THÈSE

Pour l'obtention du grade de
DOCTEUR DE L'UNIVERSITÉ DE POITIERS
UFR des sciences fondamentales et appliquées
Institut de chimie des milieux et matériaux de Poitiers - IC2MP
(Diplôme National - Arrêté du 7 août 2006)

École doctorale : Sciences pour l'environnement - Gay Lussac (La Rochelle)
Secteur de recherche : Chimie organique, minérale, industrielle

Cotutelle : Université libanaise

Présentée par :
Zeinab Ezzeddine

Divalent heavy metals adsorption on various porous materials: removal efficiency and application

Directeur(s) de Thèse :
Yannick Pouilloux, Zeinab Saad

Soutenue le 09 décembre 2014 devant le jury

Jury :

Président	**Bernard Legube**	Professeur des Universités, Université de Poitiers
Rapporteur	**Bénédicte Lebeau-Talamona**	Directeur de recherche CNRS, Université de Haute-Alsace
Rapporteur	**Maguy Jaber**	Professeur des Universités, Université Pierre et Marie Curie, Paris 6
Membre	**Yannick Pouilloux**	Professeur des Universités, Université de Poitiers
Membre	**Zeinab Saad**	Professeur, Université libanaise
Membre	**Hussein Hamad**	Professeur, Université libanaise
Membre	**Isabelle Batonneau-Gener**	Maître de conférences, Université de Poitiers

Pour citer cette thèse :
Zeinab Ezzeddine. *Divalent heavy metals adsorption on various porous materials: removal efficiency and application* [En ligne]. Thèse Chimie organique, minérale, industrielle. Poitiers : Université de Poitiers, 2014. Disponible sur Internet <http://theses.univ-poitiers.fr>

THÈSE

Pour l'obtention du Grade de
DOCTEUR DE L'UNIVERSITE DE POITIERS

Faculté des Sciences Fondamentales et Appliquées
(Diplôme National - Arrêté du 7 août 2006)

Ecole Doctorale : Gay Lussac, Science pour l'environnement

Secteur de Recherche : Chimie des Matériaux

Présentée par :

Zeinab EZZEDDINE

****

Divalent Heavy Metals Adsorption on Various Porous Materials: Removal Efficiency and Application

****

Directeur de Thèse :
Yannick POUILLOUX, Professeur, Université de Poitiers
Zeinab SAAD, Professeur, Université Libanaise

****

Soutenue le 9 décembre 2014 devant la Commission d'Examen

****

JURY

Rapporteurs :

B. LEBEAU	DR CNRS, Université de Haute Alsace
M. JABER	Professeur, Université Pierre et Marie Curie

Examinateurs :

B. LEGUBE	Professeur, Université de Poitiers
Y. POUILLOUX	Professeur, Université de Poitiers
I. BATONNEAU-GENER	Maître de Conférences, Université de Poitiers
Z. SAAD	Professeur, Université Libanaise
H. HAMAD	Professeur, Université Libanaise

Abstract

Access to sustainable and clean drinking water is a main concern as the Earth's human population continues its steady growth. Unfortunately, many of the available water resources are becoming increasingly polluted as a result of the direct discharge of industrial effluents. Heavy metals pollution, in particular, is an environmental problem of global interest due to their high toxicity, even at very low concentrations, and persistence in nature. Many methods are available for metal ions removal including adsorption which is attracting a lot of attention recently. Zeolites are well known for having very high exchange capacities. On the other hand, many researchers are studying the removal of heavy metals by modified mesoporous materials or carbonaceous adsorbents. In this thesis, the adsorption efficiencies of several materials for heavy metal removal in aqueous phase were investigated and compared to those of the faujasite NaX zeolite. Mesoporous silica SBA-15, SBA-16, KIT-6 were synthesized and modified with EDTA. Moreover, CMK-3 carbon was nano-casted from SBA-15 then the physic-chemical properties of these materials were characterized by different techniques. The effects of several experimental conditions on adsorption such as pH, contact time, temperature, metal ions concentration and the presence of competitors were studied in batch experiments. Then the efficiency of all these materials was also studied in a dynamic fixed bed reactor. Based on the obtained results, it could be said that all these materials are good candidates for divalent heavy metals removal from waste water even at low concentration. However, CMK-3 material has a high sorption capacity even in presence of competitor species.

Keywords: Heavy metals, NaX zeolite, EDTA, mesoporous silica, CMK-3 carbon.

Résumé

L'accès à l'eau potable est indispensable au développement de la vie. La pollution, liée aux activités anthropiques, constitue une menace pour la santé humaine et pour les espèces sauvages. Parmi les nombreux polluants retrouvés dans les eaux, la pollution par les métaux lourds constitue un problème environnemental d'intérêt mondial en raison de leur toxicité élevée, même à des concentrations très faibles, et de leur persistance dans la nature. De nombreuses méthodes peuvent être mises en œuvre pour l'élimination des métaux lourds dans l'eau. Parmi elles, les procédés d'adsorption sont très attractifs car très efficaces et peu couteux. Les zéolithes sont des matériaux bien connus pour leurs propriétés d'échange. Les matériaux mésoporeux modifiés ou adsorbants carbonés sont également très attractifs du fait de leur importante surface spécifique. Dans ce manuscrit, les performances d'adsorption de cations métalliques en phase aqueuse sur des matériaux mésoporeux, silices SBA-15, SBA-16, KIT-6 modifiées par l'EDTA et carbone CMK-3 obtenu par réplication ont été étudiées et comparées avec celles de la zéolithe NaX. Les propriétés physico-chimiques de l'ensemble des matériaux ont été caractérisées par plusieurs techniques d'analyses. L'influence des paramètres expérimentaux (pH, temps de contact, température, concentration des ions métalliques et de la présence d'ions concurrents) sur l'adsorption a été étudiée en mode batch. L'efficacité de ces matériaux a également été étudiée dans un réacteur dynamique à lit fixe. Les résultats obtenus ont montré que tous les matériaux étudiés éliminent efficacement et rapidement les métaux divalents dans les eaux même à faible concentration. Néanmoins, le carbone CMK-3 s'avère être le meilleur adsorbant du fait de sa grande capacité d'adsorption même en présence d'espèces compétitrices.

Mots-clés: métaux lourds, zéolithe NaX, EDTA, silice mésoporeuse, CMK-3 carbone.

Acknowledgements

I would like to express my deepest gratitude to my advisors in France: Professor Yannick Pouilloux and Dr. Isabelle Batonneau- Gene and in Lebanon: Professor Zeinab Saad and Dr. Hussein Hamad. I would never have been able to finish my thesis without their guidance and support.

I am very thankful for both Madame Bénédicte Lebeau and Professor Maguy Jaber for accepting evaluating my work. Special thanks also for Professor Bernard Legube the chairman of my jury.

I want to express my appreciation and acknowledgements to all the members of the SAMCat team at the IC2MP (Institut de Chimie des Milieux et Matériaux de Poitiers) and PRASE (Platform for Research and Analysis in Environmental Sciences, Hadath). Particular thanks go to Madame Aude Naveau for supplying the ground water samples.

My thesis would not be possible without the funding provided by the PRES Limousin Poitou-Charentes and the Lebanese university.

Many thanks to all my friends and colleagues who supported me during my research period. Finally, no words are enough to express my gratitude and love to my family for always standing by me.

List of Figures ……………………………………………………………………………….......... *iii*
List of Tables ………………………………………………………………………………... *vii*

General Introduction…………………………………………………………………………... 1

Chapter I

I. Water pollution………………………………………………………………………………. 6
II. Most common techniques for heavy metals removal……………………………………….. 9
III. Adsorption: an alternative for heavy metals remediation………………………………. 14
IV. Adsorbents regeneration…………………………………………………………………… 38
V. Conclusions…………………………………………………………………………………. 38
References……………………………………………………………………………………….. 39

Chapter II

I. Materials Used For Heavy Metals Removal………………………………………………… 48
II. Functionalization with amino groups………………………………………………………... 50
III. EDTA fixation on the materials……………………………………………………………... 51
IV. Physicochemical Characterization Techniques…………………………………………….. 51
V. Batch Adsorption Tests……………………………………………………………………… 56
VI. Evaluation of adsorptive properties………………………………………………………… 58
VII. Thermodynamics…………………………………………………………………………… 61
VIII. Fixed bed experiments…………………………………………………………………… 62
References……………………………………………………………………………………….. 66

Chapter III

I. NaX Faujasite zeolite structure……………………………………………………………… 68
II. Zeolites Physico-chemical characterizations………………………………………………. 69
III. Heavy metals Batch Adsorption Tests……………………………………………………... 72
IV. Kinetics study……………………………………………………………………………… 74
V. Distribution Coefficient……………………………………………………………………… 76
VI. NaX Zeolite Adsorption capacity…………………………………………………………… 76
VII. Cationic exchange selectivities: $2Na^+ \rightarrow M^{2+}$……………………………………………….. 83
VIII. Temperature Effect ……………………………………………………………………….. 86
IX. Fixed bed experiments……………………………………………………………………… 89
X. Conclusions……………………………………………………………………………..... 93
References……………………………………………………………………………………….. 94

Chapter IV

I. SBA-15 materials characterization ………………………………………………………… 97
II. SBA-16 and KIT6 Characterization ……………………………………………………… 109
III. Heavy Metals Batch Adsorption Tests ……………………………………………………….. 116
IV. Fixed bed experiments………………………………………………………………………… 128
V. Conclusions……………………………………………………………………………….. 132

References…………………………………………………………………………………………….. 133

Chapter V

I. Synthesis Route………………………………………………………………………………… 135
II. CMK-3 Characterization…………………………………………………………………......... 136
III. Heavy Metals Batch Adsorption Tests …………………………………………………….. 140
IV. Competitive Adsorption………………………………………………………………………. 146
V. Adsorption Thermodynamics…………………………………………………………………. 146
VI. Fixed bed experiments ……………………………………………………………………... 148
VIII. Conclusion... 152
References…………………………………………………………………………………………….. 153

Chapter VI

Adsorbents Comparison.. 154

General Conclusion………………………………………………………………………………. 158

List of Figures

Chapter I

Figure I.1 World Metals production from the year 1950 till 2010
Figure I.2 Primary building unit of zeolite structure
Figure I.3 The interaction configuration of metal ions onto IDA-chelating resins
Figure I.4 The interaction between PGLY and a metal ion
Figure I.5 Schematic molecular illustration of the silica gel surface modification with mercaptopropyl groups
Figure I.6 Possible model of chelation adsorption of PAO/SiO_2 for Pb^{2+} ion
Figure I.7 Co-condensation approach to the functionalization of mesoporous inorganic materials by direct co-assembly and incorporation of the functional moiety (R) species during synthesis
Figure I.8 Grafting (postsynthetic functionalization) for organic modification of mesoporous pure silica phases with terminal organosilanes of the type $(R'O)_3SiR$. R=organic functional group
Figure I.9 Illustration of the blockage of irregular narrow pores of silica gels
Figure I.10 Organo-functional groups derived from aminopropyl-, cyanopropyl-, or chloropropyl-grafted silica, which were applied to heavy metal ion binding
Figure I.11 Cation exchange mechanism with the carbon surface carboxylic group
Figure I.12 Preparation of mesoporous carbon using SBA-15 as a template
Figure I.13 Schematic illustration of formation of A) disordered carbon using a template with disconnected pores (MCM-41) and B) ordered CMK-3 carbon using a template with an interconnected pore system (SBA 15)

Chapter II

Figure II.1 Types of physisorption isotherms
Figure II.2 Types of hysteresis loops
Figure II.3 Model Presentation of Langmuir isotherm, (Θ) is the fraction of the surface sites occupied
Figure II.4 Model Presentation of Freundlich isotherm
Figure II.5 Schematic illustration of the experimental set up of the fixed bed column
Figure II.6 Breakthrough curve drawn as C/C_0 versus volume (ml), where C_B and V_B are the breakthrough concentration and volume respectively

Chapter III

Figure III.1 Schematic representation of the NaX zeolite with extra-framework cation positions
Figure III.2 XRD patterns NaX zeolite
Figure III.3 N_2 adsorption - desorption isotherm of NaX zeolite
Figure III.4 Thermogravimetric analysis of NaX zeolite
Figure III.5 Scanning Electron Microscopy (SEM) of NaX zeolite

Figure III.6 Effect of pH on the adsorption of metal ions on NaX zeolite (m/V= 0.1 mg. L^{-1}, t = 2h at 25 °C and [M^{2+}]$_i$ = 0.47 mmol.L^{-1})
Figure III.7 Effect of mass on the adsorption of Cu^{2+} on NaX zeolite (pH = 5.8, t = 2h at 25 °C and [Cu^{2+}]$_i$ = 0.47 mmol.L^{-1})
Figure III.8 Effect of competitive ions on the adsorption of Cu^{2+} on NaX zeolite (pH = 5.8, t= 2h at 25 °C and [Cu^{2+}]$_i$ = 0.47 mmol.L^{-1})
Figure III.9 Non- linear pseudo-second-order kinetic model for M^{2+} adsorption on NaX zeolite (pH = 5.8 at 25 °C and [Me^{2+}]$_i$ = 0.47 mmol.L^{-1})
Figure III.10 Cation exchange isotherms for 2Na^{+}→M^{2+} (M= Cu, Ni, Cd and Pb) exchange on the NaX zeolite
Figure III.11 Experimental Cu^{2+}, Ni^{2+}, Cd^{2+} and Pb^{2+} adsorption isotherms on NaX (open symbols) and their corresponding Langmuir modeled isotherms (lines)
Figure III.12 Speciation of Cu^{2+}, Ni^{2+}, Cd^{2+} and Pb^{2+} as a function of pH
Figure III.13 Kielland plots for 2Na^{+}→M^{2+} (M= Cu^{2+}, Ni^{2+}, Cd^{2+} and Pb^{2+}) exchange on the NaX zeolite. (pH = 5.8 at 25 °C and [M^{2+}]$_i$ = 0.47 mmol)
Figure III.14 NaX zeolite selectivity (pH = 5.8 at 25 °C and [M^{2+}]$_i$ = 0.47 mmol.L^{-1})
Figure III.15 Cu^{2+} adsorption on NaX at different temperatures
Figure III.16 Plots of ln K_d versus 1/T for the adsorption of Cu^{2+} on NaX
Figure III.17 The Thermodynamic speciation diagram of dominant copper species as a function of pH and temperature. The arrows show the change in the domain of stability of copper species with increasing temperature
Figure III.18 Breakthrough curve for Cu^{2+}, Ni^{2+}, Cd^{2+} and Pb^{2+} adsorption of on NaX (pH = 5.8 at 25 °C and [M^{2+}]$_i$ = 0.47 mmol.L^{-1}, m = 108 mg, flow rate 1 mL.min^{-1})
Figure III.19 Breakthrough curve for Cu^{2+}, Ni^{2+}, Cd^{2+} and Pb^{2+} adsorption of on NaX from natural ground water (pH = 6 at 25 °C and [M^{2+}]$_i$ = 0.47 mmol.L^{-1}, m = 108 mg, flow rate 1 mL.min^{-1})
Figure III.20 Breakthrough curves for Cu^{2+} adsorption of on NaX after regeneration (pH = 5.8 at 25 °C and [M^{2+}]$_i$ = 0.47 mmol.L^{-1}, m = 109 mg, flow rate 1 mL.min^{-1})

Chapter IV

Figure IV.1 Schematic illustration of mesoporous silicates modification with APTES and EDTA
Figure IV.2 XRD patterns of SBA-15 before and after modification
Figure IV.3 TEM micrographs of calcined SBA-15 before (A and B) and after EDTA modification (B and C) viewed from perpendicular and parallel directions
Figure IV.4 N_2 adsorption-desorption isotherms (a) and pore size distribution (b) of SBA-15, SBA-15-F, and SBA-15-F-EDTA.
Figure IV.5 Thermogravimetric curves for SBA-15 and its modified counterparts
Figure IV.6 FTIR spectra for unmodified SBA-15 and modified SBA-15 silica
Figure IV.7 N_2 adsorption-desorption isotherms for SBA-15-F prepared by post-synthesis impregnation and SBA-15-Co prepared by co-condensation
Figure IV.8 Thermogravimetric curves for SBA-15-co and SBA-15-co-F-EDTA
Figure IV.9 XRD patterns of SBA-15 before and after hydration
Figure IV.10 N_2 adsorption-desorption isotherms for SBA-15 before and after hydration
Figure IV.11 Cu^{2+} adsorption efficiencies for each of the modified SBA-15 samples (metal concentration, 0.47mmol.L^{-1} at 25°C)

Figure IV.12 A Simplified scheme for the speciation and interactions of the Surface amino Groups, M are silicon atoms
Figure IV.13 XRD patterns of KIT-6 (a) and SBA-16 (b) and before and after modification
Figure IV.14 TEM micrographs of calcined KIT-6 before (A and B) and after EDTA modification (C and D) viewed from perpendicular and parallel directions
Figure IV.15 TEM micrographs of the calcined SBA-16 mesoporous silica materials before (A and B) and after EDTA modification (C and D)
Figure IV.16 N_2 adsorption-desorption isotherms (a) and pore size distribution (b) of KIT-6, KIT-6-F, KIT-6-F-EDTA
Figure IV.17 N_2 adsorption-desorption isotherms (a) and pore size distribution (b) of SBA-16, SBA-16-F and SBA-16-F-EDTA
Figure IV.18 Thermogravimetric curves for modified KIT-6and SBA-16
Figure IV.19 Effect of contact time of Cu^{2+} adsorption (metal concentration, $0.47 mmol.L^{-1}$ at 25 °C)
Figure IV.20 Effect of mass on the adsorption of Cu^{2+} on EDTA modified SBA-15 silica (pH = 5.8, t= 2h at 25 ºC and $[Cu^{2+}]_i = 0.47$ $mmol.L^{-1}$)
Figure IV.21 Effect of pH on Cu^{2+}, Ni^{2+}, Cd^{2+} and Pb^{2+} adsorption onto KIT-6- F-EDTA (a) and SBA-15- F-EDTA (b) (metal concentration, $0.47 mmol.L^{-1}$ at 25 °C)
Figure IV.22 Effect of pH on EDTA
Figure IV.23 Cu^{2+}, Ni^{2+}, Cd^{2+} and Pb^{2+} sorption kinetics on KIT-6-F-EDTA samples fitted by non-linear pseudo-second order model ($C_i = 0.47 mmol.L^{-1}$, pH 5.8 at 25°C)
Figure IV.24 Cu^{2+}, Ni^{2+}, Cd^{2+} and Pb^{2+} sorption kinetics on SBA-15-F-EDTA samples fitted by non-linear pseudo-second order model ($C_i = 0.47 mmol.L^{-1}$, pH 5.8 at 25°C)
Figure IV.25 Correlation between the sorption rate h and the exchange velocity (k_{w})
Figure IV.26 Cu^{2+}, Ni^{2+}, Cd^{2+} and Pb^{2+} adsorption isotherms of KIT-6-F-EDTA fitted by Langmuir
Figure IV.27 Cu^{2+}, Ni^{2+}, Cd^{2+} and Pb^{2+} adsorption isotherms of SBA-15-F-EDTA fitted by Langmuir
Figure IV.28 Cu^{2+} adsorption on SBA-15-F-EDTA at different temperatures (pH = 5.8)
Figure IV.29 Plots of $\ln K_d$ versus $1/T$ for the adsorption of Cu^{2+} on SBA-15-F-EDTA
Figure IV.30 Effect of competitive ions on the adsorption of Cu^{2+} on SBA-15-F-EDTA (pH = 5.8, t= 2h at 25 ºC and $[Cu^{2+}]_i = 0.47$ $mmol.L^{-1}$
Figure IV.31 Equilibrium composition of Cu^{2+} - Cl^- system
Figure IV.32 Breakthrough curve for Cu^{2+}, Ni^{2+}, Cd^{2+} and Pb^{2+} adsorption of on SBA-15 (pH = 5.8 at 23 ºC and $[M^{2+}]_i = 0.47$ mmol, m = 106 mg, flow rate 1 $mL.min^{-1}$)
Figure IV.33 Breakthrough curve for Cu^{2+}, Ni^{2+}, Cd^{2+} and Pb^{2+} adsorption of on SBA-15-F-EDTA from natural ground water (pH = 6 at 25 ºC and $[M^{2+}]_i = 0.47$ $mmol.L^{-1}$, m = 107 mg, flow rate 1 $mL.min^{-1}$)

Chapter V

Figure V.1 A schematic illustration of CMK-3 nanocasting using SBA-15
Figure V.2 XRD patterns of CMK-3 and that of its template SBA-15

Figure V.3 Nitrogen adsorption–desorption isotherms (a) and pore size distribution (b) of CMK-3 and its SBA-15 mold
Figure V.4 TEM images of CMK-3 viewed from perpendicular and parallel directions
Figure V.5 The pH of point of zero charge of CMK-3 mesoporous carbon determined by pH shift method
Figure V.6 Cu^{2+}adsorption on HF and NaOH extracted CMK-3 (pH = 5.8 at 25 °C and $[Cu^{2+}]_i$ = 0.47 mmol)
Figure V.7 Effect of mass on the adsorption of Cu^{2+} on CMK-3 (pH = 5.8, t= 2h at 25 °C and $[Cu^{2+}]_i$ = 0.47 $mmol.L^{-1}$)
Figure V.8 Effect of pH on Cu^{2+}, Cd^{2+} and Pb^{2+} adsorption onto CMK-3 (metal concentration, 0.47$mmol.L^{-1}$ at 25 °C)
Figure V.9 Cu^{2+}, Cd^{2+} and Pb^{2+} sorption kinetics on CMK-3 fitted by non-linear pseudo-second order model (C_i = 0.47$mmol.L^{-1}$, pH 5.8 at 25 °C)
Figure V.10 Langmuir fitting of Cu^{2}, Cd^{2+} and Pb^{2+} adsorption isotherms on CMK-3
Figure V.11 Effect of competitive ions on the adsorption of Cu^{2+} on CMK-3 (pH = 5.8, t= 2h at 25 °C and $[Cu^{2+}]_i$ = 0.47 $mmol.L^{-1}$.
Figure V.12 Cu^{2+} adsorption on CMK-3 at different temperatures (pH = 5.8)
Figure V.13 Plots of ln K_d versus $1/T$ for the adsorption of Cu^{2+} on CMK-3
Figure V.14 Breakthrough curve for Cu^{2+}, Cd^{2+} and Pb^{2+} adsorption of on CMK-3 (pH = 5.8 at 25 °C and $[M^{2+}]_i$ = 0.47 $mmol.L^{-1}$, m = 105 mg, flow rate 1 $mL.min^{-1}$)
Figure V.15 Breakthrough curve for Cu^{2+}, Ni^{2+}, Cd^{2+} and Pb^{2+} adsorption of on CMK-3 from natural ground water (pH = 6 at 25 ºC and $[M^{2+}]_i$ = 0.47 $mmol.L^{-1}$, m = 105 mg, flow rate 1 $mL.min^{-1}$)
Figure V.16 Breakthrough curves for Cu^{2+} adsorption of on CMK-3 after regeneration (pH = 5.8 at 25 °C and $[M^{2+}]_i$ = 0.47 mmol. L^{-1}, m = 105 mg, flow rate 1 $mL.min^{-1}$)

List of Tables

Chapter I

Table I.1 Guidelines for heavy metals in drinking water
Table I.2 Heavy metals adsorption on various natural zeolites
Table I.3 Primary hydrolysis constant pK_1 of some metals
Table I.4 The adsorption capacities of some biosorbents
Table I.5 Different chelating resins and their adsorption capacities
Table I.6 Adsorption capacities of some modified silica gels
Table I.7 Removal of heavy metal species using organically-modified mesoporous silica adsorbents.
Table I.8 Heavy metals adsorption on modified microporous activated carbon
Table I.9 Heavy metals adsorption on modified mesoporous carbon
Table I.10 Heavy metals adsorption on nanosized metal oxides (NMOs)

Chapter III

Table III.1 Comparison of the first and the second order kinetic models for NaX zeolite
Table III.2 Distribution coefficients values for NaX
Table III.3 Langmuir parameters for adsorption isotherms
Table III.4 R_L values for NaX zeolites
Table III.5 Thermodynamic data for $2Na^+ \rightarrow M^{2+}$ exchange on NaX at room temperature
Table III.6 Velocity of exchange constants ($k_{\_w}$) for the four studied metal ions
Table III.7 Thermodynamic parameters for Cu^{2+} adsorption on NaX zeolite
Table III.8 Column capacity for Cu^{2+}, Ni^{2+}, Cd^{2+} and Pb^{2+} adsorption on NaX zeolite
Table III.9 Column capacity for Cu^{2+}, Ni^{2+}, Cd^{2+} and Pb^{2+} adsorption on NaX zeolite from natural water
Table.III.10 Regeneration efficiency after three Cu^{2+} adsorption-desorption cycles

Chapter IV

Table IV.1 Textural properties of SBA-15 before and after modification
Table IV.2 Amino and EDTA content of the modified samples
Table IV.3 Textural properties of SBA-15 before and after hydration
Table IV.4 Amino content for differently modified SBA-15 samples
Table IV.5 Textural properties of KIT-6 and SBA-16 before and after modification
Table IV.6 Amino and EDTA content of the modified samples
Table IV.7 Comparison of the first and the second order kinetic models for KIT-6-F-EDTA
Table IV.8 Comparison of the first and the second order kinetic models for SBA-15-F-EDTA
Table IV.9 Velocity of exchange constants ($k_{\_w}$) and log(β) values for metal-EDTA chelates
Table IV.10 Langmuir parameters for adsorption isotherms
Table IV.11 R_L values for SBA-15-F-EDTA and KIT-6-F-EDTA
Table IV.12 Thermodynamic parameters for Cu^{2+} adsorption on SBA-15-F-EDTA
Table IV.13 Competitive adsorption on SBA-15-F-EDTA and KIT-6-F-EDTA
Table IV.14 Column capacity for Cu^{2+}, Ni^{2+}, Cd^{2+} and Pb^{2+} adsorption on SBA-15-F-EDTA
Table IV.15 Comparison of column capacity for Cu^{2+}, Ni^{2+}, Cd^{2+} and Pb^{2+} adsorption on

SBA-15-F-EDTA from ultrapure and natural water
Table IV.16 Regeneration efficiency after three Cu^{2+} adsorption-desorption cycles

Chapter V

Table V.1 Textural properties of SBA-15 and its CMK-3 replica
Table V.2 Comparison of the first and the second order kinetic models for CMK-3
Table V.3 Parameters of intra-particle diffusion model for CMK-3
Table V.4 Langmuir parameters for adsorption isotherms
Table V.5 R_L values for CMK-3
Table V.6 Selectivity of CMK-3
Table V.7 Thermodynamic parameters for Cu^{2+} adsorption on CMK-3
Table V.8 Column capacity for Cu^{2+}, Cd^{2+} and Pb^{2+} adsorption on CMK-3
Table V.9 Comparison of column capacity for Cu^{2+}, Cd^{2+} and Pb^{2+} adsorption on CMK-3 from ultrapure and natural water
Table V.10 Regeneration efficiency after three Cu^{2+} adsorption-desorption cycles

Chapter VI

Table .VI.1 Comparison of m/V ratio and regeneration efficiency
Table VI.2 Maximum adsorption capacity q_{max} and removal efficiency at 100 ppm
Table VI.3 Batch experiments: kinetic parameters and selectivity
Table VI.4 Dynamic adsorption tests

The Industrial revolution in the last decades has been beneficial in many aspects but in the same time it has severely affected the environment. Many industrial effluents have been directly discharged in water courses making them unsuitable for consumption neither by all living organisms nor for domestic and irrigation usage. Heavy metals are considered one of the most dangerous inorganic contaminants among many others released into the environment. The reason behind this is their persistence in nature and their toxicity even at a very low concentration.

Diverse methods are available for heavy metals removal from water but the main challenge remains in treating effluents with low metal ions concentrations mainly between 10 and 100 ppm. Adsorption, in particular, using different types of materials is attracting a great deal of interest recently since it has proven to be a very promising technique for water treatment. Moreover, this process has become a significant addition to Green Chemistry endeavors. Nanotechnology has a lot to offer in this field and nano-porous adsorbents are wide spread in water treatments approaches. As an effort to enhance this method, a lot of adsorbents either naturally occurring or synthetic were tested for their efficiency. Natural zeolites and activated carbon are low cost naturally occurring adsorbents with high removal capacity. On the hand, many other synthetic materials were also developed for the same reason. Chelating resins, silica gel and modified mesoporous materials are the most researched adsorbents due to their tunable selectivity through modification using the appropriate organic ligands.

Although many studies were conducted to investigate the efficiency of each one of these mentioned adsorbents, no one has compared, in the same experimental conditions, the behavior of these materials in order to enhance their removal capacity. In an attempt to determine the most suitable adsorbent for heavy metals removal, this thesis focuses on the synthesis and modification of mesoporous silica along with nano-casted mesoporous carbon. Then the efficiencies of these thus synthesized adsorbents were compared with that of synthetic NaX Faujasite. This zeolite is known for its high exchange capacity compared to other zeolites. The adsorption tests will be carried out for several heavy metal cations (Ni^{2+}, Cd^{2+}, Pb^{2+}, Cu^{2+}) in ultrapure water and natural water. These metal cations tests will be considered for each heavy metal individually, in an equimolar mixed ions solution and in presence of other cationic competitors (Na^+, NH_4^+, Ca^{2+}).

In the first chapter an overview about the heavy metals pollution and the utilized treatment methods, including adsorption, is presented. Moreover, a detailed study was done in order to compare the efficiencies of several available adsorbents either natural or synthetic. These adsorbents include porous materials such as zeolites, ordered mesoporous silicates and carbon.

Chapter II is a description of the experimental protocols and conditions. These include the synthesis routes, modification, characterization methods and adsorption tests performed for the studied materials.

In chapter III, a complete analysis was established to understand the ion exchange mechanism that governs heavy metals removal (Cu^{2+}, Ni^{2+}, Cd^{2+} and Pb^{2+}) from water using synthetic NaX Faujasite zeolite. In addition, the different factors that affect adsorption were studied in batch experiments. These include pH effect, mass effect, contact time, temperature, the presence of competitors' ions and the initial metal ions concentrations. The exchange isotherms, kinetics and thermodynamic constant were established from the mathematical treatment of the batch adsorption results. Furthermore, dynamic adsorption experiments were done with equimolar mixture of heavy metal cation in ultrapure and natural water.

The results obtained for mesoporous silica, SBA-15, SBA-16 and KIT-6 are presented in Chapter IV. After synthesizing these ordered silicate adsorbents, they were modified with EDTA by a two step post synthetic route. EDTA is a widely recognized chelating agent known for its effectiveness in heavy metals capturing. EDTA immobilization on a silicate surface permits a facile separation of the modified adsorbent after treating contaminated water in a heterogeneous solid-liquid medium. These obtained materials were then characterized before and after modification by the mean of different techniques to access their physico-chemical properties. Then the same adsorption tests done for zeolite were also carried out here.

The mesoporous carbon CMK-3 adsorption behavior will be given in chapter V. CMK-3 carbon is the negative replica of SBA-15. For this mesoporous carbon, the effect of the method used for the template removal on the efficiency of adsorption was analyzed. The material was also fully characterized and tested by performing the same set of experiments done for the other adsorbents mentioned before. Then fixed bed experiments were carried out for all the materials in order to compare their performance in batch and dynamic experiments.

Finally, in chapter VI, the adsorption behaviors for all the studied materials were compared both in batch and dynamic conditions.

Table of Contents

I. Water Pollution 6
  I.1. Heavy Metals as Water Pollutants 6
II. Most Common Techniques for Heavy Metals Removal 9
  II.1. Chemical Precipitation 9
  II.2. Flotation 10
  II.3. Ion Exchange 10
    II.3.1. Resins 10
    II.3.2. Zeolites 11
    II.3.3. Clays 13
  II.4. Membrane Filtration 14
  II.5. Adsorption 14
III. Adsorption: An Alternative for Heavy Metals Remediation 14
  III.1. Physico-chemical Interactions in Biphasic Solid/Liquid Medium 15
    III.1.1. Metals Solubility 15
    III.1.2. Metal Hydrolysis 15
    III.1.3. Complexation in Aqueous Solutions 16
    III.1.4. Interaction Mechanism between a Solid Phase and a Cation 17
  III.2. Bioadsorbents 20
  III.3. Chelating Resins 22
  III.4. Silica Gel 25
  III.5. Modified Mesoporous Silica 28
    III.5.1. Mesoporous Silica Modified by Organo-Silanes Functionalization 29
    III.5.2. Mesoporous Silica Modified by Chelating Agents Grafting 32
  III.6. Carbonaceous Adsorbents 34
    III.6.1. Activated Carbon 34
    III.6.2. CMK-3 Mesoporous Carbons 35
  III.7. Nanosized Metal Oxides 37
IV. Adsorbents Regeneration 38

V. Conclusions 39
References 40

I. Water Pollution

There is no doubt that water is life and plays a vital role in sustaining the development of any country. Most of the water on our planet is located on oceans whereas fresh water represents only 2.5 % of the total water supply. Thus, the availability of clean water to the human population is essential. The United Nations reports that though access to improved drinking water has expanded, nearly one billion people do not have safe drinking water [1]. Furthermore, the world population continues its steady growth so water consumption will also increase. It has been estimated that by year 2025, more than half of the world population will face water crisis [2]. Unfortunately, many resources on which we all depend on are becoming increasingly polluted. Such pollution can be defined as any human-caused contamination of water that reduces its usefulness to humans and other organisms in nature [3]. Anthropogenic sources are considered the major cause of water pollution (industrial wastes, sewage, mining wastes, agriculture and pharmaceutical activities etc). These sources contain contaminants such as herbicides, pesticides, fertilizers, hazardous industrial chemicals, detergents, pathogens, heavy metals, organic solvents and textile dyes that find their way into water supplies.

All the above mentioned contaminants are highly dangerous to both aquatic and terrestrial life and subsequently to humans that are exposed to these toxins by one way or another. Some of the statistics worldwide are the proof of how really dangerous water pollution is. According to UN WWAP [4], two million tons of industrial, agricultural and sewage wastes are daily discharged into the world's water. Each year, 4 billion cases of diarrhea are caused by ingestion of unsafe water resulting in 2.2 million deaths, mostly of children. This means that 15% of child deaths each year are attributable to diarrhea – a child dying every 15 seconds [5].

I.1. Heavy Metals as Water Pollutants

Living organisms need some heavy metals such as Co, Cu, Fe and Mn at trace level while others (As, Pb…) are highly toxic even at very low concentration.

Heavy metals play an important role in industrial and technological advances due to the growing demands in modern societies (**Figure I.1**). Global extraction growth rates for copper, zinc, nickel, tin, and platinum averaged about 3.4 % annually over the past few decades, which implies a doubling of extracted material volumes every 20 years. Nowadays, heavy metals pollution is an environmental problem of worldwide concern because of their toxicity and persistence in nature. Lead, mercury, copper, cadmium, nickel and chromium are among the most common pollutants found in discharged industrial effluents.

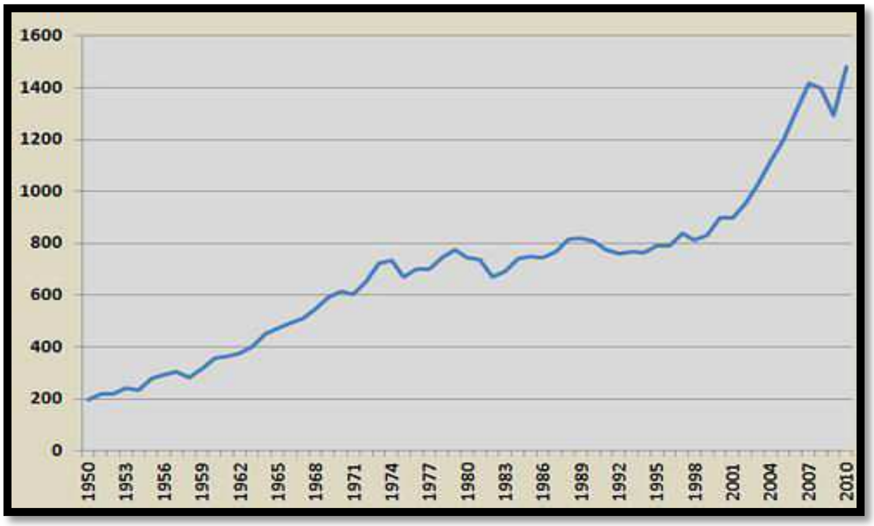

Figure I.1. World Metals production from the year 1950 till 2010[6]

Copper (Cu)

Copper, a reddish metal, is mainly used in coins, electrical wiring, and pipes. It naturally exists in rocks, soil, water and sediments so low levels of copper can be found in all water sources. Copper pipes are used extensively in plumbing systems in many countries causing elevated levels of copper in water after a long period of time. This can lead to several adverse health effects, including vomiting, diarrhea, stomach cramps, and nausea. It has also been associated with liver damage and kidney disease [7-8].

Nickel (Ni)

Nickel is mainly used in the production of stainless steels, non-ferrous alloys, nickel–cadmium batteries, welding products, and in certain electronic products. The main source of nickel in drinking-water is leaching from pipes and fittings in direct contact with water. Upon skin contact with solutions containing nickel many people develop dermatitis. Also it affects kidneys function by causing tubular lesions [9-10].

Cadmium (Cd)

Cadmium is used in for the production of rechargeable batteries, steel industry and in plastics. It is released to the environment in wastewater. Once ingested, cadmium irreversibly accumulates in kidneys and other vital organs such the lungs and the liver. In addition, it is highly toxic since it can disrupt a number of biological systems even at doses much lower than most toxic metals [11].

Lead (Pb)

Lead is one of the most toxic heavy metals discharged in water from several industries such as coating, storage batteries and aeronautical. Also it may leach into drinking water from certain types of plumbing materials. Lead causes serious health effects including hypertension, muscle and joint pain, irritability, memory or concentration problems, kidney failure and nervous diseases [12-13].

Chromium (Cr)

The oxidation degree of chromium ranges from (-2) to (+6). The most common oxidation states of chromium are (+3), and (+6). It is used in many industrial applications either melted with other metals for alloys production or plated. Hexavalent chromium is so dangerous and a dose higher than 3 g is lethal for adult humans. The first symptoms are vomiting and chronic diarrhea then convulsions occur during the final stages of the illness [14].

Mercury (Hg)

Inorganic mercury compounds such as mercuric chloride are the most common forms of mercury found in drinking water. These compounds are used in batteries paper manufacturing and the chemical industry. Overexposure to mercury causes serious brain damage and Lesions in the kidneys. Children and developing fetuses are at greatest risk from the harmful effects of mercury [15].

Potable water should contain a certain level of heavy metals that should not be exceeded in order to be considered safe for consumption. The international standards of some heavy metals are listed in **Table I.1**.

Table I.1. Guidelines for heavy metals in drinking water [16]

Metal	Standard concentration (ppm)
Copper	1.3
Nickel	0.07
Cadmium	0.005
Lead	0
Chromium (VI)	0.003
Mercury	0.002

II. Most Common Techniques for Heavy Metals Removal

Extensive research has been done concerning heavy metals removal from contaminated water especially industrial wastewater. In addition, an enormous financial budget has been dedicated to improve wastewater treatment techniques. The latter include conventional physicochemical methods such as chemical precipitation, flotation, ion exchange, membrane filtration, and currently adsorption is attracting a lot of attention in this field.

II.1. Chemical Precipitation

This technique is widely used in industries due to its simplicity, effectiveness in removing metal ions and low cost of operation [17]. The principle of chemical precipitation is the formation of insoluble complexes that can be separated from water through filtration or sedimentation and reused. Hydroxide precipitation is among the most used processes for heavy metals separation where the pH can be easily controlled [18]. In the pH range between 8 and 11 metal hydroxides solubility decreases drastically so that they can be removed by sedimentation. Various hydroxides are used in waste water treatment such as $Ca(OH)_2$ and NaOH [19] where they all have the same general mechanism for heavy metals precipitation:

$$M^{n+} + nOH^{-} \rightarrow M(OH)_n$$

On the other hand, hydroxide precipitation has some inconveniences since large quantities of low density sludge are produced posing disposal problems [20]. Also, for wastewater containing several metals, the optimal pH for one metal may put another metal back into the solution. In addition, if complexing agents are present in wastewater, they will inhibit metal hydroxide precipitation.

II.2. Flotation

Currently, flotation is extensively used in wastewater treatment. This technique allows the separation of heavy metals through bubble attachment. In Dissolved Air Flotation (DAF), suspended particles present in water attach to micro-bubbles of air thus developing agglomerates with density lower than that of water. Then, flocs rise through the water and accumulate at the surface so they can be removed as sludge [21]. Flotation offers many advantages such, high removal efficiency, high overflow rates, low detention periods, and production of more concentrated sludge [22]. But the disadvantages involve high initial capital cost, high maintenance and operation costs.

II.3. Ion Exchange

Due to the high removal efficiency and fast kinetics during operation [23], ion-exchange techniques have been widely used for heavy metals removal from water.

II.3.1. Resins

Resins have the specific ability to exchange cations with metals present in wastewater. Synthetic resins are commonly preferred because they are effective in eliminating heavy metals from the solution [24].

The most utilized cation exchangers are either strongly acidic resins with sulfonic acid groups ($-SO_3H$) or weakly acid resins with carboxylic acid groups (-COOH). Hydrogen ions serve as exchangeable ions with metal cations for both types of resins [25]. As waste water passes through the resins column, metal ions are exchanged for the hydrogen ions on the resin according to the following process:

$$nR\text{-}SO_3H + M^{n+} \rightarrow (R\text{-}SO_3\text{-})n\ M^{n+} + nH^+$$

$$nR\text{-}COOH + M^{n+} \rightarrow (R\text{-}COO\text{-})n\ M^{n+} + nH^+$$

However, chemical reagents should be used for the regeneration of resins and this can cause serious secondary pollution. Also, resins are expensive, so they cannot be used upon treating large amounts of wastewater containing low concentration heavy metals.

II.3.2. Zeolites

Zeolites are broadly present in nature and were firstly discovered by the Swedish mineralogist Axel Fredrick Crønstedt in 1756. He named the material ‘zeolite’ which emerges from the classical Greek, where (zeo) means ‘to boil’ and (lithos) means ‘stone’ [26].

Zeolites are microporous crystalline aluminosilicates composed of linked tetrahedral frameworks each consisting of a cation surrounded by four O atoms TO_4 (T = Si, Al) **Figure I.2**. When Al is incorporated into the silica framework it makes it negatively charged due to the +3 charge on the Al atom. In order to keep the overall framework neutral the presence of extra framework cations is necessary within the structure [27]. These cations are exchangeable and give rise to the rich ion-exchange chemistry of these materials. The formula describing the three components of zeolites is:

$M_{x/n} [Al_x\ Si_y\ O_{2(x+y)}],\ zH_2O$

(Where M is an alkaline earth cation having n as the valence charge, per unit cell x and y are the total number of tetrahedra per unit cell with the number of water molecules z.

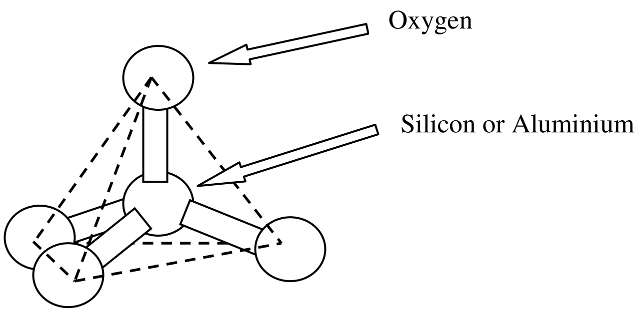

Figure I.2. Primary building unit of zeolite structure

Natural zeolites have been also used to remove heavy metal from aqueous solutions because they are inexpensive and highly abundant. Several researches showed that zeolites have good cation-exchange capacities under different experimental conditions [28-29-30]. One of the most frequently studied natural zeolites is Clinoptilolite [31-32]. Although there are many reports on the use of zeolites for heavy metal removal, they are limited compared with synthetic resins. So, more work is needed for the application of zeolites at an industrial scale since their application is still on the laboratory experimental scale. Some examples for heavy metals removal using natural zeolites are listed in **Table I.2**.

Table I.2. Heavy metals adsorption on various natural zeolites

Zeolite	Metal ions	Adsorption (mmol g^{-1})	Ref
Turkish clinoptilolite	Pb^{2+}	0.365	[33]
	Zn^{2+}	0.125	
	Cu^{2+}	0.113	
	Ni^{2+}	0.086	
Sardinian clinoptilolite	Cu^{2+}	0.170	[34]
	Cd^{2+}	0.095	
	Pb^{2+}	0.600	
	Zn^{2+}	0.05	
Natural phillipsite	Pb^{2+}	0.172	[35]
Clinoptilolite	Cd^{2+}	0.09	[36]
Natural clinoptilolite	Cr^{3+}	0.079	[37]
	Ni^{2+}	0.034	
	Zn^{2+}	0.053	
	Cu^{2+}	0.093	
	Cd^{2+}	0.041	
Bigadic clinoptilolite	Pb^{2+}	0.111	[38]
	Zn^{2+}	0.367	
	Cd^{2+}	0.003	

Scolecite	Pb^{2+}	0.028	[39]
	Cu^{2+}	0.065	
	Zn^{2+}	0.032	
	Ni^{2+}, Co^{2+}	0.015	
	Cd^{2+}	0.004	
Ukraine clinoptilolite	Pb^{2+}	0.067	[40]
	Cu^{2+}	0.202	
	Ni^{2+}	0.111	
	Cd^{2+}	0.019	
Mexican clinoptilolite	Pb^{2+}	0.7	[41]
Brazilian scolecite	Cr^{3+}	1.94	[42]
	Ni^{2+}	1.04	
	Cd^{2+}	0.89	
	Mn^{2+}	2	

II.3.3. Clays

Clays are hydrous aluminosilicates defined as minerals that make up the colloid fraction (< 2 μ) of soils, sediments, rocks and water [43]. Clays contain exchangeable cations and anions on their surfaces. The prominent cations found on clay surface are Ca^{2+}, Mg^{2+}, H^+, K^+, NH_4^+ and Na^+. These cations can be exchanged with other metal ions easily without affecting the clay mineral structure.

Heavy metals removal by natural clays has been extensively investigated due to their high cation exchange capacity. Also, clays are very abundant, have mechanical and chemical stability and low-cost [44,45,46,47]. Some of these used clays are: bentonite [48], beidellite [49], kaolinite [50] and montmorillonite [51]. The disadvantage of clays is that their removal efficiency is less than that of natural zeolites [52].

Ion-exchange in clays is affected by certain parameters as pH, temperature, initial metal concentration and contact time [53].

II.4. Membrane Filtration

Membrane filtration is highly efficient in heavy metals removal, easy to operate and saves space. Other advantages of this technique include less usage of chemicals and it can be easily combined with other separation processes for better removal efficiency. There are several filtration processes used for heavy metals separation from contaminated wastewater depending on the size of the particle that can be retained. Membrane filtration includes nanofiltration (NF), reverse osmosis (RO) and electrodialysis (ED). The main disadvantages are the high operation cost, process complexity, membrane fouling and low permeate flux [54].

II.5. Adsorption

Adsorption is currently considered as an effective and an economic method for heavy metal wastewater treatment. It offers design and operation flexibility and will produce high-quality treated effluent. Moreover, adsorption is often reversible so adsorbents can be regenerated by suitable desorption process.

Adsorption, in general, proceeds through three steps [55], first by film diffusion which is the transport of metal ions (adsorbate) from the bulk solution to the external surface of the adsorbent. Second, it proceeds by particle diffusion or the migration of adsorbate into the pores of the adsorbent. Finally there is the interaction of metal ions with the available sites on surface of the pores. It is well known that the difference between the adsorbate concentration in the solution at any time and that at equilibrium is the driving force for the adsorption process [56].

III. Adsorption: An Alternative for Heavy Metals Remediation

The dispersion of solid particles in an aqueous solution constitutes a biphasic system. The two phases are separated by an interface resulted from exchanges between them. This exchange is due to physical or chemical reactions that can be described by several models. The most important properties that interfere in these exchange reactions are the valence, the electronic configuration, the ionic radius as well as the ionization capacity in the solution. The main chemical reactions that affect metal cations in water are hydrolysis and complexation.

III.1. Physico-chemical Interactions in Biphasic Solid/Liquid Medium

The different possible chemical forms of an element (species) can be differentiated by speciation. For example, it can be distinguished between dissolved species and those bound to a solid phase or between complexes formed with different ligands in the solution and also between different oxidation states. So, metal speciation is important to understand the fate of trace metals in natural water.

III.1.1. Metals Solubility

The concentration of dissolved metals is limited by precipitation of solid phases slightly soluble. In natural water the most important solid phases for metals are hydroxides, oxides, carbonates and sulfur in anoxic conditions. The solubility of all these species in solution depends on pH so the solubility strongly depends on the presence of ligands and metal speciation [57].

III.1.2. Metal Hydrolysis

In aqueous medium, metal ions exist in their hydrated forms. The attraction and the organization of water molecules around the ions are under the effect of dipolar interactions on several layers. However, it is important to distinguish between the primary hydration sphere which consists of the water molecules in contact with the cation and the following layers that are more distant. Me^{2+} represents the simple form of hydrated ion $[Me(OH_2)_n]^{2+}$. Thus, the reaction for a divalent cation Me and a coordination number n is as follows [58]:

$Me(H_2O)_n^{2+} \leftrightarrow MeOH(H_2O)_{n-1}^{+} + H^+$ $\quad\quad K_1$

This reaction can be simplified as:

$Me^{2+} + H_2O \leftrightarrow MeOH^+ + H^+$ $\quad\quad K_1^{'}$

The pK_1 values of some metals are presented in **Table I.3**.

Table I.3. Primary hydrolysis constant pK_1 of some metals

Cation	pK_1
Hg^{2+}	2.4
Pb^{2+}	7.7
Cu^{2+}	7.7
Zn^{2+}	9
Ni^{2+}	9.7
Cd^{2+}	10.1

The deprotonation reaction successively proceeds as follows:

$Me^{2+} + H_2O \leftrightarrow MeOH^{+} + H^{+}$ K_1'

$MeOH^{+} + H_2O \leftrightarrow Me(OH)_2 + H^{+}$ K_2'

$Me(OH)_2 + H_2O \leftrightarrow Me(OH)_3^{-} + H^{+}$ K_3'

This reaction depends on pH and the hydrolysis degree of metals. In general as pH increases the degree of deprotonation increases so the metals will be present in their insoluble form.

III.1.3. Complexation in Aqueous Solutions

Metallic cations can react with ligands present in water and form complexes. These ligands have a lone pair of electrons. In general they are non metallic elements, electronegative electron donors (Lewis acid) such as O, N and S. The principle inorganic ligands that can be found in water are PO_4^{3-}, HCO_3^{-}, CO_3^{-}, Cl^{-}, SO_4^{2-}, F^{-}, carbonate and biocarbonate ions are important ligands that form complexes with metals. The complexation reaction between divalent metals and a ligand can be written as follows:

$Me^{2+} + L^{-} \leftrightarrow L\text{-}Me^{+}$

This reaction is described by the formation constant K_{MeL} which is related to the activity of ions in solution:

$$K_{MeL} = \frac{[\mathrm{MeL}^{+}]}{[\mathrm{Me}^{2+}][\mathrm{L}^{-}]}$$

This formation constant is a measure of the complex stability. The complexation rate depends on the metal concentration as well as the concentration of the ligands. Two types of complexes can be distinguished:

- Internal sphere complex, if the ligand is in direct contact with the metal
- External sphere complex, if one or more water molecules are interposed between the metal and the ligand.

The determination (all the chemical forms of a species) of metals speciation in soluble phase is so important since the thus complexes formed can react or not with solids. For example, hydroxyl-metal complexes adsorb more strongly than free ions while metal complexes formed with chlorine are less adsorbed than free ions.

III.1.4. Interaction Mechanism between a Solid Phase and a Cation

Several physico-chemical phenomena interfere in the transfer of trace elements from liquid phase to solid phase or vice versa: specific adsorption, non specific adsorption and precipitation. This physico-chemical retention can interfere simultaneously with varied importance concerning the total interaction between metallic cations and the solid phase.

Adsorption

In general adsorption is defined as the process resulting from the accumulation of a substance at the interface between two contiguous phases according to a two dimensional arrangement. It is the surface property that corresponds to electrostatic or chemical reaction: acidic-basic, oxidation-reduction, or the combination of the two.

Two types of adsorption can be distinguished based on the formation or not of chemical bonds which are: specific and non specific adsorption [59].

III.1.4.1. Non Specific Adsorption

It is also called physisorption and can be devided into surface complexation of external sphere and non specific physical adsorption.

Complexation of External Sphere

This complexation also named specific physical adsorption takes place at the level of the outer Helmotz plane (OHP). The sites on the solid surface and the metallic cations are separated by the hydration sphere that surrounds these cations. Thus Van der Waals interactions predominate (energy between 1 and 50 kJ mol^{-1}).

This type of adsorption is sometimes called weak affinity specific adsorption in order to distinguish it from the high affinity specific adsorption (chemisorption).

The surface is selective for cations by physiosorption. The affinity of the surface for the cations depends on several factors: the charge, the hydrated radius and the speciation of the cation and above all the nature of the sites on the solid surface.

Non Specific Physical Adsorption

It corresponds to charge compensation of the solid surface by hydrated ions (counter-ions) present in the diffuse layer. The latter doesn't form complexes with the functional groups at the surface and are generally called indifferent ions. This interaction is only influenced by the valence of the metallic cation and the surface charge of the solid particle. In the diffusion layer, the distribution of counter-ions and co-ions is determined at the same time by the electrostatic interaction with the surface and by the diffusion mechanism related to thermal agitation.

In the two above cases, the bonds formed are electrostatic. These bonds are relatively weak that's why the elements are easily remobilized when there are physico-chemical changes in the medium.

The increase of the ionic force which means the increase in the concentration of ions in the solution favors the non specific adsorption.

This mechanism depends on pH which:

- Regulates the value and the density of surface charges
- Determines the activity of protons that will react with the sites on the surface thus competing with the metallic cations.
- Controls the metals speciation in the solution.

III.1.4.2. Specific Adsorption

It is assimilated with the formation of complexes in the internal sphere which means that the solute and the sites on the surface are in direct contact (without interposed water molecules). This adsorption generally takes place in the inner Helmotz plane (IHP). It corresponds to the formation of chemical bonds between the electron donor atoms on the surface (surface ligands) and the electron acceptors solutes (specific ions) so this is chemisorption. The three main types of chemical bonds between atoms are:

- Ionic: the electron transfer between atoms so the electrostatic attraction of these charged ions assure the composed bond.
- Covalent: sharing equal electrons
- Covalent coordination: the shared electrons come from only one of the partner atoms.

Taking into consideration the nature of these bonds, the formed complexes are very stable so the cations will be difficultly exchanged. This type of reaction is largely influenced by the electronic structure of the metallic cation and that of the functional groups of the surface.

The specific adsorption strongly depends on pH and is also related to the metals ions hydrolysis. Particularly, the metals that are able to form hydroxyl-complexes are more specifically adsorbed on the negatively charges deprotonated surfaces. The adsorption reaction, resulting from the formation of complexes in the internal sphere, can be described according to the following process:

$Me^{2+} + H_2O \leftrightarrow MeOH^+ + H^+$

$-S-O^- + MeOH^+ \leftrightarrow -S-O-Me-OH$

In addition, after being specifically adsorbed on the mineral surface the heavy metals can diffuse and incorporate in the structure of the solid.

III.1.4.3. Ionic Exchange

It is a particular case of adsorption. An ionic exchange reaction is the replacement of an adsorbed ion by another in the solution:

$$\bar{M}^{2+} + Me^{2+} \leftrightarrow M^{2+} + \overline{Me}^{2+}$$

Where $\bar{M}^{2+}$ and $\overline{Me}^{2+}$ are the ions retained at the surface of the solid while Me^{2+} and M^{2+} are the ions in the solution.

The ionic exchange is a phenomenon of a surface which is stoichiometric in nature, isoionic or heteroionic. Usually, the term ionic exchange is wrongly used to describe a substitution mechanism. The two reactions are not localized in the same place. Ionic exchange implies an exchange between an ion in the solution and one on the surface while substitution describes the exchange between an ion on the surface with one located on its crystallographic site in the solid [60].

Several materials are available for heavy metals adsorption. Bioadsorbents, chelating resins, silica gels, modified mesoporous silicates and carbonaceous materials are the most studied adsorbents nowadays. The adsorption mechanism depends on the material surface since it governs the interaction complexes that will form with the adsorbed metal ions.

III.2. Bioadsorbents

The removal of heavy metals from water by natural biological materials is defined as biosorption [61]. Both living and dead biomass can be used for metal removal. biosorbents have different sources which are [62]: (1) non-living biomass (bark, lignin, egg shell, etc.); (2) algae; (3) microorganisms (bacteria, fungi and yeast).

The ability of some living microorganisms to accumulate heavy metals has been observed at the beginning from toxicological point of view [63]. Then, various studies have revealed that dead microbial biomass can passively bind metal ions via various physicochemical mechanisms.

Several forms of inexpensive, non-living plant material such as sawdust, Rice husk and agricultural biomass etc., were investigated as potential biosorbents for heavy metals.

Algae are considered a renewable natural biomass that abundantly proliferates in the littoral zones. They have attracted attention and tested by many investigators as new adsorbents for metal ions. The main advantages of algal biosorbent are their wide availability, low cost and high metal sorption capacity [64].

Bacteria are the most abundant microorganisms constituting of ~10^{18} g of the entire living terrestrial biomass [65]. Some of these microorganisms were found to accumulate metals with high capacity since early 1980 [66]. Bacteria can be used as biosorbents due to their small size, their ubiquity and their ability to grow under controlled conditions. Bacterial species such as Bacillus, Pseudomonas, Streptomyces and Escherichia have been tested for metals uptake.

Fungi grow easily producing high yields of biomass and can be also genetically manipulated. Fungi biosorbents include Aspergillus niger, Saccharomyces cerevisiae and Penicillium sp.

Although biosorbents have broad sources, low-cost and rapid adsorption, there are still some challenges before their application in a wide range. The first is to select the most promising types of biomass from an extremely large pool of the available biomass [67]. The second challenge is to improve biosorption process, mainly immobilization of biomaterials, improvement of regeneration and re-use, optimization of biosorption process. **Table I.4** summarizes some of the important results of metal biosorption, according to some published references.

Table I.4. The adsorption capacities of some biosorbents

Biosorbents	Metal ions	Biosorption Capacity (mmol g^{-1})	References
Non-living biomass			
Rice husk	Cu^{2+}	0.500	[68]
	Pb^{2+}	0.580	
Sawdust (cedrus deodar wood)	Cd^{2+}	0.650	[69]
Wheat bran	Cd^{2+}	0.890	[70]
Banana stem	Pb^{2+}	0.440	[71]
Carrot residues	Cu^{2+}	0.510	[72]
	Zn^{2+}	0.450	
Nipah palm shoot biomass	Cu^{2+}	1.05	[73]
	Pb^{2+}	0.250	
Dairy manure compost	Pb^{2+}	0.460	[74]
	Cu^{2+}	0.430	
	Zn^{2+}	0.240	
Algae			
Brown alga (Ascophyllum nodosum)	Cd^{2+}	1.57	[75]

Green alga (Chlorella miniata)	Cu^{2+}	0.366	[76]
Red alga (Chondrus crispus)	Ni^{2+}	0.443	
marine green macroalga (C. linum)	Cu^{2+} Zn^{2+}	1.46 1.97	
Bacteria			
Pseudomonas putida	Pb^{2+}	1.30	[77]
Pseudomonas putida	Zn^{2+}	0.270	[78]
Streptomyces rimosus	Pb^{2+}	0.650	[79]
Bacillus licheniformis	Cr^{4+}	1.33	[80]
Bacillus thuringiensis	Ni^{2+}	0.780	[81]
Fungi			
Penicillium canescens	Cd^{2+} Pb^{2+}	0.910 1.03	[82]
Penicillium chrysogenum	Ni^{2+}	0.950	[83]
Aspergillus niger	Cu^{2+} Pb^{2+}	0.450 0.160	[84]
Aspergillus terreus (mycelial waste)	Cu^{2+}	2.68	[85]

III.3. Chelating Resins

The immobilization of a chelate moiety onto a supports through a covalent bond is considered one of the most important procedures to develop highly selective adsorbents. Taking into consideration this proposal, many organic polymers and inorganic oxides have been chemically modified by immobilizing chelate groups onto the backbone chain. Chelating resins are synthetic polymers widely used to remove heavy metals from water due to their selective properties. The latter is mainly based on the nature of the functional groups of the resin in the time the physical properties of the resin may also affect its adsorption efficiency. Many researches have been done to treat wastewater using different types of resins (**Table I.5**).

Table I.5. Different chelating resins and their adsorption capacities

Chelating resin	Active Functional group	Metals ions	Adsorption capacity (mmol g^{-1})	Ref
		Cu^{2+}	1.69	
IRC748	Iminodiacetic acid (IDA)	Pb^{2+}	1.13	[86]
NDC702		Cd^{2+}	0.61	

NJC-702	Iminodiacetic acid (IDA)	Cu^{2+}	2.04	[87]
		Pb^{2+}	1.18	
		Cd^{2+}	0.580	
PS-EDTA	Ethylenediaminetetraacetic acid	Cu^{2+}	0.660	[88]
		Pb^{2+}	0.150	
PS-EDTA PS-DTPA PS-TTOA	Amino Imino Carboxylic acid	Pb^{2+}	2.41	[89]
PSDC	N,N_-di (carboxymethyl) dithiocarbamate	Cu^{2+}	1.08	[90]
		Pb^{2+}	1.40	
		Ni^{2+}	0.970	
MPGI	Iminodiacetic acid (IDA)	Cu^{2+}	0.880	[91]
		Pb^{2+}	0.810	
		Cd^{2+}	0.780	
NDC-984	Polyamine functional groups	Ni^{2+}	0.982	[92]
		Co^{2+}	0.741	
Diaion CR 11	Iminodiacetic acid (IDA)	Cu^{2+}	0.180	[93]
		Cr^{2+}	0.280	
PS-DVB	Benzothiazole	Cu^{2+}	5.68	[94]
		Pb^{2+}	1.55	
		Cd^{2+}	1.03	
Dowex M-4195	Bispicolylamine	Cu^{2+}	1.59	[95]
MF–NTA	Nitrilotriacetic acid	Cu^{2+}	0.470	[96]
PTUI	poly(thiourea imine)	Pb^{2+}	1.57	[97]
HP2MG	Cysteamine	Pb^{2+}	0.410	[98]
		Cd^{2+}	0.410	
PS-DEG-3-AP PS-TEG-3-AP	3-aminopyridine	Hg^{2+}	1.04	[99]
OABA	Orotic acid	Cu^{2+}	1.40	[100]
MF–DTPA	Diethylenetriaminepentaacetic acid	Co^{2+} Cd^{2+} Zn^{2+} Cu^{2+}	0.930	[101]
DVB-MA-HAD	Hydroxamic acid	Ni^{2+}	2.14	[102]
Purolite S950	Aminophosphonate	Ni^{2+}	0.29	[103]
		Co^{2+}	0.180	
PGLY	Poly(glycidyl methacrylate-glycine)	Cu^{2+}	1.22	[104]
		Ni^{2+}	1.07	
		Cd^{2+}	0.960	
DTMAN	Dithiocarbamate	Hg^{2+}	2.30	[105]
		Cd^{2+}	1.94	
		Pb^{2+}	1.14	
PAO-AM	Amidoxime	Cu^{2+}	2.30	[106]
		Ni^{2+}	1.94	
		Pb^{2+}	1.14	

ED resin	Ethylenediamine	Cu^{2+}	6.85	[107]
Amberlite IRA 402 Lewatit MonoPlus MP 500	Ethylenediamine-N,N_-disuccinic acid (EDDS)	Cu^{2+} Zn^{2+} Cd^{2+} Pb^{2+}	1.64 0.960 1.06 0.650	[108]

The chelating mechanisms of some of these resins are discussed according to the explanation given by the authors. Ling *et al.* [109] investigated the efficiency of two iminodiacetic acid chelating resins (IRC748 and NDC702). The adsorption capacities on both resins followed the order of Cu^{2+} > Pb^{2+}> Cd^{2+}. They explained that this selectivity is due to the complicated impacts of metal ion electronegativity as well as resin pore textures. The proposed chelating mechanism is illustrated in **Figure I.3**.

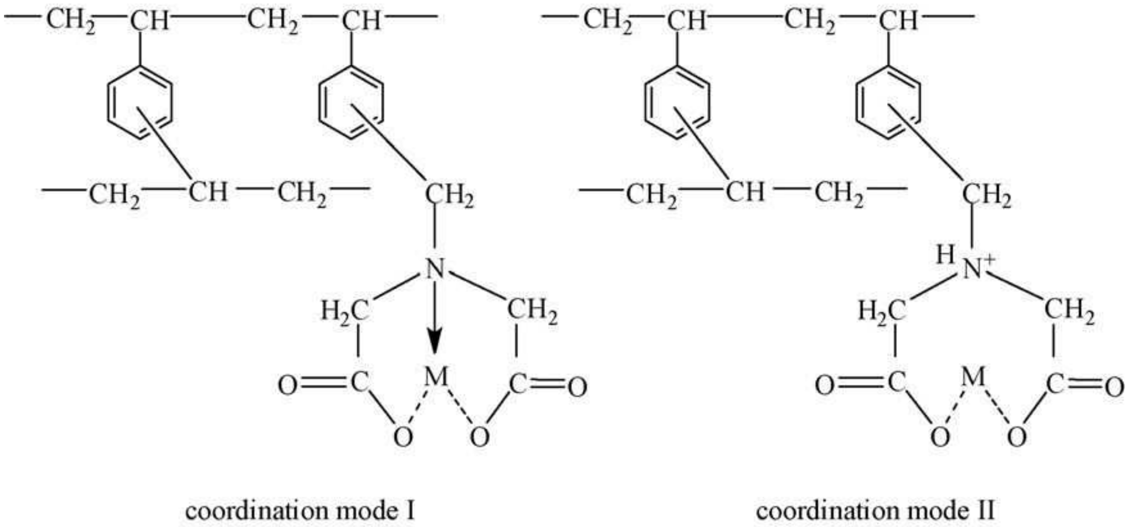

Figure I.3. The interaction configuration of metal ions onto IDA-chelating resins.

Based on their obtained information, they concluded that the chelation mechanism by iminodiacetate can be due the formation of strong complexes ML, as is the case for copper. Here, ($–L^{2–}$) coordinates to metal ions using all three donor atoms, like an iminodiacetate in solution (coordination mode I). Another complexation mode can be also formed with carboxylate $M(HL)_2$ with metal ions having lower complexation constants with the iminodiacetate, such as cadmium. In this case, two carboxylates are used for the coordination to metal ions (coordination mode II).

Moreover, Chen *et al.* [110] used a crosslinked poly(glycidyl methacrylate-glycine) (PGLY) to remove Cu^{2+}, $Ni^{2+}$and Cd^{2+} from waste water. They suggested that the removal of heavy metals was done through the strong correlations between the metal ions and both COO− and NH in glycine (**Figure I.4**).

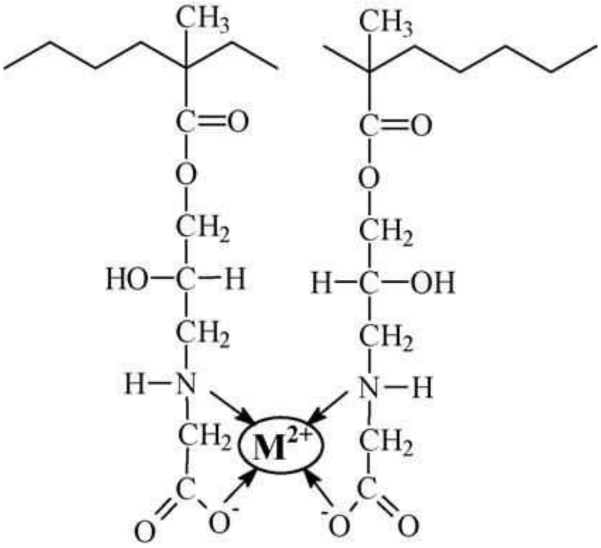

Figure I.4. The interaction between PGLY and a metal ion.

They have explained the adsorption mechanism by the coordination number of Cu^{2+}, Ni^{2+} and Cd^{2+} which is 4 so this means that these divalent metal ions need 4 electron pairs to form coordinate covalent bonds. The equilibrium adsorption capacities were in the following order $Cu^{2+} > Ni^{2+} > Cd^{2+}$, respectively. This order could be as a result of the charge density of Cu^{2+} which is greater than that of Ni^{2+} and Cd^{2+} because the ionic radius order is as follows: Cd^{2+}(0.97Å) > Ni^{2+}(0.78 Å) > Cu^{2+}(0.72 Å).

III.4. Silica Gel

Although chelating resins are effective in removing heavy metals from water, anchoring complexing agents onto more stable materials is attracting a lot of attention recently. Silica gels are among the supports having a high thermal, chemical and mechanical stability and can be chemically modified through the silanol groups dispersed on its surface. So, the ability to modify such supports leads to new materials that can be applied in different fields including wastewater treatment.

In the last years many researchers focused on modifying silica gel and presenting it as an efficient adsorbent for heavy metals removal. Silica gel can be modified with organosilanes (amino, mercapto) and used directly for heavy metals adsorption (**Figure I.5**).

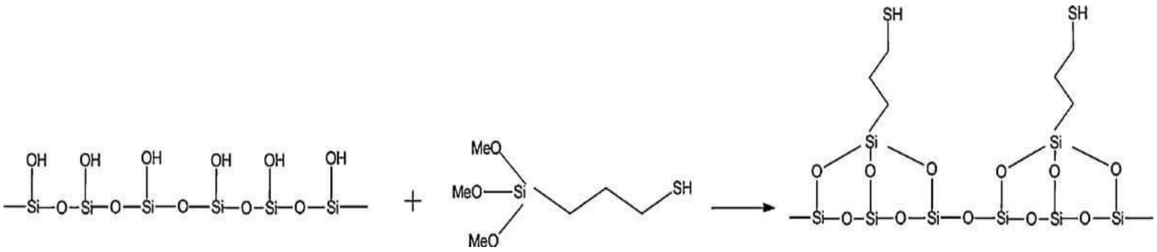

Figure I.5. Schematic molecular illustration of the silica gel surface modification with mercaptopropyl groups [111].

Where several types of adsorption complexes are possible either with the organosilane alone (1-2) or with the participation of residual silanols (3-4) [112]:

$$\equiv \mathrm{SiR(S)N}\cdot\cdot\cdot \mathrm{M}^{2+}\cdot\cdot\cdot \mathrm{N(S)RSi} \equiv \quad (1)$$

$$\equiv \mathrm{SiR(S)N}\cdot\cdot\cdot \mathrm{M}^{2+}\cdot\cdot\cdot \mathrm{OH_2} \quad (2)$$

$$\equiv \mathrm{SiO(H)}\cdot\cdot\cdot \mathrm{M}^{2+}\cdot\cdot\cdot \mathrm{N(S)RSi} \equiv \quad (3)$$

$$\equiv \mathrm{SiO(H)}\cdot\cdot\cdot \mathrm{M}^{2+}\cdot\cdot\cdot \mathrm{OH_2} \quad (4)$$

Further modification can be done by anchoring chelating agents to silica gel in order to enhance the selectivity of the adsorbent. One example is the modification with poly(amidoxime) PAO/SiO_2 [113] to remove Pb^{2+} from waste water. The proposed chelation mechanism is illustrated in **Figure I.6**. The adsorption action of PAO/SiO_2 for Pb^{2+} ion is originated from the strong chelation of amidoxime groups towards Pb^{2+} ion. Amidoxime group is a bidentate ligand, and a stable five-membered chelating ring can form between one amidoxime group and one Pb^{2+} ion.

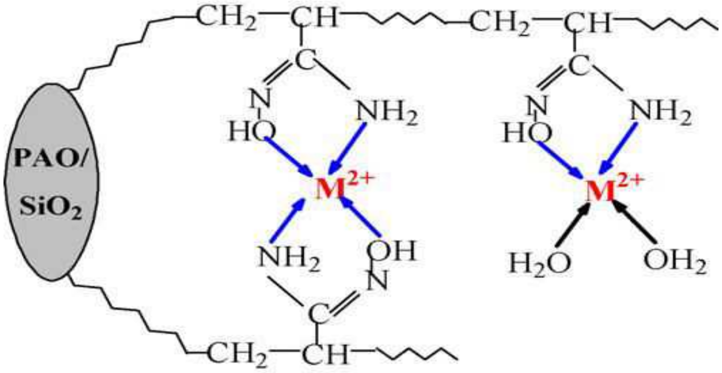

Figure I.6. Possible model of chelation adsorption of PAO/SiO_2 for Pb^{2+} ion.

The adsorption capacities of some modified silica gels are listed in **Table I.6**. It can be noticed that the adsorption capacities are lower than those found for resins although silica gels are more stable. This difference might be due to the structure of silica that could cause diffusion problems during functionalization.

Table I.6. Adsorption capacities of some modified silica gels

Chelating agent	Metal ions	Adsorption capacity (mmol g^{-1})	Ref
2-aminomethylpyridine (AMP)	Cu^{2+}	0.84	[114]
	Co^{2+}	0.67	
	Ni^{2+}	0.40	
	Zn^{2+}	0.22	
Schiff base derivative [N,N0-[1,4-phenilendi(E)methylidene]bis(2-chloroethanamine)]	Co^{2+}	0.143	[115]
	Ni^{2+}	0.073	
EDTA	Co^{2+}	0.3	[116]
	Ni^{2+}	0.35	
4,4-oxy-bis(chlorophenylglyoxime) (CPGO)	Cu^{2+}	0.055	[117]
	Co^{2+}	0.042	
	Ni^{2+}	0.034	
5-sulfosalicyclic acid (SG-PS-azo-SSA)	Cu^{2+}	0.47	[118]
Mercapto functional groups	Cu^{2+}	2.86	[119]
Amino functional groups (NH_2–SG)	Cd^{2+}	0.36	[120]
	Ni^{2+}	0.53	
	Pb^{2+}	0.47	
poly(amidoxime)	Cu^{2+}	1.2	[121]
	Ni^{2+}	0.55	
	Pb^{2+}	0.45	
	Cd^{2+}	0.4	
1,4-bis(3-aminopropyl)piperazine	Cu^{2+}	1.63	[122]

Cyanex 272 [bis(2,4,4-trimethylpentyl) phosphinic acid, HA]	Cu^{2+}	0.33	[123]
zwitterionic Schiff base ligand	Cu^{2+}	0.65	[124]
multi-carboxyl-functionalized silica gel	Cu^{2+}	0.74	[125]
	Cd^{2+}	0.37	
	Ni^{2+}	0.52	
	Zn^{2+}	0.61	
ethyleneimine	Pb^{2+}	1.27	[126]
	Cd^{2+}	1.02	
	Hg^{2+}	0.98	
2-acrylamido-2-methylpropanesulfonic acid	Cu^{2+}	0.31	[127]
Ethylenediamine	Cu^{2+}	1.04	[128]
	Co^{2+}	1.85	
	Ni^{2+}	1.89	
Nitrogen and thiol	Pb^{2+}	2.06	[129]
	Cd^{2+}	3.72	
	Hg^{2+}	5.14	
N-[3-(trimethoxysilyl)propyl]-ethylenediamine	Pb^{2+}	0.184	[130]
	Cu^{2+}	0.261	
4-amino-2-mercaptopyrimidine (AMP)	Cu^{2+}	0.44	[131]
aniline formaldehyde condensate (AFC)	Cu^{2+}	1.2	[132]

III.5. Modified Mesoporous Silica

The development of ordered porous materials with structures and pores that can be controlled is crucial in various fields including adsorption.

A couple of decades ago, mesoporous materials were developed. Since the 1980s, mesoporous pillared clays were widely investigated. Their major drawbacks were the rectangular pores that cannot be completely opened and the pore sizes are widely distributed with a disordered pores arrangement. The "template" synthesis was not realized before the early 1990s, when Japanese and Mobil scientists reported the synthesis of mesostructued silicates separately M41S [133-134-135]. They used organic surfactants (cationic templates) as templates and inorganic silica source. The mesoporous materials were formed by supramolecular assemblies of organic molecules instead of the molecular templates used for the production of zeolites. Since then, these materials had a great deal of interest and the surfactant-templating strategy has been widely used to synthesize a variety of ordered mesoporous materials with two- and three-dimensional (2D and 3D) structures [136]. The obtained materials have tunable porosities and open framework thus providing accessibility to reagents and metal ions. Also they have well-defined structural symmetry, high surface areas, and large pore volumes which make them good candidates for adsorption.

III.5.1. Mesoporous Silica Modified by Organo-Silanes Functionalization

Many examples are present in literature concerning the adsorption of heavy metals on functionalized mesoporous silica. Such modification via functional groups bonding offers a unique opportunity to engineer the interfacial properties of solid substrates while retaining their basic geometry and mechanical strength.

There are two methods to introduce functional groups into a mesoporous matrix, mainly co-condensation and post-grafting. The numerous silanol groups at the pore surfaces of mesoporous silicas can anchor large amounts of silanes and thus the functional groups are introduced into the mesoporous silicas.

Co-condensation

General processes of organic functionalization can be achieved by direct synthesis method which is known as co-condensation (**Figure I.7**). This direct approach involves co-condensation of tetraalkoxysilanes and organo-silanes. It offers a higher and more uniform surface coverage of functional groups and a better control over the surface properties of the functionalized materials. Thus this method has been widely used to functionalize mesoporous materials with various available functional groups. Co-condensation has the advantage of being simple and direct over one-step reaction. However the binding site of organo-silanes could be buried within the walls of the silica. Moreover, high functional silane loading may produce structurally unstable materials [137].

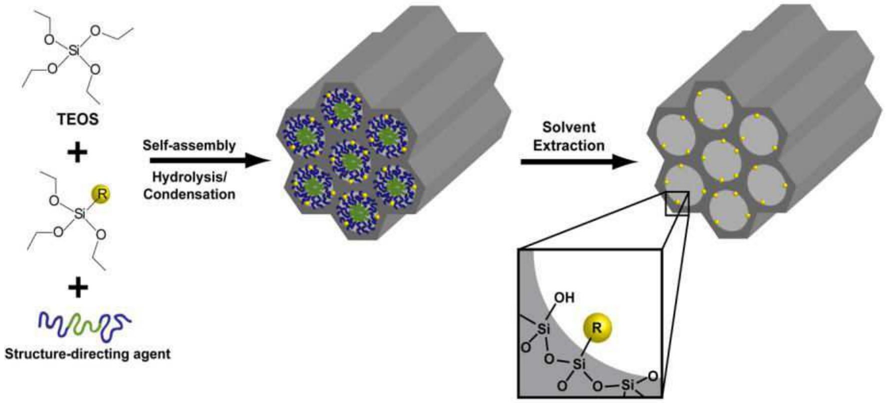

Figure I.7. Co-condensation approach to the functionalization of mesoporous inorganic materials by direct co-assembly and incorporation of the functional moiety (R) species during synthesis [138].

Post-grafting

The post grafting method is the most commonly used approach for functionalization. Through this method, calcined mesoporous silicas are modified with the organo-silanes by the reaction with the abundant silanol groups present on the mesoporous silica surface (**Figure I.8**). Specific parts of the mesoporous silica surface (external surface, pore surface, pore entrances) can be highly functionalized without altering the mesoscopic order. In general, organic functional groups are covalently attached to the pore surface by the reaction of the organo-silane usually using an appropriate solvent under reflux condition such as toluene [139].

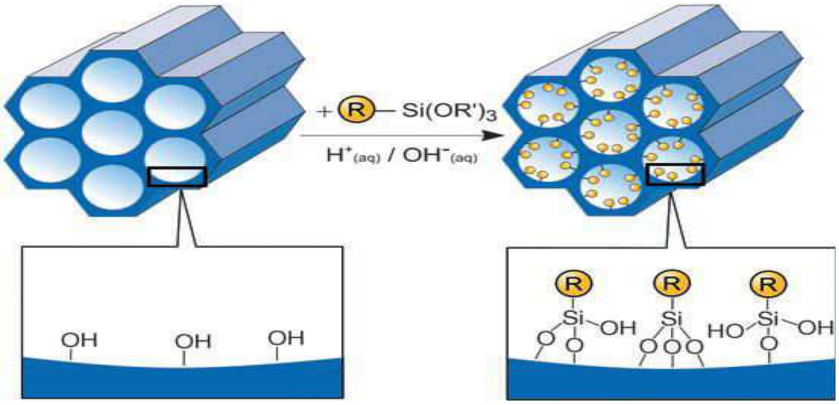

Figure I.8. Grafting (postsynthetic functionalization) for organic modification of mesoporous pure silica phases with terminal organosilanes of the type $(R'O)_3SiR$. R=organic functional group [140].

The uniform and the large framework structure of mesoporous silicates are considered as an advantage during functionalization contrary to other porous materials. This can be observed while using non-ordered silica gels as adsorbents. Functionalizing the heterogenous porous frameworks of silica gels may cause pore clogging (**Figure I.9**), so the grafted organic groups become inaccessible to metal ions.

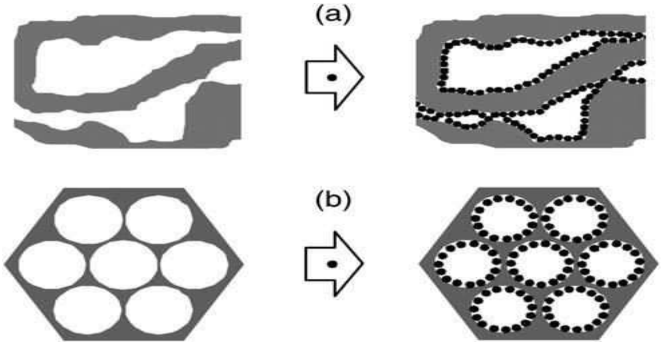

Figure I.9. Illustration of the blockage of irregular narrow pores of silica gels (a); in contrast, the uniform pore morphology of hexagonal mesoporous silica (b) leads to a grafted material with unrestricted access of ions to all of the functional sites [141].

To further increase metal ions uptake, some researchers attached polyamine-functionalized ligands to mesoporous silicates. On the other hand, other groups have modified them with more than one single ligand. This approach can extend the sorption ability to a wider range of target pollutants. The latter was achieved by co-immobilization of mercaptopropyl and propyl diethylenetriamine groups in the same mesoporous silica, resulting in efficient adsorption of many metal ions likely to be complexed with either amine and/or thiol ligands.

The choice of the functionalisation agent can be derived from the Irving-Williams stability series that relates particular ligands with particular metal ions to form the most stable complexes. According to this assumption, aminopropyl ligands (NH) are identified as being attracted to ‘hard’ metal ions such as Ni, Cr, Mn and Fe while mercatopropyl ligands (SH) are attracted to ‘soft’ metal ions such as Pb and Hg. Most environmental water samples contain a mixture of metal ions, so bi-functionalised (both aminopropyl and mercatopropyl) mesoporous silica would allow effective removal of a wider range of both hard and soft metallic ions [142].

III.5.2. Mesoporous Silica Modified by Chelating Agents Grafting

The covalent grafting of organic molecules with desired functions onto a variety of inorganic surfaces to create a heterogeneous phase during application is very beneficial. The most significant practical advantages are: improved structural and thermal stability, accessibility to the reactive centers, and insolubility in organic and aqueous solvents [143]. Recently, chelating agents are increasingly used in the removal of metal ions because they have high adsorption capacities and selectivity [144]. Chelating agents containing N-donor centers are highly specific for transition metal ions [145].

Aminopolycarboxylic acids chelating agents (APCAs) are well known to form stable structures with metal ions. APCAs are an important group of chelating agents containing several carboxylate groups bound to one or more nitrogen atoms and have the ability to sequester metal ions. Therefore, surface functionalization with these high affinity binding groups has received considerable research interest in the recent years. Iminodiacetic acid (IDA), nitrilotriacetic acid (NTA), ethylenediaminetetraacetic acid (EDTA), and diethylenetriaminepentaacetic acid (DTPA) are the most frequently used APCAs for the binding of metal ions in aqueous solutions [146].

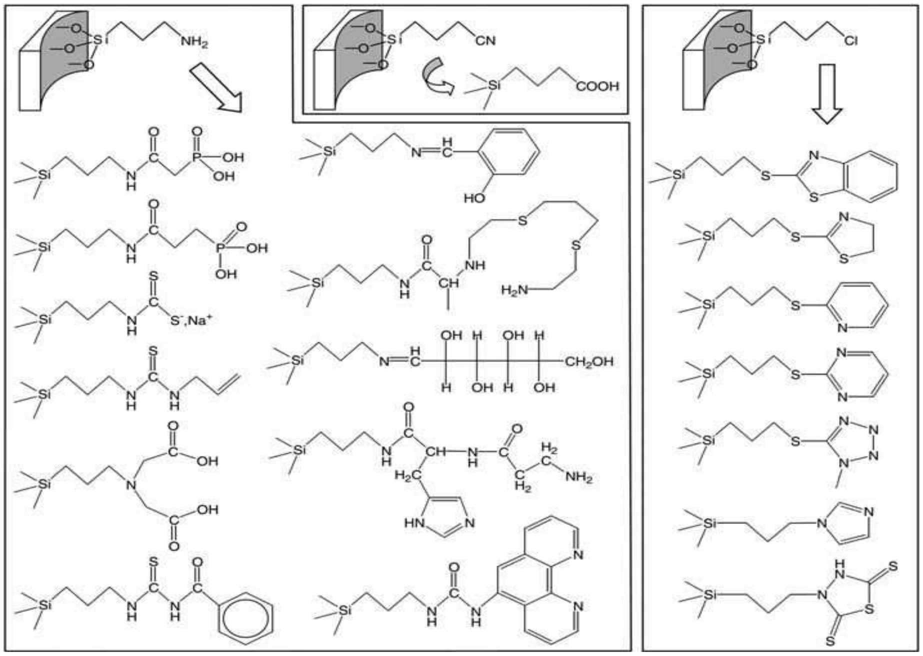

Figure I.10. Organo-functional groups applied to heavy metal ion binding and are derived from aminopropyl-, cyanopropyl-, or chloropropyl-grafted silica [135].

For modification with chelating agents, two-step derivatization from pre-formed mesoporous organosilica is needed (**Figure I.10**). However, the limitation of the two-step derivatization procedure is the presence of residual unreacted organic groups in the final material. The presence of such residual groups is due to incomplete post functionalization, which can result from restricted accessibility of these intermediary groups to large ligands. Some of the examples of modified mesoporous silica are listed in **Table I.7**.

Table I.7. Removal of heavy metal species using organically-modified mesoporous silica adsorbents.

Material	Organosilane Functional group	Metal ions	Adsorption capacity (mmol g^{-1})	Ref
SBA-15	Amino	Pb^{2+} Cd^{2+}	0.180 0.360	[147]
SBA-15	Amino	Cu^{2+}	0.540	[148]
SBA-16	Mercapto	Cu^{2+}	0.570	[149]
Mesoporous silica spheres	bi-functionalised: amino/mercapto	Cr^{3+} Ni^{2+} Fe^{3+} Mn^{2+} Pd^{2+}	0.384 0.340 0.358 0.364 0.188	[150]
MCM-41	Diethylenetriamine (DETA) Mercaptodiethylenetriamine (MDETA)	Pb^{2+}	1	[151]
MCM-48	Mercaptopropyl	Hg^{2+}	2.20	[152]
MCM-41	Amino	Ni^{2+} Cd^{2+} Pb^{2+}	0.190 0.160 0.270	[153]
SBA-15	N-propylsalicylaldimine	Cu^{2+} Co^{2+} Ni^{2+} Zn^{2+}	0.730 0.320 0.380 0.400	[154]
SBA-15	melamine-based dendrimer amines(MDA)	Pb^{2+} Cu^{2+} Cd^{2+}	0.630 1.98 0.870	[155]
SBA-15	Ethylenediamine	Pb^{2+} Cd^{2+}	1.73 0.890	[156]
SBA-15	Iminodiacetic acid (IDA)	Cd^{2+}	0.324	[157]
OSU-6-W	Ethylenediamine	Cu^{2+} Zn^{2+} Cd^{2+}	8.22 4.62 2.25	[158]

SBA-15	Ethylenediamine	Cu^{2+}	0.830	[159]
SBA-15	2-mercaptopyridine	Cr^{6+}	1.83	[160]
SBA-15	Ethylenediaminetetraacetic acid (EDTA)	Pb^{2+}	1.32	[161]

III.6. Carbonaceous Adsorbents

III.6.1. Activated Carbon

Activated carbon (AC) is a widely used adsorbent in wastewater treatment due to its high surface area ranging from 500 to 1500 $m^2\ g^{-1}$, well-developed internal microporous structure and the presence of a wide spectrum of surface functional groups [162]. It is known that chemical species removal by AC adsorption is due to the surface complex formation between the species and the surface functional groups. This is especially significant in the case of removing inorganics and metals from aqueous solutions. Many investigations dealing with metal removal from aqueous solutions tend to modify carbon surfaces by increasing their acidic surface functional groups [163]. Heavy metal ions can to form complexes with these groups as indicated in the following equation [164]:

$$M^{n+} + n(\text{–COOH}) \leftrightarrow (\text{–COO})_nM + nH^+$$

The reaction stated above occurs through cation exchange such that the metal ion exchanges site with the hydrogen ion previously attached as a whole carboxylic group as illustrated in **Figure I.11**.

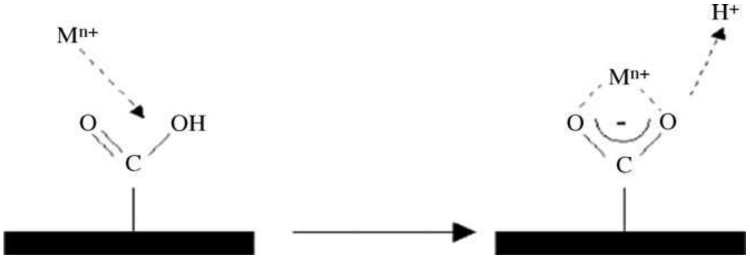

Figure I.11. Cation exchange mechanism with the carbon surface carboxylic group [165]

Although acidic treatment of AC is beneficial for metal ions adsorption, it can affect the physical aspects of AC such as BET surface area and pore volume. In most cases, treatment with oxidizing agents produces modification of the textural characteristics of the original AC, which can be a drawback in carbon materials with a narrow microporosity or a well-defined porosity [166]. Some examples of heavy metals adsorption on modified activated carbon are listed in **Table I.8**.

Table I.8. Heavy metals adsorption on modified microporous activated carbon

Carbon	Modification route	Metal ions	Adsorption capacity (mmol g^{-1})	Ref
Carbon nanotubes (CNTs)	$KMnO_4$	Cd^{2+}	0.098	[167]
Commercial coconut activated carbon	Acid-base	Cr^{6+}	0.124	[168]
Bamboo charcoal	-	Cd^{2+}	0.107	[169]
Nut shells activated carbon	SO_2 gas	Cd^{2+}	1.275	[170]
Commercial activated carbon	Polypyrrole-impregnation	Hg^{2+} Pb^{2+}	3.40 4.10	[171]
Commercial activated carbon	Immobilization of baker's yeast	Cd^{2+}	0.265	[172]
M. baccifera charcoal	H_3PO_4 and KOH	Pb^{2+}	0.259	[173]
Commercial activated carbon	HNO_3 and $SOCl_2$, followed by the reaction with ethylenediamine $C_2H_4(NH_2)_2$	Hg^{2+}	0.608	[174]
Peanut Shell Activated Carbon	HNO_3	Pb^{2+}	0.171	[175]
Olive-waste cakes Activated Carbon	H_3PO_4	Mn^{2+}	0.690	[176]
Multi-walled carbon nanotubes	Diethylenetriamine $HN(CH_2CH_2NH_2)_2$	Pb^{2+} Cd^{2+}	0.281 0.280	[177]

III.6.2. CMK-3 Mesoporous Carbons

Nanocasting Principles

Casting using hard template was known many years ago [178]. This process is based on pouring a liquid inside an object (mold) containing a hollow cavity and allowing it to solidify. Then the casting mold is broken to get the desired material so that the process is complete. When the casting procedure is done in the nanometer scale it is named nanocasting. Recently, this technique is widely studied and developed due to the need for creating nanomaterials.

Ordered Mesoporous Carbons (OMCs)

Ordered mesoporous carbons (OMCs) having high surface areas, uniform pore sizes, and large pore volumes are interesting for many applications such as catalyst supports, adsorbents, fuel cells, and electrodes for supercapacitors [179]. Several techniques for preparing OMCs are found in the literature. However, only few permit an accurate control of mesoporosity. The preparation of mesoporous carbons using mesostructured silica materials as templates was reported a few years ago [180]. The preparation method of these materials is quite simple (**Figure I.12**): firstly, the carbon source is infiltrated into the channels of a mesoporous silicate and polymerized. The obtained composite was carbonized for several hours at a high temperature (around 900 °C) then the inorganic mesoporous silica template is removed by HF or NaOH solution resulting in mesoporous carbon materials [181].

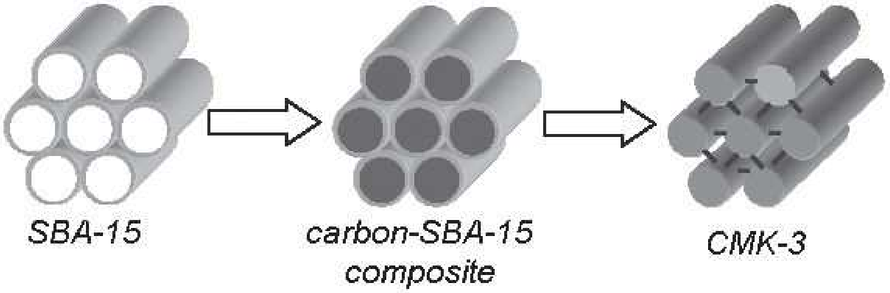

Figure I.12: Preparation of mesoporous carbon using SBA-15 as a template [182]

Earlier studies showed that zeolites and MCM-41 silica with a hexagonally ordered structure of approximately cylindrical pores was unsuitable as a template for ordered mesoporous carbon synthesis since they yielded disordered high-surface-area microporous carbon (**Figure I.13**). On the other hand, using SBA-15 silica as a hard template for carbon was a very suitable. This template choice was not obvious, since SBA-15 exhibits a structure with disconnected channel- like pores, similar to MCM-41. However, the existence of connecting micropores and small mesopores in the walls of large-pore channels of SBA-15 facilitated the synthesis of the first ordered mesoporous carbons referred to as CMK-3 [183].

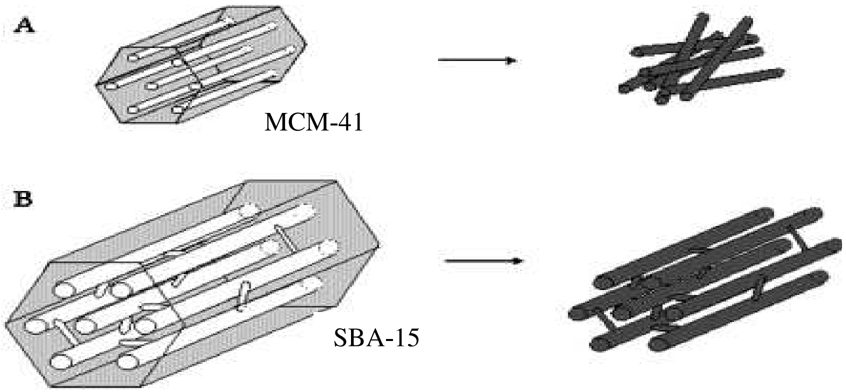

Figure I.13. Schematic illustration of formation of A) disordered carbon using a template with disconnected pores (MCM-41) and B) ordered CMK-3 carbon using a template with an interconnected pore system (SBA 15) [184].

Only few examples are found in literature dealing with heavy metals adsorption on mesoporous carbon (**Table I.9**). The results prove that OMC are very promising for heavy metals adsorption.

Table I.9. Heavy metals adsorption on modified mesoporous carbon

Mesoporous carbon	Modification route	Metal ions	Adsorption capacity (mmol g^{-1})	Ref
CMK-3	Oxidation with nitric acid	Cd^{2+} Pb^{2+}	0.360 0.450	[185]
OMC (MCM-48 as template)	Oxidation with nitric acid	Pb^{2+}	1.44	[186]
CMK-3	functionalized with 2-amino-5-mercapto-1,3,4-thiadiazole groups	Hg^{2+}	2.24	[187]
CMK-3	Functionalized with L-Cysteine	Cd^{2+}	1.76	[188]

III.7. Nanosized Metal Oxides

Another type of studied materials for heavy metals adsorption is nanosized metal oxides (NMOs). These include nanosized ferric oxides, manganese oxides, aluminum oxides, titanium oxides, magnesium oxides and cerium oxides [189-190-191]. This is partly because of their large surface areas and high activities caused by the size quantization effect [192]. **Table I.10** shows some examples for heavy metals removal using several types of NMOs.

Table I.10. Heavy metals adsorption on nanosized metal oxides (NMOs)

NMOs	Metal ions	Adsorption capacity (mmol g^{-1})	Ref
∝-MnO_2	Cu^{2+}	1.29	[193]
TiO_2	Pb^{2+} Cd^{2+} Ni^{2+}	0.390 0.070 1.14	[194]
Modified Al_2O_3	Pb^{2+} Cd^{2+} Ni^{2+}	0.480 0.740 0.310	[195]
CeO_2	Pb^{2+} Cu^{2+}	0.040 0.240	[196]
ZnO	Pb^{2+}	0.030	[197]

IV. Adsorbents Regeneration

Adsorbents regeneration is considered a very important so that they can be used several times thus reducing the operation cost. Heavy metals elution was done using several solutions depending on the nature of the adsorbents. For resins, HCl [198-199] and nitric acid [200-201-202] were mainly used but some researchers used EDTA [203]. Silica gel can be also regenerated using HCl [204] and sometimes EDTA [205] depending on the nature of the attached organic group. HCl can be also used for the regeneration of functionalized mesoporous silica [206-207] as well as nitric acid [208]. Concerning zeolites, desorption can be done using NaCl so that metal ions will be exchanged by sodium [209]. HCl can also be used for regeneration of activated carbon [210]. Nanosized metal oxides (NMOs) can be regenerated either by HCl [195] or NaOH [196] depending on the type of the metal oxide used.

V. Conclusions

Organically modified porous materials are considered promising adsorbents for heavy metals removal. This is due to the attractive properties since they can be modified even if the mechanical stability differs from one material to another. On the other hand, zeolites also have been effective in removing heavy metals from wastewater. A lot of researches have been done in order to investigate the efficiency and applicability of each adsorbent. Yet despite all these investigations, there are no real environmental applications at the commercial level of these materials. Moreover, no efforts have been done to compare the effectiveness of each material with other types of available adsorbents in order to evaluate which one can be more practical for a wider environmental use. The main challenges are the design of adsorbents that could be used in packed columns so that large volumes of waste water could be treated. To do so more efforts are required in order to increase the particle size of these adsorbents in a way that they become suitable for column application. Also, one should not forget the selectivity of each material, its stability on the long term use, and of course effectiveness of regeneration. If one of these available adsorbents could meet all the standards for real application, it could compete with commercial adsorbents in cost and stability.

References

---

[1] United Nations. The Millennium Development Goals Report 2008. New York.
[2] S. KULSHRESHTHA. Water Resour. Manag.12 (1998) 167–184.
[3] United States Environmental Protection Agency EPA-905-F-97-011, 1997.
[4] UN WWAP. 2003. United Nations World Water Assessment Program. The World Water Development Report 1: Water for People, Water for Life. UNESCO: Paris, France
[5] World Health Organization and United Nations Children's Fund. (WHO and UNICEF). (2000).
[6] Historical Statistics for Mineral and Material Commodities in the United States; USGS.
[7]Minnesota Department of Health Division of Environmental Health (2005).
[8] Environmental Health Directorate, Department of Health: Western Australia. (2010).
[9] WHO. Guidelines for drinking water Quality (2005).
[10] Lenntech. Nickel and water: reaction mechanisms, environmental impact and health effects (2014).
[11] A. Bernard, Indian J. Med. Res. 128 (2008) 557-564.
[12] T. Bahadira, G. Bakana, L. Altasb, H. Buyukgungor. 41 (2007) 98–102.
[13] I. Hajdua, M. Bodnára, Z. Csikósa, S. Weie, L. Daróczi, B. Kovácsd, Z. Gyori, J. Tamásb, J.J. Borbély. Membr. Sci. 409–410 (2012) 44–53.
[14] G. Naja, B.Volesky.. Heavy metals in the environment. Taylor & Francis Group (2009)
[15] Background document for development of WHO Guidelines for Drinking-water Quality. Mercury in Drinking-water (2005).
[16] U.S. EPA. 2011 Edition of the Drinking Water Standards and Health Advisories (2011).
[17] Y. Ku, I.L. Jung, Water Res. 35 (2001)135-142.
[18]J.L. Huisman, G. Schouten, C. Schultz. Hydrometallurgy. 83 (2006)106-113.
[19]S.A. Mirbagheri, S.N. Hosseini. Desalination 171 (2005) 85-93.
[20] N. Kongsricharoern, C. Polprasert. Wat. Sci. Technol. 31 (1995) 109-117.
[21] M.Lundh, L. Jönsson, J. Dahlquist. Water Res. 34 (2000) 21-30.
[22] J. Rubio, M. Souza, R. Smith. Miner. Eng. 15 (2002) 139-155.
[23] S.Y. Kang, J.U. Lee, S.H. Moon, K.W. Kim. Chemosphere 56 (2004)141-147.
[24] B. Alyüz, S. Veli. J. Hazard. Mater. 167 (2009) 482-488.
[25] F. Fenglian, W. Qi. J. Environ. Manage. 92 (2011) 407-418.
[26] V.H. Bekkum, E.M. Flanigen, P.A.. Jacobs, J.C. Jansen. Introduction to Zeolite Science and Practice, 2nd Revised Edn. Elsevier, Amsterdam (1991).
[27] Scott M. Auerbach, Kathleen A. Carrado, Prabir K.Dutta. Handbook of Zeolite Science and Technology. Marcel Dekker, Inc. New York (2003).
[28] T. Motsi, N.A. Rowson, M.H. Simmons. Int. J. Miner. Process 92 (2009) 42-48.
[29] I. Ostroski, M. Barros, E. Silvab, J. Dantas, P. Arroyo, O. Lima. J. Hazard. Mater. 161 (2009) 1404-1412.
[30] S.R. Taffarel, J.Rubio. Miner. Eng. 22 (2009) 336-343

---

[31] V.J. Inglezakis, M.A. Styliano, D. Gkantzou, M.D. Loizidou. Desalination 210 (2007) 248-256.
[32] K. Athanasiadis, B. Helmreich. Water Res. 39 (2005) 1527-1532.
[33] O. Oter, H. Akcay. Water Environ. Res.79 (2007) 329–335.
[34] A. Cincotti, A. Mameli, A.M. Locci, R. Orru, G. Cao. Ind. Eng. Chem. Res. 45 (2006) 1074–1084.
[35] A. Al-Haj-Ali, T. Al-Hunaidi. Environ. Technol. 25 (2004) 1009–1019.
[36] K. Gedik, I. Imamoglu. Sep. Sci. Technol.43 (2008) 1191–1207.
[37] E. Alvarez-Ayuso, A. Garcia-Sanchez, X. Querol. Water Res.37 (2003) 4855–4862.
[38] A.E. Turkman, S. Aslan, I. Ege. Fresenius Environ. Bull.13 (2004) 574–580.
[39] S.T. Bosso, J. Enzweiler. Water Res.36 (2002) 4795–4800.
[40] M. Sprynskyy, B. Buszewski, A.P. Terzyk, J. Namiesnik. J. Colloid Interface Sci.304 (2006) 21–28.
[41] M.M. Llanes-Monter, M.T. Olguin, M.J. Solache-Rios. Environ. Sci. Poll. Res.14 (2007) 397–403.
[42] S.M. Dal Bosco, R.S. Jimenez, W.A. Carvalho. J. Colloid Interface Sci. 281 (2005) 424–431.
[43] K. Bhattacharyya, S. Gupta. Adv. Colloid Interface Sci. 140 (2008) 114–131.
[44] F. Barbier, G. Duc, M. Petit-Ramel. Colloid. Surf A Physicochem. Eng. Aspects 166 (2000) 153–159.
[45] A. Chakir, J. Bessiere, K.E.L. Kacemi, B. Marouf. J. Hazard. Mater. B95 (2002) 29–46.
[46] S. Kubilay, R. Gürkan, A. Savran, T. Sahan. Adsorption 13 (2007) 41–51.
[47] D. Ozdes, C. Duran, H.B. Senturk,. J. Environ. Manage. 92 (2011) 3082–3090.
[48] L. Zhi-rong, Z. Shao-qi. Process Safety Environ. Protec. 88 (2010) 62–66.
[49] Ö. Etci, N. Bektas M.S. Öncel. Environ. Earth Sci. 61 (2010) 231–240.
[50] P. Srivastava, B. Singh, M. Angove. J. Colloid. Interf. Sci. 290 (2005) 28–38.
[51] A. Sdiri, T. Higashi, R. Chaabouni, F. Jamoussi. Water Air Soil Pollut. 223 (2012) 1191–1204.
[52] E. Padilla-Ortega, R. Leyva-Ramos, J.V. Flores-Cano. Chem. Eng. J. 225 (2013) 535–546.
[53] F. Gode, E. Pehlivan. J. Hazard. Mater. 136 (2006) 330-337.
[54] P. Sin Keng, S. Ling Lee, S. Tiong Ha, Y. Tse Hung, S. Teng Ong. Environ. Chem. Lett. 12 (2014) 15–25.
[55] A. Denizli, R. Say , Y. Arica. Sep. Purif. Technol. 21 (2000) 181-190.
[56] M. G. Lee, J.K. Cheon, S.K. Kam, J. Ind. Chem. Eng. 9 (2003) 174-180.
[57] L. Sigg, P. behra, W. stumm. chimie des milieu aquatiques 5e edition 2014, Dunod,paris.
[58] J. Duan, J. Gregory. Adv. Colloid Interface Sci. 100 –102 (2003) 475–502.
[59] S. Trasatfi , R. Parsons. Pure & App. Chem. 58 (1986) 437-454.
[60] S. Kumar, S. Jain. Journal of Chemistry. (2013) 1-14.
[61] G. Gadd. Phytologist 124 (1993) 25-60.
[62] R. Apiratikul, P. Pavasant. Bioresour. Technol. 99 (2008) 2766-2777
[63] B. Volesky. Hydrometallurgy. 59 (2001) 203–16.
[64] R. Apiratikul, P. Pavasant. Bioresour. Technol. 99 (2008) 2766-2777.

---

[65] J. Wang, C. Chen. Biotechnol. Adv. 27 (2009) 195–226.
[66] K. Vijayaraghavan, Y. Yu. Biotechnol. Adv. 26 (2008) 266–91.
[67] D. Kratochvil, B. Volesky. Trends Biotechnol. 16 (1998) 291–300.
[68] K. Wong, C. Lee, K. Low, M. Haron. Process Biochem. 39 (2003) 437–445.
[69] S. Memon, N. Memon, S. Shah, M. Khuhawar, M. Bhanger. J. Hazard. Mater. 139 (2007) 116–121.
[70] A. Özer, H. Pirinççi. J. Hazard. Mater. 137(2006) 849–855.
[71] B. Noeline, D. Manohar, T. Anirudhan. Sep. Purif. Technol. 45 (2005) 131–140.
[72] B. Nasernejad, T. Zadeh, B. Pour, M. Bygi, A. Zamani. Process Biochem. 40 (2005) 1319–1322
[73] D. Wankasi, J. Horsfall, A. Spiff. Elec. J. Biotechnol. 9 (2006) 587–592.
[74] Z. Mingliang. Chem. Eng. J. 172 (2011) 361– 368.
[75] E. Romera, F. Gonzalez, A. Ballester, M. Blazquez, J. Munoz. Crit Rev Biotechnol 26 (2006) 223–35.
[76] L. Ajjabi, L. Chouba. J. Environ. Manage. 90 (2009) 3485-3489.
[77] G. Uslu, M. Tanyol. J Hazard Mater 135 (2006) 87–93.
[78] X. Chen,Y. Wang, Q. Lin, J. Shi, W. Wu, Y. Chen. Colloid Surf B-Biointerfaces 46 (2005) 101–7.
[79] A. Selatnia, A. Boukazoula, N. Kechid, M. Bakhti, A. Chergui, Y. Kerchich. Biochem Eng J.19 (2004) 127–35.
[80] M. Zhou, Y. Liu, G. Zeng, X. Li, W. Xu, T. Fan. World J Microbiol Biotechnol. 23 (2007) 43–8.
[81] A. Ozturk A. J Hazard Mater. 147 (2007) 518–23.
[82] R. Say R, N. Yimaz, A. Denizli. Adsorpt Sci Technol. 21 (2003) 643–50.
[83] H. Su, Y. Zhao, J. Li, T. Tan. Process Biochem. 41 (2006)1422–6.
[84] A. Dursun. Biochem Eng J. 28 (2006) 187–95.
[85] R. Gulati, R. Saxena, R. Gupta. World J Microbiol Biotechnol. 18 (2002) 397 401.
[86] P. Ling, F. Liu, L.Li, X. Jing, B. Yin, K. Chen, A. Li. Talanta 81 (2010) 424–432.
[87] F. Liu, L. Li, P. Ling, X. Jing, C. Li, A. Li, X. You. Chem. Eng. J. 173 (2011) 106–114.
[88] L. Wanga, L. Yanga, Y. Li, Y. Zhanga, X. Maa, Z. Ye. Chem. Eng. J. 163 (2010) 364–372.
[89] L. Yang, Y. Li, X. Jin, Z. Ye, X. Ma, L. Wang, Y. Liua. Chem. Eng. J. 168 (2011) 115–124.
[90] X. Jing, F. Liu, X. Yang, P. Ling, L. Li, C.Long, A. Li. J. Hazard. Mater. 167 (2009) 589–596.
[91] C. Chen, C. Chiang, P. Huang. Sep. Purif. Technol. 50 (2006) 15–21.
[92] B. Li, F. Liu, J. Wang, C. Ling, L. Li, P. Hou, A. Li, Z. Bai. Chem. Eng. J. 195–196 (2012) 31–39.
[93] L. Gando-Ferreira, I. Romao, M. Quina. Chem. Eng. J. 172 (2011) 277– 286.
[94] S. Meesri, N. Praphairaksit, A. Imyim. Microchem. J. 87 (2007) 47–55.
[95] J. Gao, F. Liu, P. Ling, J. Lei, L. Li, C. Li, A. Li. Chem. Eng. J. 222 (2013) 240–247.
[96] A. Baraka, P.J. Hall, M.J. Heslop. J. Hazard. Mater. 140 (2007) 86–94.

---

[97] A. Murugesan, T. Vidhyadevi, S.S. Kalaivani, K.V. Thiruvengadaravi, L. Ravikumar,C.D. Anuradha, S. Sivanesan. J. Water. Process Eng.xxx (2014) xxx–xxx.
[98] M. Tanco, D. Tanaka, V. Flores, T. Nagase, T. Suzuki. React. Funct. Polym. 53 (2002) 91–101.
[99] C. Ji, S. Song, C. Wang, C. Sun, R. Qu, C. Wang, H. Chen. Chem. Eng. J 165 (2010) 573–580.
[100] Y. Sun, Z. Li, Y. Chin. Chem. Lett. 24 (2013) 747–750.
[101] A. Baraka, P.J. Hall, M.J. Heslop. React. Funct. Polym 67 (2007) 585–600.
[102] Y. Peng, J. Wang, X. Yang, C.Cheng, T. Wintgens. Chin. Chem. Lett. 25 (2014) 265–268.
[103] A. Deepatana, M. Valix. J. Hazard. Mater. B137 (2006) 925–933.
[104] C.Y. Chen, C.L. Chiang, C.R. Chen. Sep. Purif. Technol. 54 (2007) 396–403.
[105] A.F. Shaaban, D.A. Fadel, A.A. Mahmoud, M.A. Elkomy, S.M. Elbahy . J. Environ.Chem. Eng. 1 (2013) 208–217.
[106] A.F. Shaaban, D.A. Fadel, A.A. Mahmoud, M.A. Elkomy, S.M. Elbahy. J. Environ.Chem. Eng. 2 (2014) 632–641.
[107] C. Xiong, X. Chen, X. Liu. Chem. Eng. J. 203 (2012) 115–122.
[108] D. Kołodynska. Chem. Eng. J. 168 (2011) 994–1007.
[109] P. Ling, F. Liu, L.Li, X. Jing, B. Yin, K. Chen, A. Li. Talanta 81 (2010) 424–432.
[110] C.Y. Chen, C.L. Chiang, C.R. Chen. Sep. Purif. Technol. 54 (2007) 396–403.
[111] S. Štandeker, A.Veronovski, Z. Novak, Ž. Knez. Desalination 269 (2011) 223–230.
[112] I. Blitz, J. Blitz, V. Gun'ko, D. Sheeran. Colloids Surf., A: Physicochem. Eng. Aspects 307 (2007) 83–92.
[113] B. Gao, Y. Gao, Y. Li. Chem. Eng. J. 158 (2010) 542–549.
[114] J. Sales, F. Faria, A. Prado, C. Airoldi. Polyhedron. 23 (2004) 719–725.
[115] A.Kursunlu, E. Guler, H. Dumrul, O. Kocyigit, I.Gubbuk. Appl. Surf. Sci. 255 (2009) 8798–8803.
[116] E. Repo, R. Petrus, M.Sillanpaa, J.Warchoł. Chem. Eng. J. 172 (2011) 376– 385.
[117] I. Gubbuka, I. Hataya, A. kunb, M. Ersoz. J. Hazard. Mater. 172 (2009) 1532–1537.
[118] P. Yin, Q. Xu, R. Qu, G. Zhao. J. Hazard. Mater.169 (2009) 228–232.
[119] S. Štandeker, A.Veronovski, Z. Novak, Ž. Knez. Desalination 269 (2011) 223–230.
[120] M. Najafi, Y. Yousefi , A.A. Rafati. Sep. Purif. Technol.85 (2012) 193-205.
[121] B. Gao, Y. Gao, Y. Li. Chem. Eng. J. 158 (2010) 542–549.
[122] R. Dey, C. Airoldi. J. Hazard. Mater.156 (2008) 95–101.
[123] F. Bari, N. Begum, S. Jamaludin, K. Hussin. Hydrometallurgy 96 (2009) 140–147.
[124] Q. Wang, W. Gao, Y. Liu, J. Yuan, Z. Xu, Q. Zeng, Y. Li, M. Schröder.
[125] M. Li, M.y. Li, C. Feng, Q. Zeng. Appl. Surf. Sci., Available online 12 June 2014.
[126] L. Arakaki, V. Filha, K. Sousa, F. Aguiar, M. Fonseca, J. Espínola. Thermochim. Acta. 440 (2006) 176-180.
[127] H. Wang, J. Kang, H. Liu, J. Qu. J. Environ. Sci.21 (2009) 1473-1479.

---

[128] L. Arakaki, V. Augusto Filha, A. Germano, S. Santos, M.G. Fonseca, K.S. Sousa, J.G.P. Espínola, T. Arakaki. Thermochim. Acta. 556 (2013) 34-40.
[129] L. Arakaki, M. Fonseca, E. da Silva Filho, A. de M. Alves, Kaline S. de Sousa, A. Silva. Thermochim. Acta. 450 (2006) 12-15.
[130] N. Chiron, R. Guilet, E. Deydier. Water Research.37 (2003) 3079-3086.
[131] A.S. Pereira, G. Ferreira, L. Caetano, M. Martines, P.M. Padilha, A. Santos, G.R. Castro. J. Hazard. Mater..175 (2010) 399-403.
[132] G. Kumar, P. Kumar, S. Chakraborty, M. Ray. Sep. Purif. Technol. 57 (2007) 47-56.
[133] C.T. Kresge, M.E. Leonowicz, W.J. Roth, J.C. Vartuli, J.S. Beck. Nature. 359 (1992) 710-712.
[134] J.S. Beck, J.C. Vartuli, W.J. Roth, M.E. Leonowicz, C.T. Kresge, K.D. Schmitt, C. Chu, D.H. Olson, E.W. Sheppard, S.B. McCullen, J.B. Higgins, J.L. Schlenker. J. Am. Chem. Soc. 114 (1992) 10834-10843.
[135] T. Yanagisawa, T. Shimizu, K. Kuroda, C. Kato. Bull. Chem. Soc. Jpn. 63 (1990) 988-992.
[136] B. Naik, N. Nath Ghosh. Recent Pat. Nanotechnol.3 (2009) 213-224.
[137 J. Bae et al. J Nanosci Nanotechnol.10 (2010) 290–296.
[138] G. Athens, R. Shayib, B. Chmelka. Curr. Opin. Colloid Interface Sci. 14 (2009) 281–292.
[139] G. Fryxell. Inorg. Chem. Commun. 9 (2006) 1141–1150.
[140] F. Hoffmann, M. Cornelius, J. Morell, M. Froba. Angew. Chem. Int. Ed. 45(2006) 3 216 – 3251
[141] A. Walcarius, L. Mercier. J. Mater. Chem., 2010, 20, 4478–4511.
[142] A. Burke, J. Hanrahan, D. Healy, J. Sodeau, J. Holmes, M. Morris. J. Hazard. Mater. 164 (2009) 229–234.
[143] Z. Alothman, A. Apblett. Chem. Eng. J.155 (2009) 916–924.
[144] L. Yang, Y. Li, X. Jin, Z. Ye, X. Ma, L. Wang, Y. Liu. Chem. Eng. 168 (2011)115–124.
[145] S. Pramanik, P. Dhara, P. Chattopadhyay. Talanta 63 (2003) 485–490.
[146] E. Repo, J. Warchoł, A. Bhatnagar, A. Mudhoo, M. Sillanpaa. Water research. 47 (2013) 4812 - 4832.
[147] C. McManamon , A. Burke, J. Holmes, M. Morris. J. Colloid Interface Sci. 369 (2012) 330–337
[148] Enshirah Da'na, Abdelhamid Sayari. Chem. Eng. J. 166 (2011) 445–453.
[149] Xiaoming Xue a,b, Fengting Li. Microporous and Mesoporous Materials 116 (2008) 116–122.
[150] Aoife M. Burke, John P. Hanrahan, David A. Healy, John R. Sodeau, Justin D. Holmes, Michael A. Morris. J. Hazard. Mater. 164 (2009) 229–234.
[151] Salah A. Idris a, Christine M. Davidsona, Colm McManamonb, Michael A. Morrisb,Peter Andersonc, Lorraine T. Gibson. J. Hazard. Mater. 185 (2011) 898–904.
[152] S. WANG, J. LI. Chin. Chem. Lett. 17(2006) 221-224.
[153] A. Heidaria, H. Younesia, Z. Mehraban. Chem. Eng. J. 153 (2009) 70–79.
[154] M. Mureseanu, A. Reiss, I. Stefanescu, E. David b, V. Parvulescu, G. Renard ,V. Hulea. Chemosphere 73 (2008) 1499–1504.

---

[155] A. Shahbazia, H. Younesia, A. Badiei. Chem. Eng. J. 168 (2011) 505–518.
[156] L. Hajiaghababaei , A. Badiei, M. Reza Ganjali, S. Heydari,Y. Khaniani , G. Mohammadi Ziarani. Desalination 266 (2011) 182–187.
[157] Z. Gao, L. Wang, T. Qi, J. Chua, Y. Zhang. Colloids Surf., A. 304 (2007) 77–81.
[158] Z. Alothman, A. Apblett. J. Hazard. Mater. 182 (2010) 581–590.
[159] J. Aguado, J. Arsuaga, A. Arencibia, M. Lindo, V. Gascon. J. Hazard. Mater. 163 (2009) 213–221.
[160] D. Perez-Quintanilla, I. del Hierro, M. Fajardo, I. Sierra. Mater.Res. Bull. 42 (2007) 1518–1530.
[161] J. Huang, M. Ye, Y. Qu, L. Chu, R. Chen, Q. He, D. Xu. 2012. J. Colloid Interface Sci. 385 (2012) 13-146.
[162] P. Chingombe, B. Saha, R.J.Wakeman. Carbon 43 (2005) 3132–3143
[163] S.N. Wu, P.J. Chen, Modification of a commercial activated carbon for metal adsorption by several approaches, in: Proceedings of the 2001 International Containment & Remediation Technology Conference and Exhibition, 10–13 June, Orlando, Florida, 2001.
[164] Y. Kikuchi, Q.R. Qian, M. Machida, H. Tatsumoto. Carbon 44 (2006) 195–202
[165] R.R.V.A. Rios, D.E. Alves, I. Dalmazio, S. Fernando, V. Bento, C.L. Donnici, R.M. Lago., Mater. Res. 6 (2) (2003) 129–135.
[166] M. Domingo-Garcia, F.J. Lopez-Garzon, M. Perez-Mendoza. J. Colloid Interface Sci. 222 (2000) 233–240.
[167] Y. Li, S. Wang, Z. Luan, J. Ding, C. Xu,D. Wu. Carbon 41 (2003) 1057–1062.
[168] S. Liu, X. Chen, X.Y. Chen, Z.F. Liu, H.L. Wang. J. Hazard. Mater.141 (2007) 315–319.
[169] F. Wang, H. Wang, J.W. Ma. J. Hazard. Mater.177 (2010) 300–306.
[170] A. Tajar, T. Kaghazchi, M. Soleimani. J. Hazard. Mater.165 (2009) 1159–1164.
[171] M. Choi, J. Jang. J. Colloid Interface Sci. 325 (2008) 287–289.
[172] M. Mahmoud, M. Osman, S. Ahmed, T. Abdel-Fattah. Chem. Eng. J. 175 (2011) 84– 94.
[173] H. Lalhruaitluanga, K. Jayaram, M.N.V. Prasad, K.K. Kumar. J. Hazard. Mater.175 (2010) 311–318.
[174] J. Zhu, B. Deng, J. Yang, D. Gang. Carbon 4 7 (200 9) 2014 –2025.
[175] X. Tao, L. Xiaoqin. Chinese J. Chem. Eng.16 (2008) 401-406.
[176] R. Baccar, J. Bouzid, M. Feki, A. Montiel. J. Hazard. Mater.162 (2009) 1522–1529.
[177] G. Vukovic, A. Marinkovic, S. Skapinc, M. Ristic, R. Aleksic, A. Peric-Grujic, P. Uskokovic. Chem. Eng. J.173 (2011) 855– 865.
[178] A. Hui Lu, D. Zhao, Y. Wan. Nanocasting: A Versatile Strategy for Creating Nanostructured Porous Materials. RSC publishing. UK (2010).
[179] W. Dai, M. Zheng, Y. Zhao, S. Liao, G. Ji, J. Cao. Springer. 5 (2009)103–107.
[180] A. Fuertes, D. Nevskaia. Microporous Mesoporous Mater.62 (2003) 177–190.
[181] A. Vinu, P. Srinivasu, M. Takahashi, T. Mori, V. Balasubramanian, K. Ariga. Microporous Mesoporous Mater. 100 (2007) 20–26.
[182] E. de Oliveira, C. Pires, H. Pastore, J. Braz. Chem. Soc. 17 (2006) 16-29.

---

[183] S. Jun, S. H. Joo, R. Ryoo, M. Kruk, M. Jaroniec, Z. Liu, T. Ohsuna, O. Terasaki, J. Am. Chem. Soc.122 (2000)10 712-10713.

[184] R. Ryoo, S. Joo, M. Kruk, M. Jaroniec. Adv. Mater. 13 (2001) 677-681.

[185] R. Moreno-Tovara, E. Terrésb, J. Rene Rangel-Mendez. Appl. Surf. Sci. 303 (2014) 373–380.

[186] S. E. Moradi, M.J. Baniamerian. Chem. Ind. & Chem. Eng. Q. 17 (2011) 397−408.

[187] M.Anbia, R. Dehghan. J. Environ.Sci. 26 (2014) 1541-1548.

[188] M.Anabia, A. Davijani. Chem. Eng. J. 223 (2013) 899–907.

[189] J.E. Vanbenschoten, B.E. Reed, M.R. Matsumoto, P.J. McGarvey. Water Environ. Res. 66 (1994) 168–174.

[190] J.A. Coston, C.C. Fuller, J.A. Davis. Geochim. Cosmochim. Acta 59 (1995) 3535–3547.

[191] A. Agrawal, K.K. Sahu. J. Hazard. Mater. 137 (2006) 915–924.

[192] M.A. El-Sayed. Acc. Chem. Res. 34 (2001) 257–264.

[193] R. Koivula, J. Pakarinen, M. Sivenius, K. Sirola, R. Harjula, E. Paatero. Sep. Purif. Technol. 70 (2009) 53–57.

[194] K.E. Engates, H.J. Shipley. Environ. Sci. Pollut. Res. 18 (2011) 386–395.

[195] A. Afkhami, M. Saber-Tehrani, H. Bagheri. J. Hazard. Mater. 181 (2010) 836–844.

[196] C.Y. Cao, Z.M. Cui, C.Q. Chen, W.G. Song, W. Cai. J. Phys. Chem. C 114 (2010) 9865–9870.

[197] X.F. Ma, Y.Q. Wang, M.J. Gao, H.Z. Xu, G.A. Li. Catal. Today 158 (2010) 459–463.

[198] C.Y. Chen, C.L. Chiang, C.R. Chen. Sep. Purif. Technol. 54 (2007) 396–403.

[199] A. Murugesan, T. Vidhyadevi, S.S. Kalaivani, K.V. Thiruvengadaravi, L. Ravikumar,C.D. Anuradha, S. Sivanesan. J. Water. Process Eng.3 (2014) 132–143.

[200] C. Ji, S. Song, C. Wang, C. Sun, R. Qu, C. Wang, H. Chen. Chem. Eng. J 165 (2010) 573–580.

[201] A.F. Shaaban, D.A. Fadel, A.A. Mahmoud, M.A. Elkomy, S.M. Elbahy . J. Environ.Chem. Eng. 1 (2013) 208–217.

[202] A.F. Shaaban, D.A. Fadel, A.A. Mahmoud, M.A. Elkomy, S.M. Elbahy. J. Environ.Chem. Eng. 2 (2014) 632–641.

[203] A. Baraka, P.J. Hall, M.J. Heslop. J. Hazard. Mater. 140 (2007) 86–94.

[204] F. An, B. Gao, X. Dai, M. Wang, X. Wang. J. Hazard. Mater. 192 (2011) 956– 962.

[205] I.Gubbuk, I. Hatay, A. kun, M. Ersoz. J. Hazard. Mater. 172 (2009) 1532–1537.

[206] M. Mureseanu, A. Reiss, I. Stefanescu, E. David b, V. Parvulescu, G. Renard ,V. Hulea. Chemosphere 73 (2008) 1499–1504.

[207] A. Shahbazia, H. Younesia, A. Badiei. Chem. Eng. J. 168 (2011) 505–518.

[208] Z. Alothmana, A. Apblett. J. Hazard. Mater. 182 (2010) 581–590.

[209] W. Chunfeng, L. Jiansheng, S. Xia,W. Lianjun, S. Xiuyun. J. Environ. Sci. 21(2009) 127–136.

[210] A. Tajar, T. Kaghazchi, M. Soleimani. J. Hazard. Mater.165 (2009) 1159–1164.

Table of Contents

I. Materials Used For Heavy Metals Removal 48
  I.1. Mesoporous Silica Adsorbents Synthesis 48
    I.1.1. SBA-15 48
    I.1.2 SBA-16 48
    I.1.3. KIT-6 48
  I.2. Mesoporous Carbon CMK-3 49
    I.2.1. Synthesis Protocol 49
  I.3. Zeolites 49
    I.3.1. NaX zeolite 49
II. Functionalization with Amino Groups 50
  II.1. Post Synthesis Grafting 50
    II.1.1. Impregnation Process 50
  II.2. Co-condensation 50
III. EDTA Fixation on the Materials 51
IV. Physicochemical Characterization Techniques 51
  IV.1. N_2 Adsorption Isotherms 51
  IV.2. X-Ray Diffraction 54
  IV.3. Electron Microscopy (SEM and TEM) 54
  IV.4. Fourier Transform-Infrared Spectroscopy (FT-IR) 55
  IV.5. Thermogravimetric Analysis (TG) 55
  IV.6. Determination of Carboxyl Content 55
  IV.7. Zero Point Charge (pH_{ZPC}) of Carbonaceous Adsorbents 56
V. Batch Adsorption Tests 56
  V.1. Batch Experiments 56
  V.2. Kinetics Study 57
    V.2.1. Pseudo-First Order 57
    V.2.2. Pseudo-Second Order 58
VI. Evaluation of Adsorptive Properties 58

  VI.1. Langmuir Isotherm Model 59
  VI.2. Freundlich Isotherm Model 60
VII. Thermodynamics 61
VIII. Fixed Bed Experiments 62
  VIII.1. Experimental Set-Up 62
  VIII.2. Breakthrough Curve 63
  VIII.3. Column Regeneration 65
References 66

I. Materials Used For Heavy Metals Removal

I.1. Mesoporous Silica Adsorbents Synthesis

I.1.1. SBA-15

SBA-15 silica was synthesized as described by Zhao *et al* [1]. In a typical synthesis, 4 g of Pluronic P123 [poly(ethyleneoxide)-poly(propylene oxide)-poly(ethylene oxide)] triblock copolymer (EO20PO70EO20) were dissolved in 30 g water and 120 g of 2 M HCl at 35 °C. After dissolution, 8.5 g of TEOS (tetraethylorthosilicate) were added. The resulting mixture was stirred for 20 h at 35 °C, and then aged at 80 °C overnight. The solid obtained was filtered, washed and dried. Calcination was performed at 500 °C for 6 h with a heating ramp 1°C min^{-1}.

I.1.2. SBA-16

SBA-16 was synthesized as reported in the literature. 2 g of polymeric template F 127 (EO106PO70EO106) and 7.05 g of sodium chloride were added to 20 mL of 2 M HCl and 60 mL deionized water at 40 °C. After complete dissolution of the polymer, 8.4 g of TEOS was added dropwise and the solution was stirred for 20 h at 40 °C. The resulting slurry was aged at 100 °C for 24 h under static conditions. The precipitate was filtered, washed with deionized water, and dried at 80 °C. Then SBA-16 was calcined at 500 °C for 6 h with a heating ramp of 1 °C min^{-1}[2].

I.1.3. KIT-6

In a typical synthesis, 5 g of Pluronic P123 were dissolved in 180 g of distilled water and 9.9 g of HCl solution (37 wt %) under vigorous stirring at 35 °C. After complete dissolution, 5 g of 1-butanol was added. Following further stirring for 1 h, 10.75 g of TEOS was added immediately. Subsequently the mixture was left stirring at 35 °C for 24 h and transferred into an autoclave, which was sealed and maintained at 100 °C for another 24 h under static conditions. The resulting solid product was filtered and dried at 100 °C overnight. The final sample was calcined at 550 °C for 6 h in air with a heating rate of 1°C min^{-1} [3].

I.2. Mesoporous Carbon CMK-3

I.2.1. Synthesis Protocol

1 g of template of SBA-15 powder was added to a solution prepared by dissolving 1.5 g of sucrose in 5 g of water containing 0.17 g of H_2SO_4. The mixture was then heated at 100 °C in an oven for 6 h. Subsequently, the oven temperature was raised to 160 °C for another 6 h.

In order to obtain fully polymerized and carbonized sucrose inside the pores of the silica template, 1 g of sucrose, 0.10 g of H_2SO_4 and 5 g of water were again added to the pre-treated sample and the mixture was again subjected to the thermal treatment described above.

The template–polymer composites were then pyrolyzed under nitrogen flow at 800 °C and kept under these conditions for 6 h to carbonize the polymer.

The dissolution of silica template was achieved using 2 M NaOH solution in a 50:50 mixture of H_2O and ethanol at 65 °C for 24 h. The mesoporous carbon was recovered after dissolution of the silica framework, by filtration, washed several times with ethanol, and dried at 120 °C [4].

I.3. Zeolites

I.3.1. NaX zeolite

NaX zeolite is a large-pore Faujasite zeolite with a Si/Al ~ 1.18 kindly provided by IFP Energie Nouvelle. The unit cell composition of is given by the following formula $Na_{88}Al_{88}Si_{104}O_{384}$.

II. Functionalization with Amino Groups

Since the hydroxyl groups present on the synthesized mesoporous silica are not sufficient for heavy metals removal, chemical modifications should be done. In order to compare which functionalization route is better for loading more amino groups on the mesoporous silicates three protocols were done. The first two are post synthesis through either impregnation or reflux. The second is co-condensation of the organosilanes during the synthesis of the material.

II.1. Post Synthesis Grafting

II.1.1. Impregnation Process

The three materials were functionalized with aminopropyl groups through impregnation [5] by adding 1 g of each silica to 10 mL toluene solution containing 1 mL APTES and stirred at room temperature for 10 min. The mixture was then heated at 100 °C for 24 h. The final solid was filtered, washed with dry toluene followed twice with dichloromethane, and dried at 120 °C for 12 h. The obtained material was referred to as KIT-6-F, SBA-15-F and SBA-16-F.

II.2. Co-condensation

SBA-15 was prepared according to Zhao *et al.* but with addition of the organosilanes and KCl for enhanced stability and ordering [6]. 4 g of P123 and 8 g KCl were dissolved in 30mL of water and 120 mL of a 2 M HCl solution at 40 °C. Then, 8.5 g of TEOS was added and prehydrolyzed for 2 h before adding 1.08 g of APTES. The mixture was stirred at the same temperature for 20 h, and then heated at 100 °C for 24 h in static conditions. The white solid product was collected by filtration, dried in air at room temperature for 1 day, and then extracted with ethanol (140 mL g^{-1}) at the same temperature for 24 h to remove the organic template. The material was then filtered and dried under vacuum. To ensure complete removal of template, 1 g of the ethanol-extracted material was stirred in 50 mL of aqueous 0.1 M HCl for 1 h, filtered and dried, then neutralized in 50 mL of 0.1 M $NaHCO_3$ for 1 h and finally filtered and dried under vacuum at 100 °C for 3 h. The obtained material was referred as SBA-15-F-co.

III. EDTA Fixation on the Materials

To further enhance the removal efficiency of the amino-functionalized adsorbents, additional modification was done by EDTA. EDTA is a chelating agent widely known for its divalent heavy metals complexing properties. All the functionalized materials were added to 80 mL of 0.1 M EDTA aqueous solution and stirred for 24 h at room temperature. The mixture was then filtered, washed well with water, and dried to obtain the KIT-6-F-EDTA, SBA-15-F-EDTA, SBA-16-F-EDTA, SBA-15-F-R-EDTA and SBA-15-F-co-EDTA.

In order to access the physical and chemical properties of all the adsorbents used before and after modification, several techniques were utilized. These techniques give detailed information about the structure and the characteristics of the materials and allow knowing how modification affects their textural properties.

IV. Physicochemical Characterization Techniques

IV.1. N_2 Adsorption Isotherms

Definition and Classification of Porous Materials

All materials having deeper pores, channels, holes, or cavities than they are wide thus permitting the movement of fluids or gases are called porous material. These materials are known for more than a century. They are scientifically and technologically important due to the presence of voids of controllable dimensions at the atomic, molecular and nanometer scale. According to The International Union of Pure and Applied Chemistry (IUPAC) classification, porous solids can be arranged in three main categories, according to their pore size (diameter, *d*), in micro- ($d < 2$ nm), meso- (2 nm $< d < 50$ nm), and macroporous materials ($d > 50$ nm) [7].

The textural properties of porous materials can be deduced from their adsorption behavior. The gas adsorption isotherm represents the amount adsorbed for each equilibrium gas pressure at a fixed temperature. The isotherm shapes are directly linked to the material porosity. IUPAC classification defines 6 types of isotherms which correspond to different porosity patterns (**Figure II.1**). Microporous materials exhibit (type I) isotherm, while (type II) is characteristic of macroporous materials, and mesoporous materials will result in (type IV). Moreover, (types III and V) are characteristics of porous materials with very weak surface/ adsorbate interaction and (type VI) is for porous solids that give adsorption layers [8].

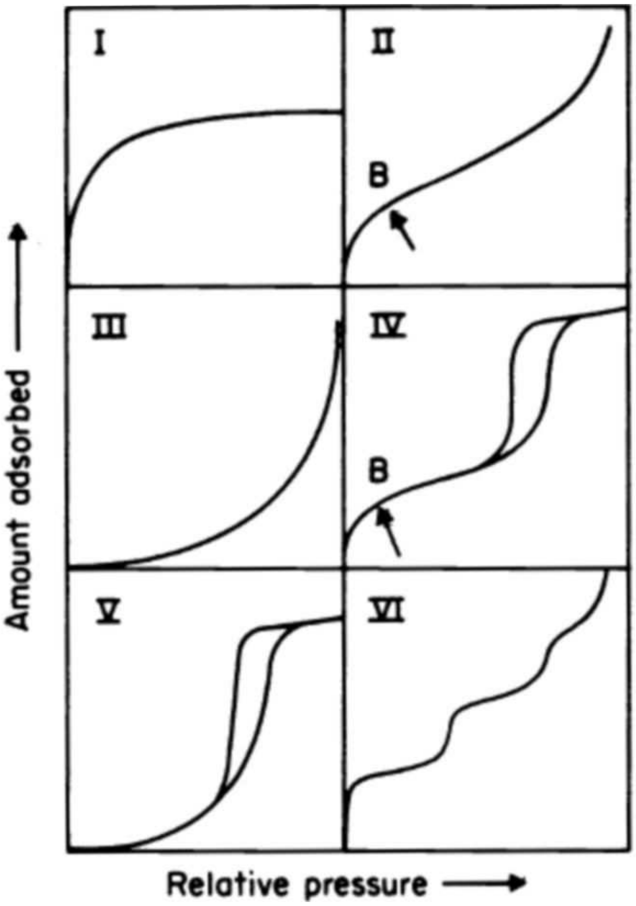

Figure II.1. Types of physisorption isotherms

Point B indicates the completion of the monolayer coverage stage. Practically, the concept of monolayer adsorption is only applied on the perfect planar surface. Real surfaces have some degree of roughness [9-10] so the adsorption progress is not homogeneous. As for the amount of molecules adsorbed on the external surface, it is considered negligible in comparison to that on the pore wall, because nanoporous materials typically possess a very large internal surface area.

Hysteresis Loops Characterization

Hysteresis loops observed in the desorption step give information about pore shape and distribution. According to IUPAC, these loops are classified into four types H1–H4 [11]. The schematic representations of the four types are shown in **Figure II.2**.

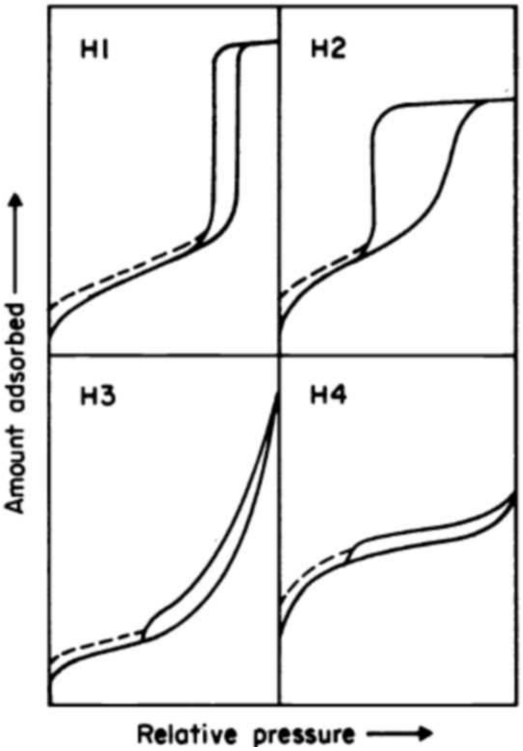

Figure II.2. Types of hysteresis loops

Hysteresis is usually associated with capillary condensation in mesopore structures since it appears in the multilayer range of physisorption isotherms. H1 and H4 are extreme types while H2 and H3 types are intermediate between these two extremes. Type H1 is related to porous materials that can agglomerate to form uniform spheres in a regular array, cylindrical pore geometry and have narrow distributions of pore size. A lot of porous materials such as inorganic oxide gels and porous glasses give H2 Type loops, but the distribution of pore size and pore shape is not well-defined. The sharp step during desorption is usually understood as a sign of pores interconnectivity. If the pores are connected to the external vapor phase through a smaller pore, so these smaller pores acts as a neck ("ink-bottle" pore). As for H3 loop it is associated with aggregates of plate-like particles giving rise to slit-shaped pores. Type H4 loop is also associated with narrow slit-like pores, but in this case the Type I isotherm character is indicative of microporosity [12].

The textural properties were determined by N_2 adsorption–desorption isotherms performed at -196 °C using the Micromeritics TRISTAR sorptiometer and Micromeritics ASAP 2010 for determining the zeolites microporosity. All samples were out gassed under vacuum for at least 5 hours at 350°C before measurement (150°C for the functionalized samples).

IV.2. X-Ray Diffraction

XRD is considered a very powerful and one of the most important method for materials characterizations. Small-angle powder X-ray diffraction (XRD) patterns were recorded on an Empyrean X-ray diffractometer using Cu Kα (λ=1.54 Å) radiation with a scanning rate of 0.008° min^{-1} from 0.65° to 5° 2θ for mesoporous silicates and CMK-3 and from 3° to 70° 2θ for zeolite.

The wall thickness of the mesoporous materials can be calculated from the obtained XRD data starting from a_0 (the unit cell parameter) for each material according to the following equations:

	SBA-15 [1]	SBA-16 [13]	KIT-6 [3]
a_0	$a_0 = 2d(100)/\sqrt{3}$	$a_0 = d(110)\sqrt{2}$	$a_0 = 6^{1/2}d(211)$
Wall thickness	a_0 - $d$pore	$\sqrt{3}a_0/2 - d$pore	$a_0/2 - d$pore

IV.3. Electron Microscopy (SEM and TEM)

Scanning electron microscopy (SEM) is used to study the surface topography and morphology of solid materials on a scale down to about 10 nm. The analysis was performed using SEM, JEOL 7001 FEG.

Transmission electron microscopy (TEM) is used to obtain direct structural information at nanometer scale resolution for porous materials. The samples were dispersed in an Epon resin and then mechanically cut to obtain a 60 nm thick resin-sample which then was analyzed. The morphology of the mesoporous materials was obtained by transmission electron microscopy (TEM, JEOL 2100 UHR at 200 kV).

IV.4. Fourier Transform-Infrared Spectroscopy (FT-IR)

Infrared spectroscopy was used to determine the functional groups on the surface of the materials. Functional groups of EDTA modified silica were identified through CaF_2 window. The analysis was done in transmission for the samples pellets of 16 mm diameter and 2 cm^2 surface prepared using a hydraulic press. The samples were out gassed in at 250°C under secondary vacuum before analysis through CaF_2 window. Fourier Transform Infrared spectra were recorded by FTIR1650 Nicolet spectrometer in the range of 1000–4000 cm^{-1}.

IV.5. Thermogravimetric Analysis (TG)

Thermogravimetric analysis (TG) was conducted in air from 25 to 900 °C with a ramp of 10 $°C.min^{-1}$ using a SDT Q600 from TA Instruments. The percentage of the weight loss was used to calculate the amount of aminopropyl groups immobilized on the mesoporous materials. This technique also was used to determine the water content in the adsorbents including zeolite NaX.

IV.6. Determination of Carboxyl Content

The amount of carboxyl groups resulting from EDTA immobilization was measured through back titration [14]. 1 g of each sample was mixed with 100 mL of deionized water. The pH of the mixture was lowered to 2 so that the COONa groups of EDTA could be transformed into COOH groups [15]. After stirring for 2 h, the mixture was separated by filtration and the obtained solid was dried at 80 °C. Then, 0.1 g of each solid was dispersed in 100 mL of $NaHCO_3$ 0.01 M standard solution and stirred for 2 h. After the suspension was filtered and titrated with HCl 0.01 M standard solution and the COOH concentration was determined from the HCl volume consumed to reach equivalence point.

IV.7. Zero Point Charge (pH_{ZPC}) of Carbonaceous Adsorbents

The surface charge properties of the CMK-3 and activated carbon (AC) were evaluated by batch equilibration technique [16] where a 100mg of each sample were introduced into a 100 mL of 0.1M NaCl solution. The initial pH value (pH_i) of the NaCl solution was adjusted from 1 to 10 by addition of 0.1 M HCl or 0.1M NaOH. The suspension was allowed to equilibrate at room temperature for 24 h by agitation, then filtered and the pH value (pH_e) was measured again.

V. Batch Adsorption Tests

V.1. Batch Experiments

Metal ions solutions (Cu^{2+}, Ni^{2+}, $Pb^{2+}$and Cd^{2+}) were prepared from their corresponding nitrate salts in ultrapure water to obtain solutions of different concentrations. The pH of the solution was adjusted using 0.1M HCl and 0.1M NaOH solution. In typical batch studies, a weighed amount (m) of the solid powder was placed in a flask containing V mL of a metal solution with the desired concentration. The m/V ratios depend on the nature of the adsorbent. The flask was continuously stirred at 25 °C at 300 rpm. At the end of each step the solution was filtered and the metal ion concentration was determined for each metal using Atomic Adsorption Spectrophotometer (Perkin Elmer AA200 atomic absorption). The same procedure was repeated for the four divalent metals used. The equilibrium time was determined as the contact time required for the metals in the solution to reach equilibrium. The abatement rate of the metal ions was calculated by equation (1):

$$R = \frac{C_0 - C_t}{C_0} \times 100 \qquad (1)$$

where R is the abatement rate (%), C_0 is the initial concentration and C_t is the concentration at time t. The adsorption capacity of the adsorbent at equilibrium was calculated by equation (2):

$$q_e = \frac{(\mathrm{C_0} - \mathrm{C_e})\mathrm{V}}{\mathrm{m}} \qquad (2)$$

Where q_e is the equilibrium adsorption capacity in mmol g^{-1}, C_0 is the initial concentration and C_e is the concentration at equilibrium, V is the volume in L of metal solution and m is the mass in g of the adsorbent.

For obtaining the isotherms, the batch experiments are done with m/V ratio as before for all adsorbents. But here the initial metal ions concentrations were varied between 0.17 mmol L^{-1} and 5 mmol L^{-1}. The solutions were stirred for 120 min at 25 °C then filtered by a 0.45 µm syringe filter and the remaining metal ions were measured by AAS in order to calculate C_e and q_e.

V.2. Kinetics Study

The study of sorption kinetics in wastewater treatment is very essential since it provides valuable insights into the adsorbent performances and the underlying sorption mechanism. It is an important parameter for the design of an appropriate adsorption process [22]. The adsorption of a solute from solution by porous adsorbents is essentially associated with three consecutive mass transport steps. (1) Film diffusion involves the transport of the sorbate to the external surface of the adsorbent, (2) particle diffusion involves the transport of the pollutant within the pores of the adsorbent and (3) adsorption involves the adherence of the adsorbate on the surface of the adsorbent. Film and pore transport are the two major factors controlling rates of adsorption from solution by porous adsorbents. Therefore, it is necessary to identify the rate-limiting step that governs the overall rate of the adsorption process.

V.2.1. Pseudo-First Order

The pseudo first-order kinetic model is based on the assumption that the adsorption rate is proportional to the number of free sites and is generally expressed as equation (3):

$$\frac{dq_t}{dt} = k_1(q_e - q_t) \tag{3}$$

Where q_t and q_e are the amounts of metal ions adsorbed (mmol g^{-1}) at time t (min) and at equilibrium respectively, and k_1 is the rate constant of adsorption (min^{-1}). The non-linear form of this order is expressed as follows (4) [17]:

$$\mathrm{q} = q_e(1 - exp^{-k_1 t}) \tag{4}$$

V.2.2. Pseudo-Second Order

The non-linear pseudo-second-order model is known to be more accurate and it is expressed in equation (5) [18]:

$$q = \frac{k_2\, q_\mathrm{e}^2\, t}{1 + k_2\, q_e\, t} \tag{5}$$

where k_2 is the pseudo-second order rate constant (g $mmol^{-1}$ min^{-1}), q_t and q_e are the amounts of metal ions adsorbed at t time and at equilibrium (mmol g^{-1}) respectively. The initial sorption rates (h= $k_2\, q_e^2$) expressed in mmol g^{-1} min^{-1} were also calculated.

VI. Evaluation of Adsorptive Properties

The adsorption isotherm provides information about how much material can be adsorbed under given conditions (pressure P and temperature for gases, concentration and temperature for molecules in solutions). The amount of adsorbed material can be given as the fraction of occupied sites that's to say surface coverage Θ or as the volume of the particles sum adsorbed in the first monolayer.

Adsorption isotherms are very important criteria for adsorption processes. Practically, the amount of adsorptive up taken by a given catalyst is a decisive quantity because high uptake generally means high catalyst efficiency. The latter is usually called 'sorption capacity' that is characterized by adsorption isotherm. The isotherm form allows the analysis of the chemical and physical properties of the material as well as how the process of adsorption proceeds over a given surface. The different kinds of isotherms are based on the nature of the catalyst and the kind of interaction [19].

After an enough contact time between the adsorbent and the adsorptive, equilibrium is established between the adsorbate and the amount of adsorptive remaining in the solution. Therefore, for heavy metals removal, the adsorption isotherm is the relation between the specific amount adsorbed at equilibrium (q_e, expressed in (mmol) of the adsorbate per (g) of the solid adsorbent) and the equilibrium concentration of metal ions in liquid phase (C_e, expressed in (mmol) of the adsorptive per (L) of the solution, when the amount adsorbed is equal to q_e.

Among the numerous models found in literature for fitting the adsorption isotherms, Langmuir and Freundlich models are the most used for describing heavy metals adsorption.

VI.1. Langmuir Isotherm Model

Langmuir Isotherm is a model that assumes monolayer coverage of a finite number of identical sites present on the surface such that no further adsorption takes place [39]. This model suggests uniform energies of adsorption and no transmigration of adsorbate in the plane of the surface (**Figure II.3**). Based on these assumptions, Langmuir represented the following equation [20]:

$$q_e = \frac{\mathrm{K_L} \times q_{max}\ C_e}{1 + \mathrm{K_L} C_e}$$

where q_{max} is the maximum adsorption capacity (monolayer coverage), i.e. mmol of the adsorbate per (g) of adsorbent and $\mathrm{K_L}$ is Langmuir isotherm constant. $\mathrm{K_L}$ depends on the initial concentration of the metal ions in the solution, the temperature of the system and the relative stabilities of the adsorbate and adsorptive species.

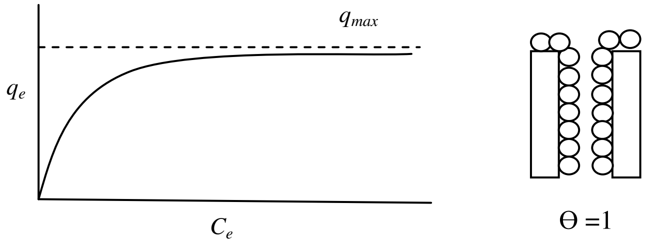

Figure II.3. Model Presentation of Langmuir isotherm, (Θ) is the fraction of the surface sites occupied

The adsorption parameters of Langmuir model can be determined from its linear form by sketching C_e/q_e versus C_e so that the values of q_{max} and K_L can be calculated from the slope and intercept of the linear plot respectively:

$$\frac{C_e}{q_e} = \frac{1}{K_L q_{max}} + \frac{C_e}{q_{max}}$$

VI.2. Freundlich Isotherm Model

This model describes the non-ideal and reversible adsorption, not limited to monolayer formation. It can be applied to multilayer adsorption, with non-uniform distribution of adsorption heat and affinities over a heterogeneous surface [21-22]. The equation is expressed as follows:

$$q_e = K_f C_e^{1/n}$$

Where K_f is Freundlich isotherm constant (mmol g^{-1}) and n is the adsorption intensity. The linear form:

$$\log q_e = \log K_f + \frac{1}{n}\log C_e$$

Currently, this model is applied for heterogeneous systems. The slope is a measure of adsorption intensity or surface heterogeneity and it ranges between 0 and 1(**Figure II.4**). If n = 1 then the partition between the two phases is independent of the concentration. If value of 1/n is below one it indicates a normal adsorption. The value gets closer to zero when the system is more heterogeneous while 1/n values above 1 indicates cooperative adsorption [23]. The limitation of Freundlich isotherm is the lack of fundamental thermodynamic basis, not approaching the Henry's law at low concentrations [24].

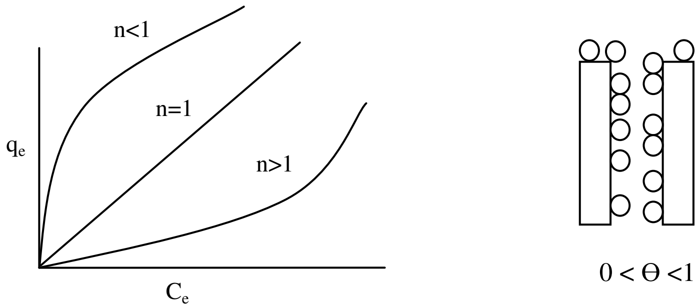

Figure II.4. Model Presentation of Freundlich isotherm

VII. Thermodynamics

To completely understand the adsorption nature, the thermodynamic parameters such as free energy change (ΔGº), enthalpy change (ΔHº) and entropy change (ΔSº) can be calculated. These thermodynamic parameters are estimated for an adsorption reaction by considering the equilibrium constants under several experimental conditions.

The thermodynamic parameters can be determined from the thermodynamic equilibrium constant, K^0 (or the thermodynamic distribution coefficient) which is defined as [25]:

$$K^0 = \frac{a_s}{a_e} = \frac{\gamma_s}{\gamma_e}\frac{C_s}{C_e}$$

where a_s is the activity of adsorbed metal ions on the adsorbent, a_e is the activity of metal ions in the solution at equilibrium, γ_s is the activity coefficient of adsorbed ions, γ_e is the activity coefficient at equilibrium, C_s is the concentration of adsorbed ions on the solid. The K^0 expression can be simplified by assuming that the concentration in the solution approaches zero resulting in $C_s \to 0$ and $C_e \to 0$ and the activity coefficients approach unity at these very low concentrations and can be written as:

$$C_s \to 0 \frac{C_s}{C_e} = \frac{a_s}{a_e} = K^0 = K_d$$

K_d values were obtained by plotting ln (q_e/C_e) versus qe and extrapolating q_e to 0 [26]. Hence, ΔG^0 (kJ mol^{-1}) at temperature T (in Kelvin) was calculated as follows:

$$\Delta G^\circ = -RT \ln K_d$$

R is the universal gas constant (8.314 J mol^{-1} K^{-1}). These parameters are obtained experimentally at different temperatures. (ΔH^o) and (ΔS^o) values are calculated respectively from the slop and intercept of van't Hoff plot of ln K_d versus 1/T [27]. ΔG° values indicate whether the adsorption process is spontaneous or not. The values of (ΔH^o) are positive when the process is endothermic in nature and negative value if exothermic so that a given amount of heat evolves during the binding of metal ions on the surface. Positive values of (ΔS^o) indicate an increase in the degree of or disorder of the adsorbed species.

VIII. Fixed Bed Experiments

Although batch studies give information about the effectiveness and the adsorption capacity of the adsorbents, column operations are important for the practical utility design. The main advantage of fixed bed is that it allows a more efficient usage of the adsorbents. In the setup the materials are in a continuous contact at the inlet end with the water to be treated having initial concentration C_0. Thus the solution concentration in contact with the adsorbents layers remains constant.

VIII.1. Experimental Set-Up

For fixed bed experiments, a stainless steel column was used with a 100 mm length and a diameter of 4.6 mm. The experimental set-up is shown on **Figure II.5**. 0.1 g of each adsorbent was packed in the column separately. The polluted water mixture was fed into the column using in HPLC pump (Gilson 307) with a constant flow rate of 1 mL min^{-1}. The treated water samples were collected then analyzed by atomic absorption spectrometry (AAS).

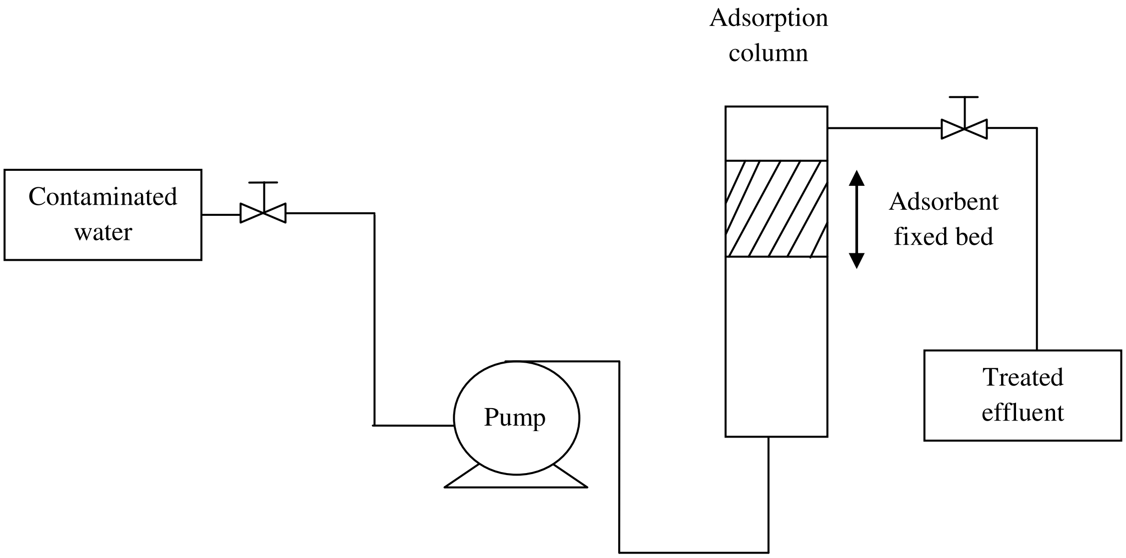

Figure II.5. Schematic illustration of the experimental set up of the fixed bed column

VIII.2. Breakthrough Curve

The breakthrough curve represents the evolution of the solution concentration as a function of adsorption parameters such as contact time and the volume eluted (**Figure II.6**). It gives information concerning the efficiency of the column and the adsorbent capacity.

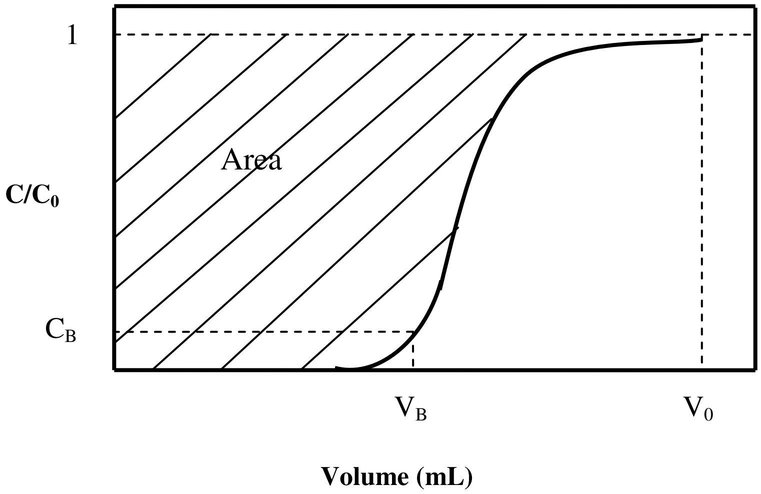

Figure II.6. Breakthrough curve drawn as C/C_0 versus volume (mL), where C_B and V_B are the breakthrough concentration and volume respectively

The column capacity is calculated starting from the area of the dashed part in the figure above, the initial concentration (C_0) of the metal solution concentration and the mass of the adsorbent used (m):

$$Capacity = \frac{\mathrm{Area} \times C_0}{\mathrm{m}} = \frac{C_0}{\mathrm{m}} \int_0^{\mathrm{V}_0} \left(1 - \frac{C}{C_0}\right) \mathrm{dv}$$

These experiments were conducted in both ultrapure water and natural ground water. The water samples were spiked with an equimolar concentration of metal ions. The characteristics of the water used are listed below. The pH of the water was adjusted to 6 before passing the samples into the column in order to avoid the precipitation of the metal ions used.

Characteristics of the natural ground water used

		pH	8,1
		Concentration Unit	**(ppm)**
Major Elements	**Anions**	Nitrate (NO_3^-)	14,6
		Nitrite (NO_2^-)	< 0,5
		Chlorure (Cl^-)	22,0
		Sulfate (SO_4^{2-})	13,1
		Phosphate (PO_4^{3-})	< 0,2
		Hydrogénocarbonates (HCO_3^-)	366
	Cations	Calcium (Ca^{2+})	216,2
		Magnésium (Mg^{2+})	6,1
		Sodium (Na^+)	18,3
		Potassium (K^+)	1,2

VIII.3. Column Regeneration

Column regeneration was carried out by using 1 M HCl for EDTA modified SBA-15and CMK-3 materials while NaX zeolite was regenerated by 1 M NaCl solution. At the end of regeneration cycle, the adsorbent was washed with distilled water. The regeneration efficiency was calculated as follows:

$$\text{Effeciency } (\%) = \frac{q_{reg}}{q_{org}} \times 100$$

where q_{reg} is the adsorptive capacity of the regenerated column and q_{org} is the sorption capacity (mmol/g) of the adsorbent after each cycle. The solution was collected after regeneration and the amount of copper desorbed was measured by AAS.

References

---

[1] D. Zhao, Q. Huo, J. Feng, B. Chmelka, G. Stucky. J. Am. Chem. Soc., 120 (1998) 6024-6036.
[2] R.M. Grudzien, B.E. Grabicka, M. Jaroniec, Appl. Surf. Sci. 253 (2007) 5660–5665.
[3] W. Da, M. Zheng, Y. Zhao, S. Liao, G. Ji, J. Cao. Springer. 5 (2010) 103.
[4] A. Vinu, P. Srinivasu, M. TakahashI, T. Mori, V. Balasubramanian, K. Ariga. (2007). Micropor. Mesopor. Mater. 100 (2007) 20–26.
[5] Z. Luan, J. Fournier, J. Wooten, D. Miser. Micropor. Mesopor. Mater. 83 (2005) 150–158.
[6] Enshirah Da’na, Abdelhamid Sayari. Chem. Eng. J.166 (2011) 445–453.
[7] L.B. Smccusker, F. Liebau, G. Engelhardt. Pure Appl. Chem. 73 (2001) 381–394.
[8] K. Sing, D. Everett.D, R. Haul,L. Moscou, R. Pierotti, J. Rou- querol, T. Siemieniewska. Pure Appl. Chem. 57 (1985) 603-619.
[9] R. Valiullin, P. Kortunov, J. Karger, V. Timoshenko. J. Phys. Chem. B. 109 (2005) 5746.
[10] J. Puibasset, J. Chem. Phys. 127 (2007) 154701.
[11] J.B. Condon. Micropor. Mesopor. Mater. 38 (2000) 359-383.
[12] K. Sing, D. Everett.D, R. Haul,L. Moscou, R. Pierotti, J. Rou- querol, T. Siemieniewska. Pure Appl. Chem. 57 (1985) 603-619.
[13] M. Mesa, L. Sierra, J. Patarin, J.L. Guth. Solid State Sci. 7 (2005) 990–997.
[14] I. Ghodbane, L. Nouri, O. Hamdaoui, M. Chiha, J. Hazard. Mater. 152 (2008) 148-158.
[15] J.A. Dean, Lange’s Hand Book of Chemistry, 15th ed., McGraw-Hill Book Company, USA, 1999.
[16] I.D. Smiciklas, S.K. Milonjic, P. Pfendt, S. Raicevic. Sep. Purif. Technol. 18 (2000) 185–194.
[17] K. Vasanth Kumar. J. Hazard. Mater. B137 (2006) 1538–1544.
[18] Vasanth Kumar.V. J. Hazard. Mater. 137 (2006) 1538–1544.
[19] K. Christmann. 2010 Adsorption. Institute of chemistry and Biochemistry, Freie University, Berlin. Lecture Series 2010/2011.
[20] I. Langmuir. J. Am. Chem. Soc. 38 (1916) 2221–2295.
[21] H.M. Freundlich. J. Phys. Chem. 57 (1906) 385–471.
[22] A.W. Adamson, A.P. Gast, Physical Chemistry of Surfaces, sixth edition, Wiley Interscience, New York (1997).
[23] F. Haghseresht, G. Lu. Energy Fuels 12 (1998) 1100–1107.
[24] Y.S. Ho, J.F. Porter, G. Mckay. Water Air Soil Pollut. 141 (2002) 1–33.
[25] A.Kumar, S. Rout, M. Ghosh, RK. Singhal, P M. Ravi. SpringerPlus.2 (2013) 530-537.
[26] K. Kumari, R.P. Singh, SK. Saxena . Colloids and Surfaces. 33 (1988) 55-61.
[27] X. Jing, F. Q. Liu, X. Yang, P. Ling, L.J. Li, C. Long, A. Li. J. Hazard. Mater. 167. (2009) 589–596.

Table of Contents

I. NaX Faujasite Zeolite Structure 68
II. Zeolites Physico-chemical Characterizations 69
  II.1 X-Ray Diffraction 69
  II. 2. N_2 physisorption at 77 K 70
  II. 3 Thermogravimetric Analysis (TGA) 70
  II. 4. Scanning Electron Microscopy 71
III. Heavy Metals Batch Adsorption Tests 72
  III.1. pH Effect 72
  III.2. Mass Effect 72
  III.3. Competitive Adsorption 73
IV. Kinetics study 74
  IV.1 Kinetic Models 74
V. Distribution Coefficient 76
VI. NaX Zeolite Adsorption Capacity 76
  VI.1. Theory of Cation Exchange in Zeolites 76
  VI.2. Exchange Equilibrium Curves for NaX Zeolite 79
VII. Cation Exchange selectivities: $2Na^+ \rightarrow M^{2+}$ 83
VIII. Temperature Effect 86
IX. Fixed Bed Experiments 89
  IX.1. Heavy Metal Mixture Breakthrough Curves in Ultrapure Water 89
  IX.2. Application to a Natural Water Sample 90
  IX.3. Column Regeneration 92
X. Conclusions 93
References 94

The zeolite framework is a tridimensional arrangement of tetrahedral SiO_4 and AlO_4^-. The tetravalent Al atoms in the zeolite framework are responsible for its net negative charge which is balanced by the presence of extra framework cations located on defined crystallographic positions. The zeolite cations are responsible for zeolite exchange properties.

I. NaX Faujasite Zeolite Structure

Faujasite NaX belongs to the space group *Fd3*. The micropore framework consists of truncated octahedrons or β-cages (Ø = 0.66 nm) connected by hexagonal prisms or double six rings. This creates a void space called supercage or α-cage (Ø = 1.3 nm) (**Figure III.1**). The supercarges are accessible through windows of 12 oxygen atoms with a diameter of about 0.74 nm. The smaller windows into β-cages are 0.22 nm in diameter [1].

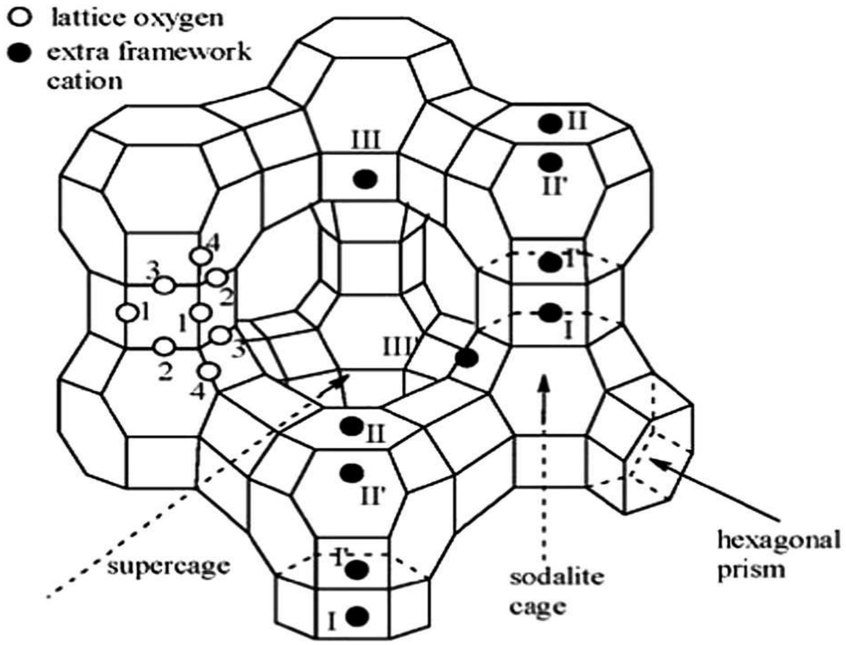

Figure III.1. Schematic representation of the NaX zeolite with extra-framework cation positions [2].

The high alumina content gives zeolite X a high affinity for polar molecules (e.g., water) and a high capacity for ion exchange. The sodium ions are usually distributed as follows: 32 Na^+ ions are in I' sites in the sodalite cages facing the six-rings of hexagonal prisms (partial occupancy of site I inside the hexagonal prism may occur); 32 Na^+ ions are in sites II facing the six-rings of sodalite cages towards the supercages; the extra cations are distributed in the supercages near the 12-ring or 4-ring windows over a variety of sites referred to as III or III' depending on their framework environment. Although the location of Na^+ ions in sites I' and II is well established, the location of the ions in the supercages is still a subject of controversy [3].

II. Zeolites Physico-chemical Characterizations

II.1. X-Ray Diffraction

The high crystallinity of the NaX zeolite used was verified by X-ray powder diffraction. The obtained XRD pattern is shown on **Figure III.2**. It was compared with these given by Treacy *et al*. [4]. The observed reflections on the XRD pattern correspond to hydrated NaX Faujasite structure. The sharp peaks in the 2θ ranges of 3–35° indicate that the microporous structure of zeolite is well crystallized.

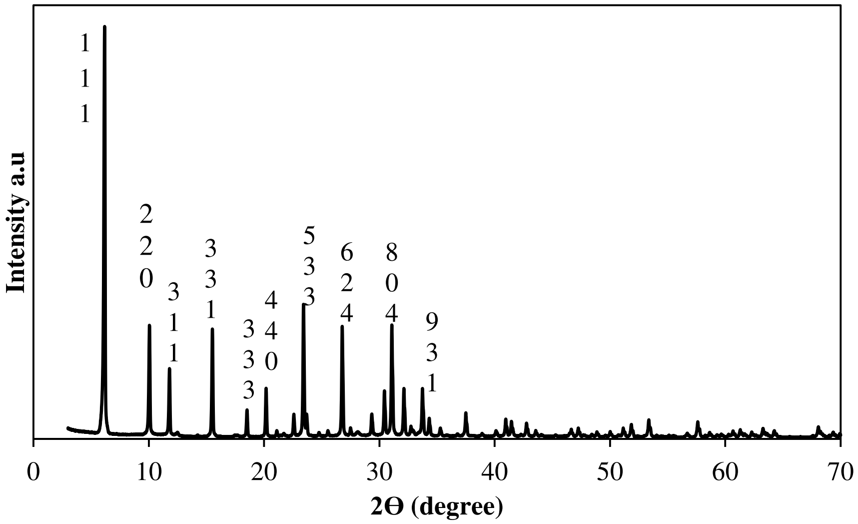

Figure III.2. XRD patterns NaX zeolite.

II. 2. N_2 physisorption at 77 K

The nitrogen adsorption-desorption isotherms for NaX are shown in **Figure III.3**. The adsorption isotherm is of type I which is characteristic of a microporous material. No important increase of N_2 adsorbed amount is noticed for high P/P_0 values indicating the absence of mesopores and external surface. The microporous volume estimated from t-plot is 0.317 $cm^3\ g^{-1}$ and the BET surface area is 745 $m^2\ g^{-1}$.

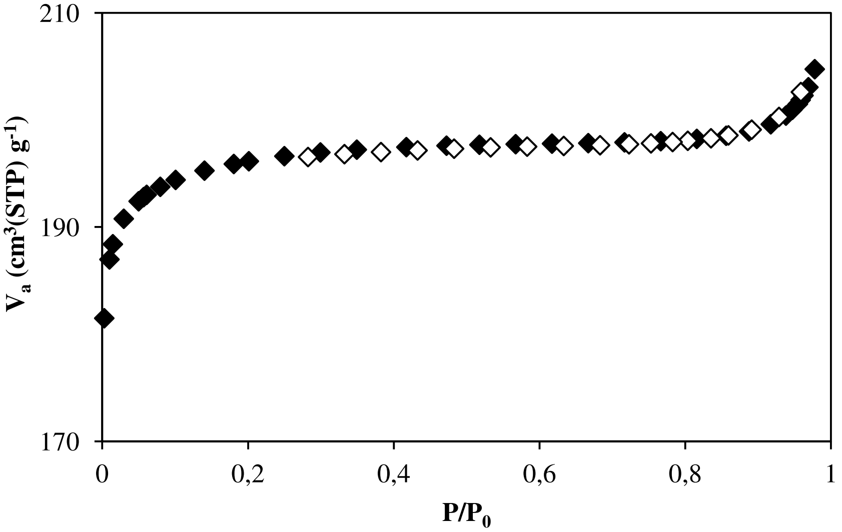

Figure III.3. N_2 adsorption - desorption isotherm of NaX zeolite

II. 3. Thermogravimetric Analysis (TGA)

TGA was used to verify the absence of organic template and to estimate the zeolite water content. The obtained signals recorded under air flow are shown on **Figure III.4**. The weight loss observed between 25 °C and 900 °C is attributed to the desorption of the physisorbed water molecules from the zeolite cavities. The desorbed water amount is estimated to be 26%. This high amount results from the strong hydrophilicity of NaX zeolite due to its low Si/Al ratio.

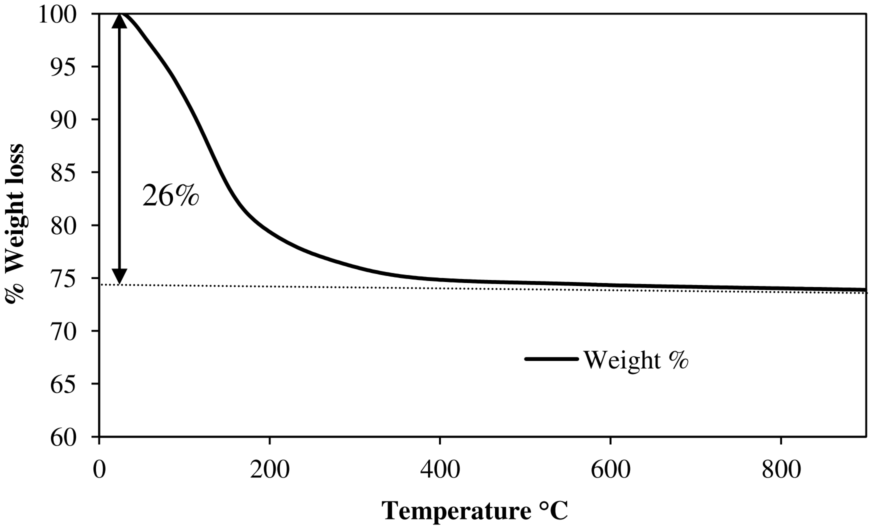

Figure III.4. Thermogravimetric analysis of NaX zeolite

II. 4. Scanning Electron Microscopy

Scanning electronic micrographs show the crystallites of NaX forming fine cubic particles with an average size 3 μm (**Figure III.5**).

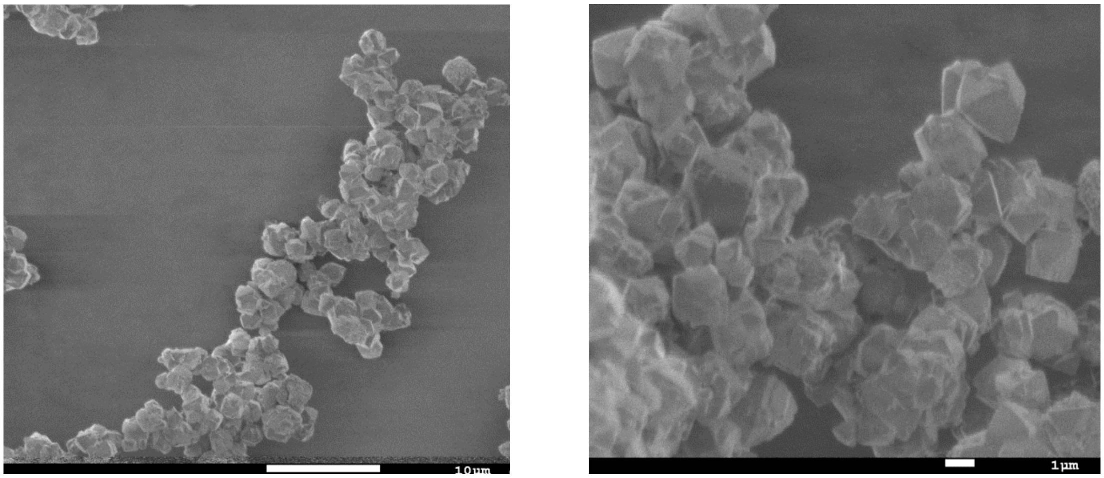

Figure III.5. Scanning Electron Microscopy (SEM) of NaX zeolite

III. Heavy Metals Batch Adsorption Tests

III.1. pH Effect

In order to study the effect of pH on the adsorption of metal ions on NaX zeolite, adsorption tests were performed in the pH range between 2 and 7. **Figure III.6** shows the adsorption of Cu^{2+}, Ni^{2+}, Cd^{2+} and Pb^{2+} at different pH values.

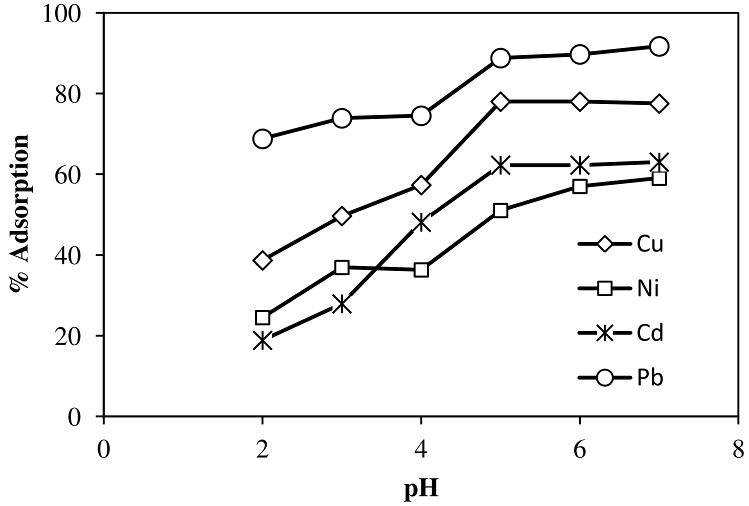

Figure III.6. Effect of pH on the adsorption of metal ions on NaX zeolite (m/V= 0.1 mg. L^{-1}, t = 2 h at 25 °C and $[M^{2+}]_i = 0.47$ mmol L^{-1})

As the pH increases from 2 to 5, adsorption increases to reach its maximum at pH 6 and 7 for all metal ions. The reason of low adsorption at low pH values is the competition between metal ions and hydronium H_3O^+ ions. Furthermore, NaX zeolite structure is not stable in strongly acidic media (dealumination). So a pH value of 6 has been chosen to carry out all the adsorption experiments. The tests were not performed above pH 7 in order to avoid hydroxide precipitation mainly for Cu^{2+} and Cd^{2+}.

III.2. Mass Effect

The mass of zeolite was varied between 10 mg and 60 mg in order to optimize the adsorbent mass while keeping the metal solution volume constant (100 mL). **Figure III.7** shows the mass effect on adsorption of Cu^{2+}. Below 30 mg, the adsorption percentage increases when the zeolite mass increases in the solution. This is due to the increase in the amount exchangeable sites. Above 30 mg, mass increasing no longer affect copper abatement since the adsorption reaches 100%. From this result, a zeolite mass of 20 mg was found to be the more suitable so all the following experiments which were done with a ratio m/V = 20 /100 (mg mL^{-1}). The m/V ratio depends on the type of zeolite used and the metal concentration range in solution. For example, Nibou *et al.* used also synthetic NaX zeolite but with different Na^+ content and they used 250 mg for 100 mL of metal solution [5]. Erdem *et al.* worked with clinoptilolite (natural zeolite) where they used 10 g of solid for 500 mL of metal solution [6]. Another study was performed by Hui *et al.* with 100 mg of synthetic zeolite 4A for 100 mL metal ions solution [7]. So by comparing the m/V ratio used in literature, it can be concluded that this type synthetic NaX (Si/Al~1) is much more efficient than other types of zeolites used elsewhere.

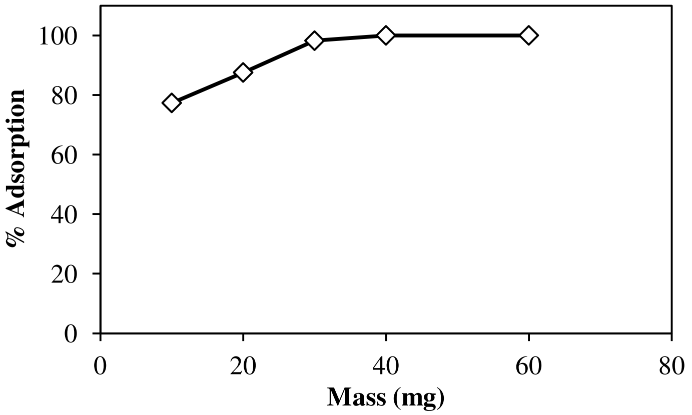

Figure III.7. Effect of mass on the adsorption of Cu^{2+} on NaX zeolite (pH = 5.8, t = 2 h at 25 °C and $[Cu^{2+}]_i = 0.47$ mmol L^{-1})

III.3. Competitive Adsorption

As it is well known, natural water contains different amounts of inorganic cationic and anionic species. So the effect of some ions usually present in natural water was studied. Copper adsorption by NaX was examined in the presence of competitor salts such as NaCl, $NaNO_3$, KCl and NH_4NO_3 for a concentration of 0.2 M. The results are shown in **Figure III.8**. The presence of these ions decreased considerably Cu^{2+} adsorption. This behavior is mainly due to the competition between Na^+, K^+, NH_4^+ and Cu^{2+}. Zeolites are good ion exchangers since they have important exchange capacities. However, they exhibit poor selectivity since the presence of other cations affects considerably heavy metals removal.

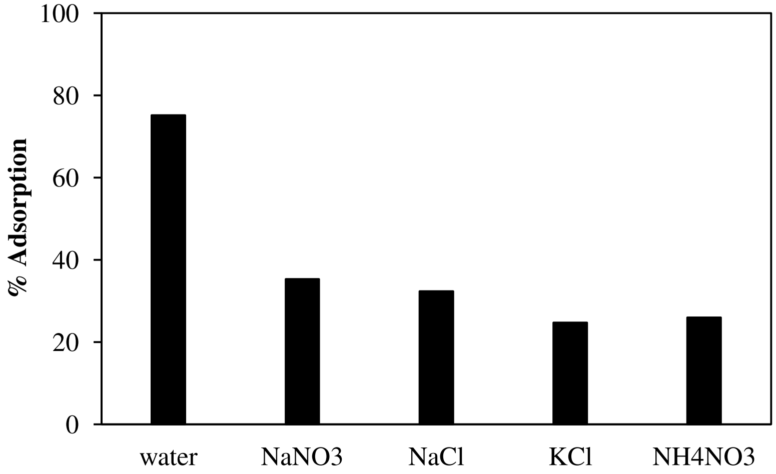

Figure III.8. Effect of competitive ions on the adsorption of Cu^{2+} on NaX zeolite (pH = 5.8, t = 2 h at 25 ºC and $[Cu^{2+}]_i = 0.47$ mmol L^{-1})

IV. Kinetics study

Adsorption tests were done in the time range between 1 min and 180 min. For all heavy metal cations, equilibrium was reached in the first 20 min which indicates the rapid exchange between zeolite Na^+ ions and the heavy metal cations. The obtained experimental data were fitted by two kinetic models, non linear pseudo first and non linear second order (detailed in chapter II §V.2.2) in order to determine the reaction order and the kinetics constants.

IV.1 Kinetic Models

The kinetic data are presented in **Table III.1**. The obtained correlation coefficients of the pseudo-second-order model are higher than those of pseudo-first-order model. Also, the equilibrium capacities (q_e values) calculated from the pseudo-second-order are closer to the experimental values. From these results, it can be concluded that the adsorption of the metal ions (Cu^{2+}, Ni^{2+}, Cd^{2+} and Pb^{2+}) on NaX zeolite follows the pseudo-second-order model which means that adsorption might be the rate limiting step involving valence forces either through sharing or exchange of electrons between adsorbent and metal ions [8]. The corresponding curves are shown in **Figure III.9**.

Table III.1. Comparison of the first and the second order kinetic models for NaX zeolite

		First order kinetic model			Second order kinetic model			
	qe^{exp} (mmol g^{-1})	k_1 (min^{-1})	qe^{cal} (mmol g^{-1})	R^2	k_2 (g $mmol^{-1}$ min^{-1})	qe^{cal} (mmol g^{-1})	h (mmol $g^{-1}min^{-1}$)	R^2
Cu^{2+}	1.82	0.700	1.69	0.935	0.900	1.80	2.94	0.997
Ni^{2+}	1.38	0.410	1.46	0.827	1.04	1.37	2.34	0.994
Cd^{2+}	1.54	1	1.35	0.978	1.19	1.45	2.52	0.996
Pb^{2+}	1.96	1	1.80	0.972	0.787	1.96	3.04	0.999

Concerning the adsorption rate *h,* it was found to be in the following order: Pb^{2+} > Cu^{2+} > Cd^{2+} > Ni^{2+} which means that the exchange process is more rapid and consequently NaX is more selective for Pb^{2+} and Cu^{2+} than for Cd^{2+} and Ni^{2+}.

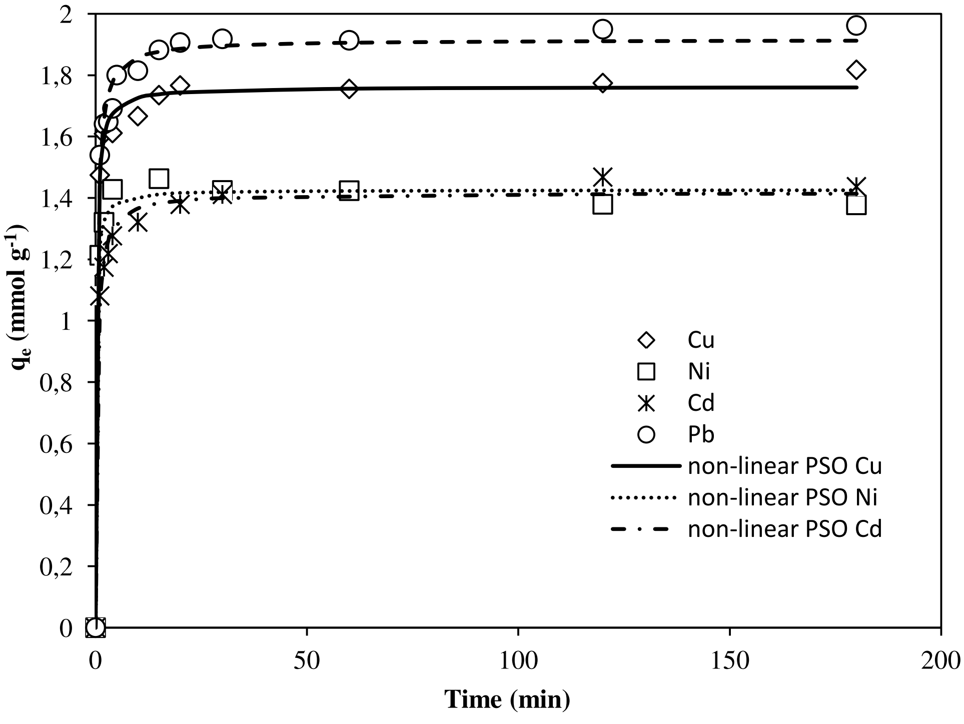

Figure III.9. Non- linear pseudo-second-order kinetic model for M^{2+} adsorption on NaX zeolite (pH = 5.8 at 25 ºC and $[Me^{2+}]_i = 0.47$ mmol L^{-1})

V. Distribution Coefficient

Based on the experimental kinetic results, the distribution coefficient (K_d) was calculated from the values of equilibrium capacities (q_e) and the concentration of the remained metal ions in solution at equilibrium (C_e) obtained from the kinetic experimental data. Information concerning the affinity of NaX towards the four heavy metal cations can be deduced from the distribution coefficients values were calculated according to the following formula [9]:

$$K_d = \frac{q_e}{C_e}$$

The obtained results are represented in **Table III.2**. K_d values were in the following order $Pb^{2+} > Cu^{2+} > Cd^{2+} > Ni^{2+}$ so NaX zeolite has higher affinity for Pb^{2+} and Cu^{2+} more than Cd^{2+} and Ni^{2+}. This information is very useful for predicting the selectivity of NaX zeolite towards a mixture of heavy metal ions. These results are in accordance with those for *h* values obtained above. This indicates that the zeolite selectivity is controlled by the sorption rate that's why Pb^{2+} which has the highest *h* value was preferentially adsorbed.

Table III.2. Distribution coefficients values for NaX

Metal ions	(K_d)
Cu^{2+}	33.5
Ni^{2+}	13.7
Cd^{2+}	15.6
Pb^{2+}	48.7

VI. NaX Zeolite Adsorption Capacity

VI.1. Theory of Cation Exchange in Zeolites

The sodium–divalent metal ion exchange process in NaX zeolite can be expressed by:

$$2\,\overline{\mathrm{Na}}^{+} + \mathrm{M}^{2+} \leftrightarrow 2\mathrm{Na}^{+} + \overline{\mathrm{M}}^{2+} \qquad (1)$$

The ion exchanger phase is represented by the bar above the symbols. The thermodynamic equilibrium constant, *K*, of the reversible ion-exchange reaction is defined by [10]:

$$K = \frac{[\mathrm{Na}^+]^2 \bar{X}_{\mathrm{M}} {\gamma_{\mathrm{Na}}}^2 f_{\mathrm{M}}}{[\mathrm{M}^{2+}] {\bar{X}_{\mathrm{Na}}}^2 \gamma_{\mathrm{M}} {f_{\mathrm{Na}}}^2} \qquad (2)$$

$[\mathrm{Na}^+]$ and $[\mathrm{M}^{2+}]$ are the molarities of the ions in solution, γ_i and f_i are the activity coefficients in the aqueous phase and in the ion-exchanger phase, respectively. The standard states for the ion-exchanger phase are taken as the exchanger in its pure Na^+ pure M^{2+} forms, and the activity coefficients, f_{Na} and f_{M}, are chosen as unity when the exchanger is at the standard state of the Na^+ form and the M^{2+} form, respectively. $\bar{X}_i$ is an equivalent fraction of ion *i* in the ion-exchanger phase, defined by:

$$\bar{X}_{Na} = \frac{[\overline{\mathrm{Na}}^+]}{2[\overline{\mathrm{M}}^{2+}] + [\overline{\mathrm{Na}}^+]}, \bar{X}_M = \frac{2[\overline{\mathrm{M}}^{2+}]}{2[\overline{\mathrm{M}}^{2+}] + [\overline{\mathrm{Na}}^+]} \qquad (3)$$

The molarities $[\mathrm{Na}^+]$ and $[\mathrm{M}^{2+}]$ can be replaced by the equivalent fractions of the ions in the solution (X_i):

$$X_{Na} = \frac{[\mathrm{Na}^+]}{2[\mathrm{M}^{2+}] + [\mathrm{Na}^+]}, X_M = \frac{2[\mathrm{M}^{2+}]}{2[\mathrm{M}^{2+}] + [\mathrm{Na}^+]} \qquad (4)$$

$$[\mathrm{Na}^+] + 2[\mathrm{M}^{2+}] = \mathrm{TN} \qquad (5)$$

where TN represents the total normality of the solution. Through using a corrected selectivity coefficient,$K_{\mathrm{Na}}^{\mathrm{M}}$, the thermodynamic equilibrium constant can be rewritten as [11]:

$$K_{\mathrm{Na}}^{\mathrm{M}} = \frac{{X_{\mathrm{Na}}}^2 \bar{X}_{\mathrm{M}} {\gamma_{\mathrm{Na}}}^2}{X_{\mathrm{M}} {\bar{X}_{\mathrm{Na}}}^2 \gamma_{\mathrm{M}}} [2(\mathrm{TN})] \qquad (6)$$

where,

$$K = K_{\mathrm{Na}}^{\mathrm{M}} \frac{f_{\mathrm{M}}}{{f_{\mathrm{Na}}}^2} \qquad (7)$$

When the total normality, TN= $[Na^+] + 2[M^{2+}]$, is lower than 0.01 N, $\gamma^2{}_{Na}/\gamma_M$ will be close to unity. $K_{\mathrm{Na}}^{\mathrm{M}}$ is dependent on the total normality as shown in equation (7).

When the corrected selectivity coefficient is larger than unity (ln $K_{\mathrm{Na}}^{\mathrm{M}}$>0), the zeolite is selective for the ion M^{2+}. If $K_{\mathrm{Na}}^{\mathrm{M}}$ is smaller than unity (ln $K_{\mathrm{Na}}^{\mathrm{M}}$<0), Na^+ ions are more preferred. When $K_{\mathrm{Na}}^{\mathrm{M}}$ is equal to unity (ln $K_{\mathrm{Na}}^{\mathrm{M}}$=0), there will be no preference between these ions.

$K_{\mathrm{Na}}^{\mathrm{M}}$ is also related to the Kielland coefficient as given below. Kielland plots show the details of the ion exchange selectivity as a function of the equivalent fraction $\bar{X}_M$.

$$\log K_{\mathrm{Na}}^{\mathrm{M}} = \sum_{m=1} (m+1) C_m \bar{X}_M^m + \log\left(K_{\mathrm{Na}}^{\mathrm{M}}\right)_{\bar{X}_{M\to 0}} \qquad (8)$$

where the coefficient, C_m, is called generalized Kielland coefficient. These plots often give linear relationships with a slope $2C_1$ so equation (8) becomes:

$$\log K_{\mathrm{Na}}^{\mathrm{M}} = 2C_1 \bar{X}_M + \log\left(K_{\mathrm{Na}}^{\mathrm{M}}\right)_{\bar{X}_{M\to 0}} \qquad (9)$$

If the Gibbs–Duhem equation is applied to the ion-exchange reaction, the thermodynamic equilibrium constant, K, is given by the integration of Kielland plot from $\bar{X}_M$=0 to $\bar{X}_M$=1.

$$\ln K = (\mathrm{Z_{Na}} - \mathrm{Z_M}) + \int_0^1 \ln K_{\mathrm{Na}}^{\mathrm{M}} \mathrm{d}\bar{\mathrm{X}}_{\mathrm{M}} + \Delta \qquad (10)$$

Here, Z_{Na} and Z_M are the number of charges on the Na^+ and M^{2+}. The third term on the right, Δ, is negligible when compared with experimental accuracy in measuring the equilibrium. Equations (9) and (10) are then combined to give the thermodynamic constant K:

$$\ln K = (\mathrm{Z_{Na}} - \mathrm{Z_M}) + 2.303 C_1 + \ln\left(K_{\mathrm{Na}}^{\mathrm{M}}\right)_{\bar{X}_{M\to 0}} \qquad (11)$$

Thus, the thermodynamic equilibrium constant is determined by the valences of the exchanged and exchanging cations, the generalized Kielland coefficient C_1 and the intercept of Kielland plot, $\left(K_{\mathrm{Na}}^{\mathrm{M}}\right)_{\bar{X}_{M\to 0}}$.

The Gibbs standard free energy change ΔG° can be calculated by:

$$\Delta G^0 = -RT \ln K \qquad (12)$$

VI.2. Exchange Equilibrium Curves for NaX Zeolite

The exchange reactions of the four heavy metals ions Cu^{2+}, Ni^{2+}, Cd^{2+} and Pb^{2+} were performed at 25 °C in the concentration range between 0.17 mmol L^{-1} and 5 mmol L^{-1} mmol L^{-1} for all. The exchange isotherms are shown in **Figure III.10** and are represented as the equivalent fraction of the divalent metal ions fraction $(\bar{X}_M)$ inside the NaX zeolite as a function of the equivalent ion fraction in the solution (X_M).

The obtained exchange isotherms almost have the same shape where they showed a steeper increase in the initial stage of $X_M^{2+} < 0.2$ and then the isotherms increased more gently. This shape is characteristic of a favorable exchange process.

It can be seen from **Figure III.10** that for $2Na^+ \rightarrow Pb^{2+}$ exchange reaction, the isotherm proceeded more steeply up to $\bar{X}_{Pb}$~0.6 which indicates higher selectivity for Pb^{2+} than for the other three heavy metals. Concerning the theoretical exchange capacity, it was calculated from the Na^+ ions contained in NaX ($Na_{88}Al_{88}Si_{104}O_{384}$). 1 gram of NaX zeolite contains 6.54 mmol Na^+. So theoretically, it has a maximum adsorption capacity for divalent ions equals to 3.27 mmol g^{-1} since every two Na^+ ions are exchanged for 1 metal divalent cation so this value was supposed to be the theoretical exchange capacity of NaX. The ion exchange capacities for all were determined from their corresponding isotherms and were found to be 93, 87, 95, and 96% of the theoretical exchange capacity for Cu^{2+}, Ni^{2+}, Cd^{2+} and Pb^{2+} respectively. These values were calculated from the equivalent fraction of cations in zeolite when the maximum exchange capacity was reached.

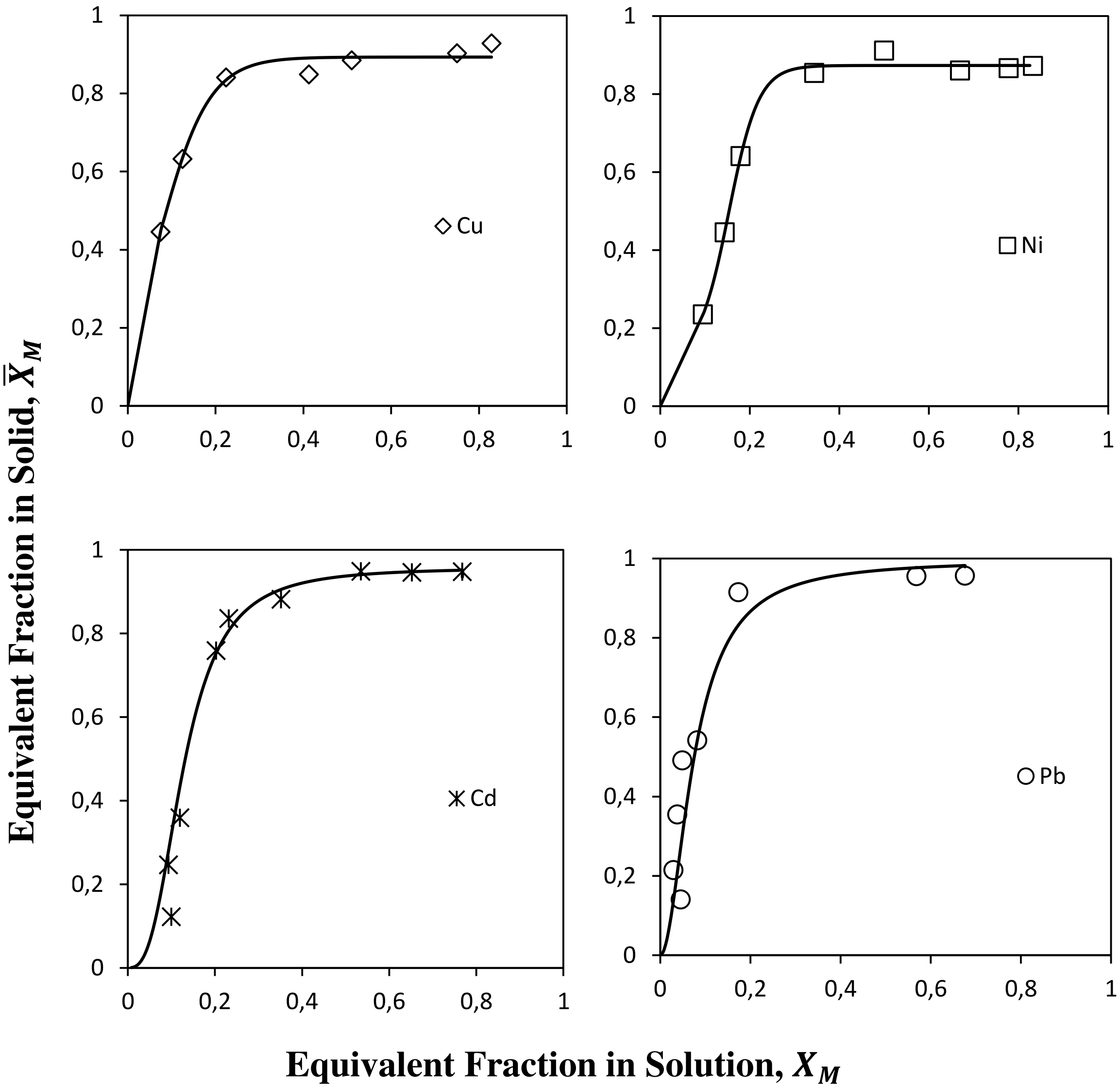

Figure III.10. Cation exchange isotherm for $2Na^+ \rightarrow M^{2+}$ (M= Cu, Ni, Cd and Pb) exchange on the NaX zeolite. (pH = 5.8 at 25 ºC and $[M^{2+}]_i = 0.47$ mmol L^{-1})

Figure III.11 represents an overview of the experimental results as equilibrium isotherms. This representation allows determining the zeolite sorption capacity for each heavy metal ion. All the isotherms have been fitted using Langmuir model. The Langmuir parameters are listed in **Table III.3**. K_L values, they are coherent with those of the distribution coefficient K_d where Pb^{2+} and Cu^{2+} showed higher Langmuir isotherm constant than Cd^{2+} and Ni^{2+}. This indicates that the zeolite has higher affinity for Pb^{2+} and Cu^{2+} than for Cd^{2+} and Ni^{2+}. It is important to specify here that the ion exchange capacities calculated from the exchange equilibrium curves are in accordance with the q_{max} values obtained from Langmuir isotherms fit except for Cu^{2+} where the exchange capacity was found to be higher (4.03 mmol g^{-1}).

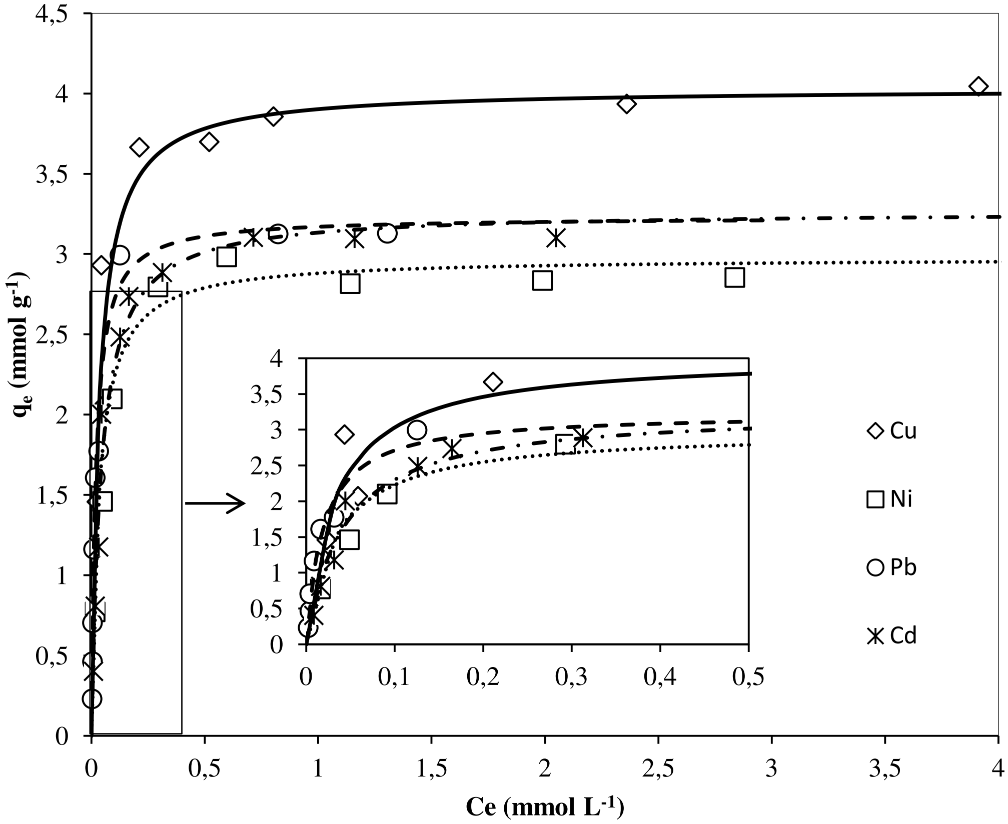

Figure III.11. Experimental Cu^{2+}, Ni^{2+}, Cd^{2+} and Pb^{2+} adsorption isotherms on NaX (open symbols) and their corresponding Langmuir modeled isotherms (lines)

Table III.3. Langmuir parameters for adsorption isotherms

Metal	q_{max} (mmol g^{-1})	K_L (L $mmol^{-1}$)	R^2
Cu^{2+}	4.03	57.7	0.991
Ni^{2+}	2.84	29.7	0.987
Cd^{2+}	3.10	23.7	0.988
Pb^{2+}	3.20	52	0.991

The elevated exchange capacity obtained for Cu^{2+} ions is due to copper speciation as a function of pH, **Figure III.12**, since the experiments were done at pH 5.8 and it is known that the dominant species of copper at this pH value will be $CuOH^+$ [12] so each molecule will be exchanged for 1 Na^{+} ion thus increasing the exchange capacity. This point was taken into consideration for the calculation all of the ion-exchange isotherm parameters. The dominant species for the other three metals will be in the form M^{2+} [13-14-15].

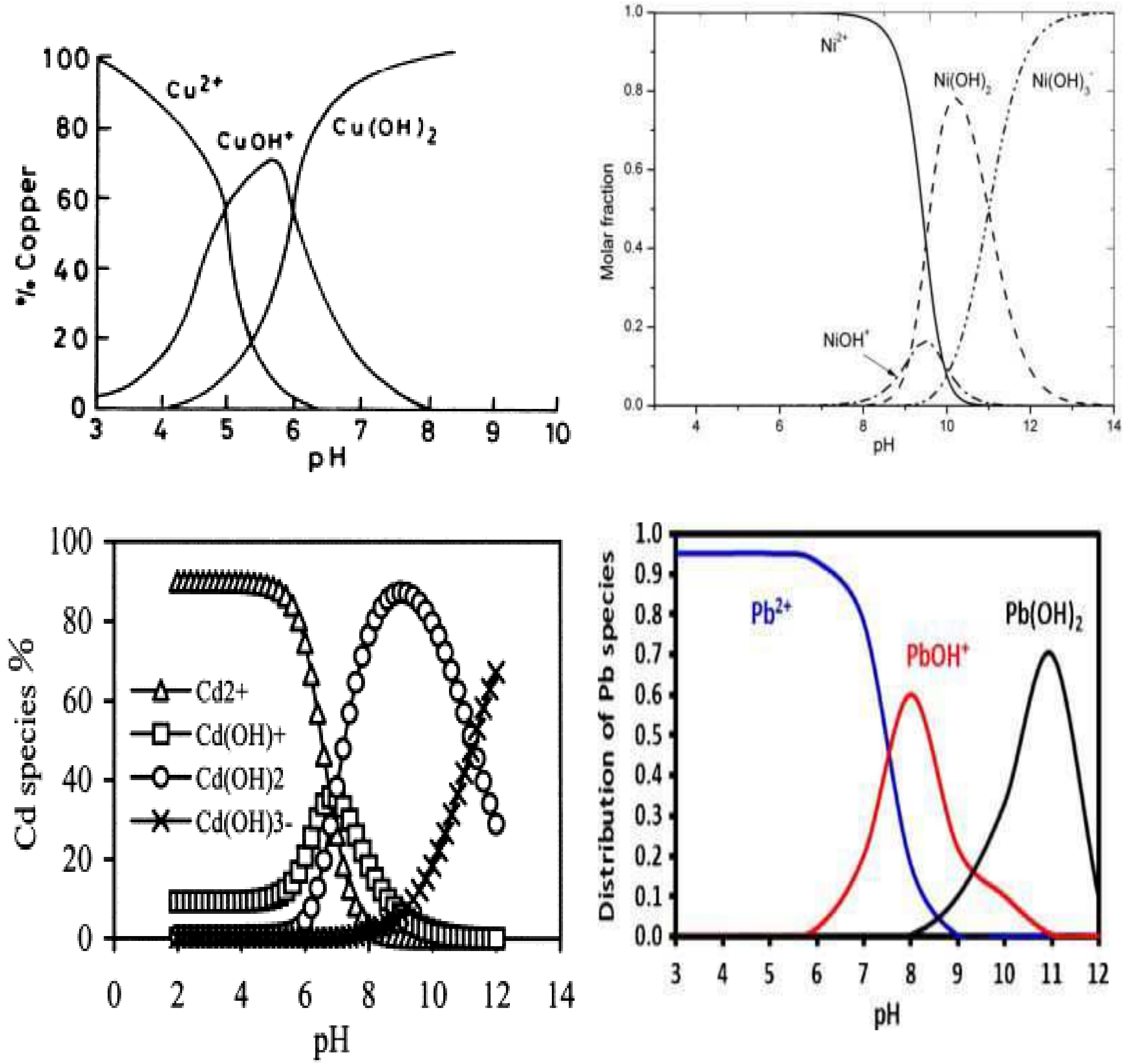

Figure III.12. Speciation of Cu^{2+}, Ni^{2+}, Cd^{2+} and Pb^{2+} as a function of pH

In order to verify if the exchange process is favorable or not a dimensionless separation factor R_L can be calculated using Langmuir parameters:

$$R_L = \frac{1}{1 + K_L\, C_0}$$

where C_0 is the highest initial solute concentration. The obtained R_L values for both adsorbents are listed in **Table III.4**.

Table III.4. R_L values for NaX zeolites

M^{2+}	R_L
Cu^{2+}	0.004
Ni^{2+}	0.006
Cd^{2+}	0.015
Pb^{2+}	0.009

R_L value indicates the nature of the adsorption process, either it is favorable if $0 < R_L < 1$or unfavorable if $R_L > 1$, linear if R_L=1, and irreversible if R_L=0. The obtained results verified that the adsorption process of all the four metal ions is favorable on the two studied adsorbents since all the R_L values are between 0 and 1.

VII. Cation Exchange selectivities: $2Na^+ \rightarrow M^{2+}$

The selectivity of NaX zeolite is further analyzed through Kielland plots where the logarithm of the selectivity coefficient (log $K_{\mathrm{Na}}^{\mathrm{M}}$) is sketched as a function of the equivalent fraction of cations in zeolites (X_M).

The Kielland plots are represented in **Figure III.13**. The plots gave a linear relation for all metals except for Cu^{2+}. The line at 0 indicates that the corrected selectivity coefficient is equal to unity ($K_{\mathrm{Na}}^{\mathrm{M}} = 1$) where there is no preference between Na^+ and M^{2+} ions. If the plots fall below this line this means that the zeolite is more selective for Na^+ while if they fall above it this indicates that the zeolite is more selective for M^{2+}.

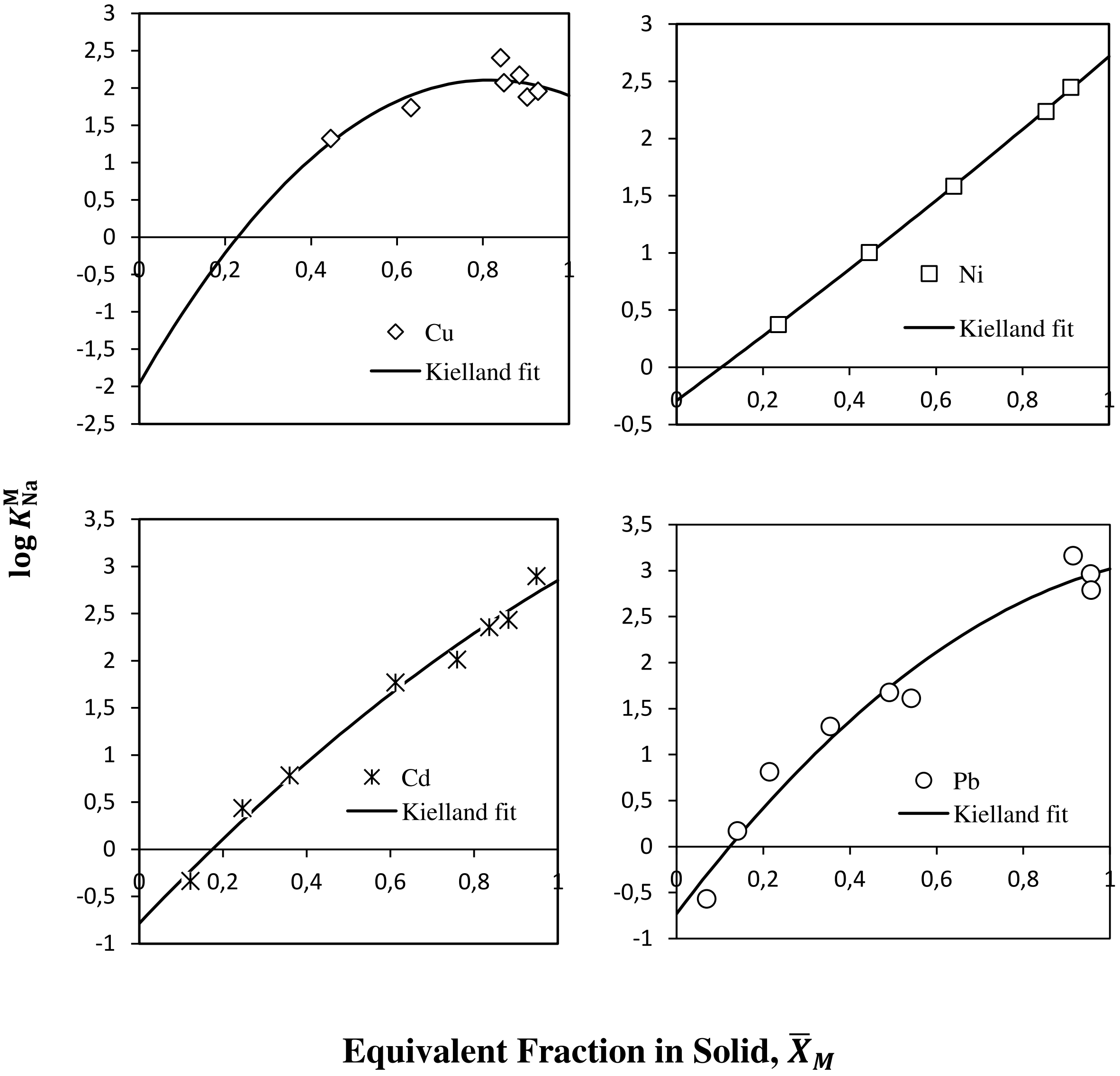

Figure III.13. Kielland plots for 2Na$^+$→M^{2+} (M= Cu, Ni, Cd and Pb) exchange on the NaX zeolite. (pH = 5.8 at 25 ºC and [M^{2+}]$_i$ = 0.47 mmol L^{-1})

From these Kielland plots, it can be deduced that for Cd^{2+} and Pb^{2+} ions the zeolite becomes more selective for the metal ions at $\bar{X}_M$> 0.2 since all Kielland plots fall above the 0 line above this value. For Cu^{2+} and Ni^{2+}, M^{2+} ions are more preferred almost throughout the 2Na$^+$→• M^{2+} exchange reaction.

Starting from the Kielland plots, the Kielland coefficient C_1, $\ln\left(K_{\mathrm{Na}}^{\mathrm{M}}\right)_{\bar{X}_{M\to 0}}$ and ΔG^0 values were estimated using the equations (9), (11) and (12). The obtained values are listed in **Table III.5**.

Table III.5. Thermodynamic data for $2Na^+ \rightarrow M^{2+}$ exchange on NaX at room temperature

M^{2+}	$\ln\left(K_{\mathrm{Na}}^{\mathrm{M}}\right)_{\bar{X}_{M\to 0}}$	C_1	ΔG^0 (kJ mol^{-1})
Cu^{2+}	2.32	1.10	-5.80
Ni^{2+}	1.69	1.50	-4.20
Cd^{2+}	1.77	1.70	-4.40
Pb^{2+}	2.65	1.60	-6.40

ΔG^0 value for Pb^{2+} was the smallest while that of Ni^{2+} was the highest. Based on this results, the order of selectivity will be $Pb^{2+} > Cu^{2+} > Cd^{2+} > Ni^{2+}$ which is in accordance with what was found before using the distribution coefficient K_d. The Kielland coefficient, C_1, is related to the energy of the steric limitation or jumping barrier for the exchanging ions in the sodalite cages [14]. In General, the energy term for the steric limitation is larger as the C_1value is larger. The energy of the steric limitation increases in the order of $Cd^{2+} > Pb^{2+} > Ni^{2+} > Cu^{2+}$ but the order of selectivity didn't follow the same order. These findings are related to the nature of the metal ions and mainly to the exchange velocities between the ligands and the aqueous metal ions which is generally expressed as follows [16]:

$$(Me(H_2O)_m)^{n+} + L \leftrightarrow (Me(H_2O)_{m-1}L)^{n+} + H_2O$$

Where L represents H_2O or other ligands and Me the metal ion. The exchange velocity constant (k_{w}) of water molecules with metallic ions (**Table III.6**) is the fundamental step controlling the rate of ions removal from water.

Table III.6. The exchange velocity constant (k_{w}) for the four studied metal ions

Cation	k_{w} (s^{-1})
Ni^{2+}	3.10^4
Cd^{2+}	3.10^8
Cu^{2+}	1.10^9
Pb^{2+}	7.10^9

The obtained selectivity results vary with the order of the exchange velocity (k_{w}) values which seems to be the main parameter that controls their adsorption. Pb^{2+} has the greatest exchange velocity (k_{w}) so it is the first to be adsorbed while Ni^{2+} has the lowest k_{w} value so its adsorption is less favorable compared to Pb^{2+} and Cu^{2+} and Cd^{2+}.

These obtained selectivity results were further experimentally verified by studying the selectivity of NaX zeolite towards these metals in an equimolar mixture of the 4 cations.

The results are shown below (**Figure III.14**); the selectivity of NaX was: $Pb^{2+} > Cu^{2+} > Cd^{2+} > Ni^{2+}$. It should be noted here that the selectivity of zeolites varies according to the zeolite type. Jha *et al.* have found the same result using Zeolite X from Coal Fly Ash [17], while Kocaoba *et al.* found that the selectivities of natural clinoptilolite which follows order $Cd^{2+} > Ni^{2+} > Cu^{2+}$ [18].

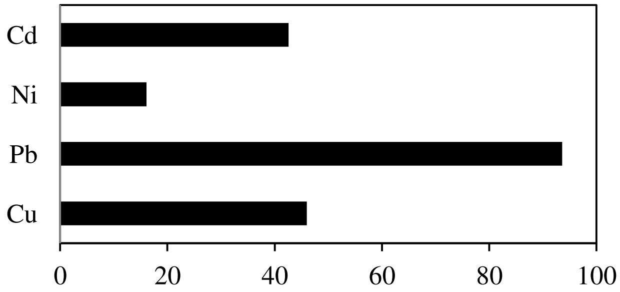

	Cu	Pb	Ni	Cd
■ % adsorption	46	93,6	16,1	42,6

Figure III.14. NaX zeolite selectivity (pH = 5.8 at 25 ºC and $[M^{2+}]_i = 0.47$ mmol L^{-1})

VIII. Temperature Effect

Cu^{2+} adsorption on NaX zeolite and the thermodynamic parameters were studied at different temperatures 25 °C, 35 °C and 45 °C. The isotherms at each temperature are presented in **Figure III.15**. The obtained results showed that Cu^{2+} adsorption slightly decreases with the increase in temperature. At 25 °C the ion exchange capacity was 93% while it decreased to 90.5% and 80% at 35 °C and 45 °C respectively.

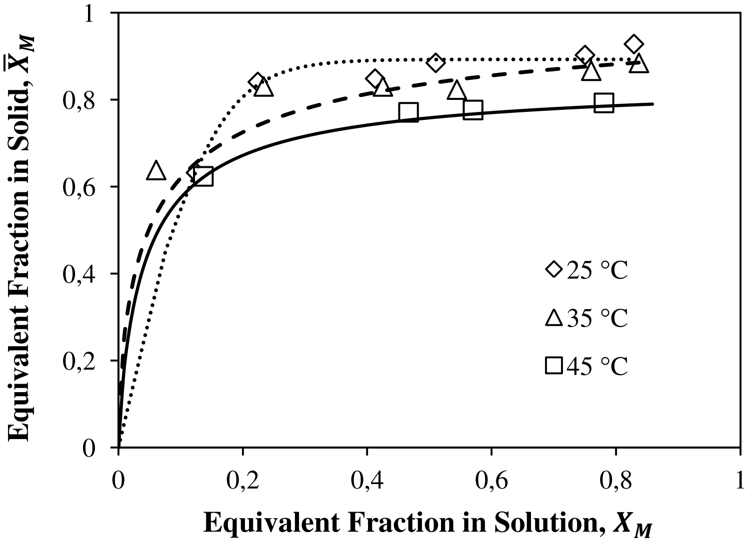

Figure III.15. Cu^{2+} adsorption on NaX at different temperatures

The van’t Hoff plot of ln K_d versus 1/T gives a straight line (**Figure III.16**) where ΔH° is obtained from the slope [19].

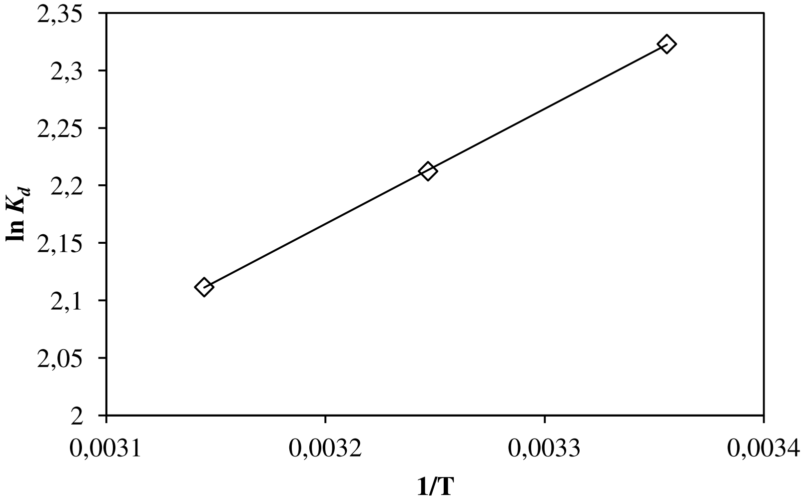

Figure III.16. Plots of ln K_d versus 1/T for the adsorption of Cu^{2+} on NaX

Table III.7 summarizes all the calculated the thermodynamic parameters. The negative value of ΔH° represents the exothermic nature of adsorption process. ΔG° negative values indicate that the reaction is spontaneous. On the other hand, the negative value decreased of ΔG° is unusual for cation exchangers since this process is generally favored when temperature increase.

Table III.7. Thermodynamic parameters for Cu^{2+} adsorption on NaX zeolite

Metal	ΔH° (kJ mol^{-1})	ΔS° (J K^{-1} mol^{-1})	T (K)	ΔG° (kJ mol^{-1})	R^2
Cu^{2+}	-8.32	-8.64	298	-5.75	0.999
			308	-5.66	
			318	-5.58	

This decrease is related to the thermodynamic speciation of copper as a function of temperature (**Figure III.17**).

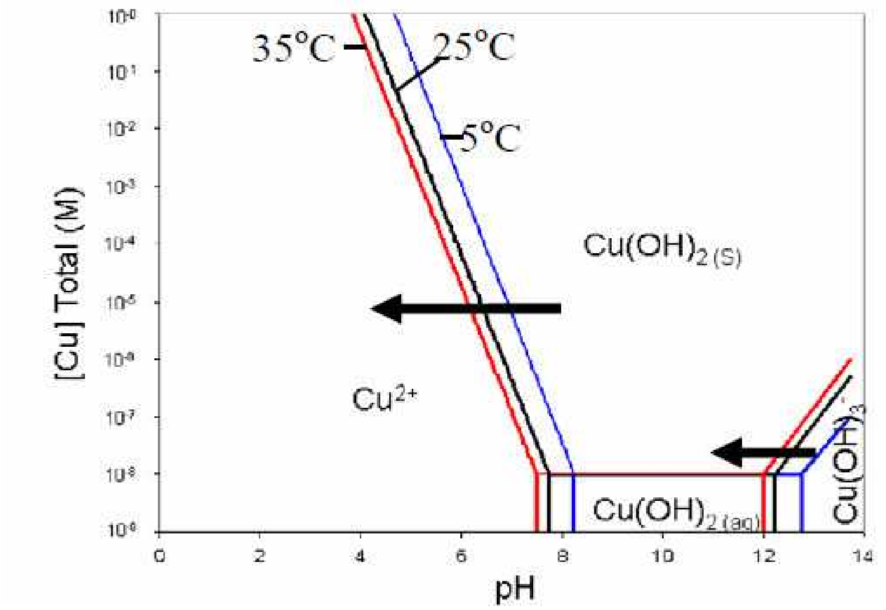

Figure III.17. The Thermodynamic speciation diagram of dominant copper species as a function of pH and temperature. The arrows show the change in the domain of stability of copper species with increasing temperature [20].

It was observed that as the temperature increases, the copper species stability domain shifts to lower pH values so copper hydroxide precipitate will form at lower pH values [21]. This change in solubility of copper hydroxide with temperature caused this decrease in the adsorbed metal fraction by the zeolite since $Cu(OH)_{2(s)}$ can't be exchanged with Na^+ ions.

The entropy change value ΔS° is negative (-162.3 J K^{-1} mol^{-1}) which means that the entropy (randomness) decreased as a result of the ion-exchange. According to Zou *et al.* this negative entropy value for Cu^{2+} removal reflects that no significant change occurs in the internal structure of the zeolite [22].

IX. Fixed Bed Experiments

IX.1. Heavy Metal Mixture Breakthrough Curves in Ultrapure Water

In addition to batch adsorption tests, fixed bed column experiments were also performed in order to test the applicability of NaX zeolites for heavy metals removal and to study their behavior in competition. These experiments are important to test the practical utility of any adsorbent. The first experiment was done using a mixed equimolar metal ions solution in ultra pure water. The obtained breakthrough curves are shown in **Figure III.18**. The curves show that saturation was reached after 700 mL of contaminated water was passed through the column. Furthermore, it was noticed that the adsorption behavior of Pb^{2+} ions was different from the other metal ions due to the high affinity of NaX zeolite towards it.

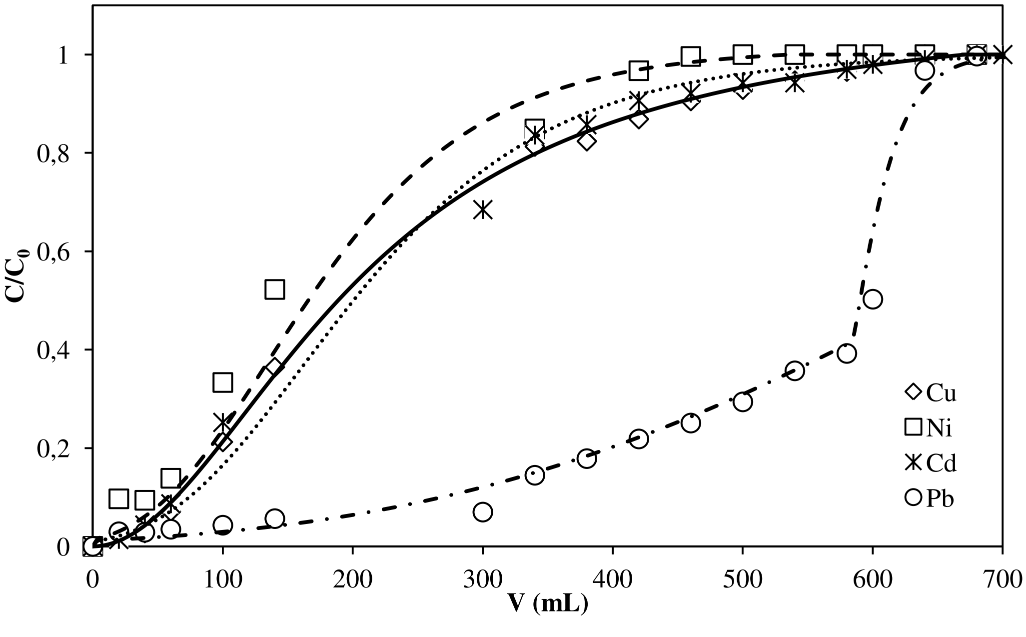

Figure III.18. Breakthrough curve for Cu^{2+}, Ni^{2+}, Cd^{2+} and Pb^{2+} adsorption of on NaX (pH = 5.8 at 25 °C and $[M^{2+}]_i$ = 0.47 mmol L^{-1}, m = 108 mg, flow rate 1 mL min^{-1})

The fixed bed adsorption capacity for each metal ion was calculated by integrating the area obtained from the breakthrough curves. The results are listed in **Table III.8**. For comparison, the capacities obtained from batch experiment done with the same equimolar mixture of heavy metal cations are also reported in **Table III.8**. The capacity obtained for Ni^{2+} was larger than that calculated for batch experiments The reason why column operation showed this higher adsorption capacity for Ni^{2+} might be due to the establishment of a continuous large concentration gradient at the interface zone when the water pass through the column contrary to batch tests where the concentration gradient decreases with time.

Table III.8. Column capacity for Cu^{2+}, Ni^{2+}, Cd^{2+} and Pb^{2+} adsorption on NaX zeolite

Metal ion	Batch capacity (mmol g^{-1})	Column capacity (mmol g^{-1})
Cu^{2+}	1.02	0.960
Ni^{2+}	0.380	0.850
Cd^{2+}	1	0.867
Pb^{2+}	2.21	2.23

IX.2. Application to a Natural Water Sample

The same fixed bed experiment was done for natural ground water as well. The water composition has been detailed in Chapter II § VIII.2. The water was spiked with the same concentration of each heavy metal as before and was then passed through a zeolite packed column. The obtained breakthrough curves are presented in **Figure III.19**.

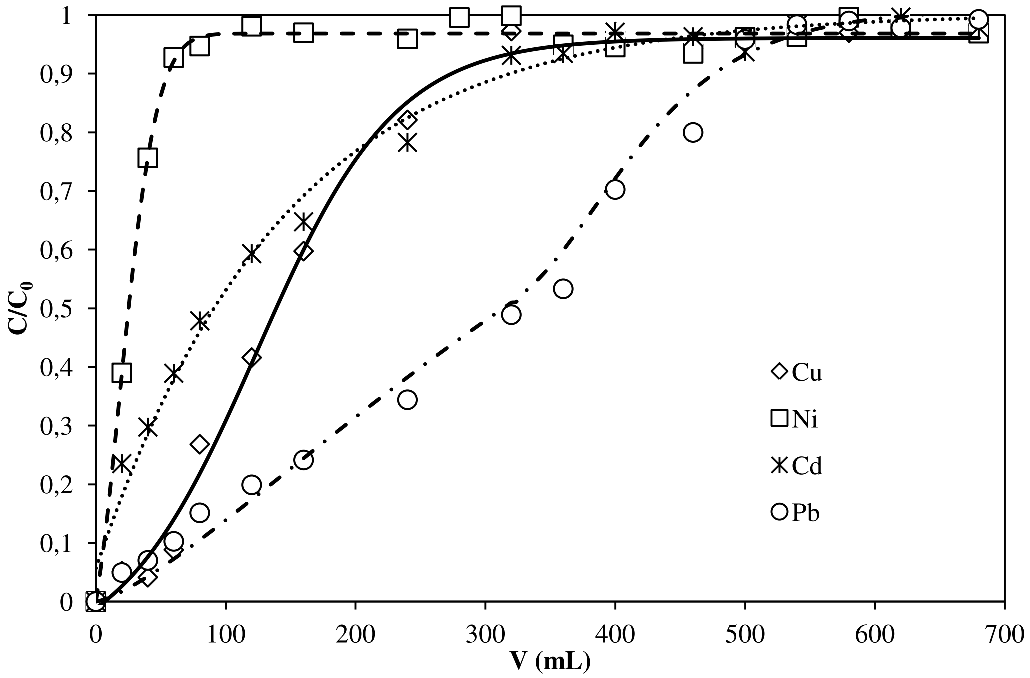

Figure III.19. Breakthrough curve for Cu^{2+}, Ni^{2+}, Cd^{2+} and Pb^{2+} adsorption of on NaX from natural ground water (pH = 6 at 25 ºC and $[M^{2+}]_i$ = 0.47 mmol L^{-1}, m = 108 mg, flow rate 1 mL min^{-1})

The fixed bed adsorption capacity for all the metal ions was also calculated and the results are listed in **Table III.9**. The capacities obtained were lower than those calculated for batch experiments and those obtained for the same experiment done with ultrapure water. This decrease is certainly due to the presence of elevated amount of calcium ions Ca^{2+} in this ground water (216 ppm) which will directly affect the adsorption of other metals since Ca^{2+} ions will be also exchanged with Na^+ ions thus leaving less exchangeable sites for the rest ions.

Table III.9. Column capacity for Cu^{2+}, Ni^{2+}, Cd^{2+} and Pb^{2+} adsorption on NaX zeolite from natural water

Metal ion	Column capacity (mmol g^{-1}) Ultrapure water	Column capacity (mmol g^{-1}) Natural water
Cu^{2+}	1.12	0.740
Ni^{2+}	0.833	0.175
Cd^{2+}	0.867	0.578
Pb^{2+}	2.30	1.38

IX.3. Column Regeneration

Column regeneration is essential for its reusability so for NaX zeolite adsorption-desorption tests were done for Cu^{2+}. Elution of adsorbed ions was accomplished by 1 M NaCl solution at flow rate 1mL min^{-1}. Then the regeneration efficiency was evaluated by performing two more adsorption cycles using the same column and regenerating it after each cycle (**Table III.10**). The three obtained curves are shown in **Figure III.20**.

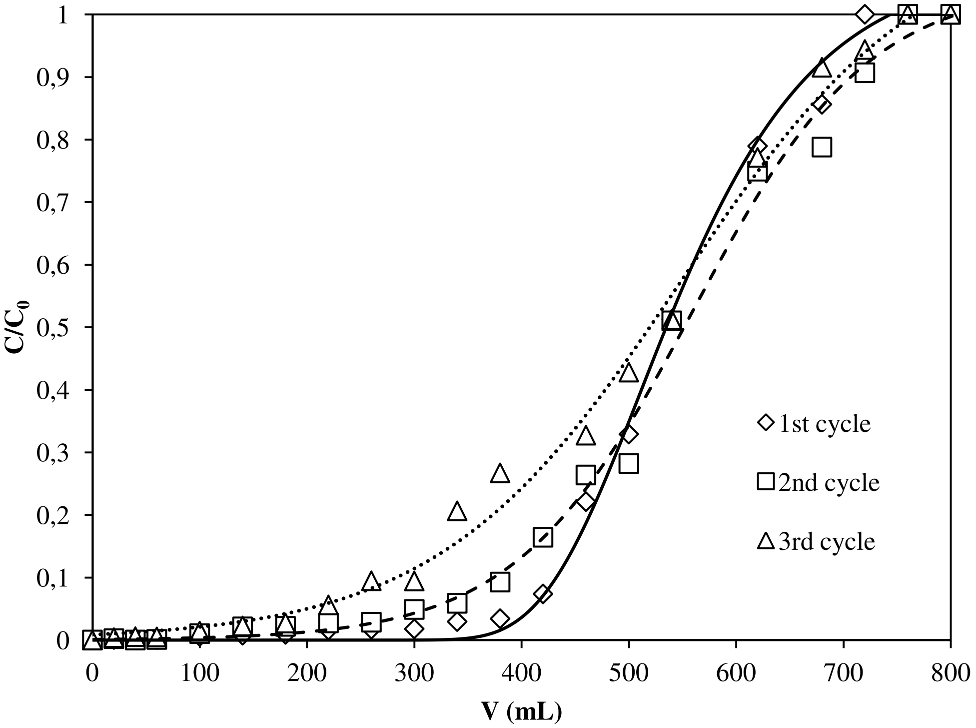

Figure 3.20. Breakthrough curves for Cu^{2+} adsorption of on NaX after regeneration (pH = 5.8 at 25 °C and $[M^{2+}]_i$ = 0.47 mmol L^{-1}, m = 109 mg, flow rate 1 mL min^{-1})

Table.III.10. regeneration efficiency after three Cu^{2+} adsorption-desorption cycles		
	Capacity (mmol g^{-1})	Regeneration efficiency (%)
1st cycle	2.43	-
2nd cycle	2.36	97.1
3rd cycle	2.24	92.2

After three consecutive Cu^{2+} adsorption-desorption cycles, the NaX zeolite packed column conserved up to 92 % of its original capacity which means that it can be used several times. Also the high efficiency conserved after regeneration proves that heavy metals can be successfully elute without degrading the structure of the adsorbent.

X. Conclusions

NaX zeolite was found to be very effective for divalent heavy metals removal from water. The obtained kinetic values were well fitted by the non linear pseudo-second-order thus proving that ion exchange process was the limiting step during adsorption. The effect of different factors on adsorption was studied as well. At low pH values, the adsorption decreased since there is competition between positively charged H_3O^+ ions and the metals. The presence of competitor ions such as Na^+ and K^+ also affected adsorption. The ion exchange mechanism was studied and presented in details thus allowing the understanding of how does the adsorption process on NaX zeolite proceed. Studying the ion exchange mechanism proved the high adsorption capacity of NaX zeolite which makes it very promising for water treatment. The removal order of the metal ions was as follows: $Pb^{2+} > Cu^{2+} > Cd^{2+} > Ni^{2+}$. This selectivity is controlled by the nature and characteristics of the metal ions where the exchange velocity (k_{w}) of each determined their exchange rate and as a result the selectivity. Moreover, the analysis of the thermodynamic parameters gave information concerning the spontaneity of adsorption on NaX. Adsorption slightly decreased as temperature increase. This decrease was caused by the speciation stability of Cu^{2+} as a function of temperature where at higher temperatures $Cu(OH)_{2(s)}$ start to form at lower pH values thus decreasing the available Cu^{2+} ions in the solution. NaX zeolite was efficient in column experiments as well and it conserved 92% of its adsorption capacity after two successive regeneration cycles.

References

[1] W.M. Meier, D.H. Olson, C. Baerlocher, Atlas of Zeolite Framework Types, Elsevier, Amsterdam, New York, 2001
[2] Y. Yang, N. Burke,J.Zhang,S.Huang, S. Lim,Y. Zhu. 4 (2014) 7279-7287.
[3] C. Mellot-Draznieks, S. Buttefey, A. Boutin, A. Fuchs. Chem. Commun. (2001) 2200–2201.
[4] M.M.J. Traecy, J.B. Higging, Collection of Simulated X Patterns for Zeolites, 4th revised ed., Elsevier, Amsterdam, 2001
[5] D. Nibou, H. Mekatel, S. Amokrane, M. Barkat, M. Trari. J. Hazard. Mater. 173 (2010) 637–646.
[6] E. Erdem, N. Karapinar, R. Donat. J. Colloid Interface Sci. 280 (2004) 309–314.
[7] K.S. Hui, C.Y.H. Chao, S.C. Kot. J. Hazard. Mater. 127 (2005) 89–101.
[8] M.A. Shavandi, Z. Haddadian, M.H.S. Ismail, N. Abdullah, Z.Z. Abidin. J. Taiwan Inst. Chem. E. 43(2012) 750-759.
[9] Mohan S, Gandhimathi R. J. Hazard. Mater. 169(2009) 351–359.
[10]T. Kodama; S. Komarneni. J. Mater. Chem. 9 (1999) 533–539.
[11] R. M. Barrer and J. Klinowski, J. Chem. Soc., Faraday Trans. 1. 70 (1974) 2080.
[12] M. Ajmal, A. Khan, S. Ahmad, A. Ahmad. Water research, 32(1998) 3085–3091.
[13] A. Bhatnagar, V. Vilar, J. Santos, C. Botelho, R. Boaventura. Chem. Eng. J. 202 (2012) 365–372.
[14] C. Lai, C. Chen, B. Wei, S. Yeh.S. Water research. 36 (2002) 4943–4950.
[15] V. Guptaa, S. Agarwalc, T. Saleh.T. J. Hazard. Mater. 185 (2011) 17–23.
[16] Sigg. L, behra. P, stumm.w. chimie des milieu aquatiques 5th Edition 2014, Dunod,paris.
[17] V. K. Jha, M. Nagae, M. Matsuda, and M. Miyake. J Environ Manage. 90 (2009) 2507-2514.
[18] S. Kocaoba, Y. Orhan, T. Akyüz. Desalination 214 (2007) 1–10.
[19] I. Hatay, R. Gup, M. Ersoz. J. Hazard. Mater. 150 (2008) 546–553.
[20] T. W. Albrecht, J. Addai-Mensah, D. Fornasiero. Effect of pH, Concentration and Temperature on Copper and Zinc Hydroxide Formation/Precipitation in Solution. Ian Wark Research Institute, University of South Australia.
[21] L. Hidmi, M. Edwards. Environ. Sci. Technol. 33(1999) 2607-2610.
[22] W. Zou, R. Han, Z. Chen, Z. Jinghua, J. Shi. Colloid Surface A: Physicochem. Eng. Aspects 279 (2006) 238–246.

Table of contents

I. SBA-15 Materials Characterization 97

I.1. Post Synthesis Modification Route 97

- I.2. Textural Properties 98
  - I.2.1. X-Ray Diffraction (XRD) 98
  - I.2.2. Transmission Electron Microscopy (TEM) 99
  - I.2.3. Nitrogen Adsorption-Desorption Isotherms 100
- I.3. Organic Groups Quantification and Characterization 102
  - I. 3.1. Thermogravimetric Analysis 102
  - I.3.2. Fourier Transform Infrared Spectroscopy (FT-IR) 103

I.4. Applying Other Modification Routes 104

- I.5. Reactivity of the Immobilized Amino Groups 108

II. SBA-16 and KIT6 Characterizations 109

- II.1. Textural Properties 110
  - II. 1. 1 X-Ray Diffraction (XRD) 110
  - II.1.2. Transmission Electron Microscopy (TEM) 111
- II.3. Nitrogen Adsorption-Desorption Isotherms 112
- II.4. Organic Content Calculation after EDTA Modification 115

III. Heavy Metals Adsorption Tests 116

- III.1. Contact Time Effect 116
- III.2. Mass Effect 117
- III.3. pH Effect 118
- III.4. Adsorption Kinetics 119
- III.5. Adsorption Isotherms 122
- III.6. Adsorption Thermodynamics 124
- III. 7. Selectivity 126
- III.8. Competitive Adsorption 126

IV. Fixed Bed Column Experiments 128

- IV.1. Heavy Metal Mixture Breakthrough Curves in Ultrapure Water 128
- IV.2. Application to a Natural Water Sample 129
- IV.3. Column Regeneration 130

IV. Conclusions 132
References 133

In this chapter, the removal of heavy metals from contaminated water was investigated using three types of ordered mesoporous silica (KIT-6, SBA-15 and SBA-16) as adsorbents. First of all, the materials were synthesized and characterized by various techniques in order to verify the order of their structure. These materials were then functionalized with 3-aminopropyltrimethoxy-silane via post synthesis modification route. The second modification step was done through anchoring ethylenediaminetetraacetic acid (EDTA) through the interaction with the previously introduced amino groups. EDTA was chosen since it is a well known as an efficient chelating agent for divalent heavy metals. After modification, the adsorbents were characterized again in order to analyze the effect of this modification on the structure of the mesoporous silicates of choice. Moreover, the amount of grafted amino and EDTA was determined. The adsorption kinetics, isotherms and thermodynamics were also studied.

I. SBA-15 Materials Characterization

I.1. Post Synthesis Modification Route

SBA-15 was synthesized using P123 as a structure directing agent and TEOS as the silica source. Then the template was removed by calcination. This ordered mesoporous material is known to have a hexagonal 2D structure. The first post-synthesis functionalization step was done by covalently grafting amino propyl groups on SBA-15 through the reaction between APTS and silanol groups present on its surface. This was done through impregnation and the obtained material was denoted as SBA-15-F. The second modification step was the fixation of EDTA on the thus obtained material. To do so, the amino modified SBA-15 was mixed with EDTA solution having a pH around 4.5 which allows the electrostatic interaction between the protonated amino groups and carboxylic acid groups of EDTA. The final material was referred as SBA-15-F-EDTA. The modification route is presented in **Figure IV.1.**

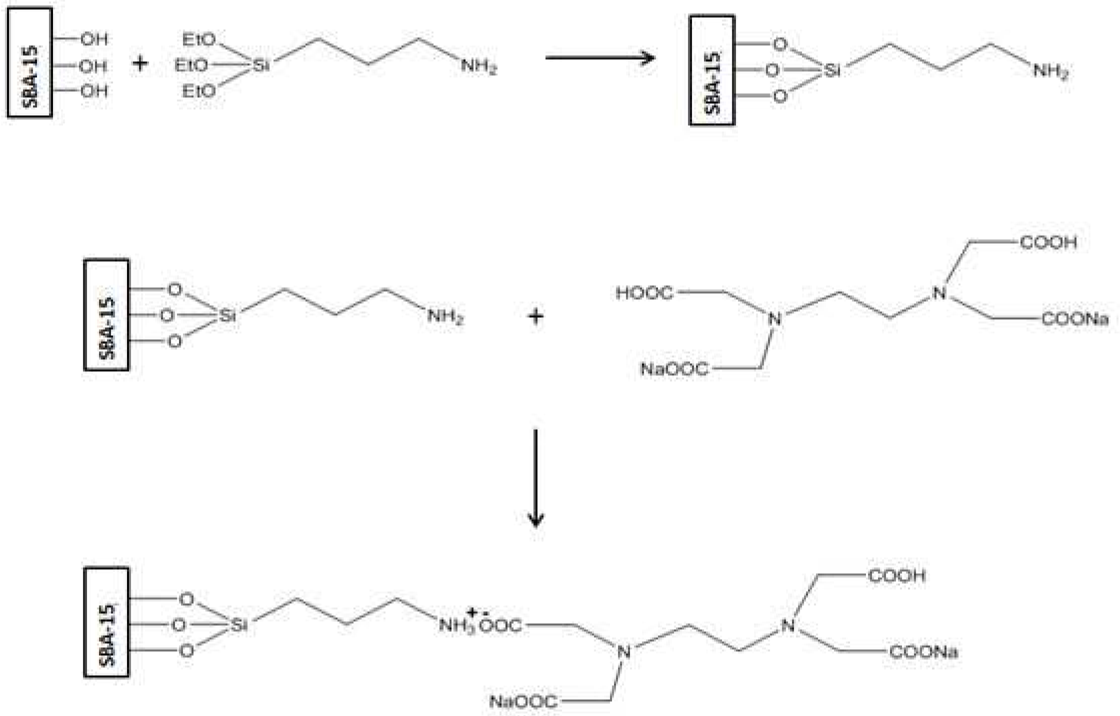

Figure IV.1. Schematic illustration of mesoporous silicates modification with APTES and EDTA

I.2. Textural Properties

I.2.1. X-Ray Diffraction (XRD)

The textural properties were then determined to access the stability of the ordered SBA-15 structure after modification. X-ray diffraction (XRD) was done to study the structural changes that took place. The obtained XRD patterns for SBA-15, SBA-15-F and SBA-15-F-EDTA are presented in **Figure IV.2.** For the unmodified SBA-15, three characteristic diffraction peaks are clearly visible. These peaks are indexed at (100), (110), and (200) planes which are characteristic of a two dimensional hexagonal symmetry (*P6mm*). These three peaks are also clearly visible after chemical modification with organic moieties. However, the XRD peak intensities decreased after modification. This crystallinity loss might be caused by the pore filling with the grafted organic ligands inside the adsorbents channels or the anchoring of ligands on their outer surface [1].

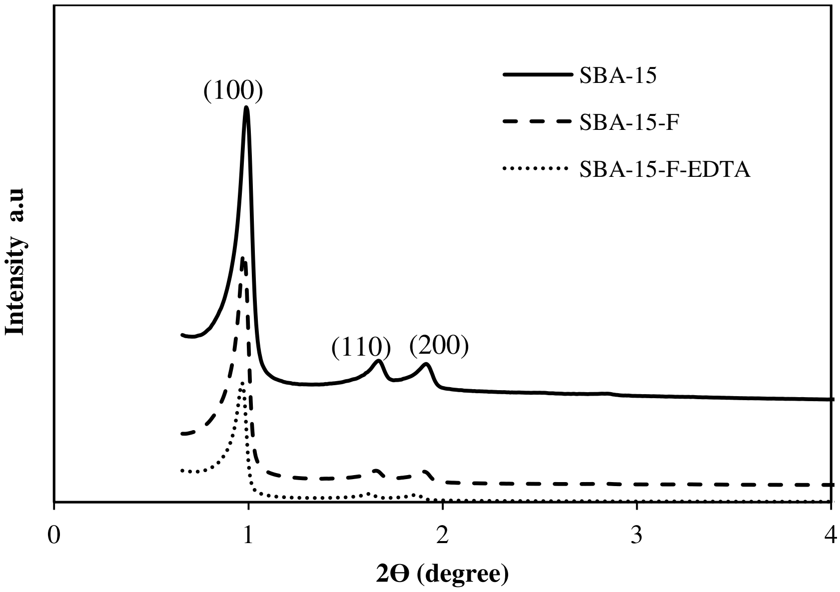

Figure IV.2. XRD patterns of SBA-15 before and after modification.

I.2.2. Transmission Electron Microscopy (TEM)

The TEM images of SBA-15 showed highly ordered 2-D hexagonal mesostructure **Figure IV.3**. The honeycomb structure and the cylindrical channels can be viewed from perpendicular and parallel directions respectively (**Figure IV.3.A and B**). After EDTA modification, the ordered structure of SBA-15 was not affected (**Figure IV.3.C and D**). The pore size estimated from TEM images were 7.8 and 5 nm before and after EDTA modification and for the wall thickness, the values were 3.7 and 6.5 respectively.

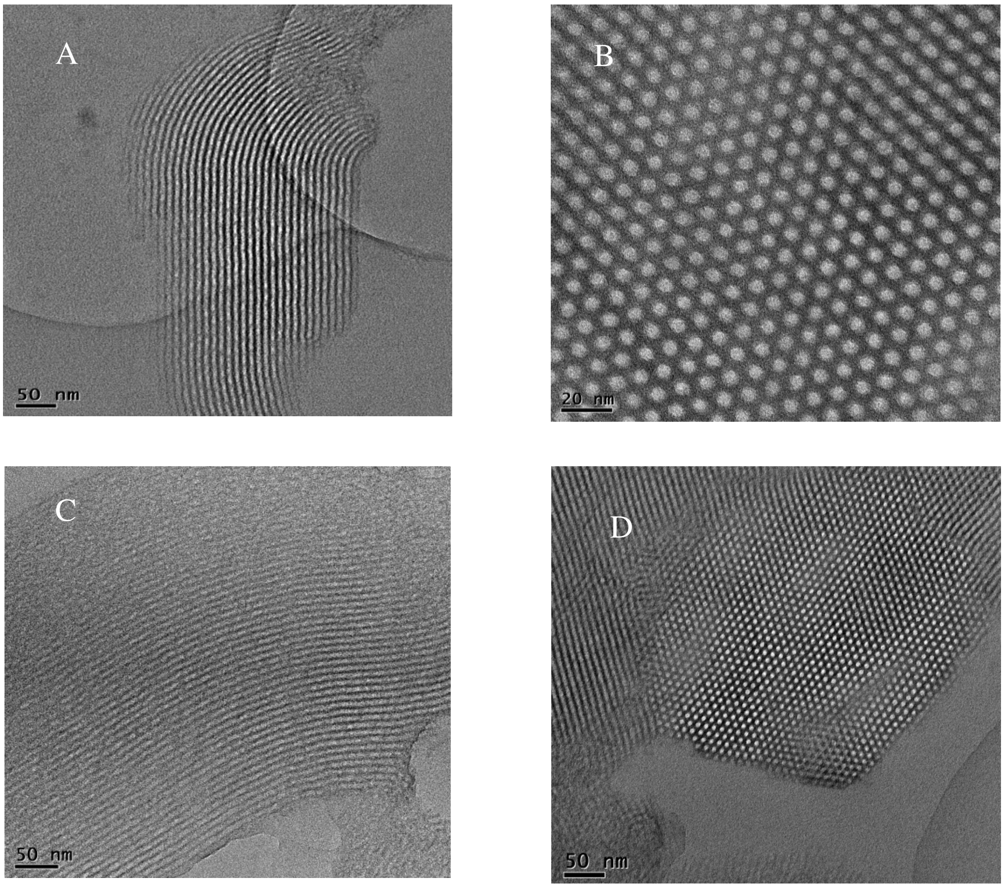

Figure IV.3.TEM micrographs of calcined SBA-15 before (A and B) and after EDTA modification (B and C) viewed from perpendicular and parallel directions

I.2.3. Nitrogen Adsorption-Desorption Isotherms

The surface area and the pore size were obtained from the nitrogen adsorption-desorption isotherms done at -196 °C. The calcined SBA-15 was characterized after each modification step. **Figure IV.4.a and b** shows the nitrogen adsorption-desorption isotherms and the pore size distribution respectively. The textural properties and pore characteristics are listed in **Table IV.1.** The specific surface area was evaluated using the BET equation, the mesopores and micropores volume from α_s-plots and the pore size distribution was calculated by BJH modified method (JKS method) from desorption branches of nitrogen isotherms. The total pore volume was taken at $P/P_0 = 0.995$.

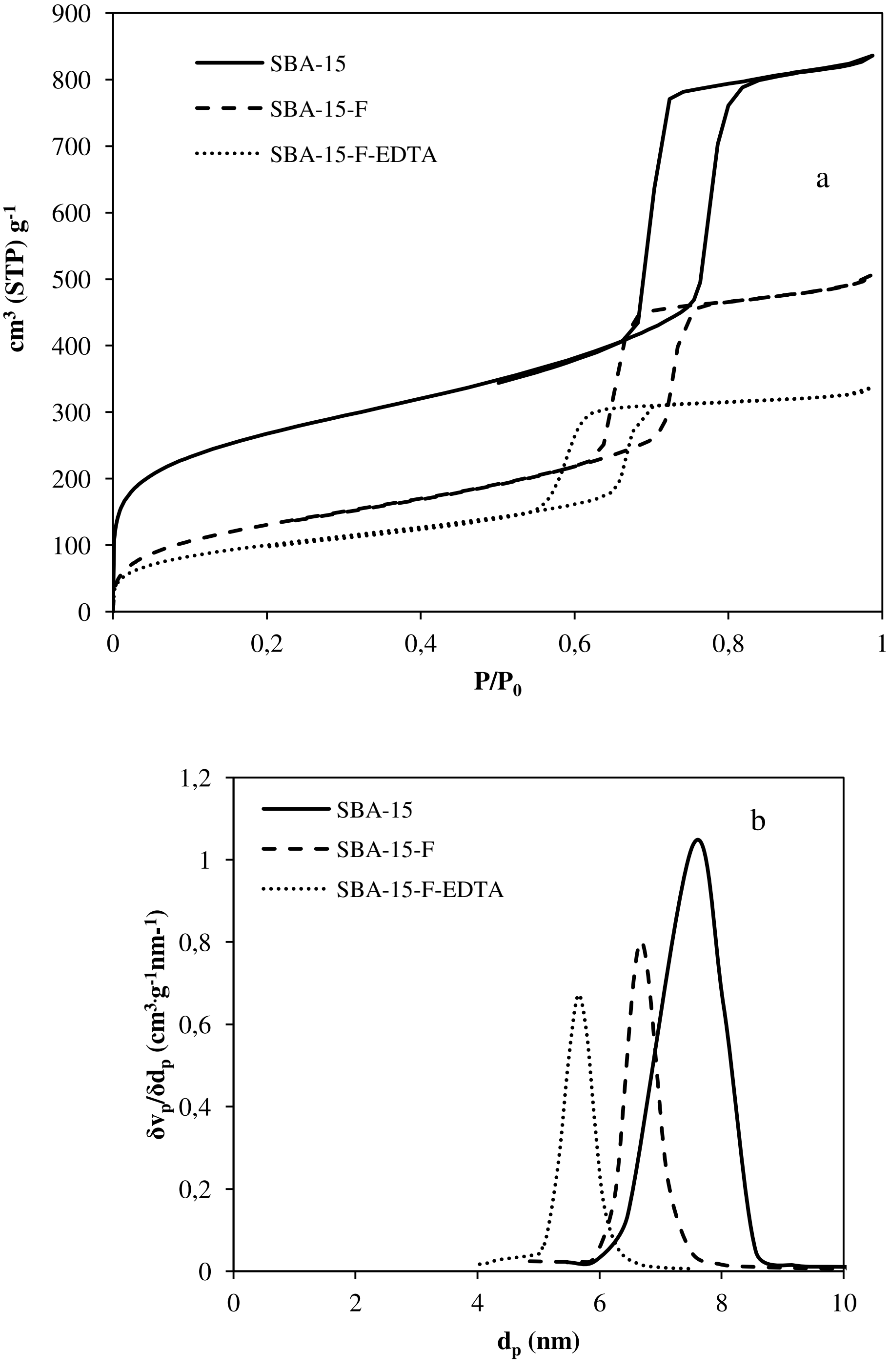

Figure IV.4. N_2 adsorption-desorption isotherms (a) and pore size distribution (b) of SBA-15, SBA-15-F, and SBA-15-F-EDTA.

Classical type IV isotherms, according to the IUPAC classification, were observed for all the samples. The hysteresis loops are of H1 type which indicates the presence of well defined cylindrical mesopores.

Table IV.1. Textural properties of SBA-15 before and after modification

sample	S_{BET}[a] ($m^2\ g^{-1}$)	pore size[b] (nm)	mesopore volume[c] ($cm^3\ g^{-1}$)	micropore volume[c] ($cm^3\ g^{-1}$)	wall thickness[d] (nm)
SBA-15	972	8	1.03	0.059	3.4
SBA-15-F	480	6.9	0.786	0	4.5
SBA-15-F- EDTA	360	5.2	0.522	0	6.2

[a] S_{BET} is the BET surface area deduced from the isotherm analysis in the relative pressure range of 0.05–0.15.
[b] pore diameter calculated using the BJH modified method.
[c] pore volume calculated by alpha-S method.
[d] Calculated by a_0 - pore size ($a_0 = 2d(100)/\sqrt{3}$)

After functionalization, the mesopores sizes and consequently the BET surface area as well as the mesopores volume decreased for all the samples whereas the wall thickness increases. Theses structural property variations result from the incorporation of the organic groups inside the pores. The residual micropore volume of SBA-15 sample becomes inaccessible after amino and EDTA modification samples.

I.3. Organic Groups Quantification and Characterization

I. 3.1. Thermogravimetric Analysis

The amount of grafted amino groups was determined by thermogravimetric analysis (**Figure IV.5**) while the amount of fixed EDTA was quantified with back titration.

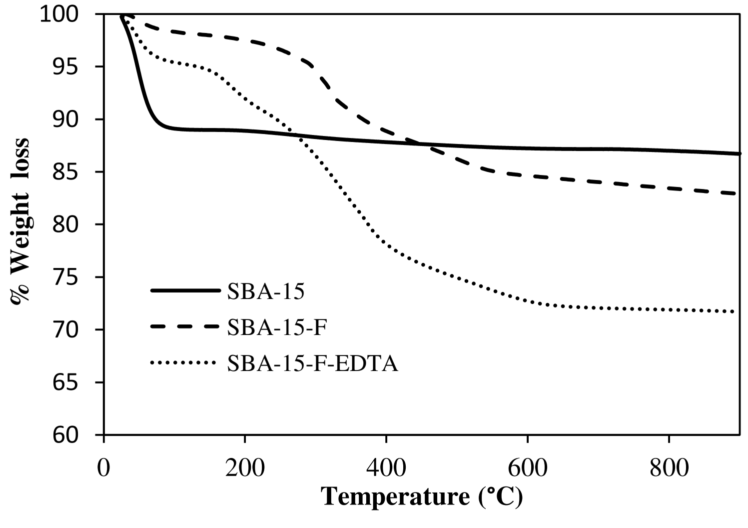

Figure IV.5. Thermogravimetric curves for SBA-15 and its modified counterparts

The weight loss observed below 200 °C is ascribed to water desorption. For pure silica samples, the weight losses between 200 and 900 °C are due to the dehydroxylation of the silicate networks. For functionalized samples, important weight losses are observed in this temperature range. Aminopropyl groups are degraded between 300 and 550 °C. EDTA decomposition occurs in the same temperature range as aminopropyl groups. So, only the quantification of the grafted amino groups will be done by ATD-ATG technique. Nevertheless, the thermograms show that EDTA molecules have been well incorporated since the mass loss increases after EDTA anchoring. EDTA quantification has been done by back titration of the carboxylate functions assuming that there are 3 free COOH for each EDTA molecule (the fourth is linked to the aminopropyl chain). The quantification of the aminopropyl groups and EDTA anchored molecules are reported on **Table IV.2**. Knowing that each EDTA molecule will react with also 1 molecule of $–NH_2$, the amount of EDTA fixed was only about the half of the available amino groups.

Table IV.2. Amino and EDTA content of the modified samples

	$C_{amino}{}^{a}$ (mmol g^{-1})	$C_{EDTA}{}^{b}$(mmol g^{-1})
SBA-15-F	2.4	0
SBA-15-F-EDTA	2.4	1.7

[a]Calculated by thermogravimetric analysis

[b]Calculated by back titration supposing that there are 3 free COOH for each EDTA molecule

I.3.2. Fourier Transform Infrared Spectroscopy (FT-IR)

All the presented IR spectra are normalized to 10 mg of dried material and the mesoporous silica have been pretreated at 450 °C under secondary vacuum whereas their functionalized counterparts at 200 °C in order to avoid organic moieties damages. The FTIR spectrum of calcined SBA-15 (**Figure IV.6**) shows typical bands at 3500–3750 cm^{-1} due to the presence of silanol groups [2]. After aminopropyl group grafting, the intensity of these bands decreases significantly with an increase of the bands characteristic of the grafted aminopropyl groups (SBA-15-F spectrum). The new bands can be attributed to both symmetric and asymmetric stretching of CH_2 groups (ν_{as} (CH_2) = 2933 cm^{-1}, ν_s (CH_2) = 2876 cm^{-1}) and of NH_2 vibration (ν_{as} = 3372 cm^{-1}, ν_s = 3300 cm^{-1}) [3]. A band at 1594 cm^{-1} that corresponds to NH_2 bending ($\delta_{as}(NH_2)$) was also identified [4]. EDTA anchoring on amino groups results in the disappearance of $–NH_2$ stretching vibration bands at 3372 and 3300 cm^{-1} [5]. In addition, the C–O asymmetrical stretching vibration of the carboxylate at 1675 cm^{-1} was observed. The band at 1744 cm^{-1} was attributed to -CO stretching vibration of carboxylic group [6]. The band at 1529 cm^{-1} refers to NH_3^+ vibration. The spectra of modified KIT-6 and SBA-16 (results not shown) are similar to those of SBA-15.

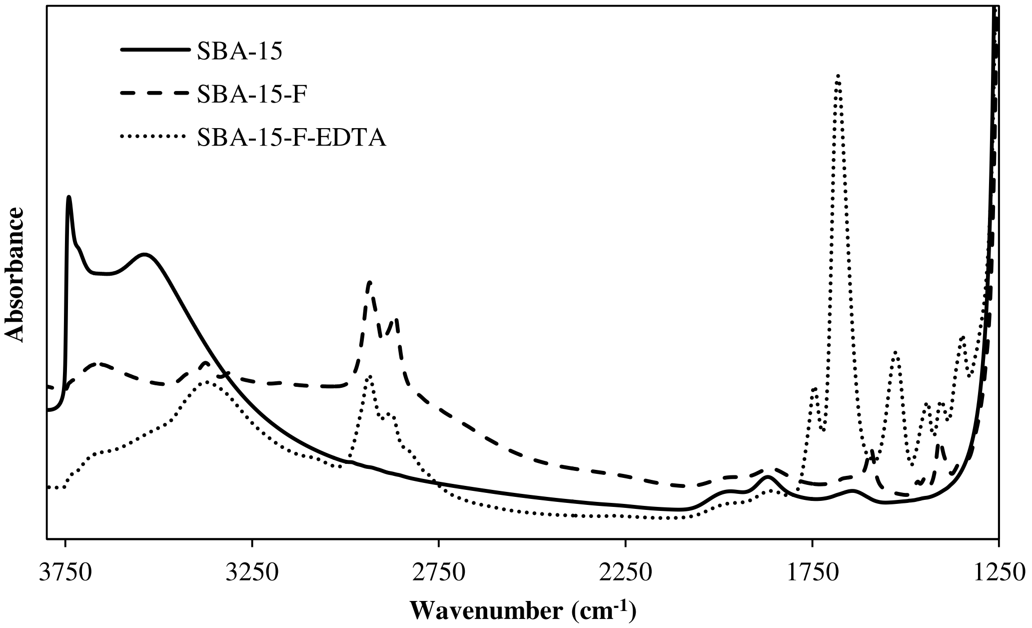

Figure IV.6. FTIR spectra for unmodified SBA-15 and modified SBA-15 silica

In order to increase the EDTA amount fixed, other available methods for amino functionalization (reflux, co-condensation, hydration of silica) were also performed. This will allow determining the most efficient route among them. Furthermore, it could be verified if by increasing the amount of amino groups it will be possible to enhance the amount of fixed EDTA.

I.4. Applying Other Modification Routes

Impregnation is not the unique post-synthesis treatment for grafting organosilane groups on mesoporous silica surface. Other protocol often used in the literature is co-condensation [7]. Amino functionalization through co-condensation was conducted to SBA-15. The experimental protocols for both functionalization routes are detailed in chapter II (§ II). Starting with co-condensation, the amino groups were introduced during the SBA-15 synthesis and the P123 template was removed by solvent extraction. The obtained SBA-15 was donated SBA-15-F-co. N_2 adsorption-desorption was performed to characterize the thus obtained material (**Figure IV.7**).

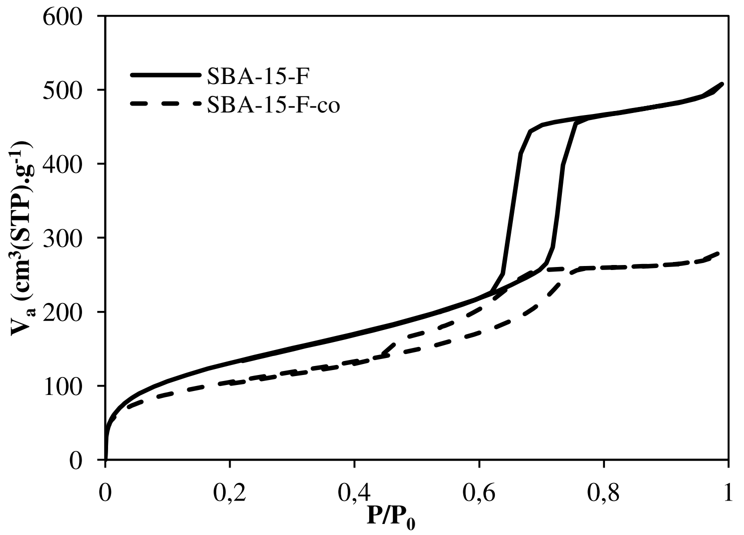

Figure IV.7. N_2 adsorption-desorption isotherms for SBA-15-F prepared by post-synthesis impregnation and SBA-15-F-co prepared by co-condensation

As it is clear in the above figure, the mesoporous channel order of the SBA-15-F-co is not as good as that of SBA-15-F. Also, since SBA-15-F has been calcined before impregnation, it will exhibit more hydrothermal stability compared to SBA-15-F-co. This property is important while applying such adsorbents for water treatments since high stability is needed. Moreover, only a small amount of EDTA could be fixed on SBA-15- F-co as it is shown on the thermogram below (**Figure IV.8**).

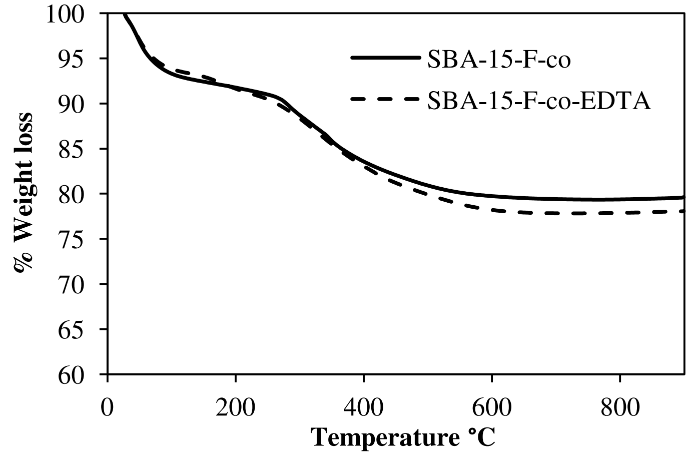

Figure IV.8. Thermogravimetric curves for SBA-15-co and SBA-15-co-F-EDTA.

These findings are due to the incorporation of amino groups in the SBA-15 walls. Thus they are not accessible for EDTA anchoring. Such incorporation results from the strong acidic conditions under which the synthesis was done. The aminopropyl of the organic precursor are protonated and can interact with both the surfactant and the silicate species [8].

The effect of hydration (denoted by –H) was also tested in order to determine if it can increase the amount of amino through increasing the amount of silanol groups by hydration before impregnation. Hydration was done by placing calcined SBA-15 in boiling water for three hours. Then the amount immobilized was calculated from thermogravimetric analysis along with the silanol content of the calcined parent SBA-15 starting from the weight loss for each sample. The obtained values are summarized in **Table IV.4**. The table analysis shows that as expected the SBA-15 silica hydration before amino grafting increases the silanol and the amino contents as well as EDTA content in case of sample SBA-15-F-H. The ordered structure was conserved after hydration as it is shown on the XRD patterns (**Figure IV.9**).

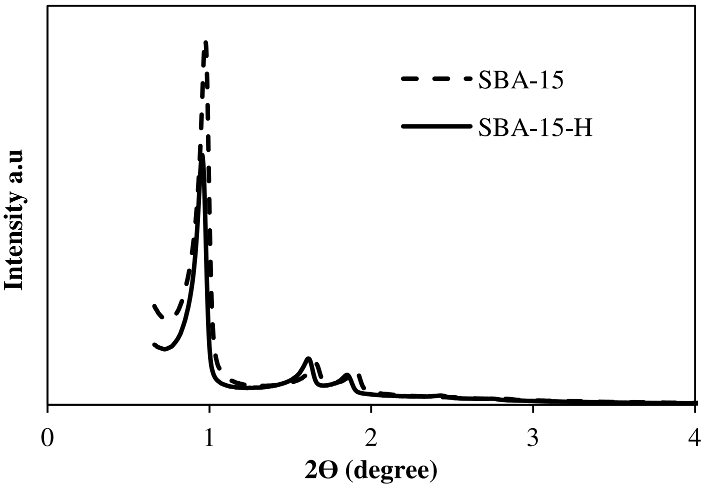

Figure IV.9. XRD patterns of SBA-15 before and after hydration

The nitrogen adsorption isotherms of SBA-15 before and after hydration are shown in **Figure IV.10**. The surface area and the pore volume decreased after hydration whereas the pore size slightly increased (**Table IV.3).** This proves that hydration has a negative effect on the structure order.

Table IV.3. Textural properties of SBA-15 before and after hydration

Sample	S_{BET} ($m^2\ g^{-1}$)	pore size (nm)	mesopore volume ($cm^3\ g^{-1}$)	micropore volume ($cm^3\ g^{-1}$)
SBA-15	774	7	1.09	0.022
SBA-15-H	548	7	0.842	0.043

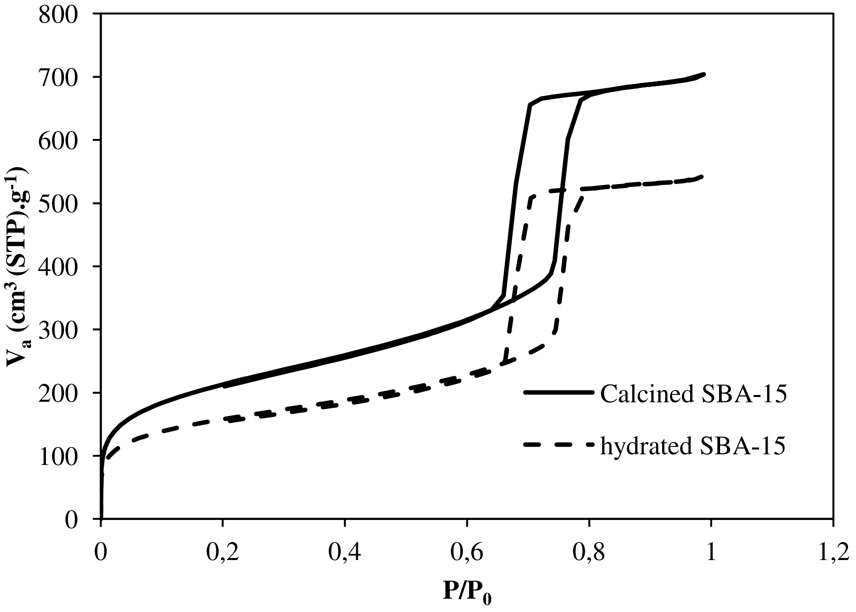

Figure IV.10. N_2 adsorption-desorption isotherms for SBA-15 before and after hydration

Table IV.4. Amino content for differently modified SBA-15 samples

Sample	Silanol content[a] (mmol g^{-1})	Amino content[a] (mmol g^{-1})	EDTA content[b] (mmol g^{-1})
SBA-15	2.50	2.40	1.70
SBA-15-F-co	-	2.45	0.140
SBA-15-F-H	3.70	2.80	2.06

[a] Calculated by thermogravimetric analysis
[b] Calculated by back titration

After characterizing all the above modified samples Cu^{2+} adsorption tests were performed in order to access the efficiency of each for the removal of copper. The results are illustrated in **Figure IV.11.** From these results, SBA-15 materials only modified with aminopropyl groups exhibit Cu^{2+} adsorption efficiency lower than those modified with EDTA. SBA-15-F-H and SBA-15-F showed the highest adsorption efficiency. Based on the above results, post synthesis impregnation was chosen as the method of modification for all the mesoporous materials used. Furthermore, no hydration will be performed before aminopropyl impregnation in order to avoid structural damage.

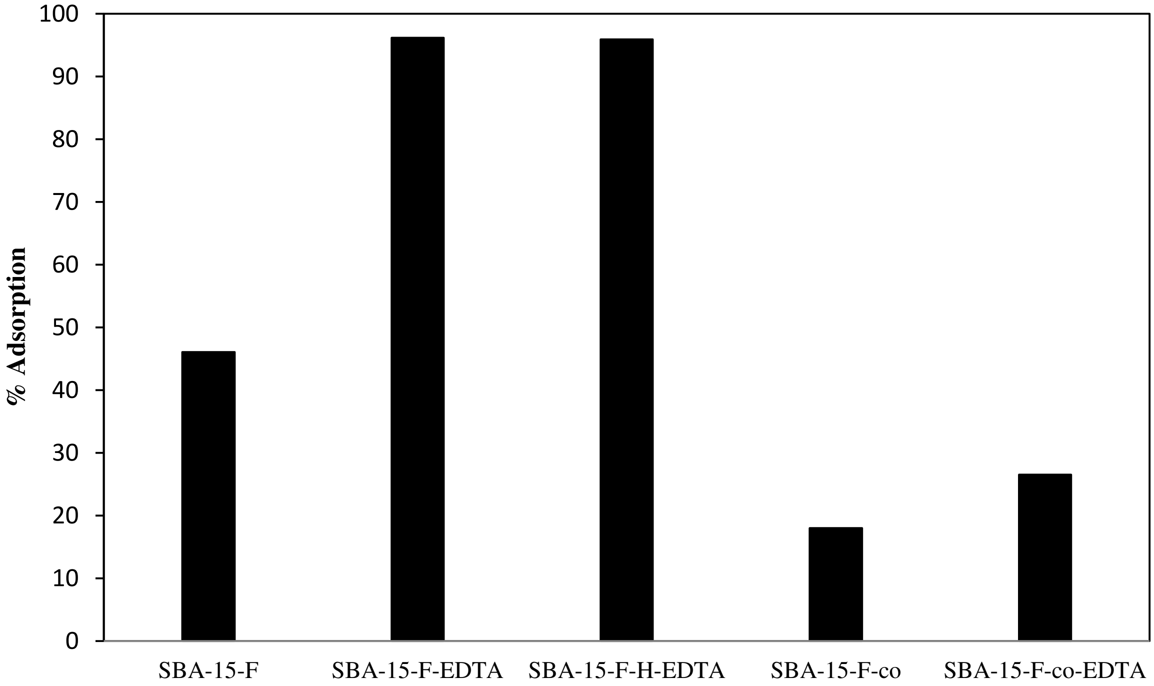

Figure IV.11. Cu^{2+} adsorption efficiencies for each of the modified SBA-15 samples (metal concentration, 0.47mmol L^{-1} at 25 °C)

According to the results shown on the **Table IV.4** above, it can be seen that the number of anchored EDTA molecule is always lower than the number of available amino groups. This can be explained by the reactivity of the grafted amino groups.

I.5. Reactivity of the Immobilized Amino Groups

In order to access the reactivity of the immobilized amino groups, a good knowledge of their availability and their interactions with the pore surface is necessary. The latter determines the amount of EDTA that will interact later with these amino groups and the behavior of the whole solid in aqueous medium. The chemical speciation and conformation of the amino functions strongly influence the reactivity and thus the possibility of achieving complex chemical systems in the mesopores [9]. The reactivity is directly related to the pH which is the main factor controlling the speciation of the different functional groups present on the surface of the adsorbent. Amino-modified SBA-15 has an isoelectric point in the range of 7-9, depending on the amino contents, while it is between 2-3 for as synthesized SBA-15 [10].When SBA-15-F interacts with acidic EDTA solution (pH = 4), ammonium functions are produced due to the protonation of NH_2 groups (Form II, **Figure IV.12**). Thus, the positive charge of the ammonium formed at low pH is counterbalanced by the anions of the solution (anions are not shown in Figure IV.12). Moreover, at very low pH values (< 2), the acidity of the ammonium groups is enhanced due to repulsion between their positive charges and the protonated silanol groups (Form I). For higher pH values (> 7) aminopropyl chain can interact with the silanol group in their vicinity forming an ion pair [$-NH_3^+ \, ^-O-Si-$] (Form III).

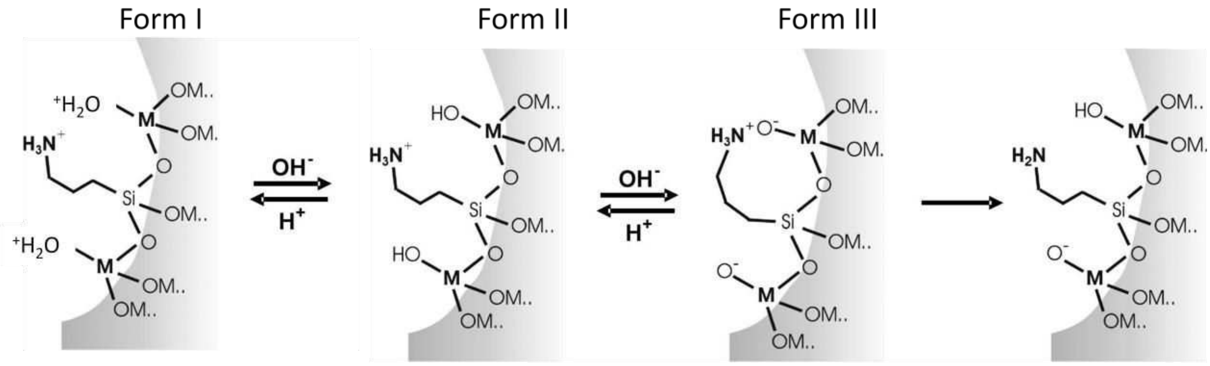

Figure IV.12. A Simplified scheme for the speciation and interactions of the Surface amino Groups, M are silicon atoms [11]

According to Calvo *et al.* [11] form II and III may be present in the solution at pH = 4. If the electrostatic interaction of the ion pair of form III is strong then this ammonium group is not available for EDTA anchoring. This could explain why the ratio of anchored EDTA /amino groups is lower than 1.

In addition to SBA-15, the efficiencies of two cubic 3D mesoporous silicates (KIT-6 and SBA-16) were further investigated. This will help understanding the effect of the mesoporous structure the heavy metals removal efficiency thus permits choosing the most promising adsorbent. The amino groups were anchored on the other two materials through impregnation since it was found to give the highest loading. As in the case of SBA-15, the obtained materials were also fully characterized before detailed adsorption experiments were done for the three modified silicates.

II. SBA-16 and KIT-6 Characterizations

After synthesizing SBA-16 and KIT-6 and modifying them by amino grafting followed by EDTA anchoring. All the prepared materials have been characterized by different techniques in order to investigate their physico-chemical properties and verify that the successive grafting treatments have not damaged the mesoporous silica structure.

II.1. Textural Properties

II. 1. 1 X-Ray Diffraction (XRD)

KIT-6 silica exhibits well-resolved hkl reflections, which correspond to (211), (220) and (332) reflections, which are characteristic of highly ordered 3-D cubic *Ia3d* structure (**Figure IV.13 a**). For SBA-16, the observed peaks correspond to (110) (211) and (220) planes which are characteristics of the cubic body centered structure (*Im3m*) (**Figure IV.13 b**). For all modified samples, the intensities of the peaks decreased after modification, which is might be caused by the pore filling effect of the adsorbents channels. From XRD patterns, the wall thickness have calculated and reported on the **Table IV.5** and the values will be discussed at the same time as the nitrogen physisorption results.

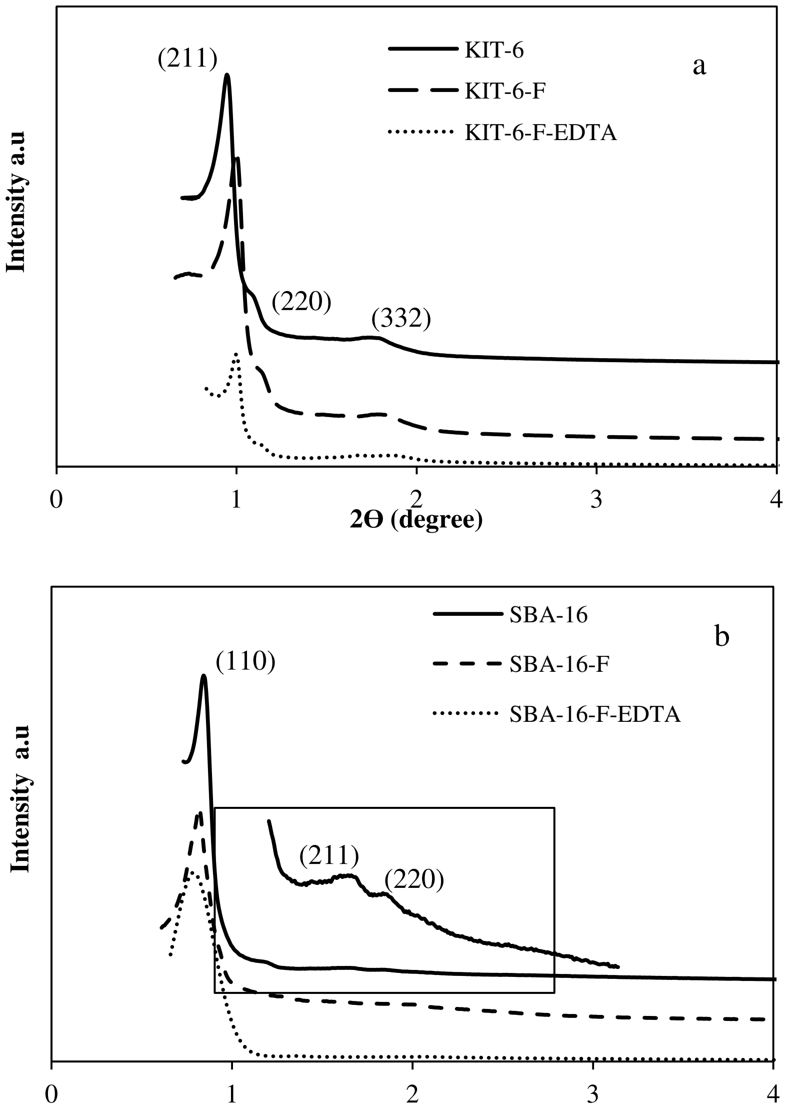

Figure IV.13. XRD patterns of KIT-6 (a) and SBA-16 (b) and before and after modification.

II.1.2. Transmission Electron Microscopy (TEM)

For KIT-6, TEM images showed the well-ordered cubic mesoporous structure materials before (**Figure IV.14. A and B**) and after EDTA modification (**Figure IV.14. C and D**). The pore sizes were 7.3 and 5 nm and the wall thickness 4.2 and 5.8 nm before and after EDTA modification.

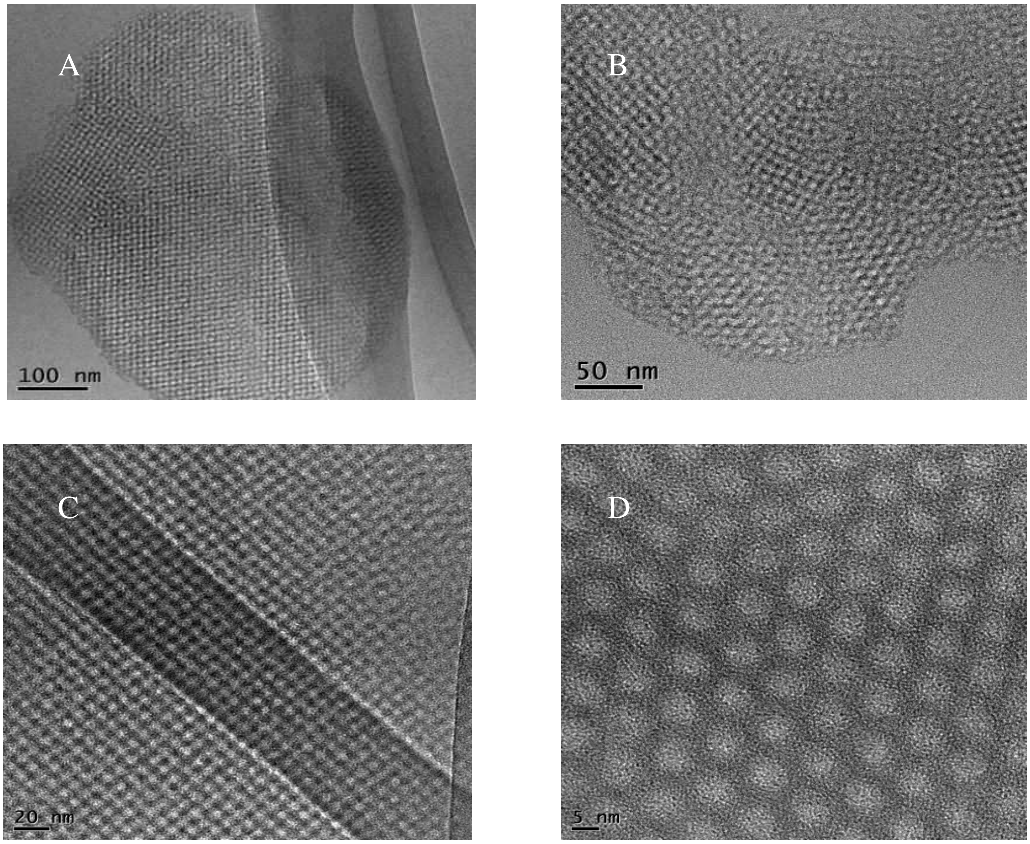

Figure IV.14. TEM micrographs of calcined KIT-6 before (A and B) and after EDTA modification (C and D) viewed from perpendicular and parallel directions.

Figure IV.15 shows the images of SBA-16 before (**Fig. IV.15.A and B**) and after EDTA fixation (**Figure IV.15. C and D**) viewed from different orientations. The arrays of the uniform cages are highly ordered demonstrating that SBA-16 has a 3D cubic structure which remained intact after modification. The pore sizes were 6.1 and 4.8 nm and the wall thickness 6 and 10 nm before and after EDTA modification respectively.

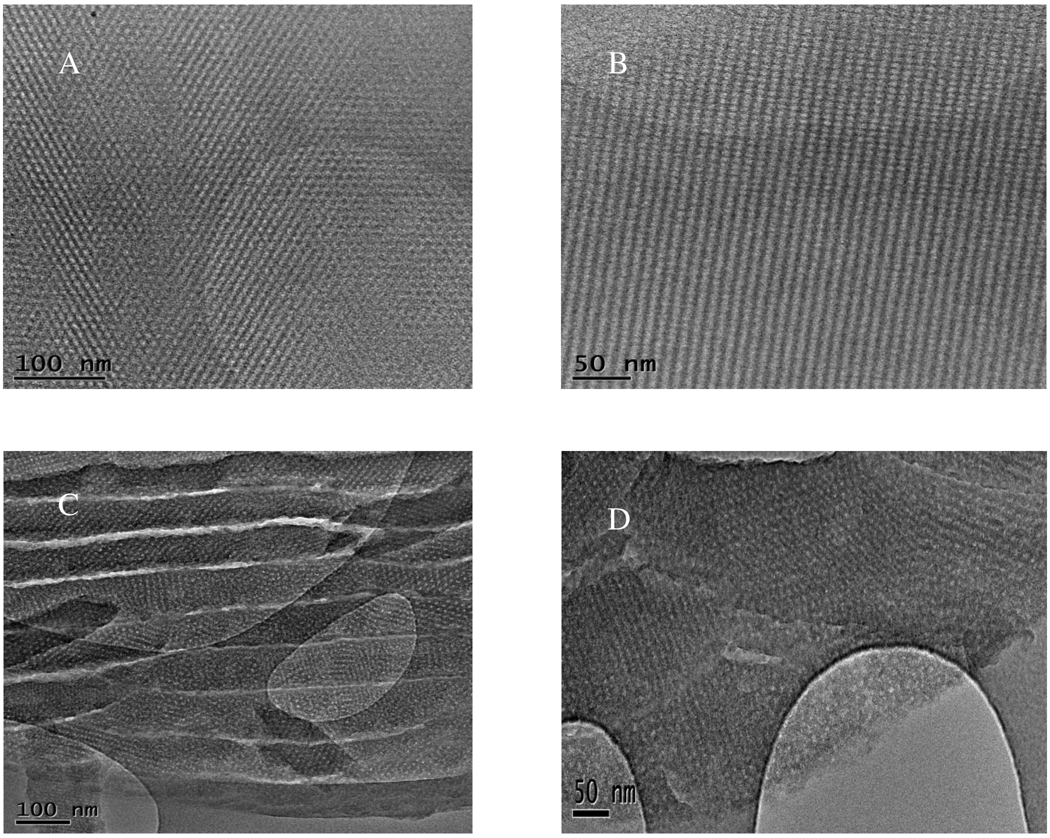

Figure IV.15. TEM micrographs of the calcined SBA-16 mesoporous silica materials before (A and B) and after EDTA modification (C and D).

II.3. Nitrogen Adsorption-Desorption Isotherms

Nitrogen adsorption-desorption isotherms for KIT-6 and SBA-16 are presented in **Figure IV.16.a,** and **IV.17.a** and the textural properties and pore characteristics are listed in **Table IV.5**. The specific surface area was also evaluated using the BET equation, the mesopores and micropores volume from α_s-plots and the pore size distribution was calculated by BJH modified method (JKS method) from desorption for KIT-6 and from adsorption for SBA-16 branches of nitrogen isotherms [12]. The total pore volume was taken at $P/P_0 = 0.995$. Classical type IV isotherms were observed for the two samples. However, KIT-6 silica exhibit H1 hysteresis loop like SBA-15. Even though H1 hysteresis loop indicates the presence of well defined cylindrical mesopores, this kind of hysteresis is also observed for KIT-6 and MCM-48 silica [13]. SBA-16 silica exhibits H2 hysteresis loop characteristic of cage like mesoporous structure with entrances much narrower than the diameter of the cage itself [14].

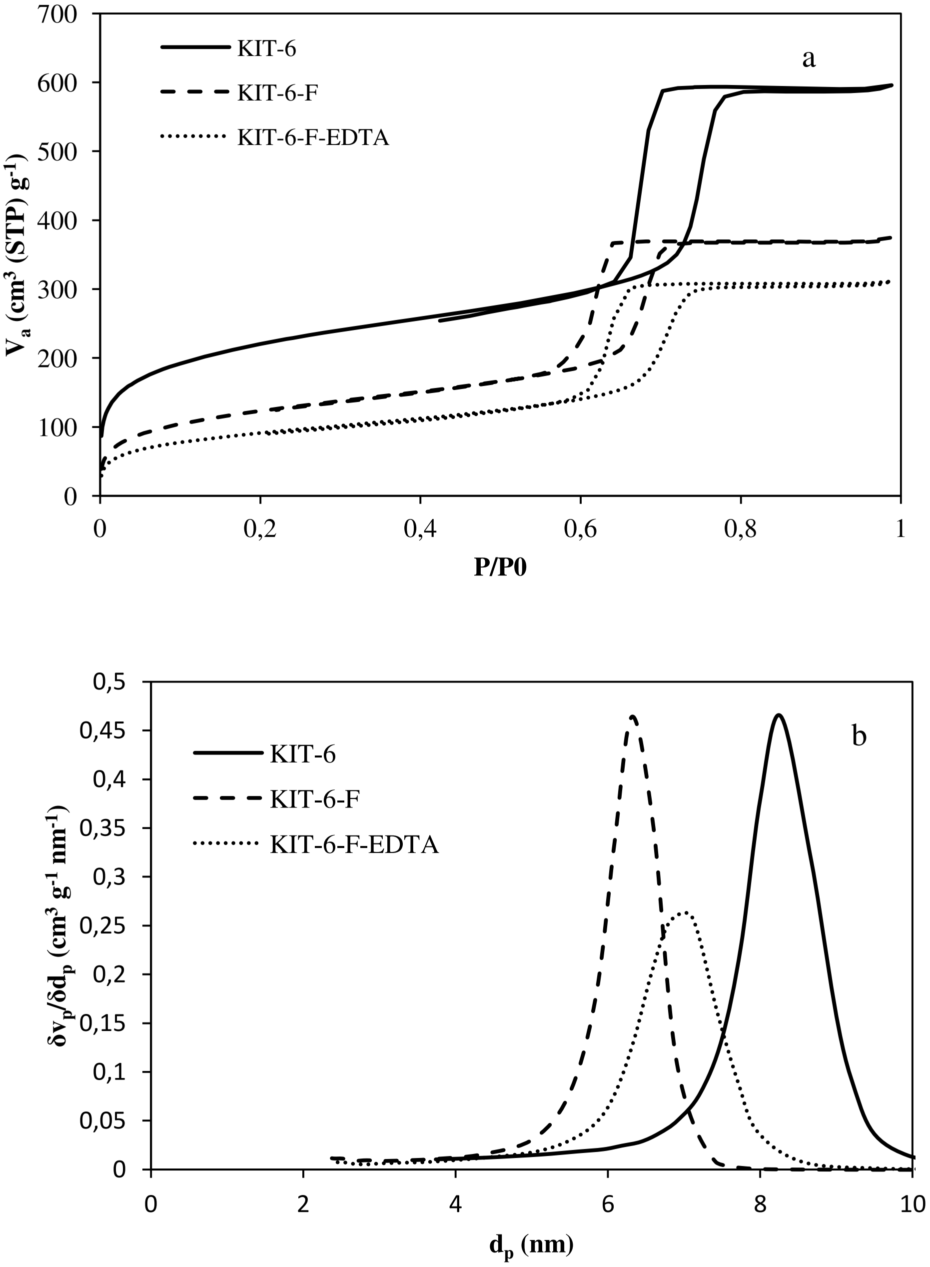

Figure IV.16. N_2 adsorption-desorption isotherms (a) and pore size distribution (b) of KIT-6, KIT-6-F, KIT-6-F-EDTA

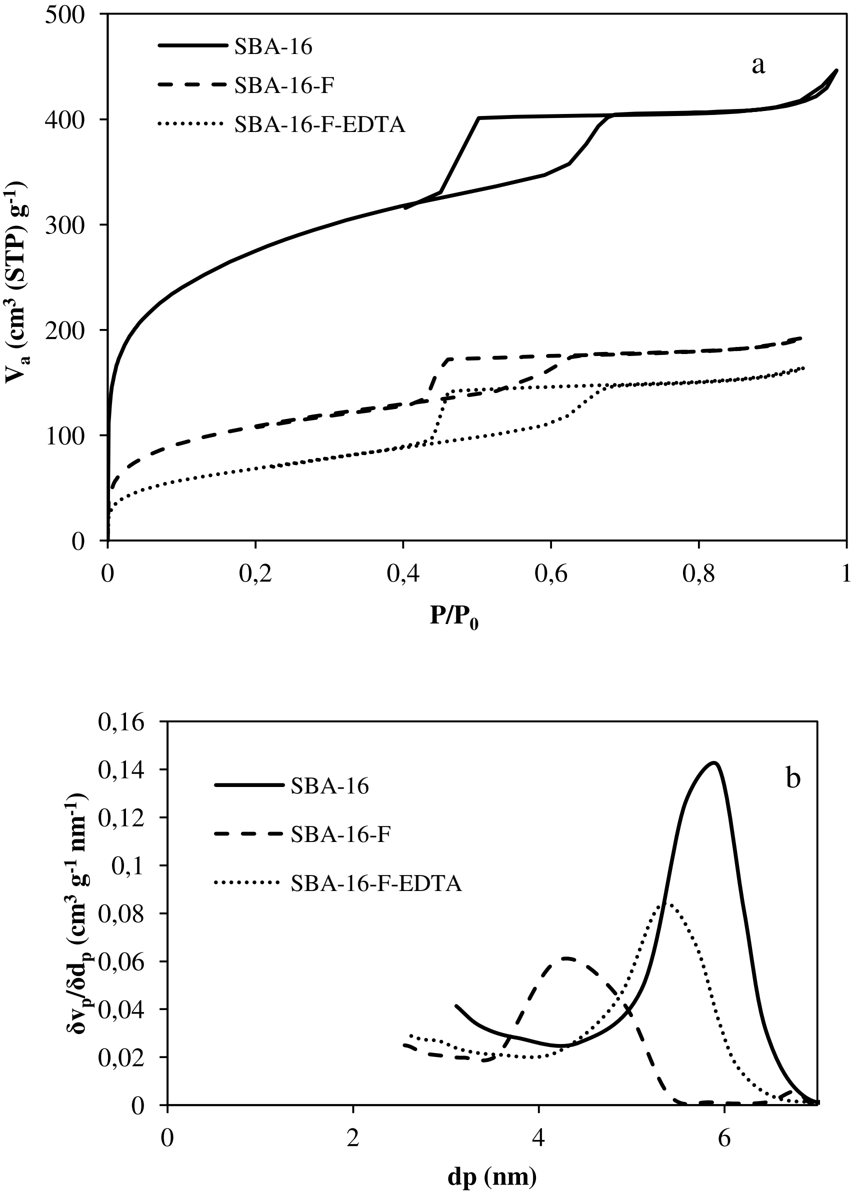

Figure IV.17. N_2 adsorption-desorption isotherms (a) and pore size distribution (b) of SBA-16, SBA-16-F and SBA-16-F-EDTA.

For KIT-6 and SBA-15 the capillary condensation occurs at relative pressure higher than for SBA-16 samples indicating that their mesopores are larger than those of SBA-16. These results of BJH distributions are illustrated on **Figure. IV.16.b** and **IV.17.b**. After functionalization, the mesopores sizes and consequently the BET surface area as well as the mesopores volume decreased for all the samples as was observed for SBA-15. The textural properties of KIT-6 and SBA-16 before and after modification are presented in **Table IV.5.** Pore size and pore volume decreased whereas wall thickness increased after modification due to the incorporation of the organic groups inside the pores. The pore size obtained from N_2 physisorption are in good agreement with the microscopy measurements.

Table IV.5. Textural properties of KIT-6 and SBA-16 before and after modification

sample	S_{BET}[a] ($m^2\ g^{-1}$)	pore size[b] (nm)	mesopore volume[c] ($cm^3\ g^{-1}$)	micropore volume[c] ($cm^3\ g^{-1}$)	wall thickness[d] (nm)
KIT-6	804	8	0.700	0.086	4
KIT-6-F	448	6	0.581	0	4.80
KIT-6-F-EDTA	331	7	0.482	0	6.10
SBA-16	885	6	0.44	0.164	6.70
SBA-16-F	398	4	0.226	0.022	11.3
SBA-16-F EDTA	246	5	0.195	0	10.2

[a] S_{BET} is the BET surface area deduced from the isotherm analysis in the relative pressure range of 0.05–0.15.

[b] pore diameter calculated using the BJH modified method.

[c] pore volume calculated by alpha-S method.

[d] Calculated by $\sqrt{3}a_0/2 - d\text{pore}$ ($a_0 = d(110)^* \sqrt{2}$) for SBA-16 and $a_0/2 - d\text{pore}$ ($a_0 = 6^{1/2}d(211)$) for KIT-6.

II.4. Organic Content Calculation after EDTA Modification

Thermogravimetric analyses were conducted under air for all samples **(Figure IV.18)**.

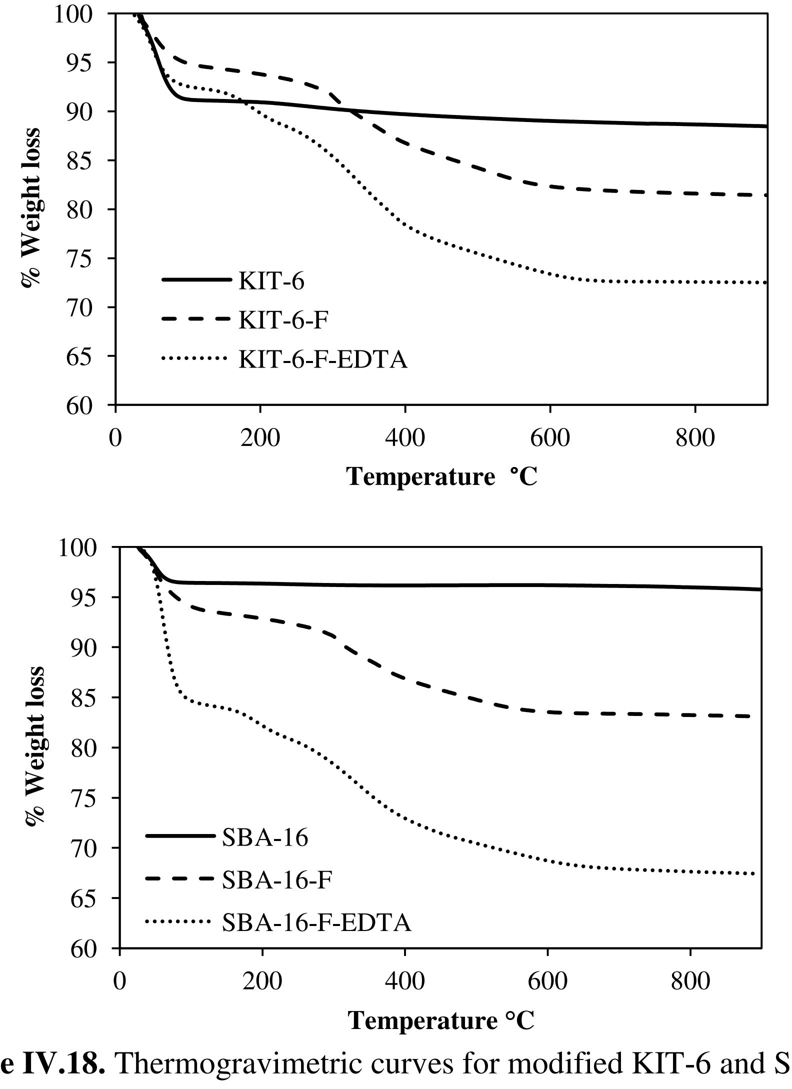

Figure IV.18. Thermogravimetric curves for modified KIT-6 and SBA-16.

As for SBA-15, the weight loss below 200 °C is due to the physisorbed water desorption. For pure silica samples, the weight losses between 200 and 900 °C are due to the dehydroxylation of the silicate networks. For functionalized samples, important weight losses are observed in this temperature range. Aminopropyl groups are degraded between 300 and 550 °C. EDTA decomposition occurs in the same temperature range as aminopropyl groups. The quantification results of the grafted amino groups along with the amount of free carboxylic groups are reported on **Table IV.6**. The number of aminopropyl groups grafted and consequently EDTA is lower for SBA-16 than for KIT-6 and SBA-15 certainly due to the smaller pore sizes of SBA-16 silica material and to their ink-bottle shape which makes the diffusion of organic molecules inside the pores more difficult.

Table IV.6. Amino and EDTA content of the modified samples

	$C_{amino}{}^{a}$ (mmol g^{-1})	$C_{EDTA}{}^{b}$(mmol g^{-1})
KIT-6-F	2.10	0
KIT-6-F-EDTA	2.10	1.40
SBA-16-F	1.50	0
SBA-16-F-EDTA	1.50	0.800

[a]Calculated by thermogravimetric analysis
[b]Calculated by back titration

III. Heavy Metals Adsorption Tests

III.1. Contact Time Effect

Metal ions sorption capacities were determined as a function of time to determine an optimum contact time for the sorption of heavy metal ions on sorbent. In this way, Cu^{2+} adsorption has been carried out for the three modified silica. For KIT-6 and SBA-15, equilibrium was reached quickly (within the first 20 min) and the amount of Cu^{2+} removed from the solution was much higher than for SBA-16 (**Figure IV.19**). The obtained results are due to the fact that KIT-6 and SBA-15 have more EDTA molecules and are more accessible for hydrated Cu^{2+} complexes than those immobilized on SBA-16.

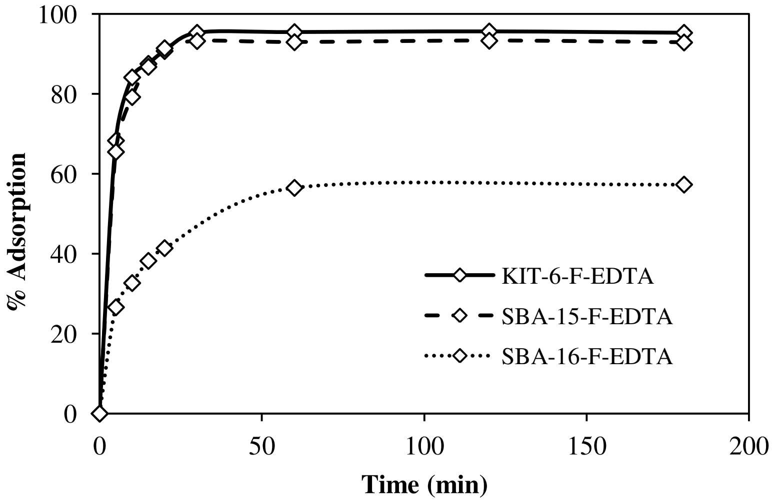

Figure IV.19. Effect of contact time of Cu^{2+} adsorption (metal concentration, 0.47mmol L^{-1} at 25 °C)

Based on the results above, the study for the other metals has only been performed on SBA-15 and KIT-6.

III.2. Mass Effect

The mass of SBA-15-F-EDTA was varied between 10 mg and 60 mg in order to optimize the mass of adsorbent for batch adsorption experiments in 20 mL Cu^{2+} solution. **Figure IV.20** shows the adsorbent dose effect on Cu^{2+} adsorption.

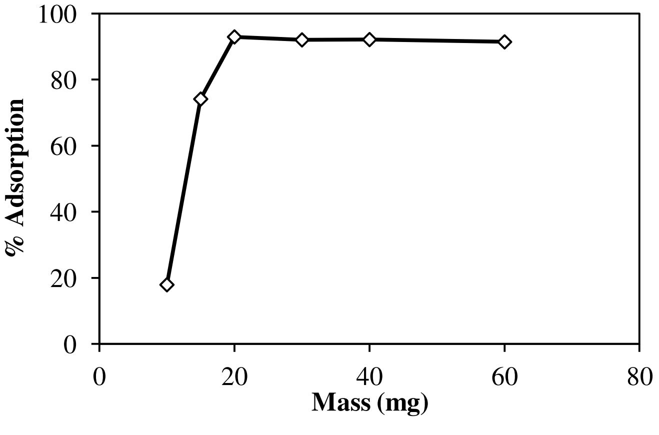

Figure IV.20. Effect of mass on the adsorption of Cu^{2+} on EDTA modified SBA-15 silica (pH = 5.8, t= 2 h at 25 ℃ and $[Cu^{2+}]_i$ = 0.47 mmol L^{-1})

The obtained results verified that metal ions removal depends on the adsorbent dose, since adsorption increased as mass increased to reach its maximum at 20 mg then it remained constant. This might be due to the fact that the concentration of Cu^{2+} in the remaining solution is too low to induce cation migration to the solid surface [15]. So, 20 mg of solid was found to be the more suitable for batch experiments. So all the batch experiments were done for m/V = 20 /20 (mg/mL) for all the mesoporous EDTA modified silica.

III.3. pH Effect

The solution pH is an important factor that affects metal ions adsorption since it controls metal ions speciation as well as the surface charge of the adsorbent [16].

The effect of initial pH on heavy metals cations adsorption is investigated and the results are shown in **Figures IV.21**. The adsorption rates increase when the pH of the solution was increased from 2 to 6 for all the metal ions. Above pH 6, lead and nickel adsorption rates reach a plateau whereas they decreased for copper and cadmium. The observed curve shapes are typical of those found in the literature [17-18-19] for heavy metal adsorbed on various mineral supports.

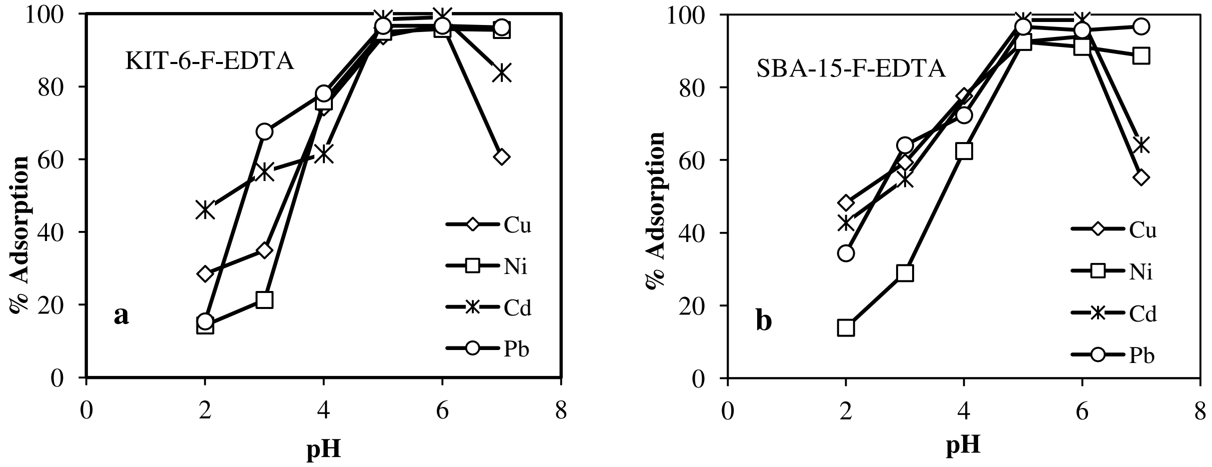

Figure IV.21. Effect of pH on Cu^{2+}, Ni^{2+}, Cd^{2+} and Pb^{2+} adsorption onto KIT-6- F-EDTA (a) and SBA-15- F-EDTA (b) (metal concentration, 0.47mmol L^{-1} at 25 °C)

At low pH values equals to 2 and 3, the EDTA acid groups are under carboxylic form which is not favorable for metallic cation chelation ($pKa_1 = 0$, $pKa_2 = 1.5$, $pKa_3 = 2$, $pKa_4 = 2.66$). The pKa values for the EDTA amino groups are $pKa_5 = 6.16$ and $pKa_6 = 10.24$. Furthermore, the free amino groups grafted on the mesoporous walls are also protonated which induces positive charge repulsions. For pH values higher than 3, EDTA molecules are on carboxylate form resulting in the increase of metallic ions complexation. Above pH 6, precipitation reaction of metal cation as hydroxide competes with the complexation reaction (**Figure IV.22**).

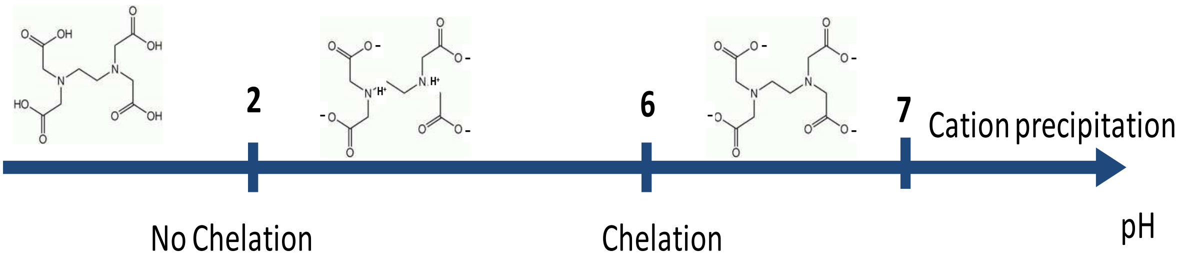

Figure IV.22. Effect of pH on EDTA

Copper and cadmium hydroxides are formed above pH 6 [15-20] whereas nickel and lead hydroxide precipitations begin at pH 8 [21-22]. This explains why a longer plateau is observed on the curves for these two cations. So, from these results, the pH value of 5.8 has been chosen to carry out adsorption experiments for all the heavy metal cations.

III.4. Adsorption Kinetics

The kinetics experimental data have first been analyzed by the non linear pseudo first and second order models. The kinetic parameters as well as the correlation coefficients (R^2) and the observed experimental equilibrium capacities are reported in **Table IV.7** for KIT-6-F-EDTA and in **Table IV.8** for SBA-15-F-EDTA samples. The obtained results show that Pb^{2+}, Cu^{2+}, Cd^{2+} and Ni^{2+} adsorption on EDTA modified silica followed the pseudo-second order kinetic model for KIT-6-F-EDTA (**Figure IV.23**) and SBA-15-F-EDTA (**Figure IV.24**). This suggests that the rate of Pb^{2+}, Cu^{2+}, Cd^{2+} and Ni^{2+} ions adsorption depends mainly on the concentration of ions at the adsorbent surface which will determine the amount adsorbed at equilibrium [23].

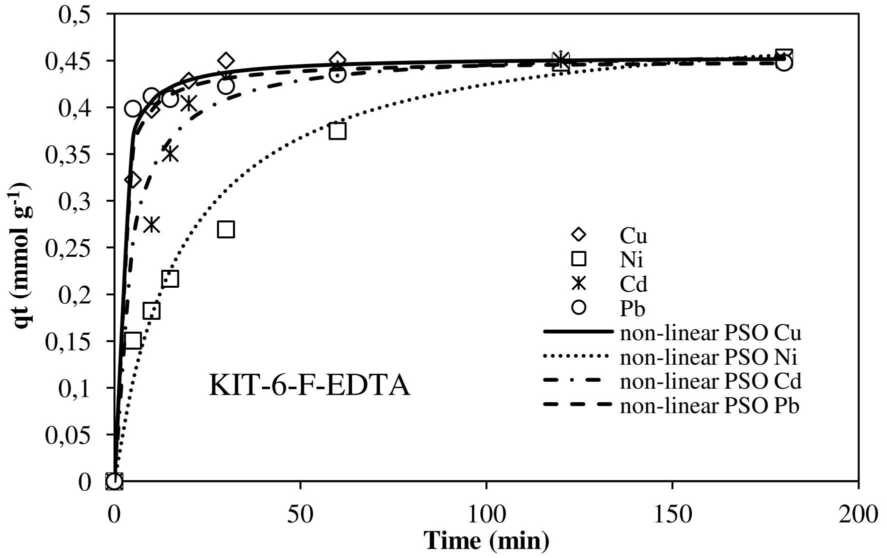

Figure IV.23. Cu^{2+}, Ni^{2+}, Cd^{2+} and Pb^{2+} sorption kinetics on KIT-6-F-EDTA samples fitted by non-linear pseudo-second order model (C_i = 0.47mmol L^{-1}, pH 5.8 at 25 °C)

Table IV.7. Comparison of the first and the second order kinetic models for KIT-6-F-EDTA

		First order kinetic model			Second order kinetic model			
	q_e^{exp} (mmol g^{-1})	k_1 (min^{-1})	q_e^{cal} (mmol g^{-1})	R^2	k_2 (g mmol^{-1} min^{-1})	q_e^{cal} (mmol g^{-1})	h (mmol g^{-1} min^{-1})	R^2
Cu^{2+}	0.451	0.050	2.10	0.914	1.84	0.454	0.380	0.999
Ni^{2+}	0.453	0.015	1	0.975	0.110	0.500	0.030	0.995
Cd^{2+}	0.450	0.020	0.355	0.873	0.538	0.563	0.170	0.999
Pb^{2+}	0.447	0.010	3.60	0.977	6.89	0.450	1.30	0.999

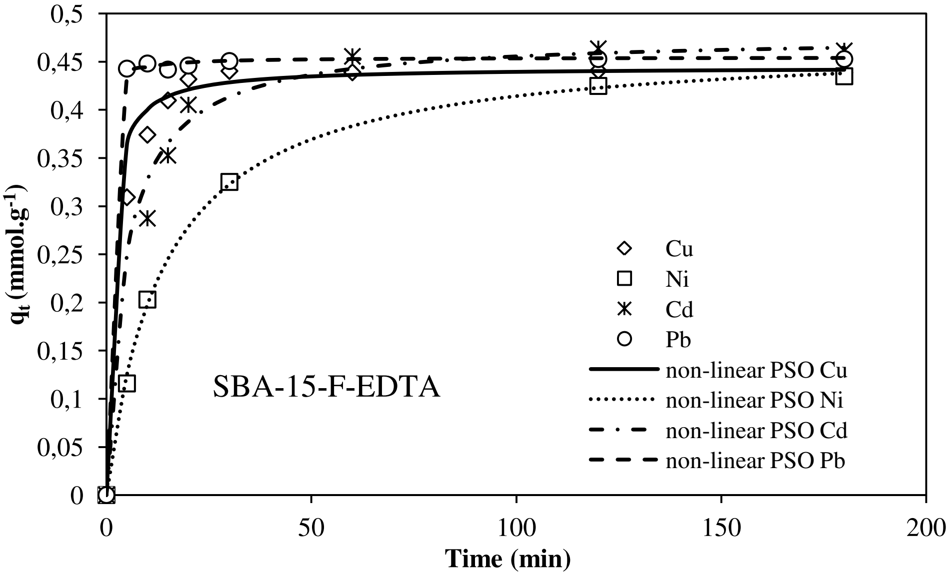

Figure IV.24. Cu^{2+}, Ni^{2+}, Cd^{2+} and Pb^{2+} sorption kinetics on SBA-15-F-EDTA samples fitted by non-linear pseudo-second order model (C_i = 0.47mmol L^{-1}, pH 5.8 at 25 °C)

Table IV.8. Comparison of the first and the second order kinetic models for SBA-15-F-EDTA

		First order kinetic model			Second order kinetic model			
	q_e^{exp} (mmol g^{-1})	k_1 (min^{-1})	q_e^{cal} (mmol g^{-1})	R^2	k_2 (g mmol^{-1} min^{-1})	q_e^{cal} (mmol g^{-1})	h (mmol g^{-1} min^{-1})	R^2
Cu^{2+}	0.440	0.212	1.90	0.979	2.05	0.443	0.402	0.999
Ni^{2+}	0.434	0.030	3.15	0.992	0.150	0.470	0.033	0.999
Cd^{2+}	0.456	0.060	52.2	0.975	0.460	0.476	0.104	0.999
Pb^{2+}	0.453	0.064	16.5	0.759	9.52	0.452	1.95	0.999

The initial sorption rate (*h* values) are not affected by the textural properties of the adsorbent. Since for the both adsorbents, *h* values decrease as follows: $Pb^{2+} > Cu^{2+} > Cd^{2+} > Ni^{2+}$. This selectivity does not depend on the equilibrium constant of complexing with EDTA or the hydrated radius of each metal as it was usually considered in the literature [24] but it is mainly related to the exchange kinetics between the ligand and the aqueous metal ions which is generally expressed as follows [25]:

$$(Me(H_2O)_m)^{n+} + L \underset{2}{\overset{1}{\rightleftharpoons}} (Me(H_2O)_{m-1}L)^{n+} + H_2O$$

Where L represents H_2O or other ligand such as EDTA molecule, Me is the metal ion. The exchange velocity (k_$_w$) of water molecules with metallic ions (**Table IV.9**) is the fundamental step controlling the rate of ions removal from water. k_$_w$ values are weakly related to the nature of the ligands so the velocity constants of metal ions with organic ligands are comparable to these calculated for the exchange with k_$_w$ values [26] in aqueous phase are in their hydrated forms and those with higher k_$_w$ values loses water molecules more easily thus interacting more favorably with organic ligands present. Therefore the properties of the metal ions affect adsorption efficiency. From **Table IV.9**, it can be observed that h values are directly related to k_$_w$ values and not to log(β) values which are the logarithm of the complexation constant (β) with EDTA . So, the weak k_$_w$ value for Ni ions is certainly responsible for its low adsorption rate. **Figure IV.25** shows the linear relationship between k_$_w$ and initial sorption rate *h*.

Table IV.9. values for the complexation constant metal-EDTA chelates [27]

Cation	log(β)
Ni^{2+}	20.11
Cd^{2+}	18.10
Cu^{2+}	20.49
Pb^{2+}	19.71

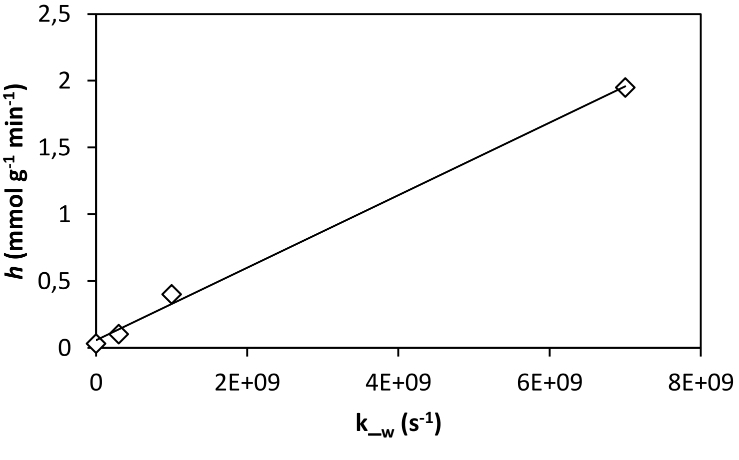

Figure IV.25. Correlation between the sorption rate h and the exchange velocity (k_$_w$)

III.5. Adsorption Isotherms

The adsorption isotherms for the two modified EDTA silica are shown in **Figure IV.26 and 27**. These isotherms are L shape in Giles classification [28] and exhibit a sharp initial slope indicating that the material is very efficient at low metal concentrations. Then, a plateau is observed indicating that the maximal adsorbent capacity is reached and the isotherms were well fitted by Langmuir equation. The corresponding K_L and q_{max} Langmuir parameters have been reported in **Table IV.10**.

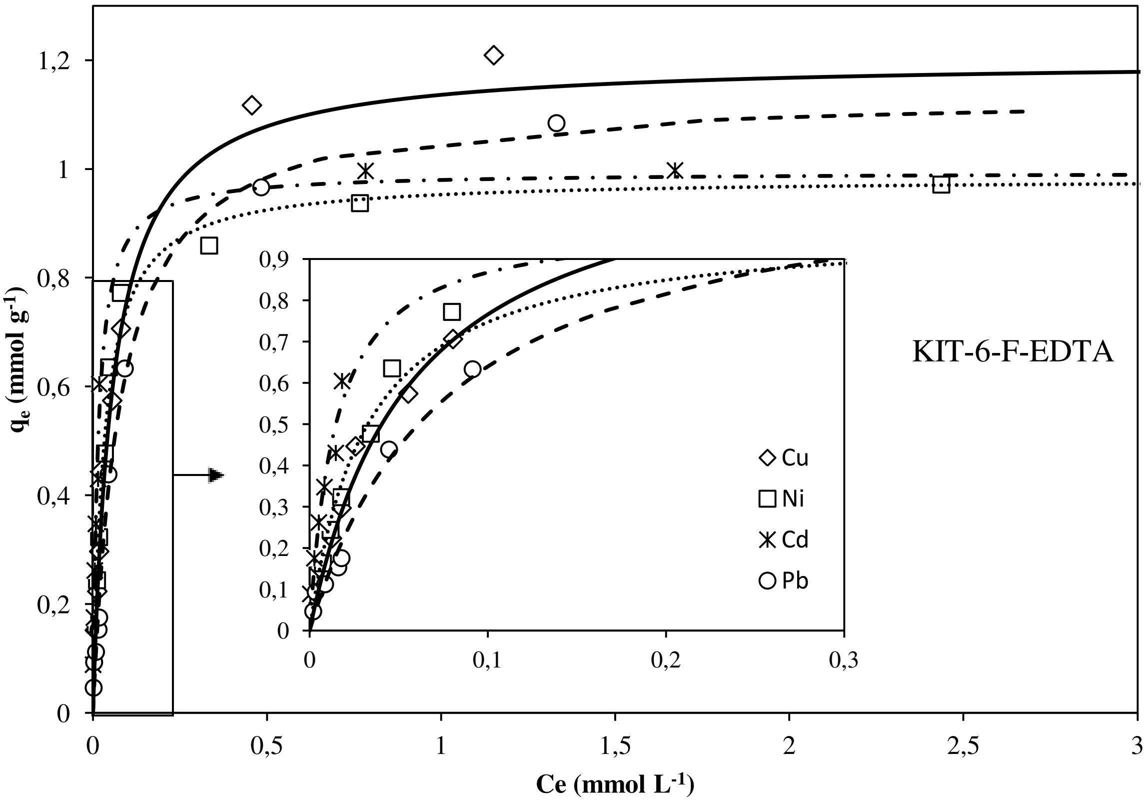

Figure IV.26. Cu^{2+}, Ni^{2+}, Cd^{2+} and Pb^{2+} adsorption isotherms of KIT-6-F-EDTA fitted by Langmuir

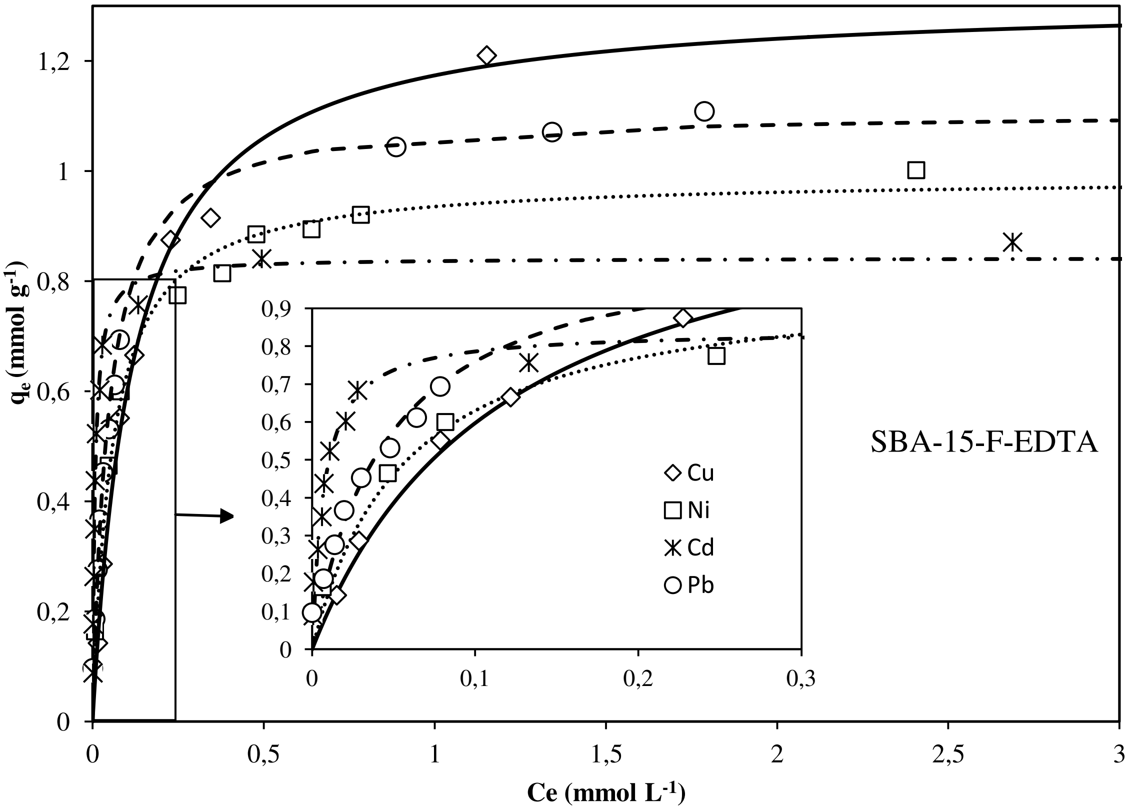

Figure IV.27. Cu^{2+}, Ni^{2+}, Cd^{2+} and Pb^{2+} adsorption isotherms of SBA-15-F-EDTA fitted by Langmuir

Table IV.10. Langmuir parameters for adsorption isotherms

Metal	SBA-15-F-EDTA			KIT-6-F-EDTA		
	q_{max} (mmol g^{-1})	K_L (L $mmol^{-1}$)	R^2	q_{max} (mmol g^{-1})	K_L (L $mmol^{-1}$)	R^2
Cu^{2+}	1.39	7.10	0.992	1.23	19.7	0.997
Ni^{2+}	1	16.3	0.991	0.980	28.7	0.992
Cd^{2+}	1.10	41.1	0.992	1.14	41	0.994
Pb^{2+}	1.12	20.8	0.996	1.15	15.7	0.998

The maximum sorption capacities for both adsorbents are very close and are directly related to the amount of EDTA immobilized on the adsorbents. This result indicates that EDTA moieties immobilized on a mesoporous matrix are able to form 1:1 complexes with Pb^{2+}, Cu^{2+}, Cd^{2+} and Ni^{2+} ions. Approximately, all the EDTA grafted (1.4 mmol g^{-1}) molecules formed complexes with Cu^{2+} ions. However, the values obtained for the other metals were smaller which means that q_{max} depends also on the metal nature as it was discussed before since the exchange velocity k_$_w$ affects directly the adsorption process.

Moreover, R_L which is of a dimensionless separation factor is an essential characteristic of the Langmuir equation can be expressed as follows [29]:

$$R_L = \frac{1}{1 + K_L C_0}$$

where C_0 is the highest initial solute concentration. The obtained R_L values for both adsorbents are listed in **Table IV.11**.

Table IV.11. R_L values for SBA-15-F-EDTA and KIT-6-F-EDTA

	R_L	
	SBA-15-F-EDTA	KIT-6-F-EDTA
Cu^{2+}	0.022	0.011
Ni^{2+}	0.007	0.007
Cd^{2+}	0.007	0.007
Pb^{2+}	0.016	0.021

The obtained results verified that the adsorption process of all the four metal ions is favorable on the two studied adsorbents since all the R_L values are between 0 and 1.

III.6. Adsorption Thermodynamics

The temperature effect on heavy metal ions adsorption on SBA-15-F-EDTA was studied. The amount of metal ions adsorbed increased with temperature as it is shown in **Figure IV.28**.

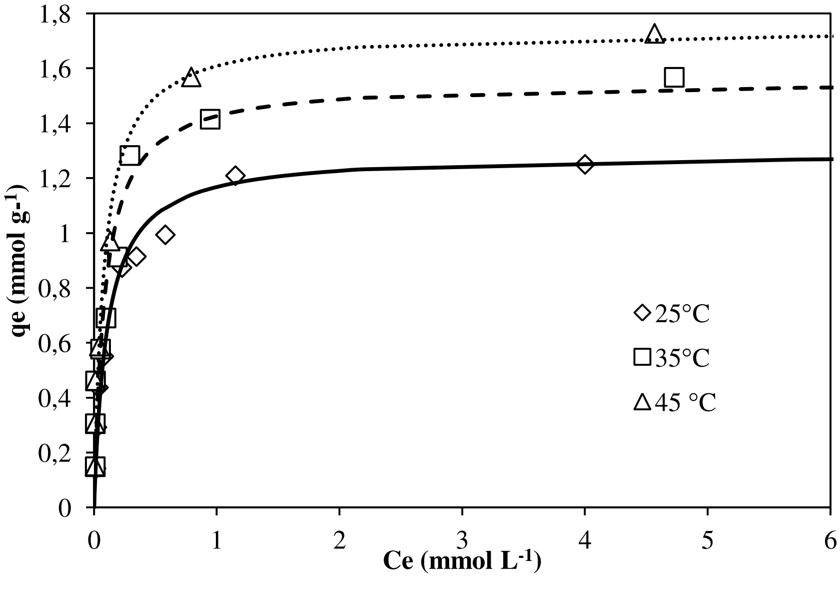

Figure IV.28. Cu^{2+} adsorption on SBA-15-F-EDTA at different temperatures (pH = 5.8)

The thermodynamic parameters were calculated from the plot of the distribution coefficient values K_d versus temperatures **Figure IV.29**. K_d values were obtained by plotting ln (q_e/C_e)

versus qe and extrapolating q_e to 0 [30]. It was found that K_d increased as the temperature increased revealing the endothermic nature of the adsorption process.

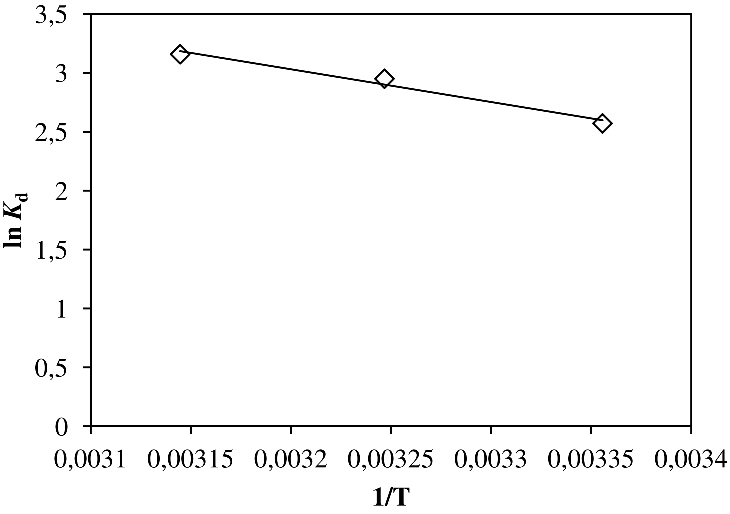

Figure IV.29. Plots of ln K_d versus $1/T$ for the adsorption of Cu^{2+} on SBA-15-F-EDTA

The thermodynamic parameters obtained for the adsorption processes are listed in **Table IV.12**. ΔH° positive values suggest the endothermic nature of the adsorption as it was mentioned before. Such endothermic behavior may be related to the chemisorptions nature of the adsorption process [31].

Table IV.12. Thermodynamic parameters for Cu^{2+} adsorption on SBA-15-F-EDTA

Metal	ΔH° ($kJ\ mol^{-1}$)	ΔS° ($J\ K^{-1}\ mol^{-1}$)	T (K)	ΔG° ($kJ\ mol^{-1}$)	R^2
Cu^{2+}	23.19	99.22	298	-6.37	0.978
			308	-7.55	
			318	-8.35	

Concerning the Gibb energy, ΔG° values are negative indicating that the adsorption process is spontaneous. These values increase with temperature, so the adsorption of Cu^{2+} on SBA-15-F-EDTA becomes more favorable at higher temperatures which is coherent with ΔH° values. The ΔS° values are positive meaning that the randomness at the solid/solution interface increased during adsorption. Metal ions are hydrated in aqueous media so when these ions get absorbed, water molecules are released and dispersed in the solution; this results in an increase in the entropy. This is mainly due to the displacement of water molecules from the coordination sphere of the metal ions which gain more energy thus increasing the randomness of the system [32]. Jing *et al.* obtained the same results where heavy metals adsorption on N,N-di(carboxymethyl) dithiocarbamate chelating resin increased with temperature [33]. Also, Da'na *et al.* reported an increase of Cu^{2+} adsorption with temperature on amino modified SBA-15 [36].

III. 7. Selectivity

In order to study the selectivity, 20 mg of each adsorbent was stirred with 20 mL of mixed metal solution containing equimolar amounts of each cation (0.47 mmol L^{-1}) for 120 min at pH 5.8. The results are reported in **Table IV.13**. Adsorption only occurred for copper and lead which have larger k_{w} than Ni^{2+} and Cd^{2+}. These results are in accordance with the kinetic data since Cu^{2+} and Pb^{2+} adsorption rates were much faster than those of Ni^{2+} and Cd^{2+}. The selectivity was calculated as the follows:

$$\alpha_{\text{Cu/Pb}} = \frac{X_{Cu}}{Y_{Cu}} \times \frac{Y_{Pb}}{X_{Pb}}$$

Where X_{Cu} and X_{Pb} are the molar fraction adsorbed at equilibrium, Y_{Cu} and Y_{Pb} are the molar fraction remaining in the solution at equilibrium. $\alpha_{\text{Cu/Pb}}$ = 0.61for SBA-15 and 0.88 KIT-6, these values are less than 1 in both cases which means that the two adsorbents are selective for Pb^{2+} more than Cu^{2+}.

Table IV.13. Competitive adsorption on SBA-15-F-EDTA and KIT-6-F-EDTA

Metal	SBA-15-F-EDTA				KIT-6-F-EDTA		
	C_i (mmol L^{-1})	C_f (mmol L^{-1})	Adsorption (%)	Selectivity $\alpha_{\text{Cu/Pb}}$	C_f (mmol L^{-1})	Adsorption (%)	Selectivity $\alpha_{\text{Cu/Pb}}$
Cu^{2+}	0.47	0.17	65		0.15	69	
Ni^{2+}	0.47	0.47	0	0.61	0.47	0	0.88
Cd^{2+}	0.47	0.47	0		0.47	0	
Pb^{2+}	0.47	0.12	74.1		0.14	62	

III.8. Competitive Adsorption

Cu^{2+} adsorption by SBA-15 was examined in the presence of competitors such as NaCl, $NaNO_3$, KCl and NH_4NO_3 of concentration 0.2 M. The results are shown in **Figure IV.30**; the presence of these ions affected Cu^{2+} adsorption remarkably which indicates that these competitors affected the chelating activity of EDTA thus decreasing its efficiency in complexing Cu^{2+}.

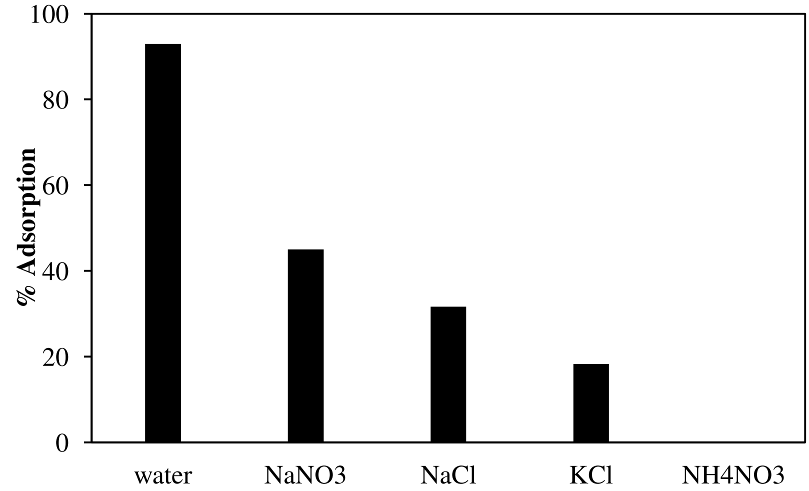

Figure IV.30. Effect of competitive ions on the adsorption of Cu^{2+} on SBA-15-F-EDTA (pH = 5.8, t= 2 h at 25 ºC and $[Cu^{2+}]_i = 0.47$ mmol L^{-1}

In the presence of KCl and NaCl the adsorption of Cu^{2+} decreased even more than in the presence of $NaNO_3$. This result could be due to the formation of stable complexes between Cu^{2+} ions and Cl^-. The charges and masses of these complexes are different from those non-complexed metal ions. This may change significantly the interaction between the adsorbent surface and metal ions. Equilibrium compositions in Cu^{2+}-Cl^- systems are shown in **Figure IV.31.** Cu^{2+} ions form relatively stable monocomplexes $CuCl^+$ which is present in a broad range of Cl^- concentrations. The monocomplex becomes dominative when the concentration of NaCl exceeds 0.08 M. Other copper complexes are on very minor importance and their contribution is less than 3–5% [34].

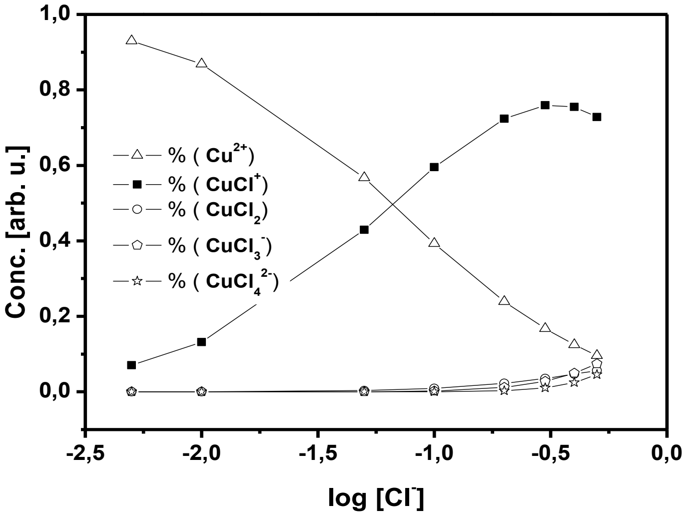

Figure IV.31. Equilibrium composition of Cu^{2+} - Cl^- system [34].

IV. Fixed Bed Column Experiments

Fixed bed column experiments were also performed for SBA-15-F-EDTA along with the batch adsorption tests so that the packed column efficiency of this adsorbent could be studied. These experiments are important to test if this type of modified materials could be applied in water treatment.

IV.1. Heavy Metal Mixture Breakthrough Curves in Ultrapure Water

The breakthrough curves in ultra pure water containing an equimolar mixture of heavy metal cation are shown in **Figure IV.32**. The curves show that the adsorbent saturation is reached after 300 mL of contaminated water was passed through the column.

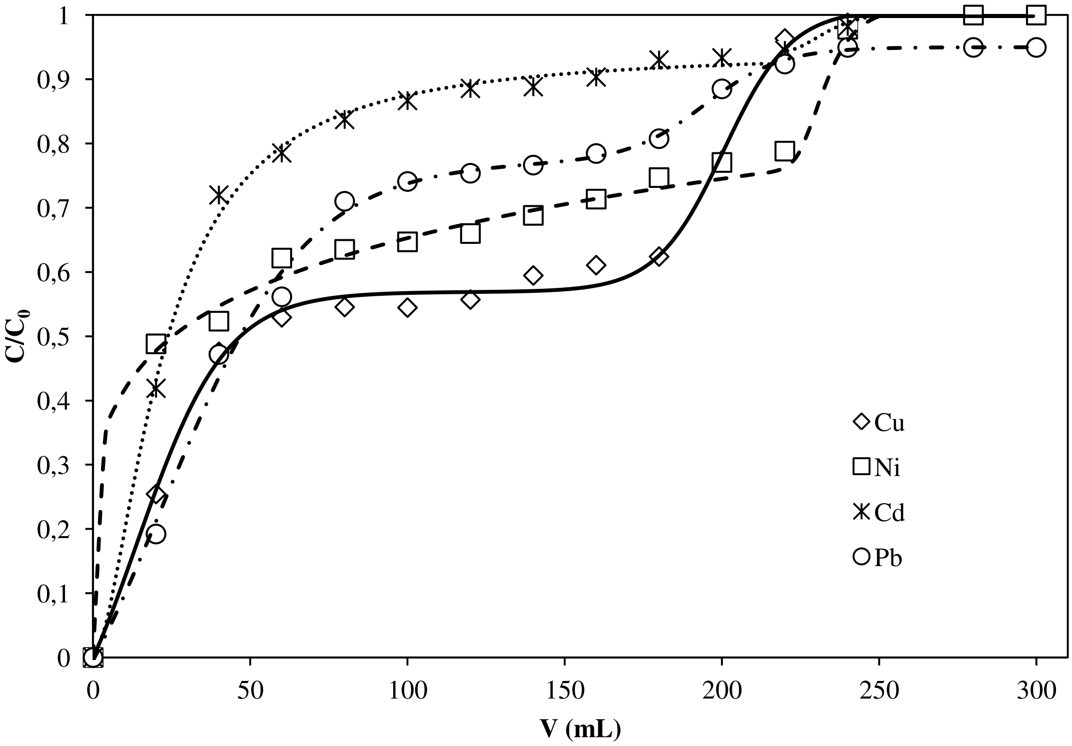

Figure IV.32. Breakthrough curve for Cu^{2+}, Ni^{2+}, Cd^{2+} and Pb^{2+} adsorption of on SBA-15-F-EDTA (pH = 5.8 at 25 ºC and $[M^{2+}]_i = 0.47$ mmol L^{-1}, m = 106 mg, flow rate 1 ml min^{-1})

The fixed bed adsorption capacity for each of one of these four metals was calculated by integration of the breakthrough curves and reported in **Table IV.14**. For comparison, the capacities obtained from batch experiment done with the same mixture of heavy metal cations have also been reported.

Table IV.14. Column capacity for Cu^{2+}, Ni^{2+}, Cd^{2+} and Pb^{2+} adsorption on SBA-15-F-EDTA

Metal ion	Batch capacity (mmol g^{-1})	Column capacity (mmol g^{-1})
Cu^{2+}	0.29	0.416
Ni^{2+}	0	0.231
Cd^{2+}	0	0.176
Pb^{2+}	0.35	0.312

The capacities obtained were larger than those calculated for batch experiments except for Pb^{2+}. In batch experiments the initial concentration of metal ions decreases with time while it remains constant in fixed bed column experiments. Furthermore, no adsorption is observed for both Ni^{2+} and Cd^{2+} in batch experiments while they were adsorbed in fixed bed. This result can be related to the fact that that these two metal ions lose their hydration sphere with lower exchange velocity (k_{w}) than Cu^{2+} and Pb^{2+}. In column experiments, the contact time is higher than in batch which permits a better interaction with the available EDTA molecules and Ni^{2+} and Cd^{2+}. The shape of the obtained curves is unusual which might be related to the adsorption kinetics of these metals in a mixed solution which differ between batch and fixed bed experiments.

IV.2. Application to a Natural Water Sample

The same experiment was also performed for natural ground water. The sample was spiked with the same concentration of each heavy metal as before and was then passed through the SBA-15-F-EDTA packed column. The obtained breakthrough curves are presented in **Figure IV.33**. The shapes of the curve are very different than those obtained in ultra pure water. The equilibrium is reach very quickly indicating that heavy metal ions are not very well adsorbed on the material. This is certainly due to the presence in large quantity of calcium cations which are also complexed by EDTA molecules.

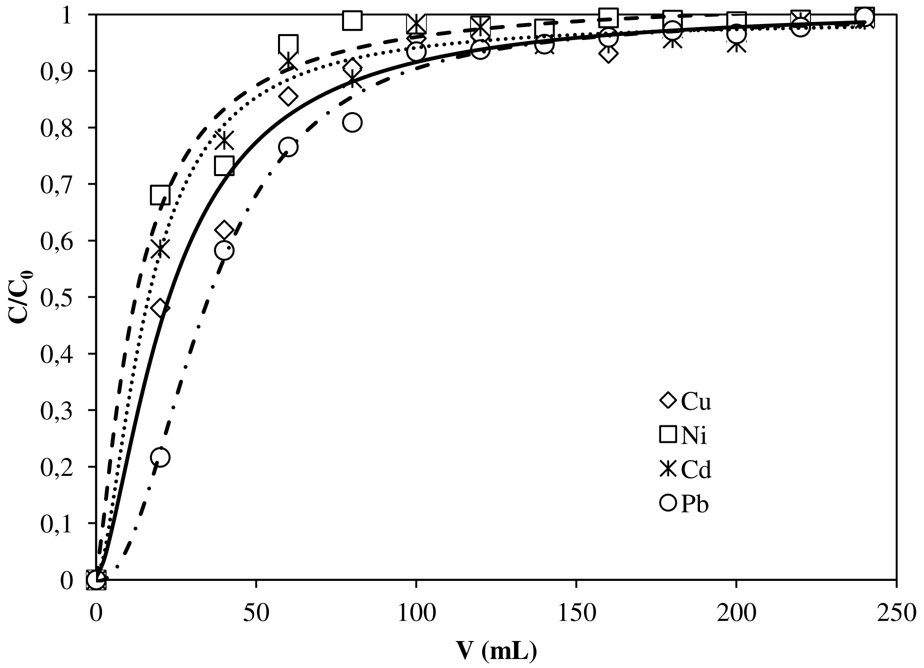

Figure IV.33. Breakthrough curve for Cu^{2+}, Ni^{2+}, Cd^{2+} and Pb^{2+} adsorption of on SBA-15-F-EDTA from natural ground water (pH = 6 at 25 °C and $[M^{2+}]_i$ = 0.47 mmol L^{-1}, m = 107 mg, flow rate 1 mL min^{-1})

The fixed bed adsorption capacity for all the metal ions was also calculated and the results are listed in **Table IV.15**. The capacities obtained decreased significantly compared to those values obtained while using heavy metals contaminated ultrapure water. This decrease is due to the presence of elevated amount of calcium ions Ca^{2+} in this ground water. Ca^{2+} ions which will form complexes with EDTA thus competing with the rest of the metal ions and it is well known that EDTA forms stable complexes with calcium ions.

Table IV.15. Comparison of column capacity for Cu^{2+}, Ni^{2+}, Cd^{2+} and Pb^{2+} adsorption on SBA-15-F-EDTA from ultrapure and natural water

Metal ion	Column capacity (mmol g^{-1}) Ultrapure water	Column capacity (mmol g^{-1}) Ground water
Cu^{2+}	0.416	0.161
Ni^{2+}	0.231	0.104
Cd^{2+}	0.176	0.124
Pb^{2+}	0.312	0.174

IV.3. Column Regeneration

Several adsorption-desorption tests were done for Cu^{2+} using the same SBA-15-F-EDTA packed column after regenerating it. Elution of adsorbed ions was accomplished by 1 M HCl solution at flow rate 1mL.min^{-1}. Then the regeneration efficiency was evaluated by performing two more adsorption cycles using the same column and regenerating it after each cycle. The three obtained curves are shown in **Figure IV.34**.

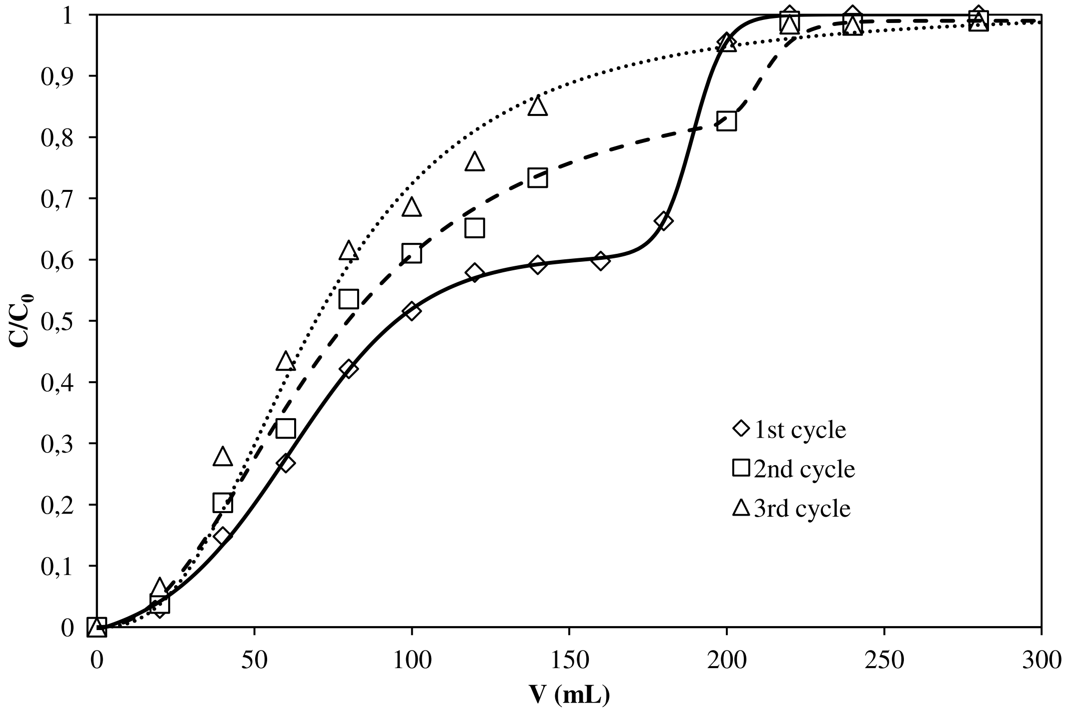

Figure IV.34. Breakthrough curves for Cu^{2+} adsorption of on NaX after regeneration (pH = 5.8 at 25 ºC and $[M^{2+}]_i$ = 0.47 mmol L^{-1}, m = 109 mg, flow rate 1 mL min^{-1})

Table IV.16. Regeneration efficiency after three Cu^{2+} adsorption-desorption cycles

	Capacity (mmol g^{-1})	Regeneration efficiency (%)
1st cycle	0.503	-
2nd cycle	0.450	89.5
3rd cycle	0.370	73.5

After three consecutive Cu^{2+} adsorption-desorption cycles, the SBA-15-F-EDTA packed column conserved up to 73.5 % of its original capacity which means that it can be used several times. It can be noticed also that the shape of the breakthrough curves changed after each regeneration cycle and the adsorption capacity also decreased. This decrease might be attributed to possible EDTA leaching after acid regeneration.

IV. Conclusions

Metal ions adsorbents have been prepared by EDTA immobilization on KIT-6, SBA-15 and SBA-16 mesoporous silica. The ordered mesostructure of the resulting hybrid organic/inorganic materials was well preserved. Modified KIT-6 and SBA-15 showed high efficiency for eliminating Cu^{2+}, Ni^{2+}, Cd^{2+} and Pb^{2+} compared to SBA-16 due to their favorable structure characteristics (pore size). The kinetic data well fits the non-linear pseudo-second-order model and the rate of the adsorption process depends on the exchange kinetics between the ligand and the aqueous metal ions. Therefore, the selectivity for Cu^{2+} and Pb^{2+} is controlled by the exchange velocity (k_{w}) of water molecules with metallic ions. These results suggest the possibility of applying these adsorbents for the selective recovery of Cu^{2+} and Pb^{2+} ions from a mixed metal ions solution. Equilibrium data were also fitted by Langmuir isotherm. The maximum adsorption capacities depend on the amount of EDTA immobilized. As for thermodynamics, the adsorption process was found to be spontaneous and endothermic where adsorption increased with temperature. Both adsorbents were selective for Pb^{2+} and Cu^{2+} with preference to lead. In the presence of competitors' ions adsorption on SBA-15-F-EDTA decreased. In column experiments the adsorption capacities of the metals ions increased and after two regeneration cycles the packed column reserved 73.5 % of its original capacity.

References

[1] Z. Liang, B. Fadhel, C.J. Schneider, A.L. Microporous Mesoporous Mater. 111 (2008) 536–543.

[2] J. Gallas, J. Goupil, A.Vimont, J. Lavalley, B. Gil, J. Gilson, O. Miserque, Langmuir. 25 (2009)5825-5834.

[3] A. Maria, X. Zhao, J. Phys. Chem. B. 107 (2003) 12650–12657.

[4] M. Mureseanu, A. Reiss, I. Stefanescu, E. David , V. Parvulescu, G. Renard,V. Hulea, Chemosphere, 73(2008) 1499–1504.

[5] X. Wang, K. Lin , J. Chan,S.Cheng, J. Phys. Chem. B 109 (2005) 1763-1769.

[6] J. Yu, M. Tong, X. Sun, B. Li, Bioresour. Technol. 99 (2008) 2588-93.

[7] E. Da'na, A. Sayari. Desalination. 285 (2012) 62–67.

[8] A.S.M. Chong, X.S. Zhao. J. Phys. Chem. B. 107 (2003) 12650–12657.

[9] N. Liu, R.A. Assink, B. Smarsly, C.J. Brinker. Chem. Commun. 10 (2003) 1146-1174.

[10] J.M. Rosenholm, M. Linden. Chem. Mater. 19 (2007) 5023-5034.

[11] A. Calvo,P. C. Angelome,V. M. Sanchez,D. A. Scherlis,F. J. Williams, G. J. A. A. Soler-Illia. Chem. Mater. 20 (2008) 4661–4668.

[12] M. Kruk, M. Jaroniec, A. Sayari, Langmuir 13(1997) 6267–6273.

[13] F. Kleitz, F.Bérubé, R.Guillet-Nicolas, C. M. Yang, M.Thommes, J. Phys. Chem. C 2010, 114, 9344 s. .

[14] Z. Jin, X. Wang, X. Cui, J. Colloid Interface Sci. 307 (2007) 158–165.

15 A. Shahbazi, H. Younesi, A. Badiei. Chem. Eng. J. 168 (2011) 505–518

[16] A. Agrawal, K. Sahu, B. Pandey, Colloids Surf., A. 237 (2004) 133–140.

[17] L. Hajiaghababaei, A. Badiei, M. R. Ganjali, S. Heydari, Y. Khaniani, G. M. Ziarani. Desalination 266 (2011) 182–187.

[18] Y. Jiang, Q. Gao, H. Yu, Y. Chen, F. Deng. Microporous Mesoporous Mater. 103 (2007) 316–324.

[19] C. Cheng, J. Wang, X. Yang, A. Lia, C. Philippe. J.Hazard. Mater. 264 (2014) 332– 341.

[20] C.Lai.,C.Chen,B.Wei, S.Yeh. Water research, 36 (2002) 4943–4950.

[21] A.Bhatnagar, V.Vilar, J.Santos, C.Botelho, R.Boaventura. Chem. Eng. J. 200 (2012) 365–372.

[22] V.Guptaa, S.Agarwalc, T.Saleh. J. Hazard. Mater. 185 (2011) 17–23.

[23]S.L. Sun, A.Q. Wang, J. Hazard. Mater. 131 (2006) 103.

[24] X. Jing, F. Liu, X. Yang, P. Ling, L. Li, C. Long, A. Li. J.Hazard. Mater. 167 (2009) 589–596.

[25]Sigg. L, behra. P, stumm.w. chimie des milieu aquatiques 5e edition 2014, Dunod,paris.

[26] F.M. Morel and J.G. hering.1993. Principles and applications of aquatic chemistry, john wiley & sons,Inc., new York.

[27] E. Repo, J. K. Warchoł , A. Bhatnagar, A. Mudhoo, M. Sillanpaa. Water research 47 (2013) 4812 -4832.

[28] C. Giles, D. smith, A. huitson, J. Colloid Interface Sci., 47 (1974) 755-765.

[29] B. H. Hameed, A. A. Ahmad, N. Aziz. Chem. Eng. J. 133 (2007) 195 – 203.

[30] K. Kumari, R.P. Singh, SK. Saxena . Colloids and Surfaces. 33 (1988) 55-61.

[31] E. Da'na, A. Sayari . Chem. Eng. J. 166 (2011) 445–453.

[32] Y. Liu, Y.J. Liu. Sep. Purif. Technol. 61 (2008) 229–242.

[33] X.Jing , F. Liua, X. Yang, P.Ling, L. Li, C. Long, A. Li. J.Hazard. Mater.167 (2009) 589–596.

[34] K. Pyrzynska, M.Bystrzejewski. Colloids Surf., A. 362 (2010) 102–109.

Table of Contents

I. Synthesis Route 135

II. CMK-3 Characterization 136

- II. 1. Textural Analysis 136
  - II.1.1. X-Ray Diffraction (XRD) 136
  - II.1.2. Nitrogen Adsorption-Desorption Isotherms 137
  - II.1.3. Transmission Electron Microscopy (TEM) 138
- II.2. Chemical Surface Analysis 139
  - II.2.1 Point of Zero Charge (pH_{zpc}) Determination 139

III. Heavy Metals Batch Adsorption Tests 140

- III.1. Effect of Extraction Method on Adsorption Efficiency 140
- III.2. Mass Effect 141
- III.4. pH Effect 141
- III.5. Adsorption Kinetics 142
- III.6. Adsorption Isotherms 144
- III.3. CMK-3 Selectivity 145

IV. Competitive Adsorption 146

V. Adsorption Thermodynamics 146

VI. Heavy Metal Mixture Adsorption in Dynamic Conditions 148

- VI.1. Heavy Metal Mixture Breakthrough Curves in Ultrapure Water 148
- VI.2. Application to Ground Water 149
- VI.3. Column Regeneration 151

VIII. Conclusions 152

References 153

Ordered mesoporous carbons (OMCs) are interesting materials for various application fields including adsorption. OMCs have high hydrothermal, chemical and mechanical stabilities. They are synthesized through the polymerization of a carbon source using mesoporous silica as templates. Thus CMK-3 is the negative replica of well-ordered hexagonal SBA-15 mesoporous silica. The use of OMCs for heavy metals adsorption has not been extensively studied. In this chapter, CMK-3 synthesis route, the physico-chemical characterizations are presented as well as its efficiency in heavy metals removal from aqueous solutions.

I. Synthesis Route

Highly ordered mesoporous SBA-15 silicate is considered as an ideal hard template for carbon nanocasting. Using SBA-15 as a mold allows obtaining nano-arrays with diameter smaller than 10 nm. The obtained carbon is referred to CMK-3. The presence of micropores in the SBA-15 structure ensures that the replicated carbon arrays will be connected by bridges thus forming its tunable order structure. The resulted CMK-3 will possess a 2-D mesostructured framework which is the negative image of the SBA-15 porous volume.

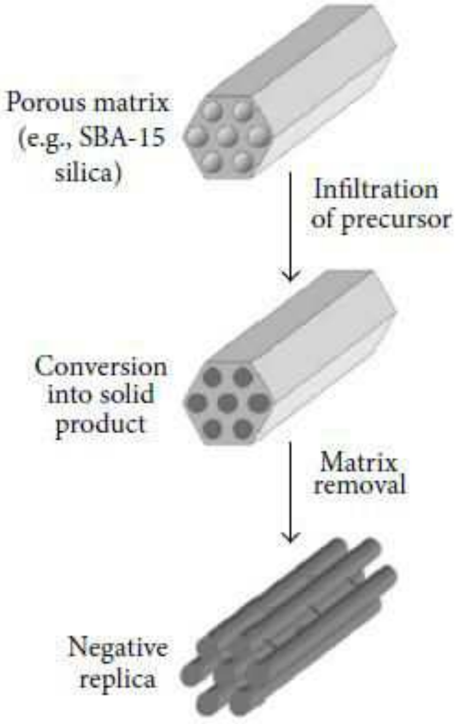

Figure V.1. A schematic illustration of CMK-3 nanocasting using SBA-15 [1].

As it is shown in **Figure V.1**, the first synthesis step is the filling of the SBA-15 pores with the carbon source (sucrose). The polymers are then converted to carbon by pyrolysis under high temperature (800 °C) and inert atmosphere. The final step is the removal of the silica template by dissolution using either aqueous NaOH or HF. The CMK-3 material was fully characterized in order to determine accurately its physico-chemical properties.

II. CMK-3 Characterization

II. 1. Textural Analysis

II.1.1. X-Ray Diffraction (XRD)

The X-Ray diffraction patterns of the mesoporous carbon CMK-3 is illustrated in **Figure V.2**. CMK-3 exhibits three well-resolved XRD diffraction peaks at low angle. The first sharper peak is indexed at (100) and the two other at (110) and (200) which all correspond to the 2D hexagonal space group *p6mm*. This result indicates that the obtained carbon possesses a uniform hexagonally ordered mesoporous structure similar to that of its hard template SBA-15 with a little structural shrinkage.

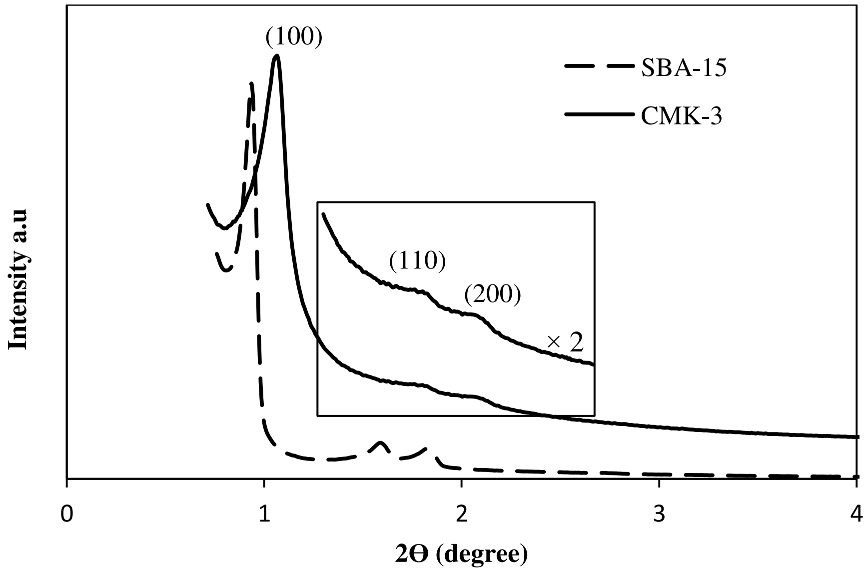

Figure V.2. XRD patterns of CMK-3 and that of its template SBA-15

II.1.2. Nitrogen Adsorption-Desorption Isotherms

The nitrogen adsorption– desorption isotherms of SBA-15 and its mesoporous CMK-3 replica are given **Figure V.3 a**. The CMK-3 isotherm is of type IV similar to SBA-15 according to the IUPAC classification with H2 type hysteresis loop. CMK-3 isotherm exhibited a sharp step pressure increase at $P/P_0 > 0.35$ while for SBA-15 it was at $P/P_0 > 0.6$ due to capillary condensation in the mesopores that are narrower than those of SBA-15 silica. This result is well illustrated by the pore size distribution calculated by BJH modified method (JKS method) from adsorption branch for CMK-3 and desorption branch for SBA-15 silica of the nitrogen isotherms (**Figure V.3 b**).

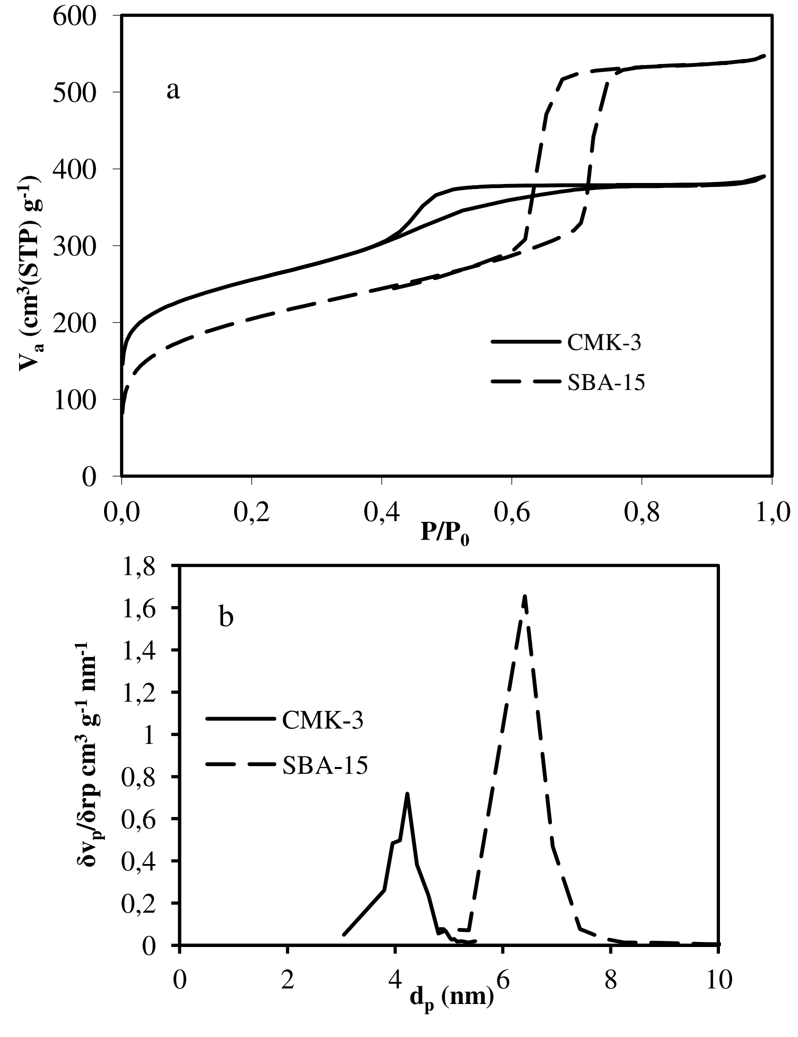

Figure V.3. Nitrogen adsorption–desorption isotherms (a) and pore size distribution (b) of CMK-3 and its SBA-15 mold

The textural properties calculated from N_2 physisorption data are summarized in **Table V.1**. The specific surface area was evaluated using the BET equation and the mesopores volume from α_s-plots. CMK-3 exhibited larger surface area but less pore volume and pore size and a larger number of micropores than SBA-15 silica. This decrease observed for both the pore volume and pore size is expected due to the filling of the carbon precursor inside the SBA-15 pores.

Table V.1. Textural properties of SBA-15 and its CMK-3 replica

Sample	S_{BET} (m^2 g^{-1})	pore size (nm)	mesopores volume (cm^3 g^{-1})	micropores volume (cm^3 g^{-1})
SBA-15	746	6	0.744	0.054
CMK-3	929	4	0.464	0.11

It should be noted here that the contrary to SBA-15, the pore size of CMK-3 and ordered mesocarbons in general is difficult to control [2]. The pore size in mesoporous silicates can be controlled by varying the temperature for example or by adding organic swelling agents [3] whereas the pore size of ordered mesocarbons (OMCs) lies in the thickness of the silica walls, which cannot be easily tuned. The pore diameters of OMCs are found around 4nm [2].

II.1.3. Transmission Electron Microscopy (TEM)

The TEM images of CMK-3 mesoporous carbon are shown in **Figure V.4**. It is clear from these images that the hexagonal structure of SBA-15 was well preserved. CMK-3 exhibited a uniform array of hexagonal pores indicating its ordered structure. Transmission electron microscopy (TEM) images of CMK-3 further confirm that the obtained material is composed of highly ordered hexagonally packed nano-rods with uniform diameter.

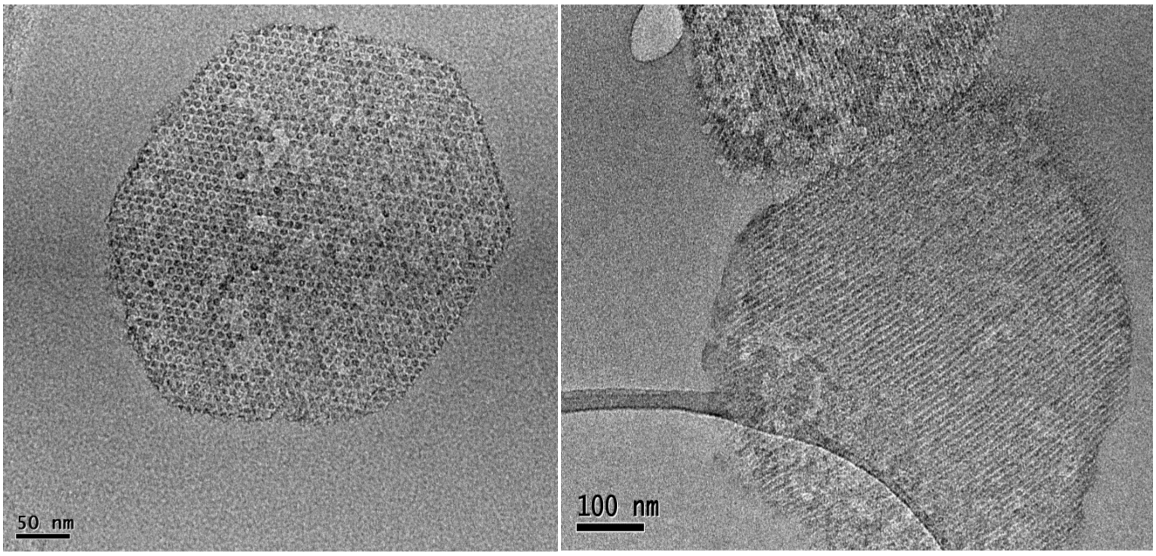

Figure V.4. TEM images of CMK-3 viewed from perpendicular and parallel directions

II.2. Chemical Surface Analysis

II.2.1 Point of Zero Charge (pH_{zpc}) Determination

The point of zero charge is defined as the pH of the aqueous solution wherein the solid is in a neutral electrical potential. This information is very important since the global charge at the adsorbent surface governs its adsorption behavior. Thus, the pH shift method (chapter II § IV.7) was used herein for determining the pH_{ZPC}.

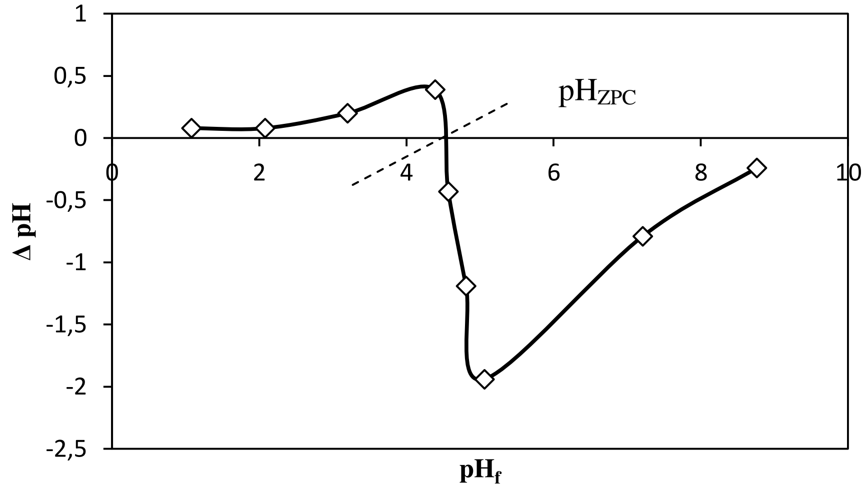

Figure V.5. The pH of point of zero charge of CMK-3 mesoporous carbon determined by pH shift method

As shown in **Figure V.5**, ΔpH is plotted versus pH_f. The obtained curve cuts the $pH_{initial} = pH_{final}$ line at 4.39 where $\Delta pH = 0$. This obtained value is the pH_{zpc} and it is of significant importance since it allows expecting the adsorption behavior of CMK-3. The removal of metal ions is not possible below this pH value because of the repulsion phenomena between the net positively charged adsorbent surface and heavy metal cations.

III. Heavy Metals Batch Adsorption Tests

III.1. Effect of Extraction Method on Adsorption Efficiency

In the literature, two protocols were found to remove the mesoporous silicate template: NaOH or HF dissolution. In order to compare the influence of the template removal protocol on the heavy metal removal, two CMK-3 materials extracted by the two mentioned protocols have been tested for Cu^{2+} adsorption. 10 mg of each CMK-3 was mixed with 20 mL of 0.47 mmol.L^{-1} Cu^{2+} solution (m/V = 10/20 mg/mL). The two mesoporous carbons were used just after template removal without any further modification. The results are presented on **Figure V.6**. The CMK-3 for which the template has been removed by NaOH exhibits 97% removal of Cu^{2+} ions whereas for the second one (template dissolution in HF) adsorbed only 48 %. Another test has been also performed using commercial activated carbon (AC) with a close zero point charge (pH_{zpc} around 5) in order to compare its removal efficiency with that of HF and NaOH extracted CMK-3. This test shows that the NaOH extracted mesoporous CMK-3 carbon is a better adsorbent than the other two (**Figure V.6**).

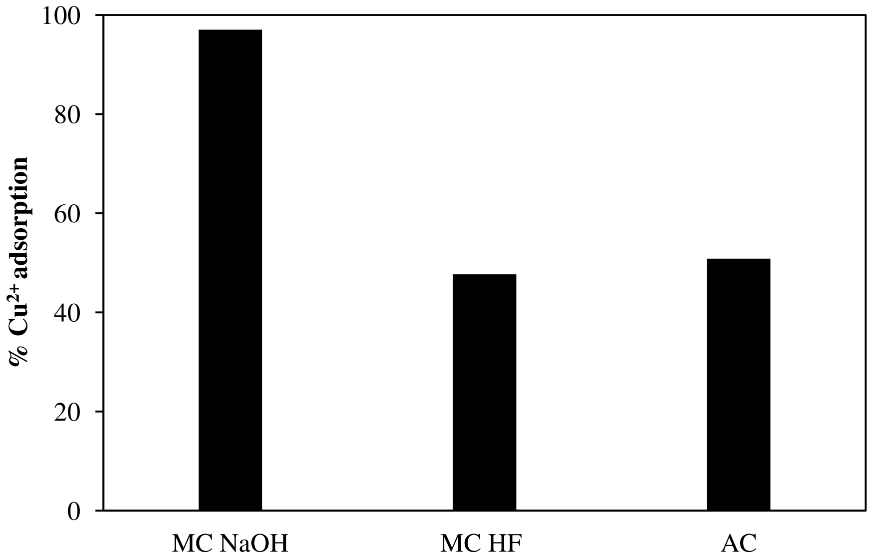

Figure V.6. Cu^{2+}adsorption on HF and NaOH extracted CMK-3 (pH = 5.8 at 25 ºC and $[Cu^{2+}]_i$ = 0.47 mmol L^{-1})

These results show that the chemical agent used to extract silica template has a significant impact on the adsorption performance of the obtained CMK-3. All the following results have been obtained with CMK-3 mesoporous carbon for which the silica template has been extracted with NaOH.

Based on these findings, the detailed study for heavy metals removal was conducted for NaOH extracted CMK-3. This extraction has proved to be very effective since no further oxidation treatments are needed to enhance the heavy metals removal efficiency.

III.2. Mass Effect

The optimization of the m/V ratio for heavy metal adsorption on CMK-3 was carried out contacting increasing masses of adsorbent (5 mg to 60 mg) with 20 mL of Cu^{2+} 0.47 mmol L^{-1} solution for 120 min. The obtained results are shown on **Figure V.7**. The adsorption percentage increase very quickly with the CMK3 mass. All the copper II ions are adsorbed for mass value higher than 10 mg (**Figure V. 7**). So m/V ratio of 10/20 mg/mL will be used in all the following experiments.

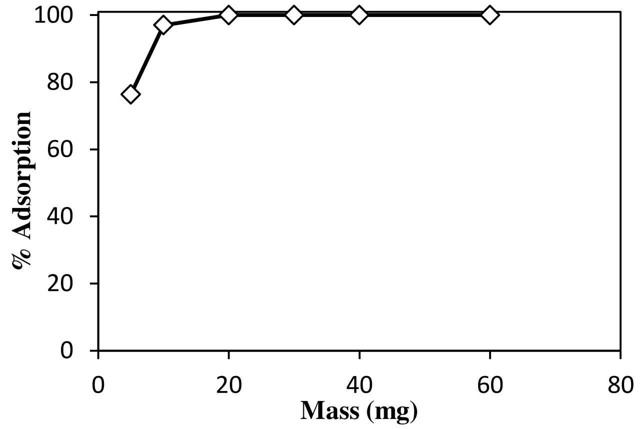

Figure V.7. Effect of mass on the adsorption of Cu^{2+} on CMK-3 (pH = 5.8, t = 2h at 25 °C and $[Cu^{2+}]_i$ = 0.47 mmol L^{-1})

III.4. pH Effect

As the pH of the solution increases from 2 to 7, adsorption on CMK-3 increases to reach its maximum at approximately pH 5 (**Figure V.8**). These obtained results matches with the pH_{pzc} value determined above. When the pH values are higher than 4.39 the CMK-3 surface will negatively charged thus it attracts the positively charged metal ions. Below pH_{pzc} the carbon surface is positively charged so it will not adsorb metal ions, that's why adsorption decreased significantly when adsorption tests were done in acidic medium. It is worth mentioning here that CMK-3 was not efficient for Ni^{2+} adsorption as it was the case for the other ions so the rest of the experiments were done for Cu^{2+}, Cd^{2+} and Pb^{2+}.

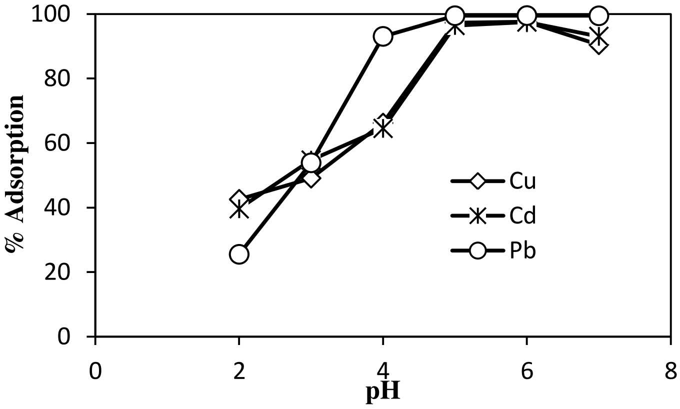

Figure V.8. Effect of pH on Cu^{2+}, Cd^{2+} and Pb^{2+} adsorption onto CMK-3 (metal concentration, 0.47mmol L^{-1} at 25°C)

III.5. Adsorption Kinetics

The kinetics sorption experiments have been carried out for Cu^{2+}, Cd^{2+} and Pb^{2+} at pH 5.8 (**Figure V.9**). Two kinetic models were used as before in order to find the best fit. The kinetics data were fitted by the non linear pseudo first and the non linear second order models. The fit parameters are summarized on **Table V.2**. The calculated parameters showed that Pb^{2+}, Cu^{2+} and Cd^{2+} adsorption on CMK-3 followed the pseudo-second order kinetic model with higher correlation coefficients (R^2). Also, the calculated qe values from pseudo-second order model were much closer to those obtained experimentally.

The initial sorption rate (*h* values) is higher for Pb^{2+} and Cu^{2+} than it is for Cd^{2+}. These results are similar to those found for NaX zeolite and mesoporous materials. This can be explained depending on the water exchange kinetic constant of the metal ions.

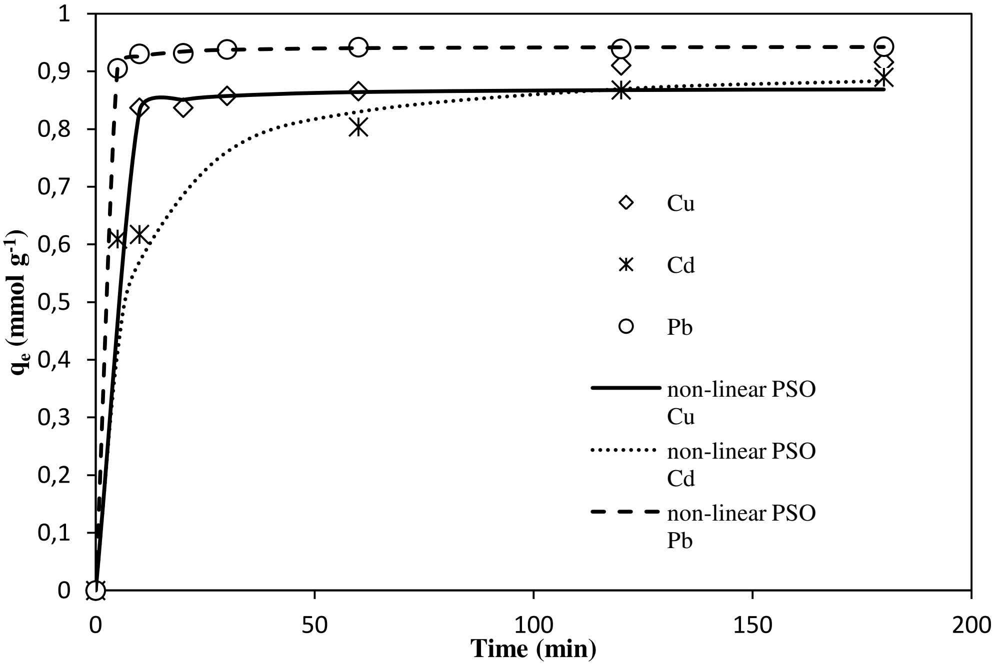

Figure V.9. Cu^{2+}, Cd^{2+} and Pb^{2+} sorption kinetics on CMK-3 fitted by non-linear pseudo-second order model (C_i = 0.47 mmol L^{-1}, pH 5.8 at 25°C)

Table V.2. Comparison of the first and the second order kinetic models for CMK-3

		First order kinetic model			Second order kinetic model			
	q_e^{exp} (mmol g^{-1})	k_1 (min^{-1})	q_e^{cal} (mmol g^{-1})	R^2	k_2 (g $mmol^{-1}$ min^{-1})	q_e^{cal} (mmol g^{-1})	h (mmol g^{-1} min^{-1})	R^2
Cu^{2+}	0.916	0.023	8.36	0.926	2.39	0.871	1.12	0.999
Cd^{2+}	0.889	0.003	1.03	0.923	0.182	0.913	0.152	0.998
Pb^{2+}	0.943	0.057	28.3	0.954	5.60	0.943	4.98	0.999

These findings prove that the selectivity of the adsorbent is directly related to the nature of the metals while the adsorption capacity is only influenced by the chemical nature of sorption or exchange sites. It is important to mention here that CMK-3 didn't adsorb Ni^{2+} in the same efficiency as for the others (only 30% adsorption). Bearing in mind that this metal has the lowest k_w value among these four ions it could be said that main reason for its low removal efficiency is its low exchange velocity of water molecules with metallic ions.

III.6. Adsorption Isotherms

The adsorption isotherms for Cu^{2+}, Cd^{2+} and Pb^{2+} on CMK-3 are shown in **Figure V.10**. These isotherms are well fitted by Langmuir and exhibit a sharp initial slope indicating that the material is very efficient at low metal concentrations. Then, a plateau is observed indicating that the maximal adsorbent capacity is reached. The corresponding K_L and q_{max} values are reported in **Table V.3**.

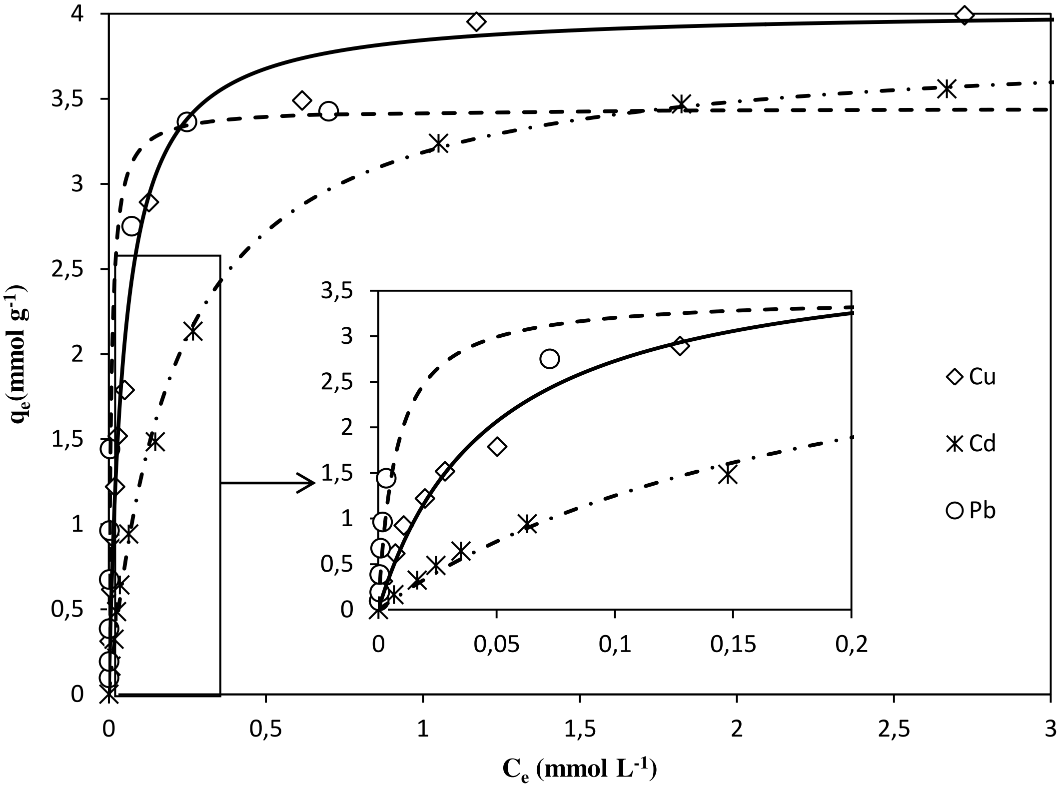

Figure V.10. Langmuir fitting of Cu^{2}, Cd^{2+} and Pb^{2+} adsorption isotherms on CMK-3

The obtained maximum adsorption capacity (q_{max}) values are high indicating the high efficiency of CMK-3. K_L values are very different and follow the same order of selectivity verifying that CMK-3 has a high affinity for $Pb^{2+.}$

Table V.3. Langmuir parameters for adsorption isotherms

Metal	q_{max}^{exp} (mmol g^{-1})	K_L (L $mmol^{-1}$)	R^2
Cu^{2+}	4	18.17	0.996
Cd^{2+}	3.86	4.72	0.999
Pb^{2+}	3.45	226	0.992

R_L values for CMK-3 were also calculated (**Table V.4**). The obtained values verified that the adsorption process of the three metal ions is favorable on CMK-3 since all the R_L values are between 0 and 1. These results are similar to those obtained for NaX and mesoporous materials.

Table V.4. R_L values for CMK-3

Cu^{2+}	0.011
Cd^{2+}	0.045
Pb^{2+}	0.002

III.3. CMK-3 Selectivity

The selectivity of CMK-3 was determined by mixing 10 mg of each adsorbent with 20 mL of equimolar mixed metal solution (0.47 mmol L^{-1} of Cu^{2+}, Cd^{2+} and Pb^{2+} ions) for 120 min at pH 5.8. The results are reported in **Table V.5**. Adsorption only occurred for these three metals with different removal percentages ($Pb^{2+} > Cu^{2+} > Cd^{2+}$). This result is expected since Pb^{2+} has the largest k_w value. These results are in accordance with the kinetic data (*h* values) since Pb^{2+} adsorption rate was much faster than Cu^{2+} followed by Cd^{2+}. The selectivity was calculated as the following:

$$\alpha_{Cu/Pb} = \frac{X_{Cu}}{Y_{Cu}} \times \frac{Y_{Pb}}{X_{Pb}} \text{ , } \alpha_{Cd/Cu} = \frac{X_{Cu}}{Y_{Cu}} \times \frac{Y_{Cd}}{X_{Cd}} \text{ and } \alpha_{Pb/Cd} = \frac{X_{Pb}}{Y_{Pb}} \times \frac{Y_{Cd}}{X_{Cd}}$$

Where X_{Cu} , X_{Pb} and X_{Cd} are the molar fraction adsorbed at equilibrium for each metal, Y_{Cu}, Y_{Cd} and Y_{Pb} are the molar fraction remaining in the solution at equilibrium. $\alpha_{Cu/Pb}$ = 0.095 and (**Table V.5**), this values isless than 1 which means that CMK-3 is more selective for Pb^{2+} more than Cu^{2+} while $\alpha_{Cu/Cd}$ = 6.4 and $\alpha_{Pb/Cd}$ = 67 so CMK-3 is more selective for Cu^{2+} and Pb^{2+} than Cd^{2+}.

Table V.5. Selectivity of CMK-3

	C_0 (mmol L^{-1})	C_f (mmol L^{-1})	Adsorption (%)	Selectivity		
				$\alpha_{Cu/Pb}$	$\alpha_{Cu/Cd}$	$\alpha_{Pb/Cd}$
Cu^{2+}	0.470	0.024	94.8	0.095	6.4	67
Cd^{2+}	0.470	0.124	73.6			
Pb^{2+}	0.470	0.002	99.5			

IV. Competitive Adsorption

Copper adsorption by CMK-3 was examined in the presence of NaCl, $NaNO_3$, KCl and NH_4NO_3 of concentration 0.2 M. As it is shown in **Figure V.11**, the presence of electrolytes in water slightly affected Cu^{2+} adsorption on CMK-3 contrary to zeolites and SBA-15-F-EDTA. These obtained results might be due to specific interaction of CMK-3 with heavy metal ions or to the very important number of adsorption sites on the CMK-3 surface. Furthermore, the adsorption properties of CMK-3 for Cu^{2+} ions is not affected by the presence of organic molecules such as dyes which are also able to be adsorbed by the CMK-3 (**Figure V.11**). In fact, the competitive adsorption of methylene blue and Cu^{2+} ions experiment have shown that the two compounds were highly adsorbed by the material. This observation indicates that CMK-3 materials are promising adsorbent for heavy metal removal from water since the presence of other species seems not to affect its adsorption properties.

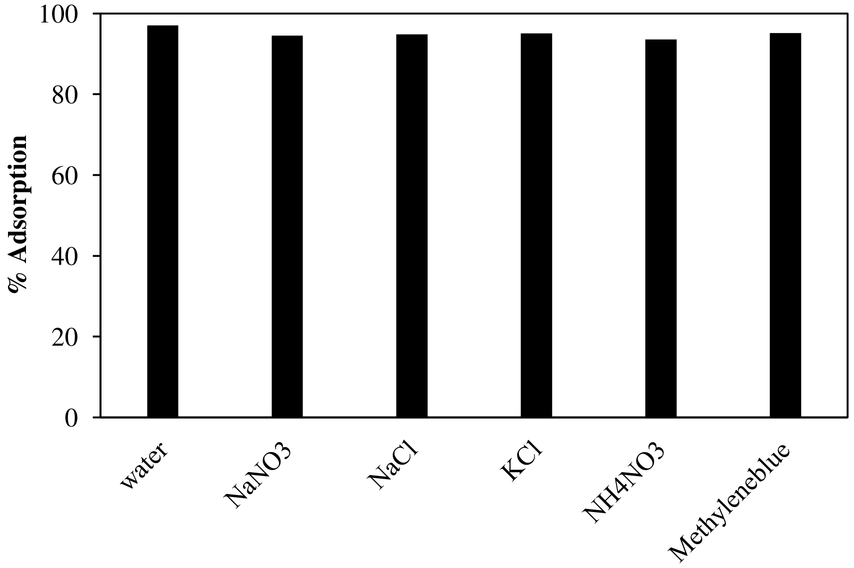

Figure V.11. Effect of competitive ions on the adsorption of Cu^{2+} on CMK-3 (pH = 5.8, t = 2 h at 25 °C and $[Cu^{2+}]_i = 0.47$ mmol L^{-1}.

V. Adsorption Thermodynamics

The effect of temperature on Cu^{2+} adsorption was also studied for CMK-3 (**Figure V.12**). The results obtained showed that adsorption slightly increases with the temperature. The calculated thermodynamic parameters are listed in **Table V.5**.

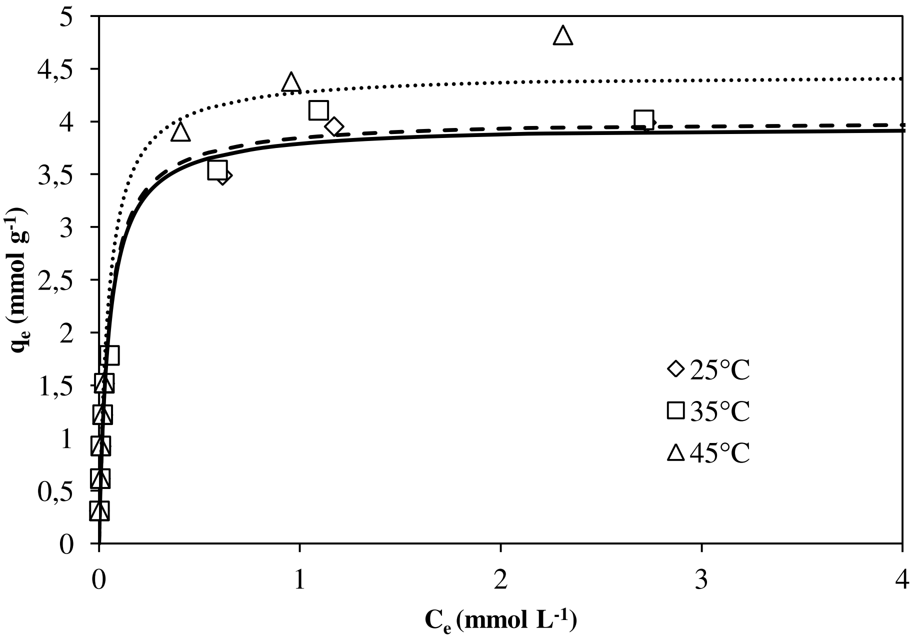

Figure V.12. Cu^{2+} adsorption on CMK-3 at different temperatures (pH = 5.8)

The thermodynamic parameters were calculated from the plot of the distribution coefficient values K_d versus temperatures **Figure V.13**. K_d values were obtained by plotting ln (q_e/C_e) versus qe and extrapolating q_e to 0 as it was done before for the other adsorbents. It was found that K_d slightly increased as the temperature increased revealing the endothermic nature of the adsorption process.

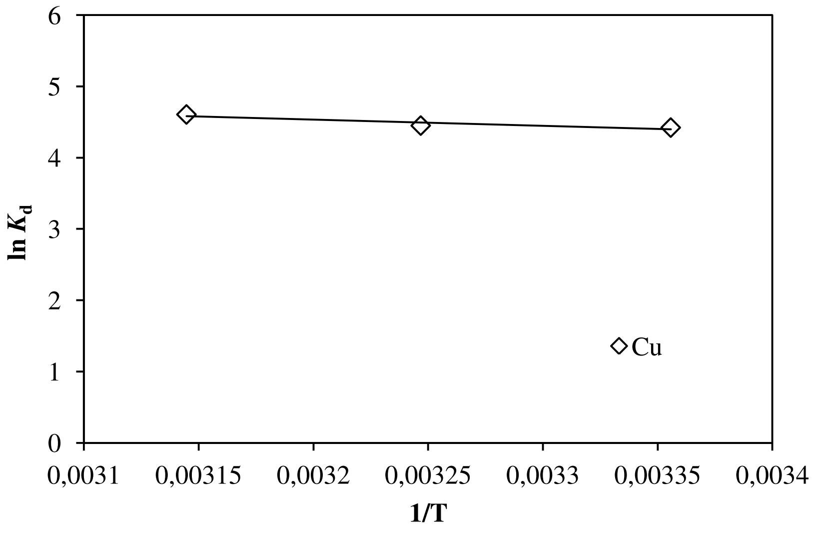

Figure V.13. Plots of ln K_d versus 1/T for the adsorption of Cu^{2+} on CMK-3

The positive value of ΔH° confirms the endothermic nature of the adsorption process on CMK-3. CMK-3 possesses also high porosity so as temperature increases diffusion becomes more favorable inside the pores of CMK-3.

Table V.6. Thermodynamic parameters for Cu^{2+} adsorption on CMK-3

Metal	ΔH° (kJ mol^{-1})	ΔS° (J K^{-1} mol^{-1})	T (K)	ΔG° (kJ mol^{-1})	R^2
Cu^{2+}	7.2	61	298	-10.9	0.848
			308	-11.4	
			318	-12.2	

ΔG° values are negative indicating the spontaneity of the adsorption process. The values of ΔG° increased with temperature, so the adsorption of Cu^{2+} on CMK-3 becomes more favorable at higher temperatures. The positive entropic value is consistent with the fact that the adsorption is favorable. The positive values of ΔS° mean that the randomness at the solid/solution interface increased during adsorption [4]. Cu^{2+} ions are hydrated in water so when these ions get absorbed, water molecules will be released and dispersed in the solution; this results in an increase in the entropy. This is mainly due to the displacement of water molecules from the coordination sphere of the metal ions which gain more energy thus increasing the randomness of the system.

VI. Heavy Metal Mixture Adsorption in Dynamic Conditions

VI.1. Heavy Metal Mixture Breakthrough Curves in Ultrapure Water

Fixed bed column experiments were performed for CMK-3 for an equimolar mixture of heavy metal cations as well so that the packed column efficiency could be studied and compared with the batch adsorption tests. The first experiment was done using a mixed metal ions solution in ultrapure water. The obtained breakthrough curves are shown in **Figure V.14**. The curves show that the adsorbent saturation is reached after 350 mL of contaminated water was passed through the column.

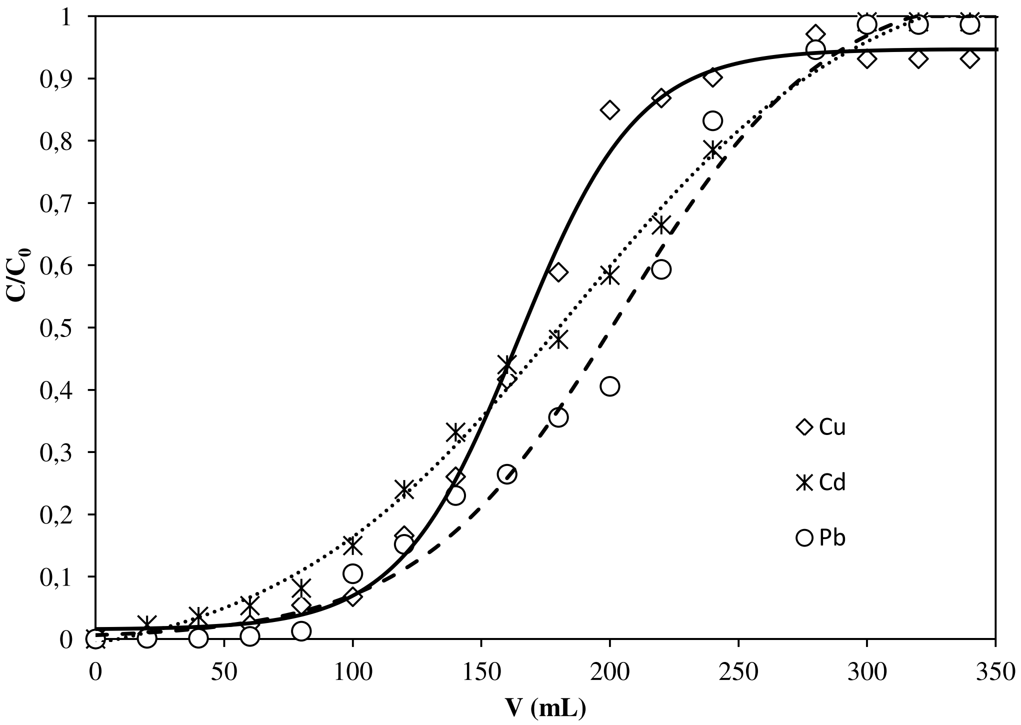

Figure V.14. Breakthrough curve for Cu^{2+}, Cd^{2+} and Pb^{2+} adsorption of on CMK-3 (pH = 5.8 at 25ºC and $[M^{2+}]_i$ = 0.47 mmol L^{-1}, m = 105 mg, flow rate 1 mL min^{-1})

The fixed bed adsorption capacity for each metal cation were calculated by integration of the breakthrough curves and reported in the **Table V.7**. For comparison, the capacities obtained from batch experiment done with the same mixture of heavy metal cations have also been reported. The capacities obtained were slightly smaller than those calculated for batch experiments but the selectivity remained in the same order.

Table V.7. Column capacity for Cu^{2+}, Cd^{2+} and Pb^{2+} adsorption on CMK-3

Metal ion	Batch capacity (mmol g^{-1})	Column capacity (mmol g^{-1})
Cu^{2+}	0.895	0.732
Cd^{2+}	0.694	0.716
Pb^{2+}	0.940	0.886

VI.2. Application to Ground Water

The same experiment was also performed for natural ground water. The sample was spiked with the same concentration of each heavy metal as before and was then passed through the CMK-3 packed column. The obtained breakthrough curves are presented in **Figure V.15**.

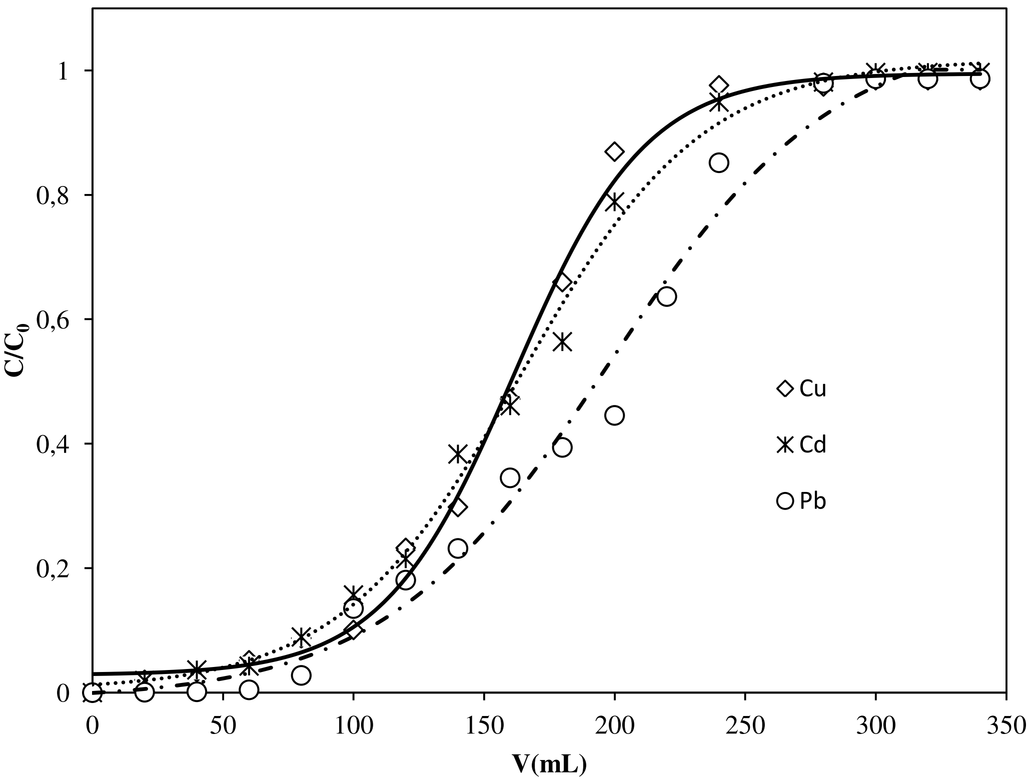

Figure V.15. Breakthrough curve for Cu^{2+}, Cd^{2+} and Pb^{2+} adsorption of on CMK-3 from natural ground water (pH = 6 at 25 ºC and $[M^{2+}]_i$ = 0.47 mmol L^{-1}, m = 105 mg, flow rate 1 mL min^{-1})

The fixed bed adsorption capacity for all the metal ions was also calculated and the results are listed in **Table V.8**. The capacities obtained slightly decreased compared to those values obtained while using heavy metals contaminated ultrapure water. This decrease certainly is due to the presence of elevated amount of calcium ions Ca^{2+} in this ground water. Nevertheless, the decrease in capacity for CMK-3 is lower than that observed for NaX and mesoporous silica. This result is in accordance with results obtained upon performing the adsorption in the preence of competitors' ions where the removal efficiency was slightly affected for CMK-3 as compared with NaX and SBA-15-F-EDTA.

Table V.8. Comparison of column capacity for Cu^{2+}, Cd^{2+} and Pb^{2+} adsorption on CMK-3 from ultrapure and natural water

Metal ion	Column capacity (mmol g^{-1}) Ultrapure water	Column capacity (mmol g^{-1}) Natural water
Cu^{2+}	0.732	0.680
Cd^{2+}	0.716	0.700
Pb^{2+}	0.886	0.747

VI.3. Column Regeneration

Several adsorption-desorption tests were done for Cu^{2+} using the same CMK-3 packed column after regenerating it. Elution of adsorbed ions was accomplished by 1 M HCl solution at flow rate 1mL.min^{-1}. Then the regeneration efficiency was evaluated by performing 3 adsorption cycles using the same column and regenerating it after each cycle. The three obtained adsorption curves are shown in **Figure V.16**.

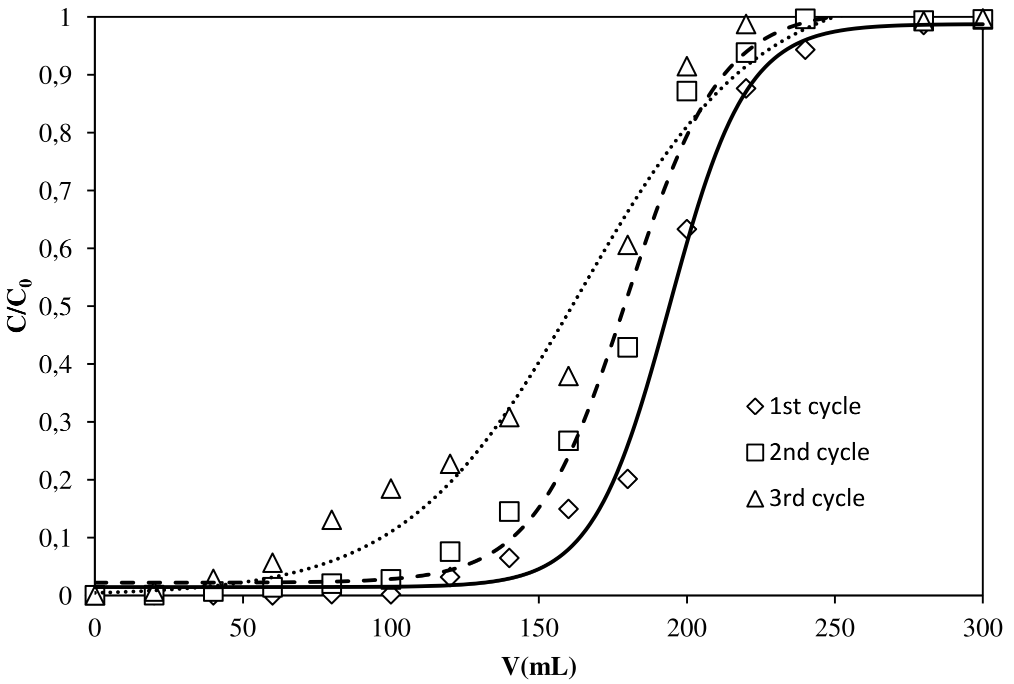

Figure V.16. Breakthrough curves for Cu^{2+} adsorption of on CMK-3 after regeneration (pH = 5.8 at 25 ºC and $[M^{2+}]_i$ = 0.47 mmol L^{-1}, m = 105 mg, flow rate 1 mL min^{-1})

Table V.9. regeneration efficiency after three Cu^{2+} adsorption-desorption cycles

	Capacity (mmol g^{-1})	Regeneration efficiency (%)
1st cycle	0.87	-
2nd cycle	0.796	91.5
3rd cycle	0.738	84.8

After three consecutive Cu^{2+} adsorption-desorption cycles, the CMK-3 packed column conserved up to 84.8 % of its original capacity which means that it can be used several times. However after the second regeneration the shape of the breakthrough curves change indicating that modifications of the solid surface chemical properties occur. The modifications seem to weaken the interaction between Cu^{2+} cations and the solid surface.

VIII. Conclusions

In this chapter the efficiency of nanocasted CMK-3 carbon for heavy metals removal was analyzed. This type of carbon was synthesized using mesoporous SBA-15 as a hard template then it was removed by NaOH. This method used for eliminating the silica template was proved to be more efficient than using HF. Moreover, the efficiency of the thus synthesized CMK-3 in adsorbing heavy metals was found to be high without the need of any further modification contrary to other nanocasted carbon extracted by HF. The kinetic data were well fitted by the non-linear pseudo second order and the metal ions adsorption was in this order: $Pb^{2+} > Cu^{2+} > Cd^{2+}$. CMK-3 was not selective for Ni^{2+} since the removal percentage was low (only 30 %) compared to the other three ions. The maximum adsorption capacity was high (up to 4 mmol g^{-1}) and the isotherms were fitted by Langmuir. Also the presence of competitors ions in the water treated didn’t affect the removal efficiency of CMK-3. The adsorption increased with temperature so the adsorption process was endothermic. Fixed bed experiments showed good results concerning adsorption efficiency and regeneration. Based on the obtained results, CMK-3 could be considered a promising adsorbent for heavy metal removal.

References

---

[1] Á.B. Murcia. ISRN Nanotechnology. Volume 2013, Article ID 257047, 29 pages.

[2] J. S. Lee, S. H. Joo and R. Ryoo, J. Am. Chem. Soc. 124(2002) 1156-1157.

[3] D. Zhao, Q. Huo, J. Feng, B. F. Chmelka and G. D. Stucky, J. Am. Chem. Soc. 120 (1998) 6024- 6036.

[4] F.J.V.E. Oliveira, E.C. da Silva Filho, M.A. Melo, C. Airoldi. Surf. Sci. 603 (2009) 2200–2206.

Comparison of the Adsorbents Used

All the adsorbent studied in this manuscript have been tested under the same experimental conditions. They have shown very good adsorption capacities and high sorption rates for all of them. However, a comparative study is now necessary to better evaluate which material is more efficient for heavy metal removal in aqueous media.

I. Batch Adsorption Comparison

From the set of results shown in **Table VI.1**, all the adsorbents maximum efficiencies are in the same pH range which corresponds to the range of the majority of natural waters. The Cu^{2+} removal efficiencies obtained for an initial copper concentration of 30 ppm are very high for the three adsorbents. However, the m/V ratios used to reach these rates are very different for the three materials. NaX zeolite exhibits the lower m/V ratio indicating that this material is more effective than the other two which require m/V ratios 3.3 and 1.6 times higher for EDTA modified mesoporous silica and CMK-3, respectively. This assumption is clearly visible on the resulting Cu^{2+} capacities which vary as follows: NaX > CMK-3> mesoporous silica.

Table .VI.1. Comparison of m/V ratio and regeneration efficiency

	NaX	**SBA-15-F-EDTA**	**KIT-6-F-EDTA**	**CMK-3**
$[Cu^{2+}]_i$ (ppm)	30	30	30	30
m/V ratio (mg mL^{-1})	30/100	20/20	20/20	10/20
Cu removal efficiency (%)	98	93	95	97
Cu capacity (mmol g^{-1})	2.32	0.440	0.450	0.916
Optimum pH	5-7	5-6	5-6	5-7
Regeneration (%)	92.2	73.5	-	84.8

A good adsorbent needs to be regenerated in order to be reused several times. NaX zeolite and CMK-3 mesoporous carbon have shown a very good adsorption behavior after two regeneration cycles. The lower regeneration percentage of EDTA modified mesoporous silica could be explained by the damaging of the adsorption sites due to EDTA leaching.

Table VI.2 represents the maximum adsorption capacities (q_{max}) calculated from the Langmuir fits for the adsorption isotherms. The maximum sorption capacities are mainly dependent on the number of the adsorption sites on the materials. CMK-3 and NaX zeolite have higher maximum sorption capacities compared to EDTA modified mesoporous silica. This result is not surprising since NaX zeolite could theoretically adsorb 3.27 mmol g^{-1} of divalent metal cations compared to only 1.7 mmol g^{-1} for EDTA modified silica. Furthermore, Cu^{2+} removal efficiency for high initial concentration (100 ppm) have also been reported in **Table VI.2**. These values can be compared with those obtained for lower copper initial concentration (30 ppm) reported on **Table VI.1**. The results show that Cu^{2+} removal efficiency of CMK-3 is slightly affected in the concentration range [30 ppm-100 ppm] which is not the case for the others adsorbent. EDTA-mesoporous silica losses around 25% of their efficiency even though the m/V ratio is 2 times higher than CMK-3 whereas NaX zeolite losses 50%. However, in case of NaX, the m/V ratio is 1.6 times lower than that of CMK-3. So it can be supposed that for the same m/V ratio as CMK-3, NaX zeolite will give a very similar adsorption efficiency.

Table VI.2. Maximum adsorption capacity q_{max} and removal efficiency at 100 ppm

Experimental parameter	**NaX**	**SBA-15-F-EDTA**	**KIT-6-F-EDTA**	**CMK-3**
$[Cu^{2+}]_i$ (ppm)	100	100	100	100
Cu abatement rate (%)	49	68.2	71	91.9
q_{max} (mmol g^{-1})				
$Cu^{2+}/Cu(OH)^+$	4.03	1.39	1.23	4
Ni^{2+}	2.84	1	0.98	-
Cd^{2+}	3.10	1.10	1.14	3.86
Pb^{2+}	3.20	1.12	1.15	3.45

In water treatment processes the sorption rates are very important in order to reduce the treatment time. The initial sorption rates calculated from the pseudo second order kinetic model are listed in **Table VI.3**. NaX zeolite sorption rates are very high for all the metal cations tested compared to the other materials. Pb^{2+} ions have the highest sorption rate whereas Ni^{2+} ions have the lowest sorption rate This behavior is rather linked to their water exchange velocity constant (high for Pb^{2+} and low for Ni^{2+}) than the chemical nature of the adsorbent. The elevated adsorption rates for zeolite compared to the other materials could be explained by its high number of exchange sites (3.27 mmol g^{-1}) compared to EDTA modified mesoporous silica (1.7 mmol g^{-1}).

Table VI.3. Batch experiments: kinetic parameters and selectivity

	NaX	**SBA-15-F-EDTA**	**KIT-6-F-EDTA**	**CMK-3**
Kinetics				
Model applied	pseudo-second order	pseudo-second order	pseudo-second order	pseudo-second order
h **(mmol $g^{-1}min^{-1}$)**				
Cu^{2+}	2.94	0.402	0.380	1.12
Ni^{2+}	2.34	0.033	0.030	-
Cd^{2+}	2.52	0.104	0.170	0.152
Pb^{2+}	3.04	1.95	1.30	4.98
Capacities (mmol g^{-1}) for mixture adsorption in batch experiments				
Cu^{2+}	1.02	0.292	0.300	0.895
Ni^{2+}	0.38	0	0	-
Cd^{2+}	1.00	0	0	0.694
Pb^{2+}	2.21	0.350	0.330	0.940

Furthermore, the batch selectivities observed for a mixture of heavy metals in ultrapure water are the same whatever the chemical nature of the adsorbent. These selectivities are directly connected to the values of the kinetic sorption rates. That is why the selectivity order is the same for all the materials $Pb^{2+} > Cu^{2+} > Cd^{2+} > Ni^{2+}$. It should be mentioned also that zeolite possesses the highest adsorption capacity in batch experiments.

Contrary to CMK-3, the presence of other cations such as Na^+, NH_4^+ affects the sorption capacities of Cu on zeolite and EDTA modified silica materials.

II. Dynamic Adsorption Comparison

Dynamic adsorption experimental results (equimolar mixture of heavy metal cation) are compared in **Table VI.4** for the three adsorbents in ultrapure water and in natural water.

Table VI.4. Dynamic adsorption tests

Experimental parameter	**NaX**	**SBA-15-F-EDTA**	**CMK-3**
Dynamic adsorption capacities (mmol g^{-1})			
Ultrapure water			
Cu^{2+}	1.12	0.420	0.730
Ni^{2+}	0.83	0.230	-
Cd^{2+}	0.87	0.180	0.720
Pb^{2+}	2.30	0.310	0.890
Natural water			
Cu^{2+}	0.740	0.161	0.680
Ni^{2+}	0.175	0.104	-
Cd^{2+}	0.578	0.124	0.700
Pb^{2+}	1.61	0.174	0.747

For ultrapure water, the adsorption capacities follow the same order for all the materials: $Pb^{2+} > Cu^{2+} > Cd^{2+} > Ni^{2+}$. In natural water, the adsorbed capacities decrease significantly for NaX zeolite and EDTA-SBA-15. For CMK-3, only a slight decrease is observed. This decrease is certainly explained by the competition with Ca^{2+} cations which are present with in concentration in the used natural water. As observed in batch tests, CMK-3 material seems to be more selective for heavy metal cation than for alkaline or alkaline earth ions

The work done in this thesis is dedicated to heavy metals removal from wastewater. This can be accomplished by several methods including adsorption on porous materials. Adsorption is considered an inexpensive and efficient method for removing heavy metals even at low concentrations. Several adsorbents with different physical and chemical properties have been studied. However, comparing the adsorption performance of these materials is difficult because the experimental conditions vary from one study to another. Among the various materials studied in literature, a great deal of attention is paid nowadays to organically modified mesoporous silicates and nanocasted mesoporous carbons. In this study the goal was to immobilize EDTA, which has good divalent cations chelating properties, on different types of mesostructured silica (SBA-15, SBA-16 and KIT-6). Then their efficiencies in removing Cu^{2+}, Ni^{2+}, Cd^{2+} and Pb^{2+} from aqueous solutions were compared with that of mesoporous carbon CMK-3 and Faujasite zeolite type X that served as the reference material.

The parent mesoporous silica (SBA-15, SBA-16 and KIT-6) have been synthesized and fully characterized. EDTA immobilization has been done via the interaction with the aminopropyl groups grafted on the silica surface. The physico-chemical characterizations have shown that the mesostructure of the sample is preserved after the organic solidification and that EDTA is well anchored to the silica surface. The physico-chemical characterization of CMK-3 mesoporous carbon obtained by nanocasting using SBA-15 silica as template have shown highly ordered material with a high specific surface area. NaX zeolite used as reference is a highly microporous solid containing 6.54 mmol g^{-1} of Na^{+} ions.

The adsorption performances of the studied materials were different both in dynamic experiments and in the presence of competitors' ions.

The three studied materials herein were effective for heavy metals removal in aqueous media. Moreover, the metal selectivity order is the same for all the materials: $Pb^{2+} > Cu^{2+} > Cd^{2+} > Ni^{2+}$. This fact has been explained by the fact that the selectivity is not governed by the chemical surface of the adsorbent but the water velocity exchange k_{w}.

EDTA modified mesoporous silica didn't have the expected efficiency for heavy metal removal in aqueous media. EDTA immobilization on SBA-16 have given rise to low amount of EDTA molecule grafted certainly due to diffusion limitations of EDTA molecules in the pores. Concerning KIT-6 and SBA-15 materials, the obtained behaviors in batch experiment adsorption are rather the same. The heavy metal capacities and sorption rates are always lower than those obtained for NaX zeolite and CMK-3. This is essentially due to the lower number of adsorption sites (EDTA molecule anchored) than NaX zeolite and CMK-3 carbon. Despite of all the synthesis conditions tested for enhancing the number of EDTA molecule anchored, the maximum EDFTA molecule immobilized didn't exceed 1.7 mmol g^{-1}.

NaX zeolite has showed the best for removal efficiency taking into consideration the m/V ratio. This efficiency was much higher than those found for natural zeolites in literature which makes it very attractive for application over a big scale. Furthermore, this type of synthetic adsorbent is not expensive, stable and can be easily regenerated and reused over several adsorption cycles. Furthermore, NaX zeolite exhibits also the highest heavy metal capacities and sorption rates even though CMK-3 is not very far behind. Indeed, CMK-3 material exhibits also good adsorption properties for high copper concentration (>100 ppm) whereas zeolite behavior seems less efficient at the used m/V. Furthermore, batch and dynamic adsorption experiments have shown that CMK-3 material is less sensitive to the presence of competitors such as alkaline cations (Na^+ and K^+) or ammonium ions than zeolite. The presence of calcium divalent cations greatly affect EDTA modified SBA-15 silica, this effect is lower on NaX and slightly affects CMK-3 is.

The regeneration experiments have shown that NaX zeolite and CMK-3 material can be used in three successive adsorption-desorption cycles for copper ion without an important decrease of their adsorption capacity. EDTA modified SBA-15 material undergoes a clearly visible degradation certainly due to EDTA leaching.

Thus, NaX zeolite and CMK-3 mesoporous carbon are promising materials for heavy metal removal in aqueous media. However, a significant difference exists between these two materials for industrial applications. NaX zeolite is a cheap commercial adsorbent which it can be easily obtained in pellets for dynamic adsorption applications.

For CMK-3 more research should be done in order to study the exact mechanism of adsorption on such type of materials. Moreover, the possibility of the application over a large scale should be taken into consideration as well.